SYNTHESIS AND DESIGN OF LIGAND COPPER COMPLEXES AS ANTI-INFLAMMATORY DRUGS

A dissertation submitted to the

University of Cape Town

In fulfilment of the requirements for the degree of

DOCTOR OF PHILOSOPHY

By

Fatin. M. Ali. Elmagbari

Supervisor:

Prof. Graham E. Jackson

Department of Chemistry
University of Cape Town
Rondebosch
7701
South Africa

January 2015

DEDICATION

This thesis is dedicated to my husband, Ahmed, who has been a constant source of support and encouragement during my graduate degree and composition of the thesis. This work is also dedicated to my parents, Mohammed Magbari and Ashia Busen, for their endless love, and whose good examples have taught me to work hard, and all I have and will accomplish are only possible due to their love and sacrifices during all these years of study.

DECLARATION

I, Fatin M. Elmagbari do sincerely and solemnly declare that **"Synthesis and Design of Ligand Copper Complexes as Anti-Inflammatory Drugs"** is my own unaided work both in concept and execution, and that all sources that I have used and quoted have been indicated and acknowledged by means of complete and clear references. This thesis is submitted for the Doctor of Philosophy (Ph.D.) degree, to the Department of Chemistry, Faculty of Science, University of Cape Town it has not been submitted before for any degree or any examination at the University of Cape Town or any other university.

…….

Fatin Elmagbari

January 2015

ACKNOWLEDGEMENTS

I would like to express my gratitude to Allah (God) for giving me strength and ability to complete this Ph.D. work. May Peace and Blessings of Allah be upon His Prophet Muhammad (peace be upon him). I also would like to ask him that this project would be another tool to help in the treatment of rheumatoid arthritis.

Foremost, I would like to express my sincere gratitude to my advisor Prof. Graham Jackson for the continuous support of my Ph.D. study and research, for his patience, motivation, enthusiasm, and immense knowledge, added considerably to my graduate experience. His useful advice was available to me all the time of research and writing of this thesis. I could not have imagined having a better advisor and mentored for my Ph.D. study.

I would like to deeply thank Prof Kelly Chibale and his group, especially Dr. Yassir Younis for his help, insights and good advices at organic stages to make this thesis able completed. I am extremely grateful to Dr. Shirley Churms for spending time reading this and providing useful suggestion, insights and good advices and made this thesis completed.

I would like to thank all the administrative and technical staff at Department of Chemistry, UCT for their contributions, seminars and conferences, especially thanks to Mr. Peter Roberts for running the NMR experiments and Dr Hong Su for the X-ray structural determination of some of my complexes.

I sincerely thank; my friends Shankari Nair and Taigh Anderson are helpful, to colour my life, during the period of three years. A big thanks is given to my colleagues in the research group for their contribution and discussion.

I would like to thank my husband Ahmed for his personal support and great patience at all times. My parents, brothers and sisters have given me their unbelievable support throughout, as always, for which my mere expression of thanks likewise does not suffice.

Finally, I would like to acknowledge the financial assistance of The Libyan Ministry of Higher Education that provided the necessary financial support for my study.

CONFERENCES PROCEEDINGS

Parts of the results in this thesis have been presented in the following conferences;

- **41st** National Convention of the South African Chemical institute (**SACI2013**) (1-6th December 2013) in the East London, South Africa. (***Potentiometric and spectroscopic study of the interaction of Cu(II), Ni(II) and Zn(II) ions with N-(2-aminoethyl)-N-((pyridin-2-ylmethyl)ethanediamide and rheumatoid arthritis*****).***

- International Conference on Pure and Applied Chemistry (**ICPAC2014**) (23rd to 27th June 2014) in Mauritius. (***Determination of Octanol/water partition coefficients and Blood–plasma modelling of H(555)NMe$_2$, NHH$_2$ and [H$_2$(555)]N copper(II) and rheumatoid arthritis*****).**

- **41st** International Conference on Coordination Chemistry (**ICCC-41**) (21st -25th July 2014) in Singapore. (***Synthesis and Structure Solution of Copper-Based Anti-Inflammatory Drugs*****).**

ABSTRACT

Rheumatoid arthritis is a debilitating disease for which there is no cure. Copper has been used for centuries to alleviate the inflammation associated with the disease. The aim of this research was to design and test new ligands which are able to promote the percutaneous absorption of copper and/or mobilize endogenous copper reserves. Formation constants of H^+, Cu(II), Ni(II) and Zn(II) with five low molecular ligands 2-((2-aminoethyl)amino)-*N*-(pyridin-2-ylmethyl)acetamide) [H(555)NH_2], 2-((2-dimethyl-amino)ethyl)amino)-*N*-(pyridin-2-ylmethyl) acetamide [H(555)NMe_2], *N*-(2-aminoethyl)-*N*′-(pyridin-2-ylmethyl)ethanediamide [H_2(555)NH_2], 3-(2-aminoacetamido)-*N*-(pyridin-2-ylmethyl)propanamide [H_2(565)NH_2], 3-amino-*N*-(pyridin-2-lmethyl)-propanamide [H(56)NH_2] were measured at 25±0.01^{o}C and at an ionic strength of 0.15M (NaCl) using glass electrode potentiometry.

The structures of the different Cu(II) species formed with these ligands were investigated using ultraviolet-visible (Uv-visible), nuclear magnetic resonance (NMR) spectroscopy and X-ray crystallography as well as molecular mechanics calculations. The Uv-visible spectra obtained for the different species in solution were typical of tetragonally distorted Cu(II) complexes. The active binding sites were identified as the pyridine nitrogen, the amide nitrogen and the terminal amino group. The pyridine nitrogen was involved in coordination first, followed by the amide and then the terminal amine groups. The X-ray crystal structure of two of the Cu(II) complexes were solved; one formed a rectangular pyramidal geometry and the other a distorted square planar geometry. Molecular mechanics was used to determine the lowest energy conformation of different possible geometries.

Since the preferred route of administration is through the skin, the rate of dermal absorption and the bioavailability of copper are important. For this reason, the drugs were designed so that they could be administered dermally and be selective for Cu(II) so that they do not affect the speciation of other metal ions in blood plasma. Speciation calculations using a blood plasma model were used to estimate the complexing ability of the ligands *in vivo*. This result showed that [H(555)NH_2] was the best at mobilising copper *in vivo*.

This study also considered dermal absorption studies. Octanol/water partition coefficients and Franz cell permeation studies showed that the Cu(II) complexes are hydrophilic but that [H(555)NMe_2] caused a three-fold increase in membrane permeability of Cu(II).

LIST OF ABBREVIATIONS AND SYMBOLS

amide-O	-Amide carbonyl
amide-N	-Amide nitrogen
amine-N	-Amino nitrogen
c	-Speed of light ($m.s^{-1}$)
C_i	-The concentration of species i
COX	-Cyclooxygenase
CP	-Ceruloplasmin
ΔH°	-The standard enthalpy change of reaction
δ	-NMR chemical shift (ppm)
DNA	-Deoxyribonucleic acid
DMARD	-Disease modifying anti-rheumatic drugs
Ɛ	-Molar absorption coefficient ($dm^3.mol^{-1}.cm^{-1}$)
E_{angle}	-The angle strain energy
E^{bend}	-The total bond deformation strain (bend)
E_{bond}	-bond energy
ECCLES	-Evaluation of Constituent Concentrations in Large Equilibrium Systems
E_{cell}	-Electrode potential
$E_{internal}$	-Internal energy
Esff	-Extensible systematic force field
ESTA	-Equilibrium Simulations for Titration Analysis
E^{strain}	-Total strain energy
$E^{stretch}$	- The total bond deformation strain (stretching)
$E_{torsion}$	-The torsional strain energy
E_{Oop}	-out-of-plane energy
E^{VDW}	-The total steric strain (van der Waals strain)
F	-Faraday's constant
g	-Gerade
GEP	-Glass-electrode potentiometry

HSA	-Human serum albumin
h	-Planck's constant (J.s)
I_0	-Intensity of incident radiation
I	-Intensity of transmitted radiation
J	-Flux in g/cm^{2}h
K	-Equilibrium constant
$k^{stretch}$,k^{bend}	-The stretch and bend force constants
K_p	-Permeability coefficient in cm/h
K_w	-Dissociation constant of water
[L]	-Free ligand concentration (mol dm^{-3})
l.m.w	-Low molecular weight
Log β	-Logarithm (to base 10) of the cumulative equilibrium constants
Log K	-Logarithm (to base 10) of the equilibrium constants
Log $P_{oct/aq}$	-Octanol/water partition coefficient
λ_{max}	-Wavelength of maximum absorption
MeCN	-Acetonitrile
NSAIDs	-Non-steroidal anti-inflammatory drugs
N	-Number of binding sides on the ligand
n-bar	-The formation function
NMR	-Nuclear magnetic resonance
n_P	-Number of titration points
n_T	-Number of titrations
OH^-	-Hydroxide oxygen
PG's	-Prostaglandins
pH	-(-Log H^+)- A measure of acidity or alkalinity
p.m.i	-Plasma mobilizing indices
pyridyl-N	-Pyridine nitrogen
Q_M-bar	-The deprotonation function
R	-The universal gas constant
RA	-Rheumatoid arthritis

r,α	-The bond distance and angle
r^{eq},α^{eq}	-The equilibrium bond length and bond angle
R_{lim}^{H}	-R_{lim} is the Hamiltonian R-limit
R_{f}^{H}	-The Hamiltonian R- factor
ROS	-Reactive oxygen species
SAARDs	-Slow acting anti-rheumatic drugs
σ	-Standard deviation
SOD	-Superoxide dismutase
TEA	-Triethylamine
T	-Temperature
T_H	-Total proton concentration (mol dm^{-3})
THF	-Tetrahydrofuran
T_L	-Total ligand concentration (mol dm^{-3})
TLC	-Thin-layer chromatography
T_M	-Total metal concentration (mol dm^{-3})
TMS	-Tetramethylsilane
u	-Ungerade
U_{obj}	-Objective function
Uv-Vis	-Ultraviolet-Visible
ν	-Frequency (s^{-1})
Z_i	-The charge of the ion
Z_H-bar	-The protonation function
Z_M-bar	-The metal formation function

LIGAND ABBREVIATIONS USED

Asp-Ala-His	-L-aspartyl-L-alanyl- L-histidine
Ala-Gly-Ha	-alanylglycylhistamine
cageL	-3,5-diaminodiamido-4-oxahexacyclododecane
EDTA	-ethylenediaminetetraacetic acid
dien	-diethylenetriamine
dtda	-3,6,9-triazaundecanedioate
$[Cu(NH_3)_4]$	-Copperammonium complexes
en	- ethylenediamine
Gly-Gly-Ha	-glycylglycylhistamine
Gly-Gly-His	-glycylglycylhistidine
Gly-His	-glycyl-L-histidine
Gly-His-Gly	-glycyl-L-histidylglycine
Gly-Gly-Gly	- glycylglycylglycine
[H(555)NH_2]	-2-((2-aminoethyl)amino)-*N*-(pyridin-2-ylmethyl)acetamide
[H(555)NMe_2]	-2-((2-(dimethylamino)ethyl)amino)-*N*-(pyridin-2-ylmethyl)acetamide
[H_2(555)NH_2]	-*N*-(2-aminoethyl)-*N*′-(pyridin-2-ylmethyl)ethanediamide
[H_2(565)NH_2]	-3-(2-aminoacetamido)-*N*-(pyridin-2-ylmethyl)propanamide
[H(56)NH_2]	-3-amino-*N*-(pyridin-2-ylmethyl)propanamide

[555-N]	-N^1-(2-aminoethyl)- N^2-(pyridin-2-ylmethyl)ethane-1,2-diamine
[H(555)-N]	-*N*-(2-(2-aminoethylamino)ethyl)- picolinamide
[H_2(556)-N]	-2-amino-*N*-(2-*oxo*-2-(2-(pyridin-2-yl)ethylamino)ethyl)acetamide
ttda	-3,6,9,12-tetraazatetradecanedioate

LIST OF FIGURES

LIST OF TABLES

TABLE OF CONTENTS

Chapter one

Rheumatoid Arthritis

1. Rheumatoid Arthritis

1.1 Background of the Disease

Rheumatoid arthritis (RA) is a chronic, inflammatory, systemic, debilitating disease that leads to the destructions of diarthrodial joints[1,2] (synovial joints).[3] It is considered to be an autoimmune disease, although the exact cause is still unknown.[1-7] The disease occurs first in the knuckle joints and chiefly affects the synovial membranes of multiple joints in the body.[8,9] It is characterized by massive synovial proliferation and subintimal (the underlying tissue includes blood and lymphatic vessels)[10] infiltration of inflammatory cells, which along with angiogenesis (the process for new capillaries from existing blood vessels)[11], appears as a slight swelling accompanied by stiffness, and leads to the formation of a very aggressive tissue called pannus[12,13], as shown in Figure 1.1. Expansion of the pannus induces cartilage thinning and bone erosion, leading to the loss of joint function. The rheumatoid pannus can be considered as a local tumor.[8,9]

Figure 1.1: Chronic Rheumatoid Arthritis.

The development of pannus is well represented in Figure 1.2, by a comparison of normal joint and one damaged by rheumatoid arthritis as well as swelling and thickening of the synovial membrane.

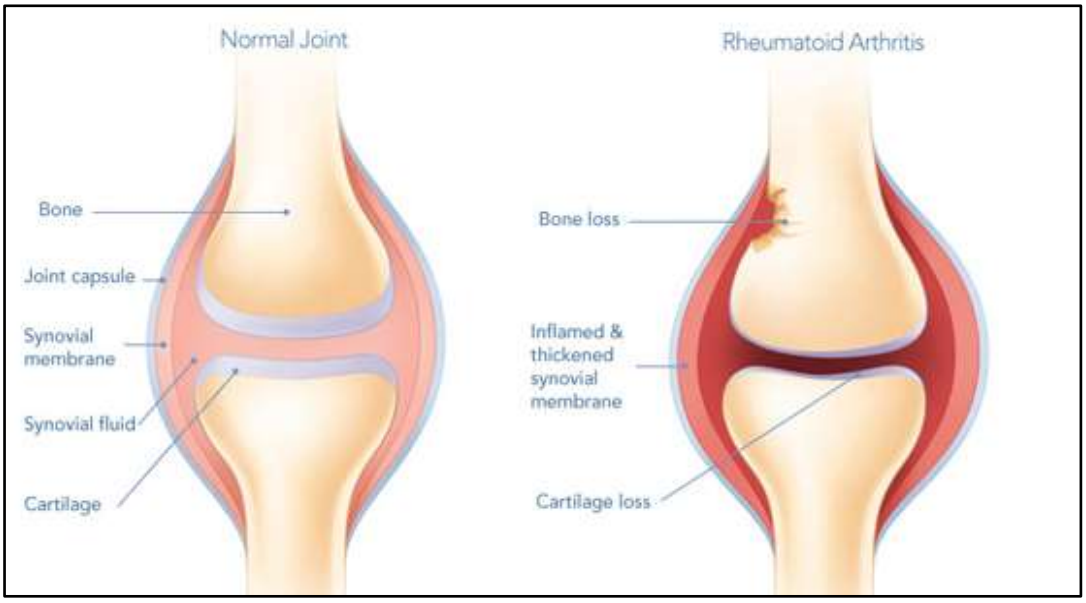

Figure 1.2: Normal joint (left) and joint affected by RA (right).

Although RA affects 1–5% of the world's population, it remains a medical challenge.[8,14] As the cure for RA has not yet been found, treatment of chronic RA remains largely symptomatic.[15,16] There is little evidence to suggest that the disease is hereditary.[17] It can develop at any age, but most commonly starts between the ages of 30 and 50. It is about three times more common in women than in men.[18] Why this disease is prevalent among women is unknown, but it is presumably related to the hormonal milieu.[14,19,20]

The symptoms of RA are weight loss, fatigue, morning stiffness, joint pain, swelling and tenderness around the joints, as well as loss of functioning and mobility of joints.[21-24] RA can affect many joints in the body, including knees, ankles, elbows and wrists.

The aetiology of RA is not known. Clinical evidence suggests that several factors together result in the onset of RA. It is believed to be related to a complex of genetic, endogenous (e.g. hormonal, endocrine, or metabolic factors), and exogenous factors (e.g. geographic, infectious agents such as viruses, bacteria, and fungi, or occupational factors).[25,26] All of these have been shown to be implicated in the progression of RA yet none is shown to be its primary cause.[27]

Macrophages, fibroblasts and T-lymphocytes, are three cell populations which are found abundantly in the rheumatoid arthritis synovium.[28] These cells are shown to play a substantial role in the progression and the development of RA.[29] However, evidence coming from different experimental approaches[30-33] strongly supports the hypothesis that RA is a disease initiated and driven mostly by T-cells irrespective of its cause. The chronic inflammatory environment in which T-cells operate within the rheumatoid synovium is likely to influence their function greatly, although the effector phases responsible for the processes that lead to joint destruction involve several different cell types such as cytokines, and also catalytic enzymes.[30,34-36]

There is no cure for this debilitating disease. However, the symptoms associated with the disease can be alleviated by the use of anti-inflammatory drugs and also controlled by the use of immunosuppressive drugs.[7,8]

1.2 Drugs used in the Treatment of Rheumatoid Arthritis

The uses of drug therapy for RA is mainly for the relief of pain, the inhibition of inflammation and the restoration of normal immune mechanisms[37], as well as, multidisciplinary health care to preserve functional capacity of joints.[38] An effective treatment program for arthritis is reported to consist of drug therapy (steroidal and non-steroidal), exercise and rest.[39] Highly effective drug treatments exist but early treatment is critical for reducing inflammation, relief of pain, slowing or stopping joint damage, and improving patient function and wellbeing.[40] Furthermore, surgical treatment (joint replacement) is done if the joints have been severely deformed.[41-43] However, pharmaceutical drugs that are commonly given to patients fall into three categories;

1. Non-steroidal anti-inflammatory drugs (NSAIDs).
2. Disease-modifying anti-rheumatoid drugs (DMARD).
3. Glucocorticosteroids.

1.2.1 NSAIDs

Non-steroidal anti-inflammatory drugs are usually the first class of drugs prescribed and most commonly used because they are well tolerated by patients, and they decrease the inflammatory response of the body to disease or injury.[44] Examples of these are aspirin,

ibuprofen and naproxen. Non-steroidal anti-inflammatory drugs alleviate inflammation and pain by blocking cyclooxygenase (COX) which is an enzyme that is responsible for the production of prostaglandins[45,46] (Prostaglandins play a key role in the generation of the inflammatory response). Their biosynthesis is significantly increased in inflamed tissue and they contribute to the development of the cardinal signs of acute inflammation).[47] NSAID's are effective, but they are associated with side-effects, and gastrointestinal side-effects have become the most prevalent complication of chronic therapy with NSAIDs.[48] As well as causing nausea, loss of appetite, vomiting, diarrhoea, constipation, rash, dizziness, drowsiness and headache[45,46], NSAIDs do not modify the progression of the disease.[45,46,49]

1.2.2 DMARDs

Disease-modifying anti-rheumatoid drugs can be divided further into two classes namely: disease-modifying antirheumatic drugs (DMARDs) and biologic agents; they reduce the progression of RA and prevent bone damage.[50] Examples of DMARDs include low doses of methotrexate, leflunomide, D-penicillamine, sulfasalazine, gold therapy, minocycline, azathioprine, hydroxychloroquine (and other antimalarials), and cyclosporine.[51,50] DMARDs prevent disease progression before it can cause irreparable joint damage. While DMARDs are powerful arthritis fighters, an instant result should not be expected; hence they are also called slow acting anti-rheumatic drugs (SAARDs).[52] Biological agents are a new type of therapy that decreases or stops the progression of RA. They act as response modifiers that block specific immune factors that lead to RA.[53] However, prostaglandins (PG's) have also been recognized as an important contributor to the body's inflammation reaction. The use of DMARD's is also associated with some side-effects. These include gastrointestinal symptoms, sore and dry mouth, nausea, and skin rash. Prolonged usage may lead to gastrointestinal irritation, renal and liver toxicity.[54,55]

1.2.3 Glucocorticosteroids

Glucocorticosteroids can be taken during the final stage of RA. These drugs suppress inflammation, and they have a high potency compared to NSAID's and DMARDs but they can compromise the immune system.[56-58] Examples of corticosteroids are cortisone, prednisone and dexamethasone. They act to reduce heat, swelling and tenderness at the inflamed joint and have proved to be the best for combating inflammation. However, their mode of

anti-inflammatory action is unclear. They are neither antiviral nor antibacterial.[44,56,59] These drugs work very well but tend to have too many side-effects. The most feared complication in patients with RA has been the effects of steroids on the bone and gastrointestinal tract.[52,60,61] Additional side effects include a puffy face, increase in appetite, weight gain, mood swings, water retention and fractures.[57,58]

This inefficiency of current drugs against arthritis has challenged scientists to develop an anti-inflammatory drug having very few side-effects. Pharmacological evidence suggests the use of copper complexes to be beneficial in alleviation and treatment of RA and that these compounds have disease-remitting qualities.[62-64] Sorenson in 1987 has discussed the physiological basis for pharmacological activities of copper complexes as well as the anti-arthritic, anti-ulcer and analgesic activities of copper complexes.[65]

1.3 Biochemistry and Metabolism of Copper

Copper, after iron and zinc, is the third most abundant essential trace mineral in the body. It has been known as an essential nutrient since the 1920's.[66] Copper occurs as the metal in oxidation states (0), (I), (II) and unstable (III), but in aqueous solution it occurs only as Cu(II) ion.[67] Like other essential component such as amino acids, fatty acids, or vitamins, copper is not synthesized in the body but must be ingested. Sources of this essential nutrient include dried beans, nuts, animal liver, and crustacean sea food.[68,69] It is associated with a number of copper-dependent enzymes that are key in mammalian biological processes. Their functions are listed in Table 1.1.

Table 1.1: Recognized copper-dependent enzymes and their biochemical function.[70,71]

Cu-dependent enzyme	Function
Cytochrome C oxidase	Oxygen reducing agent
Superoxidase dismutase (**Cu/Zn-SOD**)	Catalyses the dismutation of superoxide in oxygen and hydrogen peroxide. It plays the most important role in the antioxidant protection of almost all cells which are in contact with oxygen to any extent.
Tyrosinase (catechol oxidase)	Formation of melanin.
Dopamine-β-hydroxylase	Hydroxylase of dopamine for catecholamine synthesis.
α-Amidating enzyme	Modifies C-terminal ends of hypothalamic peptide hormones ending in glycine.
Diamine oxidase	Inactivation of histamine and polyamines? (cellular and extracellular).
Amine oxidase (extracellular)	Inactivation of histamine, tyramine, dopamine, serotonin.
Peptidylglycine monooxygenase	Bioactivation of peptide hormones.
Hephaestin	Ferroxidase, in trans-golgi of enterocytes; aids iron absorption homology to ceruloplasmin.
Cartilage matrix glycoprotein (**CMGP**)	Ferroxidase/amine oxidase, homologous to ceruloplasmin (chondrocytes and eye ciliary epithelia).
β-Amyloid precursor protein	Normal function currently unknown.
Prion protein (PrPC)	Copper binding properties suggests that it may protect against ROS*; has SOD-like activity; may return copper to Neurons at synapses (many cells).
S-Adenosylhomocysteine	Sulfur amino acid metabolism hydrolase.
Angiogenin	Induction of blood vessel formation.
Blood clotting factors V and VIII	Blood clotting.
Ceruloplasmin	Accumulation and preservation of iron reserve, iron oxydase, copper transport, SOD mimetic activity.

* (ROS) Reactive oxygen species

The body contains between 50 and 120 milligrams of copper.[52,53] Copper from an exogenous source enters the body *via* rapid absorption through the stomach and small intestine

(jejunum) by a facilitated diffusion, using transport proteins that transport it to the liver. It then passes through the phospholipid membranes as a serum albumin complex, and it is finally stored in the liver *via* ligand exchange processes in the form of a metallothionine complex[52,72,73] or converted into ceuroplasmin that is released into the blood to meet normal metabolic needs.[59,74,75] It also forms part of important antioxidant enzymes, copper-zinc superoxide dismutase.[69] Other functions of copper in the body include bone formation, keratinisation, reproduction, fertility, development of central and peripheral nervous systems, cellular respiration, nerve function, cardiac function, extracellular connective tissue formation, pigmentation and regulation of the monoamine concentration.[68,69,76] However, excess copper in the tissue leads to the production of damaging free radicals and subsequent DNA cleavage.[77] Tissue requirements for copper are considered to be met and controlled in a homeostatic fashion based on the absorption, storage, utilization and excretion of the copper.[78]

In blood plasma, at least 90% of copper is irreversibly bound to ceruloplasmin in a non-exchangeable form, while about 10% is reversibly bound to serum albumin and less than 1% is distributed amongst low molecular weight (l.m.w) complexes, predominantly [Cu(histidinate)(cystinate)] as the exchangeable copper fraction in the blood.[79,80]

The medicinal property in the beneficial effects of copper (II) complexes was reviewed by Sorenson's report in 1976, which stated that the active forms of anti-inflammatory drugs are the Cu-complexes of such drugs *in vivo*. These analogues were also reported to be more active than their parent drug or inorganic copper salts.[81] In metal-tissue distribution studies of copper in individuals with rheumatoid arthritis, elevated levels of serum copper were found during the inflammatory stage of the disease.[43,81,82] There was a two to three fold increase in endogenous copper, mainly serum albumin and ceruloplasmin (CP), returning to normal with remission.[52,83] Furthermore, the accumulation of copper-thionine in the liver decreased on remission with inflammation.[52,83,84] It has however been shown; that ceruloplasmin is a powerful antioxidant and could thus provide protection against cellular destruction, which may be the reason for its increased synthesis. However, this would then bring about decrease in the concentration of serum albumin copper, as well as the labile low molecular weight copper complexes.[59]

The l.m.w copper complexes are thought to be involved in the transportation of copper between cells in the body; this is because they are formally uncharged.[52] Also, it is the

decrease of these copper complexes in the body that is thought to increase the progression of RA.

Two ways have been proposed by which copper concentration can be adjusted; either from serum albumin by a direct complexation using a powerful ligand or from the ceruloplasmin using destructive chelators (e.g. penicillamine).

1.4 Copper Inflammation and Arthritis

Historically copper has been used therapeutically for over 300 years[59] and since the Middle Ages for the treatment of arthritis.[85] The copper bracelet, specifically, has long been used as a folk remedy for the treatment of arthritis. Cupriphores from sweat solubilise the copper and promote its dermal absorption into the blood stream,[86,87] where it will be transported to the affected areas.[88] Another traditional treatment, but less common, is by wearing stainless steel bracelets with neodymium magnets encapsulated in them. These bracelets do not provide useful chelates (for treatment of RA) but the magnetic field accelerates the circulation of blood to all parts of the body[89,90], thus distributing copper evenly throughout the body.

L.m.w copper complexes are reported to have superoxide dismutase (SOD) activity by controlling the hydroxide and superoxide radical levels in blood serum.[72] such radicals have been associated with the development of inflammation in tissues.[52,69,72] The inflammation is characterized by macrophage activation. Macrophages are phagocytic cells, which produce and release reactive oxygen species (ROS).[91] The role of SOD, a copper containing enzyme, is to remove the highly pro-inflammatory superoxide radical anion O_2^-. The superoxide radical O_2^- has been implicated in the promotion of arthritis due to its ability to degrade hyaluronic acid (HA) that is an important component of the synovial fluid.[59]

In order to improve the bioavailability of copper and hence improve the efficacy of complexes, Sorenson[62] and Jackson *et al*.[43,80] have investigated Cu(II) complexes and shown that they are effective in reducing the inflammation associated with RA, enhancing bio-availability of copper, while having reduced toxicity.[92,93] Jackson *et al.* in 2007, investigated Cu(II), Zn(II) and Ca(II), complexes of N^1-(2-aminoethyl)-N^2-(pyridin-2-ylmethyl)- ethane-1,2-diamine ([555-N]) and *N*-(2-(2-aminoethylamino)ethyl)picolinamide ([H(555)-N]), and found that these ligands form more stable complexes with Cu(II) than *in vivo* competitors, Zn(II) and Ca(II). This is an essential factor in the development of copper-based

therapeutics[43], i.e., the ligand should not alter the bio-distribution of other metal ions. A similar result was found for (1,15-bis(*N*,*N*-dimethyl)-5,11-dioxo-8-(*N*-benzyl)-1,4,8,12,15-pentaazapentadecane)].[84] The high stability of this complex was attributed to the ease with which copper deprotonates the donor nitrogen atom of the amide groups. Although, this complex was neutral under physiological conditions, it was reported to be hydrophilic. Also, calculations using a computer model of plasma revealed that the complex dissociates *in vivo*.[84] This indicated that further work was needed to improve the lipophilicity and the stability of the l.m.w. copper(II) complexes.

1.5 Research Hypothesis

The hypothesis then is that endogenous l.m.w copper has anti-inflammatory activity and should therefore be beneficial in the treatment of RA. There are two ways in which the blood plasma concentration of l.m.w. Copper can be increased; by release from high molecular mass sources, e.g., ceruloplasmin or HSA, or by administration of exogenous copper. Exogenous copper can be administered *via* intravenous injection or oral absorption. These two methods are natural drug administration routes but injection is painful, and orally the complex would have to tolerate the harsh conditions in the stomach. Therefore, the dermal route is preferred as the best route of administration because it is slow (no acute response), tolerable and painless. For dermal absorption to be effective, the copper complex must be stable enough to be dermally absorbed, but once it enters the blood plasma, the copper must be released to that it can exert its pharmacological effect. Were the copper not to be released, it is likely that the complex would be excreted, unchanged, in the urine. This was found by Jackson *et al*. in 2000, for a number of their complexes.[8] So, the design of ligand should focus on its role in enhancing copper(II) absorption through the skin. The concentration of all labile copper(II) complexes in plasma will thus be elevated although the percentage distribution of endogenous and added copper(II) amongst the l.m.w will remain essentially constant. As a result, the overall concentration of the neutral copper(II) complexes present will be increased.

1.6 Aim of this Study

Based on the hypothesis that an increase in endogenous copper will have a beneficial anti-inflammatory effect, the aim of this project was to design, synthesize and evaluate new ligands that are able to promote the percutaneous absorption of copper.

1.7 Objectives

1. Design a ligand which forms stable, labile copper complexes with a high level of specificity for copper binding and which is still able to diffuse across a lipid bilayer membrane.
2. Synthesis of ligands.
3. Measure equilibrium constant with H^{+}, Cu^{2+}, $Zn^{2+}$and Ni^{2+} using glass electrode potentiometry in an aqueous solution of 0.15M NaCl over a pH range of 2-11.
4. Investigate the structure of complexes using UV-Visible spectrophotometry and NMR spectroscopy.
5. Study the solubility of the complexes in lipids and in water with octanol/water partition coefficients, and the diffusivity with the Franz cell.
6. Evaluation of the ligands using a blood plasma model.
7. Verify the postulated solution structures for Cu(II) complexes using molecular mechanics calculation.

References

1. S. Odisitse and G. E. Jackson, *Inorganica Chim. Acta*, 2009, **362**, 125–135.
2. D. Wang, S. C. Miller, X.-M. Liu, B. Anderson, X. S. Wang and S. R. Goldring, *Arthritis Res. Ther.*, 2007, **9**, R2.
3. L. W. Koopman and W. J. Moreland, *Arthritis and allied conditions : a textbook of rheumatology*, Lippincott Williams & Wilkins, Philadelphia, 15th edn., 2005.
4. C. M. Weyand, *Rheumatology (Oxford).*, 2000, **39 Suppl 1**, 3–8.
5. E. Choy, *Rheumatology (Oxford).*, 2012, **51 Suppl 5**, v3–11.
6. S. Odisitse, G. E. Jackson, T. Govender, H. G. Kruger and A. Singh, *Dalton Trans.*, 2007, 1140–9.
7. S. Odisitse and G. E. Jackson, *Polyhedron*, 2008, **27**, 453–464.
8. G. E. Jackson, L. Mkhonta-Gama, A. Voyé and M. Kelly, *J. Inorg. Biochem.*, 2000, **79**, 147–152.
9. J. N. Zvimba and G. E. Jackson, *Polyhedron*, 2007, **26**, 2395–2404.
10. M. D. Smith, *Open Rheumatol. J.*, 2011, **5**, 100–6.
11. R. Oklu, T. G. Walker, S. Wicky and R. Hesketh, *J. Vasc. Interv. Radiol.*, 2010, **21**, 1791–805; quiz 1806.
12. M. Feldmann, F. M. Brennan and R. N. Maini, *Cell Press*, 1996, **85**, 307–310.
13. A. E. Koch, *Arthritis Rheum.*, 1998, **41**, 951–62.
14. M. Fischbach, *Rheumatoid Arthritis*, Churchill Livingstone, New York, New York, 1991.
15. D. T. Felson, *Ann. Intern. Med.*, 2000, **133**, 726.
16. W. D. Blackburn, *Am. J. Med.*, 1996, **100**, 24S–30S.
17. M. Kelly, *PhD Thesis*. University of Cape Town, 1998.
18. S. J. Richmond, *Trials*, 2008, **9**, 1–17.
19. W. N. Kelley, W. Ruddy and E .D. Jr Harris, *Textbook of Rheumatology*, PA:W.B. SaundersCompany, Philadelphia, 5th edn., 1997.
20. P. J. Maddison, D. A. Isenberg, P. Woo and D. N. Glass, *Oxford textbook of rheumatology*, Oxford University Press, Oxford, 1993.

21. R. Khurana and S. M. Berney, *Pathophysiology*, 2005, **12**, 153–65.

22. T. Pincus, L. F. Callahan, W. G. Sale, A. L. Brooks, L. E. Payne and W. K. Vaughn, *Arthritis Rheum.*, 1984, **27**, 864–72.

23. S. E. Gabriel, C. S. Crowson and W. M. O'Fallon, *J. Rheumatol.*, 1999, **26**, 2529–33.

24. E. Suresh, *J. R. Soc. Med.*, 2004, **97**, 421–424.

25. D. McCarty, *Arthritis and allied conditions*, Lea & Febiger, Philadelphia, USA, 1989.

26. T. Doan and E. Massarotti, *J. Clin. Pharmacol.*, 2005, **45**, 751–62.

27. H. R. Jr, Schumacher, *Primer on the Rheumatic Diseases*, Arthritis Foundation, Atlanta, Georgia, 10th edn., 1993.

28. C. N. Tran, S. K. Lundy and D. A. Fox, *Pathophysiology*, 2005, **12**, 183–9.

29. A. P. Cope, *Arthritis Res.*, 2002, **4 Suppl 3**, S197–211.

30. G. S. Panayi, V. M. Corrigall and C. Pitzalis, *Rheum. Dis. Clin. North Am.*, 2001, **27**, 317–334.

31. A. P. Cope, M. Londei, N. R. Chu, S. B. Cohen, M. J. Elliott, F. M. Brennan, R. N. Maini and M. Feldmann, *J. Clin. Invest.*, 1994, **94**, 749–60.

32. G. S. Firestein, *Rheumatoid synovitis and pannus, in Rheumatology*, Mosby International, London, United Kingdom, 2nd edn., 1998.

33. K. Yudoh, H. Matsuno, F. Nakazawa, T. Yonezawa and T. Kimura, *Arthritis Rheum.*, 2000, **43**, 617–27.

34. I. L. Bonta, J. Thompson, (medycyna) and K. Brune, *Inflammation : mechanisms and their impact on therapy*, Basel ; Stuttgart : Birkhauser Verlag, Conference., 1977.

35. J. R. Vane and S. H. Ferreira, *Inflammation*, Springer-Verlag, Berlin, Vol. 1&2, 1978.

36. M. Maiotti, G. Monteleone, U. Tarantino, G. F. Fasciglione, S. Marini and M. Coletta, *Arthroscopy*, 2000, **16**, 522–6.

37. R. F. Wilkens and S. L. Dahl, *Therapeutic controversies in rheumatic diseases*, Grune and Stratton, Orlando, 1987.

38. F. Ayhan, *Turkish J. Rheumatol.*, 2011, **26**, 135–144.

39. M. Rudolf, C. Deighton, J. Hall, A. Hammond and *et al.*, *Rheumatoid Arthritis*: *National clinical guideline for management and treatment in adults.*, Royal College of Physicians. London NW1 4LE, 2009.

40. S. Odisitse, *MSc Thesis*. University of Cape Town, 2003.

41. B. F. Morrey and R. A. Adams, *J. Bone Joint Surg. Br.*, 1995, **77**, 67–72.

42. F. Wolfe and S. H. Zwillich, *Arthritis Rheum.*, 1998, **41**, 1072–82.

43. J. N. Zvimba and G. E. Jackson, *J. Inorg. Biochem.*, 2007, **101**, 148–58.

44. P. T. Zvimba N. John, *PhD Thesis*. University of Cape Town, 2005.

45. T. J. Schnitzer, *Am. J. Med.*, 1998, **105**, 45S–52S.

46. M. S. Bergh and S. C. Budsberg, *J. Vet. Intern. Med.*, 2005, **19**, 633–643.

47. E. Ricciotti and G. A. FitzGerald, *Arterioscler. Thromb. Vasc. Biol.*, 2011, 31, 986–1000.

48. F. L. Lanza, F. K. L. Chan and E. M. M. Quigley, *Am. J. Gastroenterol.*, 2009, **104**, 728–38.

49. M. M. Ward, *Arthritis Rheum.*, 2005, **52**, 1634–6.

50. K. G. Saag, G. G. Teng, N. M. Patkar, J. Anuntiyo, C. Finney, J. R. Curtis, H. E. Paulus, A. Mudano, M. Pisu, M. Elkins-Melton, R. Outman, J. J. Allison, M. Suarez Almazor, S. L. Bridges, W. W. Chatham, M. Hochberg, C. MacLean, T. Mikuls, L. W. Moreland, J. O'Dell, A. M. Turkiewicz and D. E. Furst, *Arthritis Rheum.*, 2008, **59**, 762–84.

51. J. R. O'Dell, *N. Engl. J. Med.*, 2004, **350**, 2591–602.

52. J. G. Hardin and G. L Longenecker, *Handbook of Drug Therapy in Rheumatic Deseases*, Little, Brown and Company, London, 1st edn., 1992.

53. I. L Bonta, M. J. Parnham, J. E Vincent and P. C. Bragt, *Progress in Medicinal Chemistry*, North Holland Biomedical Press, North Holland, 1980.

54. M. Mohajane, *MSC Thesis*. University of Cape Town, 2013.

55. M.L. Grove, A.B. Hassell, E. M. Hay and M. F. Shadforth , *Q J Med*, 2001, **94**, 309–319.

56. C. Moncur and H. J. Williams, *J. Am. Phys. Ther.*, 1995, **75**, 511–525.

57. M. S. Nieminen, M. P. Rämö, M. Viitasalo, P. Heikkilä, J. Karjalainen, M. Mäntysaari and J. Heikkilä, *Eur. Heart J.*, 1996, **17**, 1576–83.

58. R. M. Stanbury and E. M. Graham, *Br. J. Ophthalmol.*, 1998, **82**, 704–708.

59. E. U. Tsumbu, *MSc Thesis*. University of Cape Town, 2010.

60. M. H. Weisman and M. E. Weinblatt, *Treatment of the rheumatic diseases : companion to the textbook of rheumatology*, Philadelphia : Saunders, ©1995., Philadelphia, USA, 1995.

61. S. G. West, *Rheumatology secrets*, Philadelphia : Hanley & Belfus, ©2002, Philadelphia, USA, 2nd edn., 2002.

62. J. R. Sorenson, *J. Med. Chem.*, 1976, **19**, 135–48.

63. J.R.J. Sorensen, *Metal Ions in Biological Systems*, Marcel Decker, New York, 1982.

64. J. R. J. Sorenson, *Chem. Br.*, 1984, **19**, 1110–1113.

65. J. R. J. Sorenson, *Biology of copper complexes*, Clifton, N.J. : Humana Press, New Jersey, 1987.

66. E . B . Hart , H . Steenbock, J . Waddell and C . A . Elvehjem, *J. Biol. Chem*, 1928, **77**, 797–833.

67. P. G. Georgopoulos, A. Roy, M. J. Yonone-Lioy, R. E. Opiekun, and P. J. Lioy, J. Toxicol. Environ. Health. B. Crit. Rev., 2011, 4, 341–394.

68. J. J. E. Weder , C. T. Dillon , T. W. Hambley , B. J. Kennedy, P. A. Lay and N. M. D. R. Biffin , H. L. Regtop, *Copper complexes of non-steroidal drugs. a Centre for Heavy Metals Research*, School of Chemistry, University of Sydney, Sydney NSW, 2006.

69. J. C. Frölich, *Trends Pharmacol. Sci.*, 1997, **18**, 30–4.

70. S. Ghazaryan, *Eur. Medical, Heal. Pharm.*, 2011, **2**, 4–13.

71. H. Tapiero, D. M. Townsend and K. D. Tew, *Biomed. Pharmacother.*, 2003, **57**, 386–398.

72. C. Furnival, P.M. May and D.R. Williams, *Trace Elements in the Pathogenesis and Treatment of Inflammation*, Birkhäuser Verlag, Basel, 1981.

73. J. R. J. Sorenson, *In Metal Ions in Biological Systems*, Marcel Dekker, New York, Vol.14 edn., 1982.

74. S. Odisitse, *PhD Thesis*. University of Cape Town, 2006.

75. I. Bremner, in *Ciba Foundation Symposium 79*, Excerpta Medica, Armsterdam, 1980, pp. 23–48.

76. L. S. Simon and J. A. Mills, *N. Engl. J. Med.*, 1980, **302**, 1179–85.

77. D. W. Cox, *Br. Med. Bull.*, 1999, **55**, 544–55.

78. J. R. J. Sorenson, *Prog. Med. Chem.*, 1978, **15**, 211–260.

79. M. C. Linder and M. Hazegh-Azam, *Am. J. Clin. Nutr.*, 1996, **63**, 797S–811S.

80. G. E. Jackson, P. M. May and D. R. Williams, *J. Inorg. Nucl. Chem.*, 1978, **40**, 1227–1234.

81. K. Mokalane, *MSc Thesis*. University of Cape Town, 2011.

82. P. M. May, P. W. Linder and D. R. Williams, *J. Chem. Soc. Dalt. Trans.*, 1977, **2**, 588–595.

83. B. L. O`Dell, *Trace elements in human health and disease*, Academic Press, New York, USA, Vol.1. zin., 1976.

84. T. E. Nomkoko, G. E. Jackson, B. S. Nakani and R. Hunter, *Dalton Trans.*, 2006, 4029–38.

85. T. C. Pederson and S. D. Aust, *Biochem. Biophys. Res. Commun.*, 1973, **52**, 1071–8.

86. W. R. Walker and D. M. Keats, *Agents Actions*, 1976, **6**, 454–9.

87. M. Pasqualicchio, R. Gasperini, G. P. Velo and M. E. Davies, *Mediators Inflamm.*, 1996, **5**, 95–9.

88. H. H. A. Dollwet and J. R. J. Sorenson, *Trace Elem. Med.*, 1985, **2**, 80–87.

89. M. Ostergaard, M. Hansen, M. Stoltenberg, P. Gideon, M. Klarlund, K. E. Jensen and I. Lorenzen, *Arthritis Rheum.*, 1999, **42**, 918–29.

90. M. a Quinn, P. G. Conaghan, P. J. O'Connor, Z. Karim, A. Greenstein, A. Brown, C. Brown, A. Fraser, S. Jarret and P. Emery, *Arthritis Rheum.*, 2005, **52**, 27–35.

91. I. Fridovich, *Science*, 1978, **201**, 875–80.

92. W. R. Walker, R. R. Reeves, M. Brosnan and G. D. Coleman, *Bioinorg. Chem.*, 1977, **7**, 271–276.

93. J. E. Weder, T. W. Hambley, B. J. Kennedy, P. a. Lay, D. MacLachlan, R. Bramley, C. D. Delfs, K. S. Murray, B. Moubaraki, B. Warwick, J. R. Biffin and H. L. Regtop, *Inorg. Chem.*, 1999, **38**, 1736–1744.

Chapter Two

Ligand Design and Synthesis

2.1 Ligand Design

2.1.1 Introduction

The ligand design for selective complexation of metal ions in solution for therapeutic purposes as an alleviation of inflammation associated with RA is of great importance. During inflammatory conditions, there is an increase in the total labile low molecular weight (l.m.w) concentration of copper in particular compartments of the body such as synovial fluid. The increase is due to the formation of complexes in plasma that can diffuse into synovial fluid through the separating membrane.[1] Only neutral complexes can pass through the membrane separating these compartments whereas charged complexes tend not to, in the absence of specific uptake pathways. However, the endogenous reserve or exogenous sources of Cu(II) for this therapeutic activity requires ligands that can successfully mobilize the metal ion at the site of inflammation. However, for this to happen, the ligands must possess certain desirable features.

2.1.2 Ligand Properties and Design

The design of the ligands that can successfully mobilize Cu(II) in biofluids depends on the stability of the complexes formed. They must be strong chelators in order to form thermodynamically stable complexes with Cu(II) ion. The increase in the stability of Cu(II) complexes has been associated with an increase in the number of donor atoms.[2] The chelate effect is observed in Cu(II) complexes of ethylenediamine, $[Cu(en)_2]^{2+}$ which are 10^7 times more stable than copper ammonia complexes $[Cu(NH_3)_4]$.[3]

In general, the stability of the complexes is affected by the size of the chelate rings formed upon coordination. For example, five-membered chelate rings are more stable than six- membered chelate rings. If more than one chelate ring is formed, then 5,5 is better than 5,6 which is better than 6,6. This order of stability has been attributed to entropy changes associated with chelate formation.[4,5] With three or more contiguous chelate rings, however, ring strain or enthalpy also has an effect and so 5,6,5 membered chelate systems are more stable than 5,5,5 chelate analogues.[6-9] The low stability in the structure of the 5,5,5 membered chelate system is due to steric constraints.[10]

The ligands should form bioavailable Cu(II) complexes and at the same time not disrupt the homeostasis of other endogenous metal ions. Therefore, the ligand should contain primarily nitrogen donor atoms which will increase the selectivity for copper over

most bivalent cations[11,12], such as Ca(II) and Zn(II) which are found in large concentrations in blood plasma[13] and thus can interfere with ligands designed to bind Cu(II)[2], since to form a neutral Cu(II) complex, the ligand has to include anionic groups or dissociable protons. Ligands containing amide groups where amide hydrogen atoms dissociate on complexation have been preferred in this study because they are reasonable models of peptide bonds of proteins. Moreover, on loss of amide protons, these ligands can coordinate to a metal ion *via* four nitrogen atoms, giving rise to three chelate rings.

In addition, the ligands should form kinetically labile complexes to be able to release Cu (II) at the biological sites where it is needed.[14] The complexes should be lipophilic to enable transport across cell membranes and uncharged to prevent urinary excretion.[15]

From previous studies, the pyridyl group has a high Cu(II) mobilizing ability and is found in most NSAID drugs.[16-18] The aromatic ring would increase the rigidity to the ligand system and hence the stability and lipophilicity of the metal complex.[16] The nitrogen on the pyridyl group is envisioned to increase the stability of the complex by the chelate effect.

Ligands that contain the pyridyl residue that have been studied before are 2-amino-*N*-(2-*oxo*-2-(2-(pyridin-2-yl)ethylamino)ethyl)acetamide [H_2(556)-N],a pseudo-mimic of human serum albumin, N^1-(2-aminoethyl)- N^2-(pyridin-2-ylmethyl)ethane-1,2-diamine [555-N] and *N*-(2-(2-aminoethylamino)ethyl)- picolinamide [H(555)-N] see Figure 2.2. They form stable complexes and are more selective for Cu(II) *in vivo* than Ca(II) and Zn(II).[17,19]

In blood plasma, copper is transported by proteins; human serum albumin (HSA) being the most effective protein.[20,21,22] (HSA) is a major metal-binding protein in the body[23], Cu(II) binding sites of HSA (shown in Figure 2.1) involves the α-NH_2 nitrogen, two peptide nitrogens and the imidazole nitrogen of the N-terminal Asp-Ala-His residues.[17,24]

Human serum albumin is more selective to Cu(II) than are most proteins.[25,26] This makes Cu(II) less bioavailable when complexed with HSA than when complexed with other protein molecules.[26]

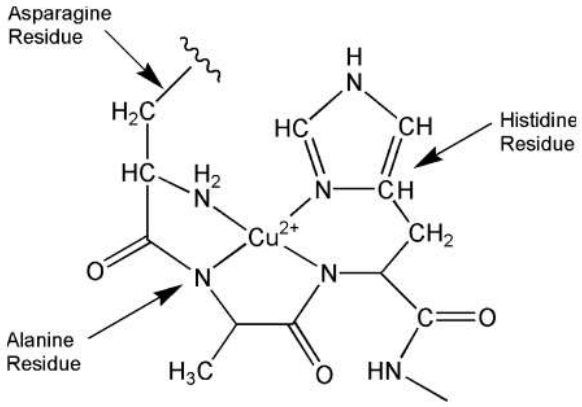

Figure 2.1: Structure of Cu(II) binding site.

The designs of the ligands in this study were based on the structure of HSA. Amines are good, selective coordinators of Cu(II)[11,12], while especially Ca(II), and Zn(II) do not form strong complexes. However, copper complexes of polyamino ligands like ttda (3,6,9,12-tetraazatetradecanedioate) and dtda (-3,6,9-triazaundecanedioate) as shown in Figure 2.2, have been shown to be too stable.[27] In animal studies, these complexes were excreted unchanged in the urine. Although they are formally neutral, they are very hydrophilic.

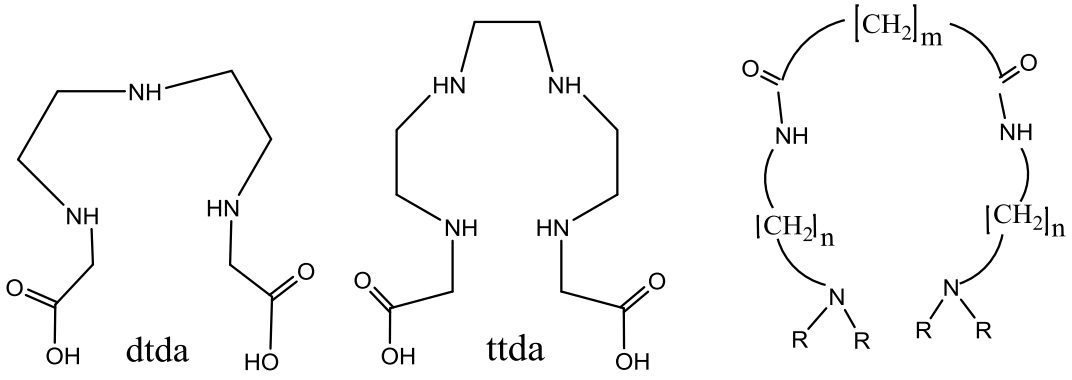

L	m	n	R
L^1	0	2	Me
L^2	1	2	Me
L^3	0	3	Me
L^4	0	2	Et

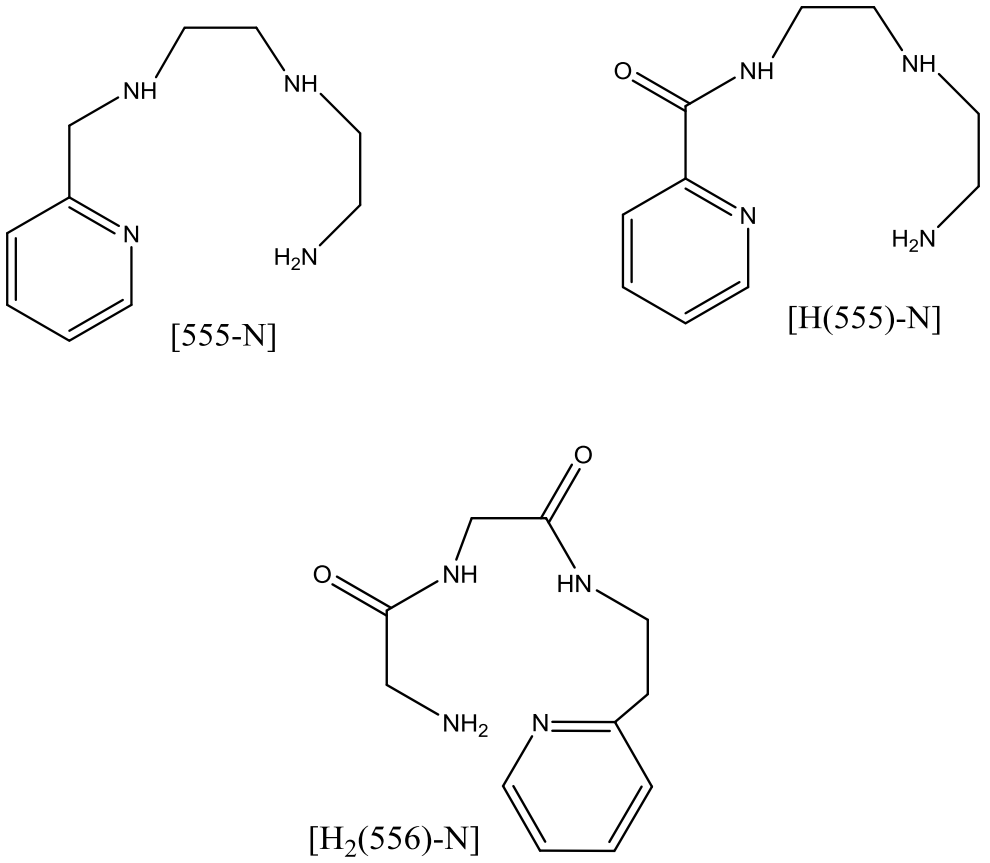

Figure 2.2: Schematic representation of ligands discussed in this chapter

In order to decrease the hydrophilicity and bury the charge of the ligand within the complex, the ligands in the present study were designed. These ligands all have an amide group which deprotonates upon metal ion coordination.[28] Furthermore, their complexes with Cu(II) would be formally neutral.[29,30]

Using the criteria outlined above and based on previous studies the following ligand have been designed. The ligands designed (Figure 2.3) in this project have included all three design features. They include the amino group, an amido group and a pyridyl group.

[H(555)NH_2]

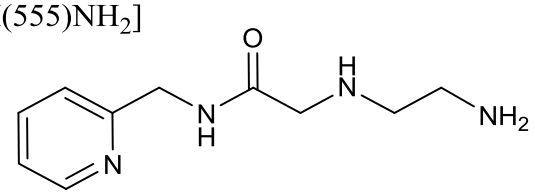

2-((2-aminoethyl)amino)-*N*-(pyridin-2-ylmethyl)acetamide

[H(555)NMe_2]

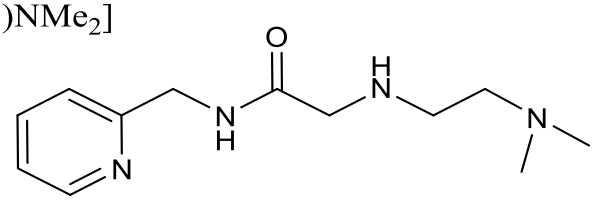

2-((2-(dimethylamino)ethyl)amino)-*N*-(pyridin-2-ylmethyl)acetamide

[H_2(555)NH_2]

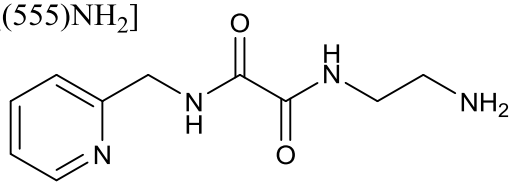

N-(2-aminoethyl)-*N*'-(pyridin-2-ylmethyl)ethanediamide

[H_2(565)NH_2]

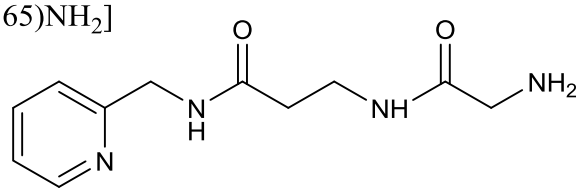

3-(2-aminoacetamido)-*N*-(pyridin-2-ylmethyl)propanamide

[H(56)NH_2]

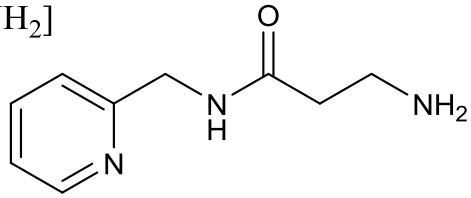

3-amino-*N*-(pyridin-2-ylmethyl)propanamide

Figure 2.3: Structures of proposed Ligands.

The above ligands have been carefully designed to achieve successful metal ion administration and subsequent mobilization in the body fluids.

2.2 Synthesis of Ligand

2.2.1 Experimental

All solvents and reagents were purchased from either Sigma-Aldrich or Aldrich and were used without further purification. Tetrahydrofuran (THF) was dried using the stand Alone SP-1 solvent purification system from LC Technology Solutions Incorporated, USA. Reactions were monitored by thin-layer chromatography (TLC) using Merck F254 aluminium-backed precoated silica gel plates and were visualized by ultraviolet light at 254nm. ^{1}H and ^{13}C NMR spectra were recorded on a Varian Unity Plus 300/400 MHz or Bruker (^{1}H at 400 MHz, ^{13}C at 100.6 MHz) instrument, using tetramethylsilane (TMS) as an internal reference. Mass spectroscopy was carried out on JEOL GCmateII in Electron Ionisation mode.

$[H(555)NH_2]$, $[H_2(565)NH_2]$, $[H(56)NH_2]$, $[H_2(555)NH_2]$, were purchased from FCH group and UORSY/ UKrorgsyntez Ltd.

2.2.2 Synthesis

$H(555)NMe_2$ ligand was successfully synthesized. The synthesis of that ligand was followed by a complete characterization procedure using nuclear magnetic resonance (N.M.R).

2.2.2.1 Synthesis of 2-(2-(dimethylamino)ethylamino)-*N*-((pyridin-2-yl)methyl)acetamide

The compound was synthesized according to the literature procedure.[31] The first step of the synthesis was preparation of 2-chloro-*N*-(pyridine-2-yl-methyl)acetamide from 2-aminomethylpyridine and chloroacetylchloride. The second step of the synthesis involves *N,N*-dimethylethylenediamine, where one nitrogen atom was protected by a methyl group as shown in Figure 2.4. Polymerization is common where the amino group is not protected.[30]

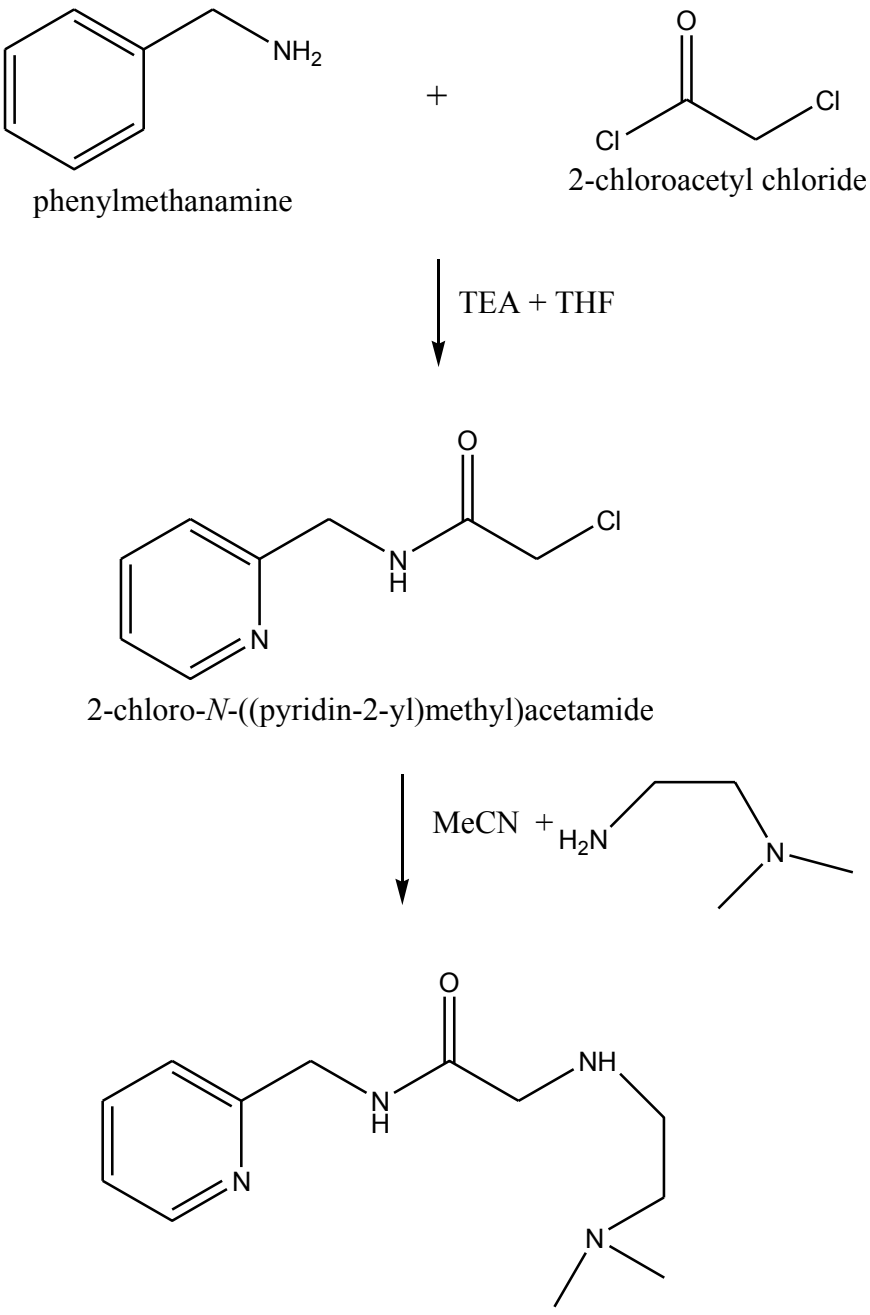

phenylmethanamine

2-chloroacetyl chloride

2-chloro-*N*-((pyridin-2-yl)methyl)acetamide

2-(2-(dimethylamino)ethylamino)-*N*-((pyridin-2-yl)methyl)acetamide

Figure 2.4 Scheme of synthesis [H(555)NMe_2].

2.2.2.2 Preparation of 2-chloro-*N*-(pyridine-2-yl-methyl) acetamide

2-Aminomethylpyridine (1.90 mL, 18.50 mmol), was dissolved by use of a magnetic stirring bar in dry THF (20 mL) after cooling to 0°C in an ice water bath. TEA (Triethylamine) (2.82 mL, 19.50 mmol) as a base and chloroacetylchloride (1.55mL, 19.5mmol) was used as the alkylating agent in dry THF (40 mL); the reagents were added dropwise to the previous mixture over 1 hour. The mixture was stirred at room temperature for 5 hours under nitrogen. The reaction was essentially complete as monitored by TLC (EtOAc:MeOH; 9:1). The resulting mixture was filtered, washed with THF and concentrated under vacuum. To the oily residue was added EtOAc (50 mL) and the resulting mixture was washed with saturated $NaHCO_3$ solution (3×20 mL). The organic layers were pooled, dried over anhydrous $MgSO_4$, filtered and the solvent was removed under reduced pressure to give a residue which was subjected to column chromatography on silica gel using (EtoAc:MeOH; 9:1) as eluent to afford the product, as a pale brown oil (2.60g, 76%).
δ_H (300MHz, CD_3Cl-d) 4.04(2H, S, H_1); 4.57(2H, d, J 5.09Hz, H_2); 7.16-7.25(2H, m, H_3, H_5); 7.62-7.64(1H, m, H_4); 7.85(1H, s, NH); 8.53(1H, d, J 4,84Hz, H_6). δ_C (100.6 MHz, CD_3Cl-d) 42.49, 44.49, 121.84, 122.41, 136.70, 149.07, 155.43, 165.98.

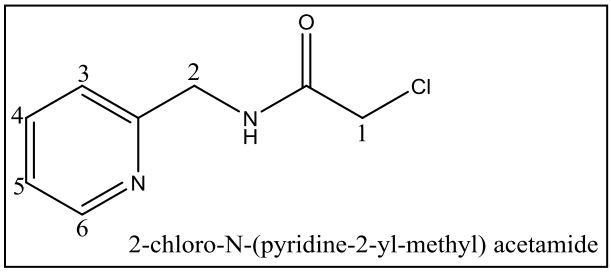

2-chloro-N-(pyridine-2-yl-methyl) acetamide

2.2.2.3 Preparation of (2-(dimethylamino)ethylamino)-*N*-((pyridin-2-yl)met-hyl)acetamide

A solution of 2-chloro-N-(pyridine-2-yl-methyl)acetamide (2.00 g, 10.83 mmol) in dry MeCN (20 mL) was add dropwise over 1hour to a stirred solution of *N,N*-dimethylethylenediamine (53.35 mL, 0.49 mol) in dry MeCN (60 mL) under nitrogen. After cooling to 0°C in an ice water bath, the reaction was stirred at room temperature overnight. The reaction was monitored by TLC (EtOAc:MeOH; 9:1). The resulting mixture was filtered and concentrated under reduced pressure. The product was extracted with MeOH:$CHCl_3$ (1:4), and washed with saturated $NaHCO_3$ solution (2×10 mL). The combined organic layers were dried over anhydrous $MgSO_4$ and the solvent removed to

afford the product. The resultant sample was then purified by column chromatography on silica gel using MeOH: EtOAc (2:8) followed by MeOH: DCM (4:6) was used to elute. Brown oil (0.70g, 27%).

δ_H (300MHz, CD_3Cl-d) 2.21 (6H, d, J 0.77Hz, $H_{1,2}$); 2.41 (2H, dd, J 5.40, 6.43Hz, H_3); 2.71 (2H, td, J 0.78, 5.85 Hz, H_4); 3.28-3.43 (2H, m, H_5); 4.60 (2H, d, J 5.67 Hz, H_6); 7.15-7.20 (1H, m, H_9); 7.29 (1H, d, J 7.63 Hz, H_7); 7.64 (1H, t, J 7.66 Hz, H_8); 8.26 (1H, s, NH_b) 8.54 (1H, dd, J 1.60, 4.77 Hz, H_{10}). δ_C (100.6 MHz, CD_3Cl-d) 44.34 (2C), 45.34, 47.43, 52.76, 58.93, 121.94, 122.21, 136.66, 149.17, 157.91, 172.10. EI-m/z 236.17 $[M]^+$.

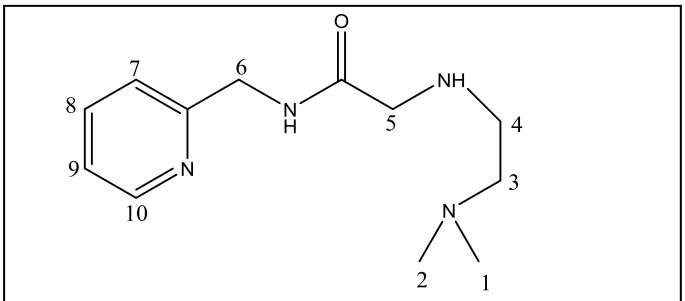

(2-(dimethylamino)ethylamino)-N-((pyridin-2-yl)met-hyl)acet amide

References

1. S. Odisitse, *MSc Thesis*. University of Cape Town, 2003.
2. G. E. Jackson and M. J. Kelly, *J. Chem. Soc. Dalt. Trans.*, 1989, 2429–33.
3. J. Burgess, *Ions in Solution*, Ellis Horwood, Chichester, 1988.
4. C. G. Spike and R. W. Parry, *J. Am. Chem. Soc.*, 1953, **75**, 2726–2729.
5. F. A. Cotton and F. E. Harris, *J. Phys. Chem.*, 1955, **59**, 1203–1208.
6. G. E. Jackson, P. W. Linder and A. Voyé, *J. Chem. Soc. Dalt. Trans.*, 1996, 4605.
7. G. E. Jackson, P. W. Linder and A. Voy/'e, *Polyhedron*, 1991, **10**, 883–884.
8. R. D. Hancock, *J. Chem. Educ.*, 1992, **69**, 615.
9. Y. Arano, M. Yabuki, T. Yahata, K. Horiuchi and A. Yokoyama, *Chem. Pharm. Bull. (Tokyo).*, 1990, **38**, 3099–101.
10. S. Odisitse, *PhD Thesis*. University of Cape Town, 2006.
11. R. P. Bonomo, A. De Flora, E. Rizzarelli, A. M. Santoro, G. Tabbí and M. Tonetti, *J. Inorg. Biochem.*, 1995, **59**, 773–784.
12. M. Valko, H. Morris, M. Mazúr, J. Telser, E. J. L. McInnes and F. E. Mabbs, *J. Phys. Chem. B*, 1999, **103**, 5591–5597.
13. N. Salsabili, a R. Mehrsai and S. Jalaie, *Andrologia*, 2009, **41**, 24–8.
14. H. Katayama, T. Utsumi, C. Ozawa, Y. Nakahara, H. Hojo and Y. Nakahara, *Tetrahedron Lett.*, 2009, **50**, 818–821.
15. J. N. Zvimba, *PhD Thesis*. University of Cape Town, 2005.
16. S. Odisitse and G. E. Jackson, *Polyhedron*, 2008, **27**, 453–464.
17. J. N. Zvimba and G. E. Jackson, *Polyhedron*, 2007, **26**, 2395–2404.
18. S. Odisitse and G. E. Jackson, *Inorganica Chim. Acta*, 2009, **362**, 125–135.
19. J. N. Zvimba and G. E. Jackson, *J. Inorg. Biochem.*, 2007, **101**, 148–58.
20. M. Sokołowska, K. Pawlas and W. Bal, *Bioinorg. Chem. Appl.*, 2010, **42**, 1–7.
21. L. Perrone, E. Mothes, M. Vignes, A. Mockel, C. Figueroa, M.-C. Miquel, M.-L. Maddelein and P. Faller, *Chembiochem*, 2010, **11**, 110–8.

22. P. Z. Neumann and A. Sass-Kortsak, *J. Clin. Invest.*, 1967, **46**, 646–58.

23. M. C. Linder and M. Hazegh-Azam, *Am. J. Clin. Nutr.*, 1996, **63**, 797S–811S.

24. M. Dockal, D. C. Carter and F. Ruker, *J. Biol. Chem.*, 1999, **274**, 29303–29310.

25. V. Karakoc, E. Yilmaz, D. Türkmen, N. Oztürk, S. Akgöl and A. Denizli, *Int. J. Biol. Macromol.*, 2009, **45**, 188–93.

26. G. Marx and M. Chevion, *Biochem. J.*, 1986, **236**, 397–400.

27. M. Kelly, *PhD Thesis*. University of Cape Town, 1998.

28. G. E. Jackson, L. Mkhonta-Gama, A. Voyé and M. Kelly, *J. Inorg. Biochem.*, 2000, **79**, 147–152.

29. S. Odisitse, G. E. Jackson, T. Govender, H. G. Kruger and A. Singh, *Dalton Trans.*, 2007, 1140–9.

30. M. Mohajane, *MSc Thesis*. University of Cape Town, 2010.

31. J. Yin, X. Guan, D. Wang and S. Liu, *Langmuir*, 2009, **25**, 11367–74.

Chapter Three

Potentiometry

3. Potentiometry

3.1 Introduction

Formation constants can be determined by techniques such as spectroscopy, electrochemistry, potentiometry and calorimetry. Potentiometry is the most extensively used technique in the determination of stability and protonation constants. Because of the availability of electrodes and reproducibility of experimental results, it is considered to be the most precise, accurate and non-invasive technique available at present.[1,2] Another advantage is that it is not subjected to interference from colored samples.[3]

Potentiometric titration is a volumetric method in which the potential (E) between two electrodes is measured as a function of the added volume of titrant (V). The indicator electrode can be selected to respond to either a reactant or a product.[3]

The advantage of potentiometric titration in the measurement of acidity and alkalinity is the reliability, dynamic range and selectivity of the glass electrode. The essence of the potentiometric experiment involving glass-electrode potentiometry (GEP) is the monitoring of the change in the hydrogen ion concentration, $[H^+]$, throughout the experiment. GEP is one of the most frequently used experimental techniques for the study of (de)protonation and coordination equilibria in solution[4] at constant ionic strength and temperature.[5-7] GEP has been employed in this study because of its linear Nernstian response, rapid reversibility and high sensitivity to aqueous hydrogen ions over a wide concentration range. However, the pH range is usually limited to between 2-12, because below pH 2 and above pH 12, the response is no longer linear due to the junction potential and the alkaline error.[8]

This chapter focuses on the general theory of potentiometry as a measurement method applied to complex equilibria, as well as presentation and discussion of experimental results.

3.2 Theory

The theory of formation constants and methods used to determine them has been extensively covered in the literature.[9-12]

For a metal M and a ligand L forming a complex ML, the thermodynamic equilibrium constant ${}^{T}K_1$ is defined as follows.

$$M + L \rightleftharpoons ML \qquad {}^{T}K_1 = \frac{\{ML\}}{\{M\}\{L\}} \tag{3.1}$$

where {ML} is the activity of ML, {M} is the activity of M and {L} is the activity of L. The activity of ML can be expressed in terms of its concentration[13];

$$\{ML\} = \Upsilon_{ML}\,[ML] \tag{3.2}$$

where Υ_{ML} is the activity coefficient of the ML species. Therefore, equation (3.1) can be expressed as:

$${}^{T}K_1 = \frac{(\Upsilon_{LM}\,[ML])}{(\Upsilon_M\,[M])\,(\Upsilon_L\,[L])} \tag{3.3}$$

Equation 3.3 can be rearranged;

$${}^{T}K_1 = \left(\frac{\Upsilon_{ML}}{\Upsilon_M\,\Upsilon_L}\right)\left(\frac{[ML]}{[M]\,[L]}\right) \tag{3.4}$$

The expression $\left(\frac{\Upsilon_{LH}}{\Upsilon_L\,\Upsilon_H}\right)$ is constant at constant ionic strength and temperature so the equilibrium constant can be expressed as;

$$K_1 = \frac{[ML]}{[M][L]} \tag{3.5}$$

Hence, the stepwise formation of the parent complexes can be described by the following set of formation constants at constant ionic strength. The charges are omitted for clarity

$M + L \rightleftharpoons ML$ $\qquad K_1 = [ML]/[M][L]$ (3.6)

$ML + L \rightleftharpoons ML_2$ $\qquad K_2 = [ML_2]/[ML][L]$ (3.7)

$ML_{n-1} + HL \rightleftharpoons ML_n + H$ $\qquad K_n = [ML_n][H]/[ML_{n-1}][HL]$ (3.8)

The equilibria represented by equations 3.6, 3.7 and 3.8 can also be expressed as overall formation constants, denoted by the symbol β, which can be expressed as:

$M + L \rightleftharpoons ML$ $\qquad \beta_1 = K_1 = \frac{[ML]}{[M][L]}$ (3.9)

$ML + 2L \rightleftharpoons ML_2$ $\qquad \beta_2 = K_1 K_2 = \frac{[ML_2]}{[M][L]^2}$ (3.10)

Therefore,

$ML_{n-1} + L \rightleftharpoons ML_n$ $\qquad \beta_n = K_1 K_2 K_3 \ldots K_n = \frac{[ML_n]}{[ML_{n-1}][L]^n}$ (3.11)

In general,

$$\beta_n = \prod_{i=1}^{n} K_i \qquad (3.12)$$

In any solution containing metal ions M, ligand L and protons/hydroxyl ions H or OH, a variety of complexes can be formed. This phenomenon occurring in solution can be described by the following general equilibrium process given by the following expression;

$$pM + qL + rH \rightleftharpoons M_pL_qH_r \tag{3.13}$$

where p, q and r are the stoichiometric coefficients of the components in the complex (metal, ligand and proton respectively), while r = -1 refers to the proton being removed or the addition of a hydroxyl ion on the complex. Therefore this equation can take into account the formation of mononuclear, binary, protonation or hydroxo, polynuclear as well as oligonuclear complexes.[14] The formation constant for this reaction is described by the mass balance equation as follows;

$$\beta_{MpLqHr} = \frac{[M_p\, L_q\, H_r\,]}{[M]^p[L]^q[H]^r} \tag{3.14}$$

Moreover, the concentrations of $M_pL_qH_r$ from each titration point can be determined and, at point k, the concentration of $M_pL_qH_r$ is expressed as;

$$[M_pL_qH_r]_k = \beta_{pqr}\,[M]_k^p[L]_k^q[H]_k^r \tag{3.15}$$

The total concentration of the metal ion (T_M), ligand (T_L) and hydrogen ion (T_H) can be expressed by the law of mass action at k ($T_{k,M}$) point:

$$T_{k,M} = [M]_k + \sum_{i=1}^{N} p\,\beta_{pqr}\,[M]_k^p\,[L]_k^q\,[H]_k^r \tag{3.16}$$

The total concentration of the free ligand at point k ($T_{k,L}$) can be expressed as;

$$T_{k,L} = [L]_k + \sum_{i=1}^{N} q\,\beta_{pqr}\,[M]_k^p\,[L]_k^q\,[H]_k^r \tag{3.17}$$

The total concentration of the free hydronium ion at point k ($T_{k,H}$) can be expressed as;

$$T_{k,H} = [H]_k + \sum_{i=1}^{N} r\, \beta_{pqr} [M]_k^p [L]_k^q [H]_k^r \qquad (3.18)$$

where $[M]_p$ is the concentration of free aquated metal ions and the summation is over the concentration of all the metal-containing species which may be protonated ($r > 0$) or may not ($r = 0$), while [L] and [H] represent the concentration of the uncomplexed ligand and proton respectively. The term r can have a negative value if the ligand loses protons upon complexation from either a coordinated ligand or a bound water molecule, or if the hydroxide ion (OH^-) is added to the complex.[15,16] If $r = 0$ then the complex is not protonated and there are no hydroxide ions attached to the complex.

Stability constants depend on temperature, as represented by the Van't Hoff equation;

$$\frac{d\ln K}{dT} = \frac{\Delta H^\circ}{RT^2} \quad \text{or} \quad \frac{d\ln K}{d(1/T)} = \frac{-\Delta H^\circ}{R} \qquad (3.19)$$

where ΔH° is the standard enthalpy change of reaction, T is absolute temperature in Kelvin and R is the universal gas constant in J $K^{-1}mol^{-1}$.

The electrode cell is the centre of any potentiometric investigation. A typical cell for pH glass electrode potentiometry consists of a reference electrode, an indicator electrode and a salt bridge. This cell can be represented as:

reference electrode| salt bridge |analyte solution | indicator electrode

A reference electrode (E_{ref}) is a half-cell having a known potential that remains constant at constant temperature and is independent of the composition of the analyte solution.[17] An indicator electrode (glass electrode, E_g) has a potential that varies with variations in the concentration of an analyte. The liquid junction potential (E_j) is the difference between the potential of the internal reference solution and the potential of the

analyte solution, and is usually small enough to be neglected, if measurements carried out well above pH 2 as in the present case.

E_{cell} can therefore be expressed as:

$$E_{cell} = E_{ref} + E_j + E_g \tag{3.20}$$

Since E_g depends on the activity of H^+ ions ($\{H^+\}$), E_g can be expressed in terms of the standard electrode potential (E^0_g) through the Nernst equation;

$$E_{cell} = E_{ref} + E_j + \left(E^0_g + \frac{RTln\{H\}}{F}\right) \tag{3.21}$$

where E_{cell} is the measured electromotive force (emf), R is the universal gas constant, T is the temperature of the system, and F is Faraday's constant. The activity of the hydrogen ion {H} ions can be expressed as;

$$\{H\} = \Upsilon_H [H] \tag{3.22}$$

where Υ_H is the activity coefficient and [H] is the concentration of H^+ ions.
The ionic strength (I) of a solution can be expressed as;

$$I = \frac{1}{2}\sum (C_i Z_i)^2 \tag{3.23}$$

where C_i is the concentration of species i and Z_i is the charge of the ion.
Since the activity coefficient is a constant at constant ionic strength and temperature, equation 3.21 becomes:

$$E_{cell} = E_{constant} + \frac{RTln[H]}{F} \tag{3.24}$$

Where $E_{constant}$ is standard electrode potential

However, the potential depends on temperature and the relationship between the two varies with the activity of the hydrogen ion. The slope (s) of the electrode can be expressed as;

$$s = \frac{2.303RT}{F} \tag{3.25}$$

The dependence of potentials on pH yields a linear curve. Substituting in the Nernst equation;

$$E_{cell} = E_{constant} + s \log[H] \tag{3.26}$$

Calibration of the electrode requires the determination of both E_{const} and s.

3.3 Equilibrium Simulation for Titration Analysis

Equilibrium Simulation for Titration Analysis **(ESTA)**[2] is a computer program used for the determination of the protonation/deprotonation constants of the ligand and the stability constants of the complexes in aqueous chemical equilibria. This program has two types of program modules, namely, simulation module (ESTA1) which characterises the system on a point by point basis, and optimization module (ESTA2) which determines the best values based on a least squares procedure over a whole system of titrations. The simulation unit (ESTA1) is used to calculate the complexation functions which help in the interpretation of data. It can also be used to calculate the speciation of a solution. The other program modules are the error propagation module (ESTA3) which performs a Monte Carlo error propagation analysis that identifies which parameters need to be refined, and the error imposition unit (ESTA7) which is used to examine the effects of random errors on the values of the refined parameters. The plotting unit (ESTA5) is used to put the results calculated by ESTA1 in a graphic form.

There are three tasks from the ESTA program which were used in this study, the formation functions (Z-bar), the deprotonation function (Q-bar) and the objective function (OBJE).

The ZBAR and QBAR were respectively calculated within the ESTA1 module while OBJE (optimization with respect to the observed emf) was determined within the ESTA2 module.

The program ESTA also incorporates the task SPEC within the ESTA1 module, and this calculates the distribution of species present in an equilibrium system as a function of the pH of the solution.

3.3.1 The Objective Function

The objective function[18,19] of ESTA which optimises titration parameters, is described as the summation of all the squared residuals of the real parameter values from the calculated values. The Gauss-Newton least squares method is used to minimize the objective function, U_{obj} which is expressed as:

$$U_{obj} = (N - n_p)^{-1} \sum_{n=1}^{N} n_e{}^{-1} \sum_{q=1}^{n_e} W_{nq}({Y_{nq}}^{obs} - {Y_{nq}}^{calc})^2 \tag{3.27}$$

where N is the number of experimental titration points, n_p is the total number of points being optimised, n_e is the total number of electrodes, w_{nq} is the q^{th} residual at the n^{th} titration point, ${y_n}^{calc}$ is the calculated variable of the q^{th} residual at the n^{th} titration point and ${y_n}^{obs}$ is the observed variable of the q^{th} residual at the n^{th} titration point.

By using Gauss-Newton methods, it is assumed that the objective function is quadratic with all the parameters. U_{obj} can therefore be expressed as;

$$U_{obj} = a + p^t b + \frac{p^t H_p}{2} \tag{3.28}$$

where a and b are Gauss-Newton quadratic parameter vectors, p is the optimization parameter vector, p^t is the transpose of p and H is the Hessian, H_{sr} expressed as;

$$H_{sr} = \frac{d^2 U_{obj}}{dp_s dp_r} \tag{3.29}$$

A well-defined system with good initial estimates often converges. The calculations are terminated if the resultant shift vectors are large or if the shift vector has an upward gradient.

3.3.2 Formation Function (Z_M-bar) and Deprotonation Function (Q_M-bar)

The ZBAR task calculates the Z_H-bar curve for ligand protonation and the Z_M-bar curve for complex formation titrations. In the absence of a metal ion the protonation function (Z_H-bar) is expressed as;

$$Z_{H-bar} = \frac{T_H - [H] + [OH]}{T_{lig}} \tag{3.30}$$

where T_{lig} is the total concentration of the ligand, T_H is the total concentration of hydronium ions and where T_H is defined by;

$$T_H = [H^+] - [OH^-] + \sum r \beta_{0qr} [L]^q [H]^r \tag{3.31}$$

The Z_H-bar function is plotted against pH. Z_H-bar may be described as the average number of hydrogen ions bound to the ligand at each pH.

Figure 3.0A shows a typical Z_H-bar curve. If a ligand has two dissociable protons, Z_H-bar levels off at two and one. The pK_a values can also be estimated from the Z_H-bar curves. The pK_a's are given by the pH at the half-bar values. E.g. log K_{LH} = 8.09 and log K_{LH2} = 4.21 in Figure 3.0A.

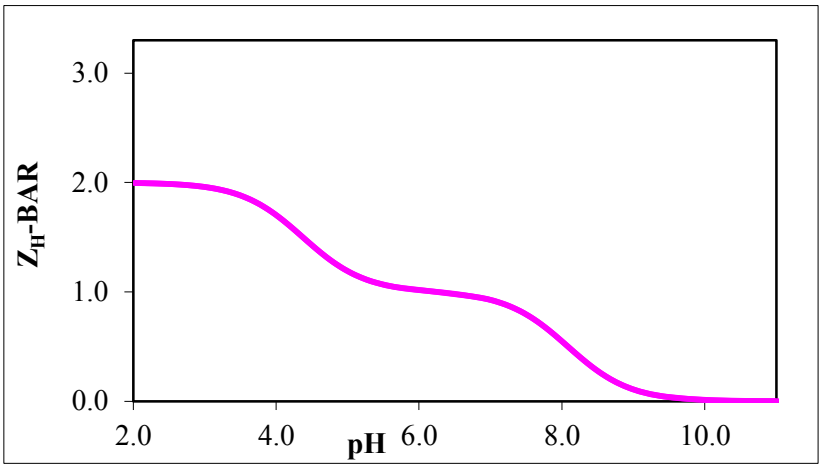

Figure 3.0 A: Typical Z_H-bar.

The complex formation function, Z_M-bar, defines the average number of ligands bound per metal ion. This can be expressed as:

$$Z_{M-bar} = \frac{T_L - [L](1 + \sum_n \beta_{LHn} H^n)}{T_M} \tag{3.32}$$

where, T_L ,and T_M are the total ligand, and total metal concentration respectively. And [L] is the free-ligand concentration;

$$[L] = \frac{T_H - H + OH}{\sum_n (\beta_{LHn} H^n)} \tag{3.33}$$

ESTA calculates the residual;

$$Z_{-bar}\text{residual} = Z^o{}_{-bar} - Z^c{}_{-bar} \tag{3.34}$$

where Z^0-bar is the observed Z-bar and Z^C-bar is the calculated Z-bar. A low residual means that there is good agreement between the observed and calculated Z-bar curves, i.e. they are superimposable. A plot of this function against pL, i.e. -log[L] gives a pictorial

representation of the equilibria. It is noted however that the Z_M-bar function applies only to mononuclear binary complexes.

Z_M-bar can be used to express the speciation of species such as ML, ML_2, …ML_n. A typical Z_M curve is given in Figure 3.0B. If ML is the most predominant species in solution, Z_M-bar levels off at 1. Log K_{ML} can be estimated from the pL that makes the mid-point of the steepest slope. If MLH is one of the species in solution, the curve splits at high pL as shown by the red plot in Figure 3.0C. The bending of the plots indicates the formation of hydroxo species. From the Z_M-bar graphs, the model of Cu(II)/ligand species can be predicted. The bending of the pink plot in Figure 3.0C shows that the formation of MLH_{-1} species begins to form at very low pH's.

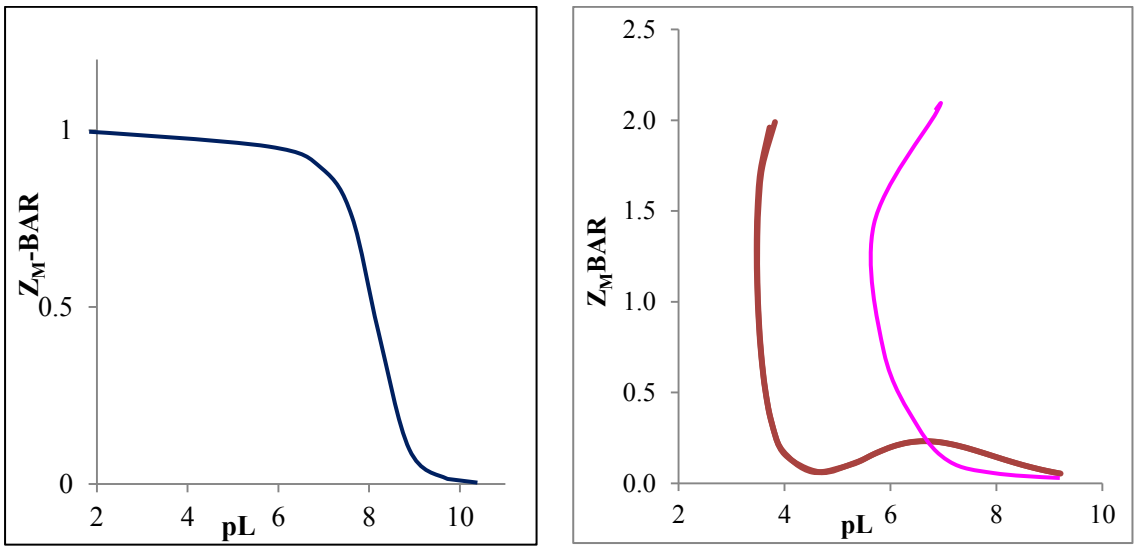

B **C**

Figure 3.0: Typical Z_M-bar curve when **(B)** ML is only species. **(C)** MLH and MLH_{-1} are present.

The deprotonation function, Q_M-bar, is the average number of protons released per metal ion upon complexation. Q-bar is expressed as;

$$Q_{M-bar} = \frac{T_H^* - T_H}{T_M} \tag{3.35}$$

where T_H is the total proton concentration and T^*_H is the calculated total concentration of protons that would be necessary to give rise to the observed pH in the absence of metal ions or rather if no complexation took place.

The mass balance equations for T^*_H and T_L can be expressed as;

$$T_H^* = H - OH + \sum_{J=1}^{NJ} r\,[M_p\,L_q\,H_r\,] \tag{3.36}$$

$$T_L = L + H - OH + \sum_{J=1}^{NJ} q\,[M_p\,L_q\,H_r\,] \tag{3.37}$$

where *NJ* is the total number of titration points. When Q_M-bar has been calculated, it can be plotted as a function of pH. ESTA plots Q_M-bar on the same graph with n-bar.

For binary systems, a formation function for a ligand subsystem is defined as follows;

$$n_{-bar} = \frac{T_H^* - H + OH}{T_L^r} \tag{3.38}$$

The average number of dissociable protons in a complex would be represented as:

$$F = qn_{bar} - Q_{bar}p \tag{3.39}$$

where p and q are the stoichiometric coefficients of the metal and the ligand respectively, and n_{bar} is the average number of protons which would be bound to the ligand in the absence of metal complexation. The agreement between the experimental plot and the theoretical plot is an indication of the validity of the proposed chemical model, a process termed pseudo-plotting.[20]

A typical Q_M-bar graph is given in Figures 3.0 D and E. The pink plot is the n-bar and the blue plot is Q_M-bar. The n-bar levels off at 1 indicating there is one dissociable

proton on the ligand. At pH 4.4 in Figure 3.0 D, there is crossover of n-bar and Q_M-bar curves. This indicates that the proton on the ligand has been displaced due to complexation; therefore the species formed is ML. At pH 6.13, the ligand lost two protons due to complexation (Q_M-bar = 1.6), the complex species formed here is the MLH_{-1}. Between pH 8.6 and 11.0, n-bar and Q_M-bar are parallel indicating that there are no more protons being displaced by the metal ion. The Q_M-bar curve can be also show the formation of hydroxol species if the curve goes-up as shown in Figure 3.0 E.

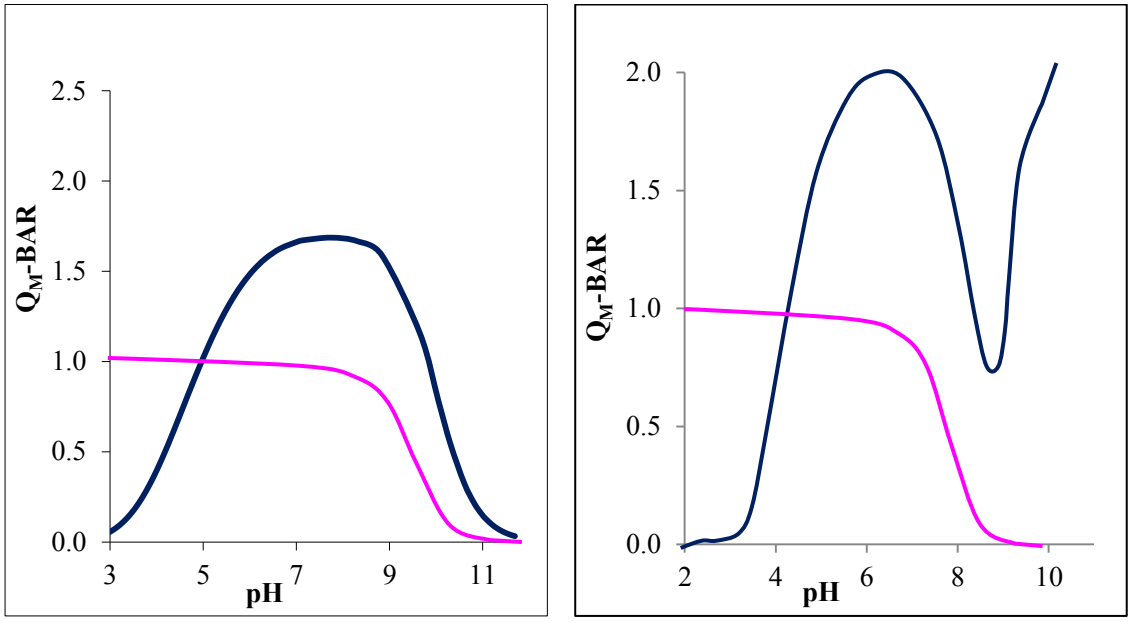

D **E**

Figure 3.0: D & E: Typical Q_M-bar curve when **(D)** ML is only species. **(E)** ML and MLH_{-1} are present.

3.3.3 Standard Deviation and Hamilton R-factor

The standard deviations[18,19] are errors estimated for the parameters being optimized by the method of least-squares. The standard deviation (σ) can be expressed as;

$$\sigma = \left(\frac{U_{obj} G_{rr}}{N - n_p}\right)^{1/2} \tag{3.40}$$

where G is the reciprocal of the Hessian, $G = H^{-1}$.

The agreement between the observed and calculated values of the refined data is determined by the Hamilton R-factor (R_f^H).[18] It is represented as:

$$R_f^H = \left(\frac{U_{obj}}{\sum n_e{}^{-1} \sum W_{nq} \, (Y_{nq}{}^{obs})^2} \right)^{1/2} \tag{3.41}$$

(R_f^H) depends on random errors and the number of variables optimised. The limiting value of R (R_{lim}^H) is expressed as;

$$R_{lim}^H = \left(\frac{N}{\sum n_e{}^{-1} \sum W_{nq} \, (Y_{nq}{}^{obs})^2} \right)^{1/2} \tag{3.42}$$

The lowest value of R that is statistically significant based on the number of variables and the random errors in the analytical data. The closer R_f^H is to R_{lim}^H the better the agreement between the experimental and theoretical data. If R_f^H is less than R_{lim}^H the model is within the maximum allowed experimental error.[20]

3.4 Experimental

3.4.1 Materials and Sample Preparation

All solutions, at ionic strength 0.15M with (Cl^-) Na^+ as the background electrode, were prepared in glass-distilled water which had been passed through a Milli-Q water purification system (Millipore Corp.) and boiled to remove dissolved carbon dioxide. Other reagents such as, $CuCl_2.2H_2O$, $NiCl_2.6H_2O$, $ZnCl_2$, NaCl, HCl, NaOH, and EDTA (Merck) were bought commercially and were of analytical grade. These were used without any further purification. Standard divalent metal solutions of Cu(II), Ni(II), and Zn(II) were prepared in calibrated volumetric flasks according to Vogel's method[21] for metal standard solution preparation. The metal ion solutions were standardized by direct titration against EDTA[16] using a Metrohm 765 Dosimat automated burette. All weighing was done to 5 decimal places on an A&D GH-202 analytical scale balance. The concentrations of the

metal ions ranged between 0.010 and 0.012 mol dm^{-3}. A solution of NaOH (0.1 mol dm^{-3}) was prepared under a nitrogen atmosphere from Merck (1.09959-Titrisol) ampoules and standardized by titrating against potassium hydrogen phthalate (KHP) using the method of Gran.[22] Ligand solutions were prepared in standard HCl solution and standardised by acid-base titration according to Gran's method.[22]

3.4.2 Potentiometric Measurements and Data Analysis

Potentiometric titrations were performed under an inert atmosphere of purified nitrogen at 25°C and at a constant ionic strength of 0.15 mol dm^{-3} (NaCl) using a Metrohm 848 Titrin plus. The pH meter was equipped with a Metrohm 6.0259.100 glass electrode. The electrode slope was calibrated using three buffers. The strong acid-strong base titrations were performed in order to calculate the values of the response intercept E^o, slope (s) and the dissociation constant of water (pK_w) by introducing titration data into an ESTA file template. The value of the Nernstian slope varied between 58.40 and 58.71 over the pH range of 2.00-11.00. The values of E^o varied from 397.87 to 409.71 millivolts, while the average pK_w value was 13.67. The metal to ligand molar ratios varied between 1:1 and 1:2. The metal ion/ligand system was then titrated with standard solutions of NaOH.

The potentiometric titration data were analysed using the ESTA suite of computer programs. The collected data were imported into a preformatted data file for the purpose of calculating the electrode parameters, protonation and formation constants. The task BETA of the ESTA programs was used to evaluate the estimated complex species and their formation constants. The output of this task was introduced into the task OBJE within the ESTA2 module to give optimised values of the stability constants and the ligand concentration describing the system. Complex formation and deprotonation functions were calculated from stability constants obtained using the tasks ZBAR and QBAR within the ESTA1 module to find out if the model fitted the system. After the completion of the model, the calculated β values from Equation 3.32 were used in the calculation of protons. The validity of the model was checked by the comparison of the resulting calculated formation and the experimental curves.

3.5 Results and Discussion

3.5.1 Protonation Formation Function

The overall protonation constants, as $\log\beta_{pqr}$ for five ligands [H(555)NH_2], [H(555)NMe_2], [H_2(555)NH_2], [H_2(565)NH_2] and [H(56)NH_2] are given in the Table 3.1. The protonation constants for H^+- L equilibria were evaluated in the pH range 2 - 11. In order to examine the experimental data, the protonation curves of the ligands and species distribution graphs have been calculated and the results are presented in Figures 3.1 - 3.10 below.

3.5.1.1 H^+-[H(555)NH_2] System

The Z_H-bar function, given in Figure 3.1, represents the variation of the mean number of protons bound to the ligand as a function of pH. The blue markers represent the experimental data points while the pink markers are the theoretical curve calculated using the model given in Table 3.1. At pH 10.90, Z_H-bar is 0, and the ligand is fully deprotonated. From pH 10.6 to 8.5 Z_H-bar rises. In this pH range, the ligand is being protonated from the L-form to the LH-form. From pH 8.1 to 6.1, Z_H-bar was fairly constant (Z_H-bar ≈ 1) indicating that no further protonation was occurring. From pH 6 to 2 the curve rises to Z_H-bar = 3, indicating the addition of two protons with similar pK_a's.

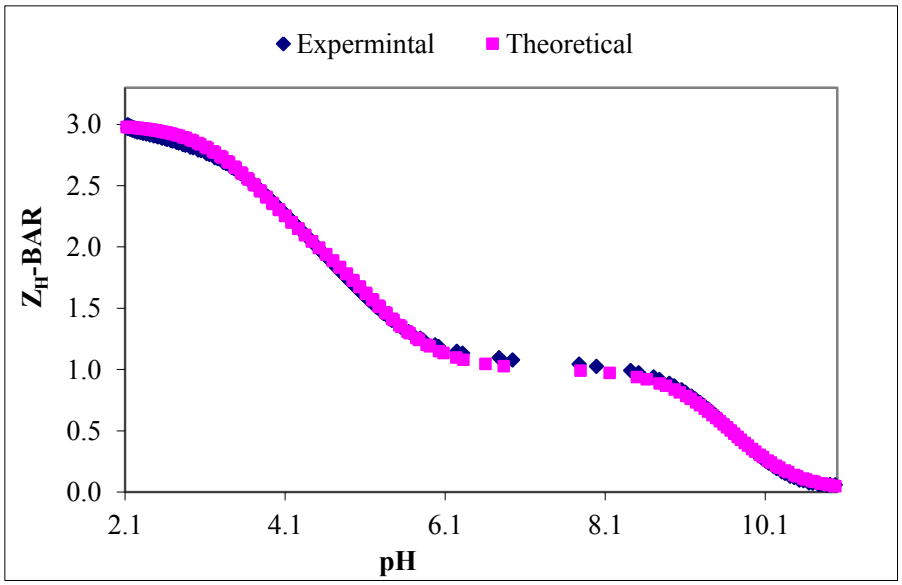

Figure 3.1: Z_H-bar for the protonation of [H(555)NH_2].

The excellent agreement between the theoretical and experimental curves in Figure 3.1, at different total ligand concentrations, the low standard deviations in the log $\beta_{pqr,}$ as well as the Hamilton R factor lends confidence to the model.

Table 3.1: Stability constants (log β_{pqr}) for [H(555)NH_2]. $\beta_{pqr} = [M_pL_qH_r]/[M]p[L]q[H]r$, I = 0.15 mol.dm^{-3} (NaCl), T = 25 ºC. S. dev denotes standard deviation in log β_{pqr}; R_f^H is the Hamilton R-factor and R_{lim}^H its limit.

p	q	r	log β_{pqr}	S.dev	R_f^H	R_{lim}^H	$n_T(n_p)$
0	1	1	9.67	0.008			
0	1	2	14.93	0.01	0.01	0.02	2(156)
0	1	3	18.69	0.01			

Figure 3.2 shows the speciation diagrams of [H(555)NH_2] from pH 2 to 11. At pH < 10.0 the most predominant species was L. The species LH dominates at pH 7. The species LH_2 and LH_3 are predominant, between pH 6.2 and 2.0 and below pH 5.00 respectively, in aqueous solution.

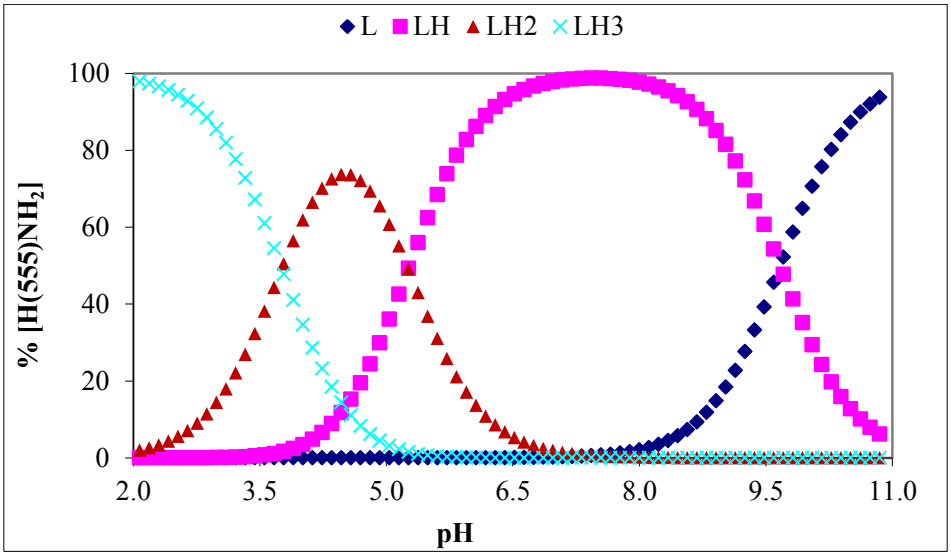

Figure 3.2: Distribution Curve for the protonation of [H(555)NH_2].

3.5.1.2 H^+-[H(555)NMe_2] System

Figure 3.3 shows Z_H-bar as a function of pH for the protonation of [H(555)NMe_2]. The ligand has three pronation sites. From the half-bar values the first two pK_a's are estimated to be 9.2 and 4.8. Since the curve does not rise to a Z_H-bar of 2.5, the last pK_a cannot be estimated. The refined beta's for this system are given in Table 3.2 and the theoretical Z_H-bar curve, calculated using these values is shown in Figure 3.3.

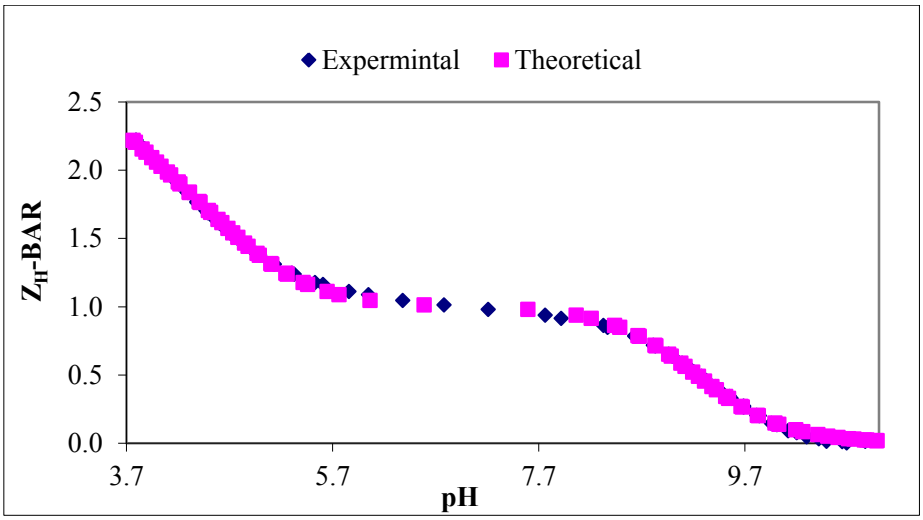

Figure 3.3: Z_H-bar for the protonation of [H(555)NMe_2].

The excellent agreement between the theoretical and experimental curves lends confidence to the results. The standard deviations σ_{pqr} and R_f^H are small

Table 3.2: Stability constants (log β_{pqr}) for [H(555)NMe_2]. β_{pqr} = $[M_pL_qH_r]/[M]p[L]q[H]r$, I = 0.15 mol.dm^{-3} (NaCl), T = 25 ºC. S. dev denotes standard deviation in log β_{pqr}; R_f^H is the Hamilton R-factor and R_{lim}^H its limit.

p	q	r	log β_{pqr}	S.dev	R_f^H	R_{lim}^H	$n_T(n_p)$
0	1	1	9.23	0.01			
0	1	2	13.97	0.02	0.01	0.01	2(73)
0	1	3	17.38	0.04			

Figure 3.4 shows the species distribution curves for [H(555)NMe_2]. The plots indicate that the ligand solution has a mixture of di-protonated and tri-protonated species at pH < 4. At pH = 7 the most predominant species was LH, whereas the neutral form of the ligand L predominates at pH > 9.5.

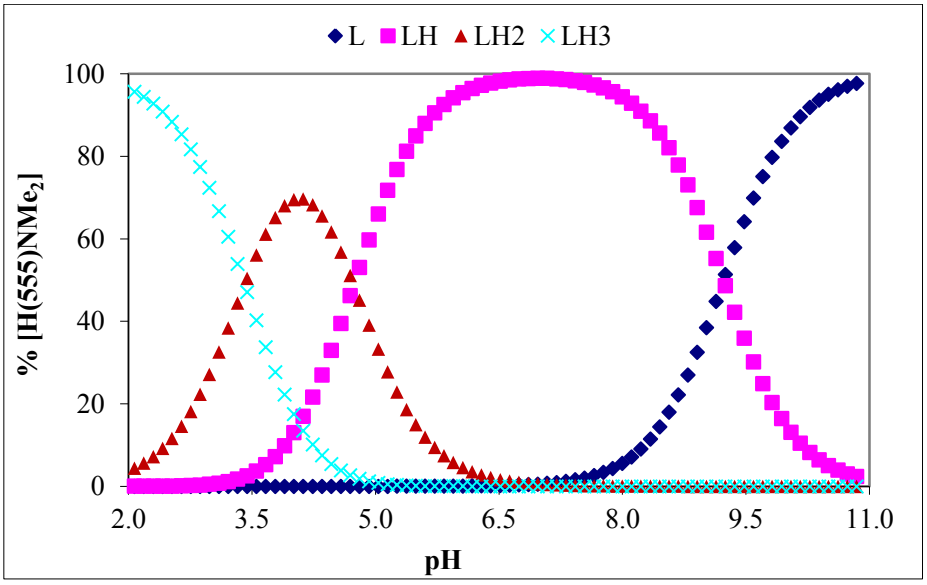

Figure 3.4: Distribution Curve for the protonation of [H(555)NMe_2].

3.5.1.3 H^+-[H_2(555)NH_2] System

Figure 3.5 shows that this ligand contains one measurable protonation site as revealed by the levelling off of the Z_H-bar function at 1.0.

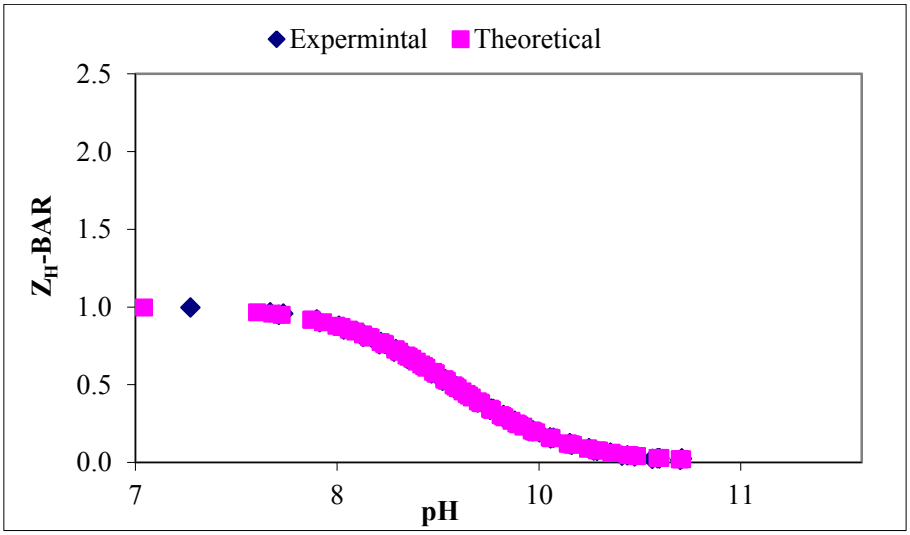

Figure 3.5: Z_H-bar for the protonation of [H_2(555)NH_2].

The theoretical and experimental curves are well superimposable, as shown in Figure 3.5. The optimised formation constant is given in Table 3.3.

Table 3.3: Stability constants (log β_{pqr}) for $[H_2(555)NH_2]$. $\beta_{pqr} = [MpLqHr]/[M]p[L]q[H]r$, I = 0.15 mol.dm^{-3} (NaCl), T = 25 ºC. S. dev denotes standard deviation in log β_{pqr}; R_f^H is the Hamilton R-factor and R_{lim}^H its limit.

p	q	r	log β_{pqr}	S.dev	R_f^H	R_{lim}^H	$n_T(n_p)$
0	1	1	8.96	0.003	0.008	0.009	3(74)

The two species of this ligand are shown by the speciation graph in Figure 3.6. The species $[H_2(555)NH_2]$ and $[H_2(555)NH_2]H^+$ are the most predominant species above and below pH 9.02 respectively in aqueous solutions of the ligand.

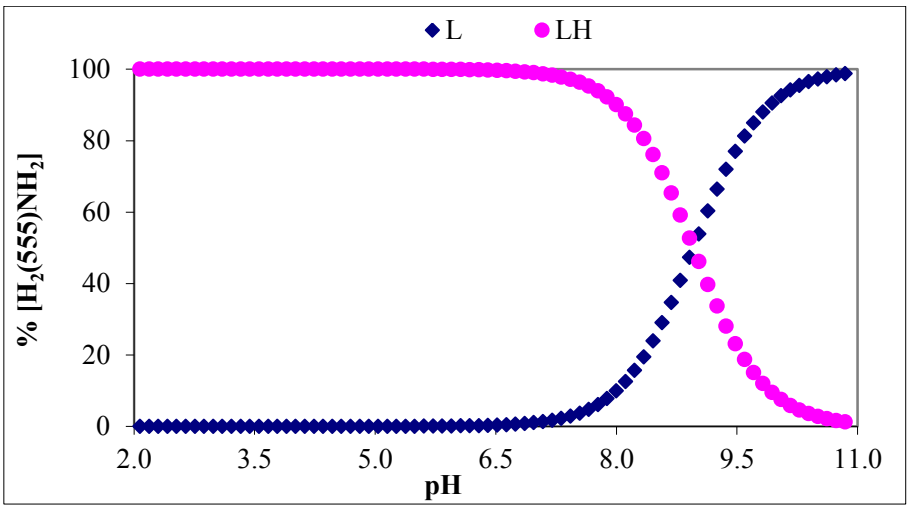

Figure 3.6: Distribution Curve for the protonation of $[H_2(555)NH_2]$.

3.5.1.4 H^+-$[H_2(565)NH_2]$ System

The Z_H-bar as a function of pH is shown in Figure 3.7. The graph rises from pH 9.04 to 7.39 indicating that one proton was added to the ligand, resulting in a mono-protonated ligand at this pH. The Z_H-bar function levels off on 1 (i.e. Z_H-bar = 1) between pH 6.86 and 5.65, and then it rises until it reaches Z_H-bar = 2 below pH 5.65. This indicates that $[H_2(565)NH_2]$ has two dissociable protons.

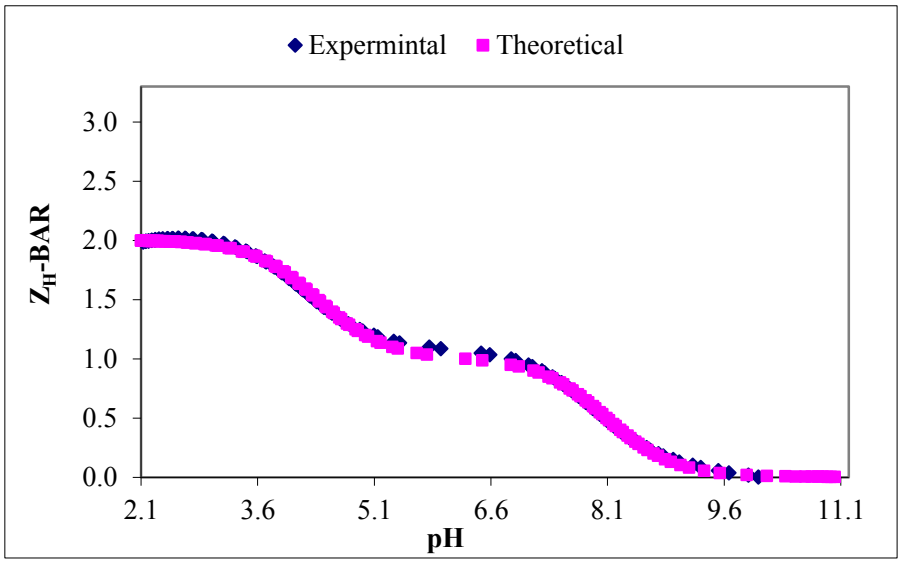

Figure 3.7: Z_H-bar for the protonation of $[H_2(565)NH_2]$.

The theoretical and experimental curves are well superimposable which support the $[H_2(565)NH_2]$ protonation model. The standard deviations are small and the model is accurate since R_f^H is less than R_{lim}^H. Optimized log β_{pqr} are given in Table 3.4.

Table 3.4: Stability constants (log β_{pqr}) for $[H_2(565)NH_2]$. $\beta_{pqr} = [M_pL_qH_r]/[M]p[L]q[H]r$, I = 0.15 mol.dm^{-3} (NaCl), T = 25 ºC. S. dev denotes standard deviation in log β_{pqr}; R_f^H is the Hamilton R-factor and R_{lim}^H its limit.

p	q	r	log β_{pqr}	S.dev	R_f^H	R_{lim}^H	$n_T(n_p)$
0	1	1	8.08	0.007	0.01	0.012	2(129)
0	1	2	12.46	0.01			

Figure 3.8 shows the distribution of species from pH 2 to 11 for $[H_2(565)NH_2]$ protonation, which confirms that the species $[H_2(565)NH_2]H^+$ dominates in the pH range 4.35 – 8.11. At pH 8.23 there is already more $[H_2(565)NH_2]$ than $[H_2(565)NH_2]H^+$ in solution. Below pH 4.24, the most predominant species is $[H_2(565)NH_2]H_2^{+2}$ in aqueous solutions of this ligand.

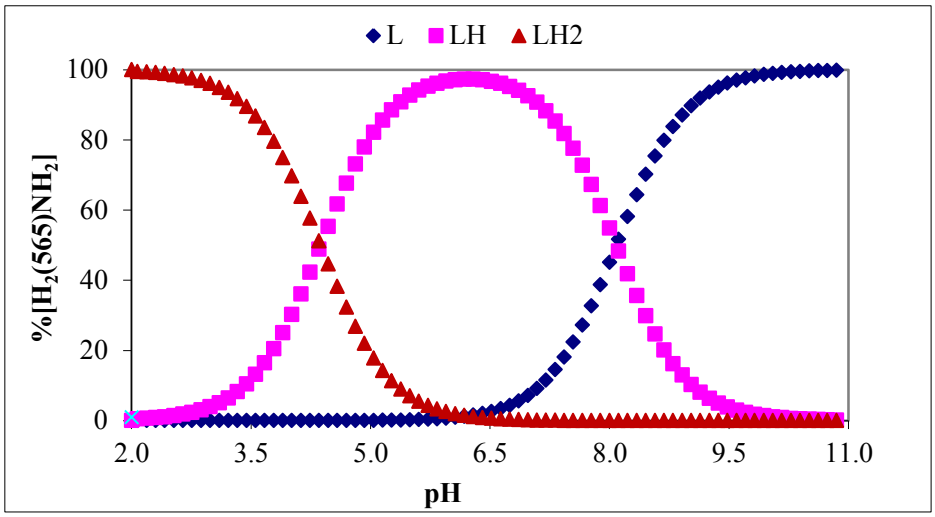

Figure 3.8: Distribution Curve for the protonation of $[H_2(565)NH_2]$.

3.5.1.5 H^+-$[H(56)NH_2]$ System

Figure 3.9 shows the plot of the formation function, Z_H-bar as a function of pH for the protonation of $[H(56)NH_2]$. The function levels to zero at a high pH of 11.10, afterwards it rises up and then levels off at Z-bar value of 1 between pH 8.10 and 6.15. Below pH 5.31 the function rises and levels off at a Z_H-bar value of 2.0. That indicating two protons have been added to the ligand making it di-protonated at low pH.

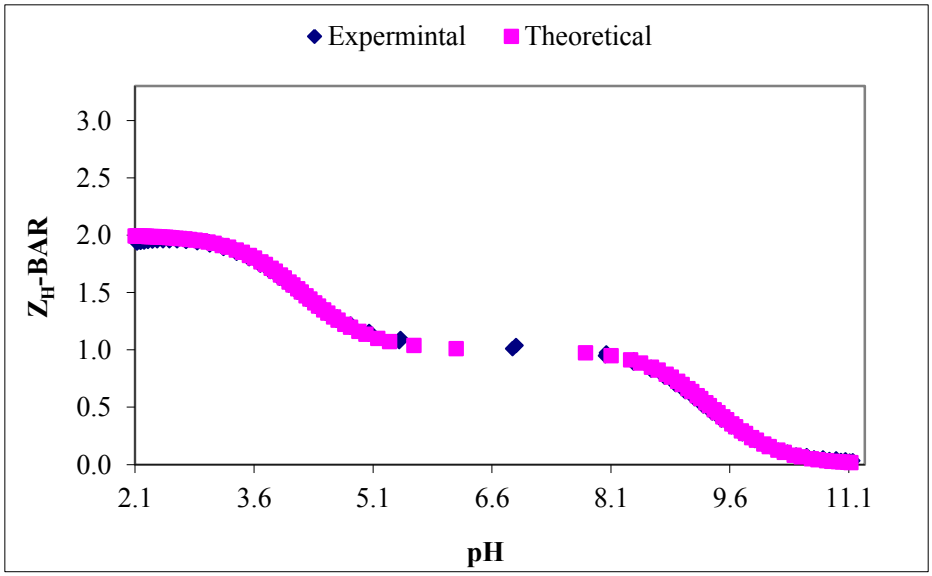

Figure 3.9: Z_H-bar for the protonation of $[H(56)NH_2]$.

Table 3.5 shows log β_{pqr} for the protonation of [H(56)NH_2]. The agreement between the theoretical and the experimental plot gives us confidence in the model.

Table 3.5: Stability constants (log β_{pqr}) for [H(56)NH_2]. $\beta_{pqr} = [M_pL_qH_r]/[M]p[L]q[H]r$, I = 0.15 mol.dm^{-3} (NaCl), T = 25 ºC. S. dev denotes standard deviation in log β_{pqr}; R_f^H is the Hamilton R-factor and R_{lim}^H its limit.

p	q	r	log β_{pqr}	S.dev	R_f^H	R_{lim}^H	$n_T(n_p)$
0	1	1	9.36	0.008			
0	1	2	13.57	0.01	0.01	0.008	2(101)

Figure 3.10 shows the speciation diagrams for [H(56)NH_2] protonation from pH 2.0 to 11.0. The most predominant species in solution from pH 11.0 to 9.48 is [H(56)NH_2] species. [H(56)NH_2]H^+ is the dominating species at physiological pH. From pH 4.13 to 2.07, [H(56)NH_2]H_2^{+2} is predominant in solution.

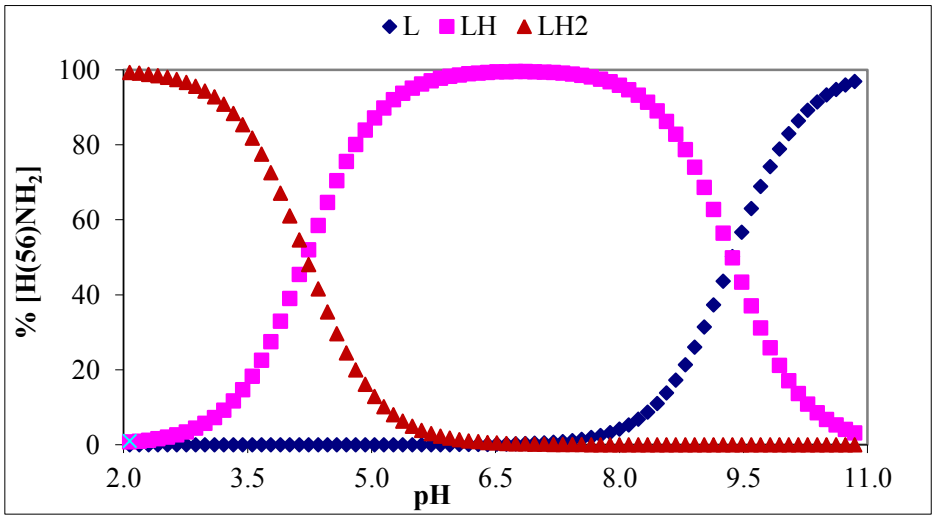

Figure 3.10: Distribution Curve for the protonation of [H(56)NH_2].

3.5.1.6 Discussion – Protonation Constants

The protonation constants results for the ligands involved in this study are presented in Tables 3.1 to 3.5. These results show low standard deviations while their R_f^H values are either close or smaller than their corresponding R_{lim}^H. This gives confidence to the chosen models. Protonation or deprotonation constants were measurable for all the available amines and pyridyl nitrogen except for the amide nitrogens which were not determined because they

are too basic ($pK_a \geq 15$)[23] and outside the pH range 2 – 11 of our glass electrode. Several other workers[24-27]have also observed that it is not possible to estimate deprotonation of the amide nitrogen outside the upper pH limit of our measurements. However, the deprotonation of the amide protons is facilitated by the presence of metal ions such as Cu(II).[28,24] So far we have always treated equilibrium constant as formation constant while pK_a is the equilibrium constant when the ligand is acting as an acid i.e deprotonation rather than formation. The measured pK_a values are given in Table 3.6.

Table 3.6: Stability and Equilibrium constants for $[H(555)NH_2]$, $[H(555)NMe_2]$, $[H_2(555)NH_2]$, $[H_2(565)NH_2]$ and $[H(56)NH_2]$. $\beta_{pqr} = [M_pL_qH_r]/[M]p[L]q[H]r$, I = 0.15 mol.dm^{-3} (NaCl), T = 25 ºC.

Ligand	p	q	r	log β_{pqr}	pK_a
$[H(555)NH_2]$	0	1	1	9.67	9.67
	0	1	2	14.93	5.26
	0	1	3	18.69	3.76
$[H(555)NMe_2]$	0	1	1	9.23	9.23
	0	1	2	13.97	4.74
	0	1	3	17.38	3.41
$[H_2(555)\text{-}NH_2]$	0	1	1	8.96	8.96
$[H_2(565)NH_2]$	0	1	1	8.08	8.08
	0	1	2	12.46	4.38
$[H(56)NH_2]$	0	1	1	9.36	9.36
	0	1	2	13.57	4.21

The three measurable acid dissociation constants of both $[H(555)NMe_2]$ and $[H(555)NH_2]$ correspond to the pyridyl nitrogen and the two amino groups. The low values of the first protonation constant (pK_{a1}) corresponding to the pyridyl nitrogens are due to the electronic repulsion effect and the base weakening effect of the adjacent amide groups.[29] The pK_a values of pyridine and 2-methylpyridine are reported as 5.34 and 6.14, respectively,[30] whereas the introduction of a carbonyl group in 2-methylpyridine results in a

pK_a value of 2.66.[23] Therefore, it would be expected that the protonation constant corresponding to the pyridyl nitrogen in [H(555)NMe_2] and [H(555)NH_2], should decrease further when an amide group is present.

The pK_{a3} for the terminal amino groups of [H(555)NMe_2] and [H(555)NH_2] is 9.23 and 9.67 respectively. This pK_a is less than the corresponding pK_a of ethylenediamine (9.89).[31,32] This is attributed to the electron-withdrawing effects of the amide group.[31,33] The observable reduction in pK_{a3} in [H(555)NMe_2] compared to that in the analogous [H(555)NH_2] is due to H-bonding and solvation effects as one moves from primary to tertiary amines.[34,25] These values are also reasonably close to the first protonation of [H(555)-N] (9.40),[31] which is an analogous ligand but with the amide carbon adjacent to the pyridine ring. pK_{a2} of [H(555)NMe_2] and [H(555)NH_2] are 4.74 and 5.26 respectively and refers to protonation of the second amine. The decrease in basicity is due to electronic repulsion when a proton is added to a molecule already containing a proton. These values are lower than the corresponds protonation of [H(555)-N][31] (6.23). This is because the secondary nitrogen donor atoms of [H(555)NMe_2] and [H(555)NH_2] are close to an electron withdrawing amide group.

Two protonation sites are available in [H_2(555)-NH_2] but only one protonation constant was determined by ESTA optimization[18] of the potentiometric data. The pK_a = 8.96 corresponds to the protonation constant of the amino group. The fact that the protonation constant is lower than that of ethylenediamine (pK_a = 9.89)[32] is due to the electron withdrawing effects of the two amide groups[31] present in the ligand, capable of drawing electrons towards themselves through inductive effects. S. Odisitse[23]reported the pK_a of the pyridyl nitrogen 3.51 in *N,N′*-bis[2(2-pyridyl)-methyl]pyridine- 2,6-dicarboxamide which is quite similar to the pK_a of the pyridyl nitrogen in [H_2(555)NH_2].

[H_2(565)NH_2] shows two pK_a values arising from the pyridyl nitrogen and the amino group, pK_{a1} = 4.38 and pK_{a2} = 8.08 respectively. The chemical environment associated with the pyridyl nitrogen is the same as that found in [H(555)NMe_2] and [H(555)NH_2] thus giving very close pK_a values differing by only 0.9 and 0.6 log unit respectively. However, the low pK_{a1} or rather acidity of the pyridyl nitrogen is due to the electronic repulsion effect and also the base weakening effect of the CONH group.[29] The amino group is observed to be less basic than the nitrogen donor atoms of ethylenediamine (pK_{a2} = 9.89).[35]

A similar protonation scheme is observed for $[H(56)NH_2]$ with $pK_{a1} = 4.21$ and $pK_{a2} = 9.39$ for the pyridyl nitrogen and amino group respectively. The pK_{a1} is almost equal to that of $[H_2(565)NH_2]$, whereas the $pK_{a2} = 9.39$ is observed to be less basic than the nitrogen donor atoms of diethylenetriamine (dien) (9.84)[35] and higher than $[H_2(565)NH_2]$ (8.08). The base weakening effect has also been attributed to the same cause as has been mentioned above.

3.5.2 Complex Formation and Deprotonation Functions

The Z_M-bar and Q_M-bar functions derived from experimental data were used to visualize the data and help with speciation model selection.

3.5.2.1 Cu(II)-L Systems

3.5.2.1.1 Cu(II)-$[H(555)NH_2]$ System

Z_M-BAR for Cu(II)-$[H(555)NH_2]$ as a function of pL is given in Figure 3.11(a). Z_M-bar should rise and level off towards a Z_M-bar limiting value of 1.0 for mononuclear ML species formation. This was not observed in this system. The Z_M-bar function levels off at 1.39 indicating that ML is not the only species in solution. The curves rise steeply and fan back at pL 8.28, indicating loss of an amide proton upon metal coordination.[36,37] The deprotonation function in Figure 3.11(b) rises to a maximum value of about 2.61 between pH 3.71 and 4.76 indicating that approximately three protons have been released from the ligand due to complexation. Between pH 4.6 and pH 7.0, Q_M-bar runs parallel to n-bar. This indicates that there is no change in complexation in this pH range.

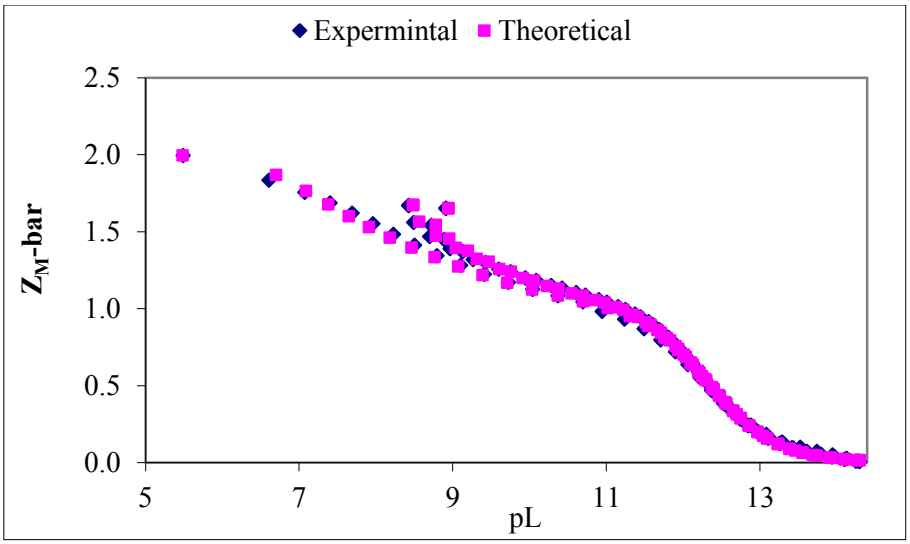

(a)

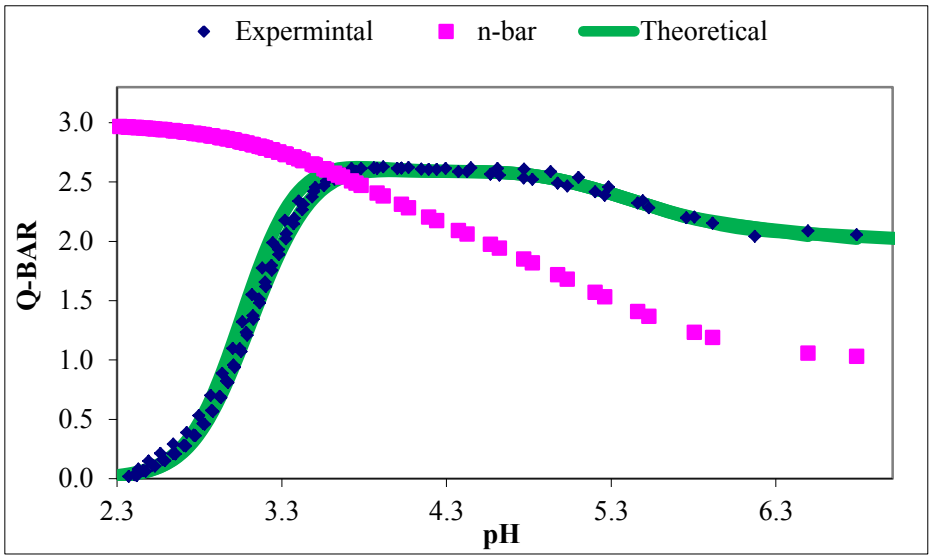

(b)

Figure 3.11 (a): Z_M-bar as a function of pL for Cu(II)-[H(555)NH_2] Complex. **(b):** Q_M-bar as a function of pH Cu^{2+}/ [H(555)NH_2] Complex.

The reproducibility of repeat titrations and excellent agreement, at different metal to ligand ratios, between the theoretical and experimental formation and deprotonation function curves. The analysis of the potentiometric data using the ESTA suite[18] of programs yielded the results given in Table 3.7. Furthermore, very low standard deviations and Hamilton R-factors were found. This lends confidence to the model selected. It is worth noting that several possible species were tried but were rejected by the optimization process.

Table 3.7: Stability constants (log β_{pqr}) for Cu(II) of [H(555)NH_2] complexes β_{pqr} = $[M_pL_qH_r]/[M]p[L]q[H]r$, I = 0.15 mol.dm^{-3} (NaCl), T = 25 ºC. S. dev denotes standard deviation in log β_{pqr}; R_f^H is the Hamilton R- factor and R_{lim}^H its limit.

Metal	p	q	r	log β_{pqr}	S.dev	R_f^H	R_{lim}^H	$n_T(n_p)$
Cu(II)	1	1	1	13.89	0.06	0.002	0.02	3(110)
	1	1	0	11.81	0.003			
	1	1	-1	7.45	0.009			

The speciation graphs in Figure 3.12 shows that ML and MLH_{-1} predominate over a wide pH range of 2.53 – 5.26 and 3.10 – 8.00 respectively. ML species reaches 81.75%

formation at pH 3.75 and at pH 7.43 MLH_{-1} species reaches 99.92% formation whereas MLH species do not exceed 5% formation.

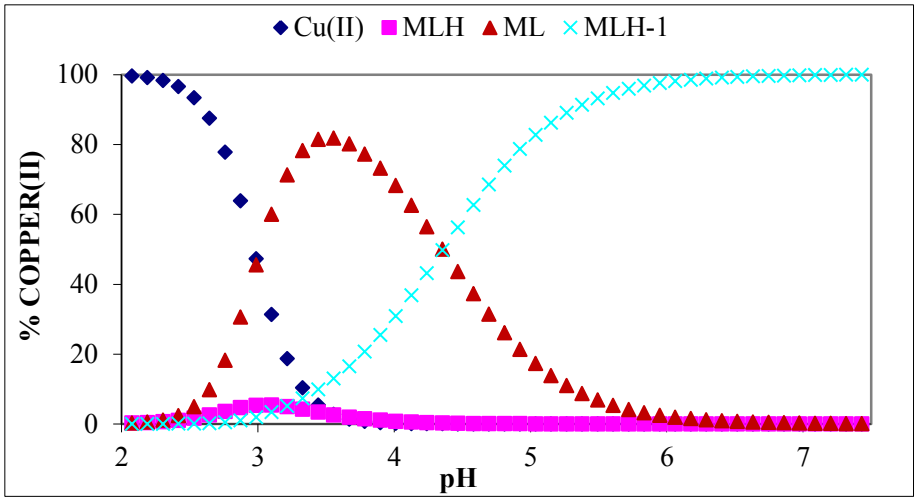

Figure 3.12: The distribution curve for Cu(II)-[H(555)NH_2] Complex. Metal to Ligand ratio 1:2.

3.5.2.1.2 Cu(II)-[H(555)NMe_2] System

The complex formation behaviour of the Cu(II)-[H(555)NMe_2] system is shown in Figure 3.13(a). like the Cu(II)-[H(555)NH_2] system, the Z_M-bar levels off at 1.2, indicating that ML is not the predominant species in solution. The fanning back of the curves at high pH is presumably due to the formation of MLH_{-1} and MLH_{-2} species. Figure 3.13(b) shows the deprotonation function as a function of pH. When the titration starts at pH of 2.94, the function is greater than zero indicating that complexation has already started. Q_M-bar then increases rapidly in the pH range 2.94 - 3.83 to a maximum value of 2.26. The n-bar curve shows that at pH 3.83 there are essentially two protons to be displaced from the ligand by the metal ion. Complexation was complete between pH 4.55 and pH 8.36. At pH > 9.50 the Q-bar curve rises, which indicates hydrolysis of the metal ion forming an MLH_{-2} species for this Cu(II)-[H(555)NMe_2] system.

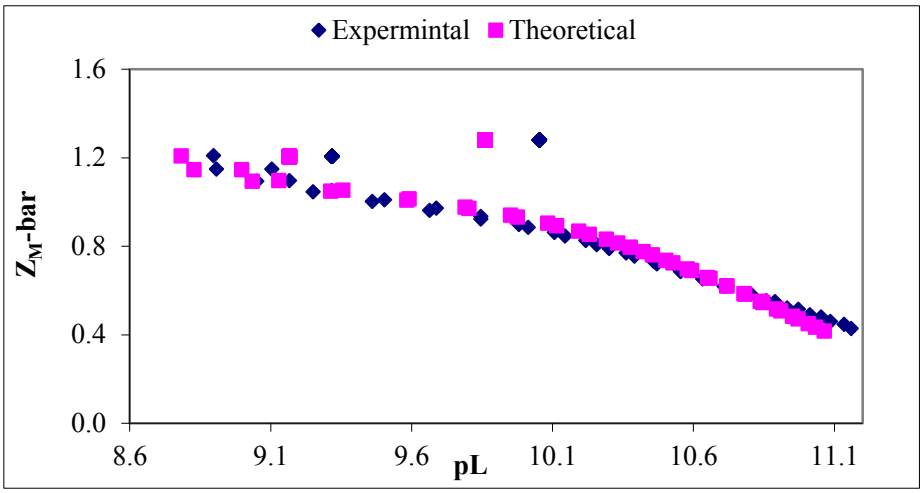

(a)

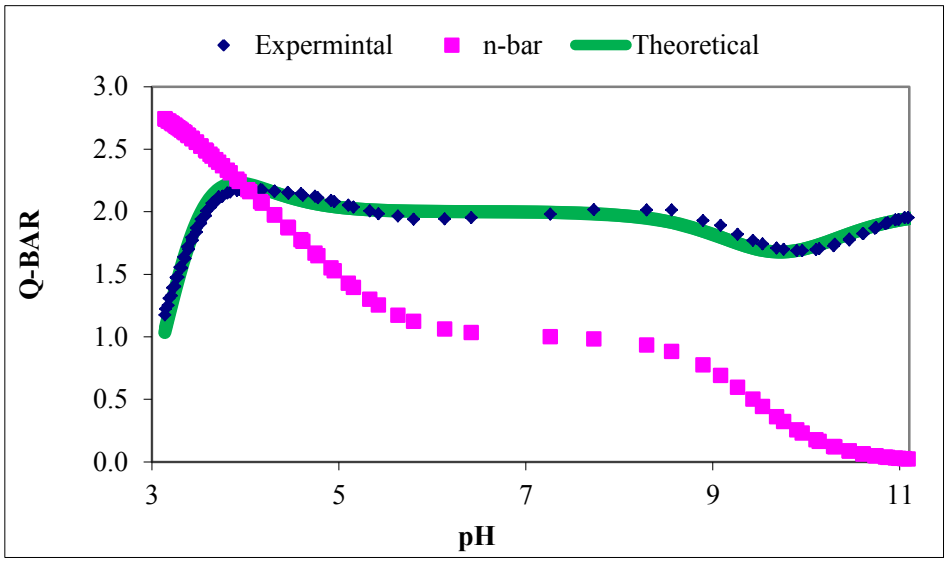

(b)

Figure 3.13 (a): Z_M-bar as a function of pL for Cu(II)-[H(555)NMe_2] Complex. **(b):** Q_M-bar as a function of pH Cu(II)-[H(555)NMe_2] Complex.

Optimised log β_{pqr} are given in Table 3.8. The standard deviations are small and R_f^H is less than R_{lim}^H. The agreement between the theoretical and experimental complex formation curves at different metal to ligand ratios supports the potentiometric model chosen in data analysis.

Table 3.8: Stability constants (log β_{pqr}) for Cu(II) of [H(555)NMe_2] complexes. β_{pqr} = $[M_pL_qH_r]/[M]p[L]q[H]r$, I = 0.15 mol.dm^{-3} (NaCl), T = 25 ºC. S. dev denotes standard deviation in log β_{pqr}; R_f^H is the Hamilton R-factor and R_{lim}^H its limit.

Metal	p	q	r	log β_{pqr}	S.dev	R_f^H	R_{lim}^H	$n_T(n_p)$
Cu(II)	1	1	0	10.90	0.02	0.009	0.02	2(84)
	1	1	-1	6.18	0.06			
	1	1	-2	-3.63	0.07			

The speciation graphs in Figure 3.14 show that ML, MLH_{-1} and MLH_{-2} are present at significant levels i.e. 89% (pH 3.5), 99% (pH 7.2) and 100% (pH 10.8) formation respectively.

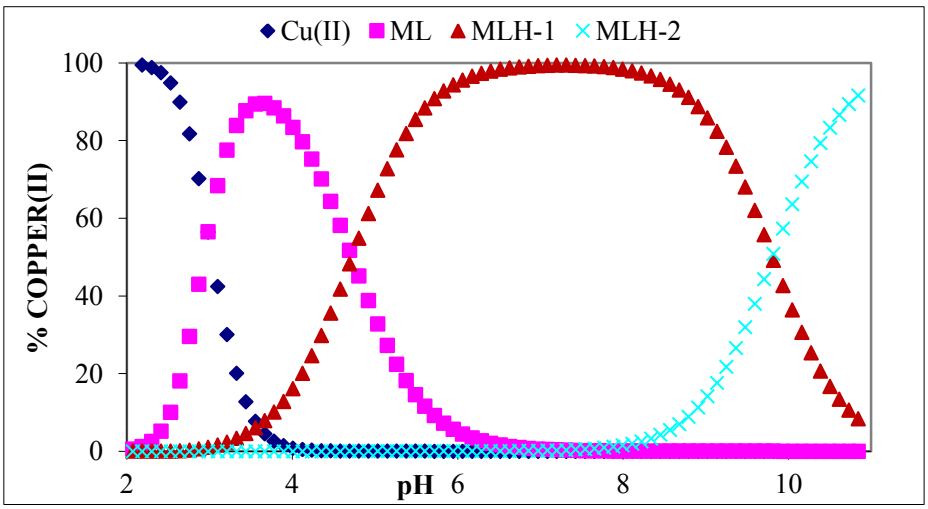

Figure 3.14: The distribution curve for Cu(II)-[H(555)NMe_2] Complex. Metal to Ligand ratio 1:1.5.

3.5.2.1.3 Cu(II)-[H_2(555)NH_2] System

The Z_M-bar curves in Figure 3.15(a) level off at ~ 0.8, indicating that ML is not the predominant species in solution. The fanning of Z_M-bar for higher metal to ligand ratios is indicative of loss of an amide proton upon metal coordination. On the other hand Q_M-bar in Figure 3.15(b) shows that at the start of the titration, at pH of approximately 2.32, Q-bar is greater than zero indicating that complexation has already commenced. The function then

rises in the pH range between 2.32 and 3.97. Between pH 4.45 and 5.94 Q-bar correspond with n-bar, indicating that no further complexation takes place in this pH range. The Q-bar curve rises above the n-bar curve at pH 8.89, due to the formation of MLH_{-1} and MLH_{-2} species.

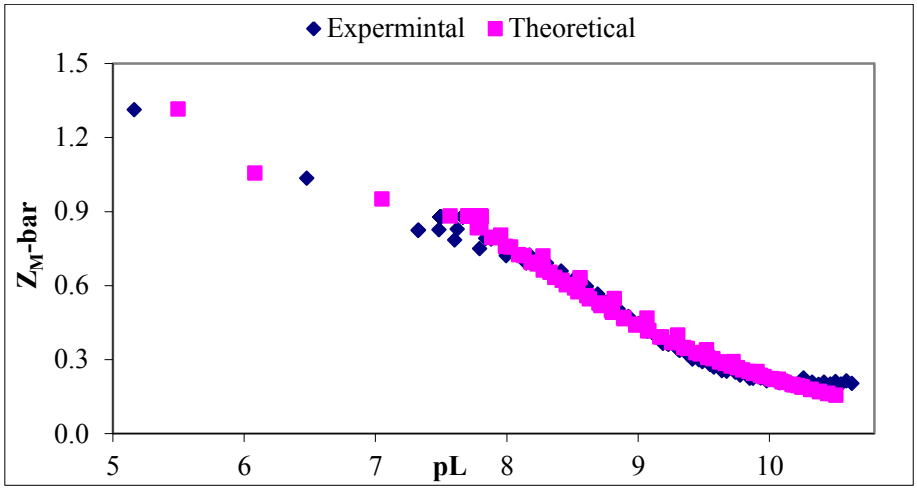

(a)

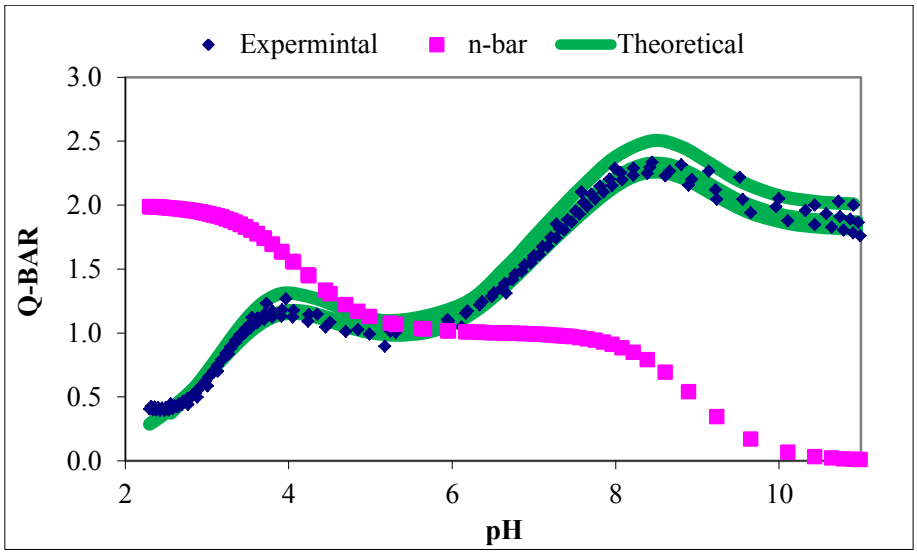

(b)

Figure 3.15 (a): Z_M-bar as a function of pL for Cu(II)-[H_2(555)NH_2] Complex. **(b):** Q_M-bar as a function of pH Cu(II)-[H_2(555)NH_2] Complex.

The stability constants are given in Table 3.9. The standard deviations are small and R_f^H is less than R_{lim}^H. This gives confidence in the model.

Table 3.9: Stability constants (log β_{pqr}) for Cu(II) of $[H_2(555)NH_2]$ complexes. β_{pqr} = $[M_pL_qH_r]/[M]p[L]q[H]r$, I = 0.15 mol.dm^{-3} (NaCl), T = 25 ºC. S. dev denotes standard deviation in log β_{pqr}; R_f^H is the Hamilton R-factor and R_{lim}^H its limit.

Metal	p	q	r	log β_{pqr}	S.dev	R_f^H	R_{lim}^H	$n_T(n_p)$
Cu(II)	1	1	1	12.80	0.01	0.01	0.012	3(157)
	1	1	0	9.39	0.009			
	1	1	-1	2.71	0.01			
	1	1	-2	-5.27	0.01			

The speciation graph for Cu(II)-$[H_2(555)NH_2]$ is given in Figure 3.16. Complexation begins at pH 2.07 for MLH. ML is the most predominant in solution in the pH range 3.44 and 6.75. MLH_{-1} is the most predominant in solution between pH 6.76 and 6.89. MLH_{-2} species is most predominant at pH > 8.11.

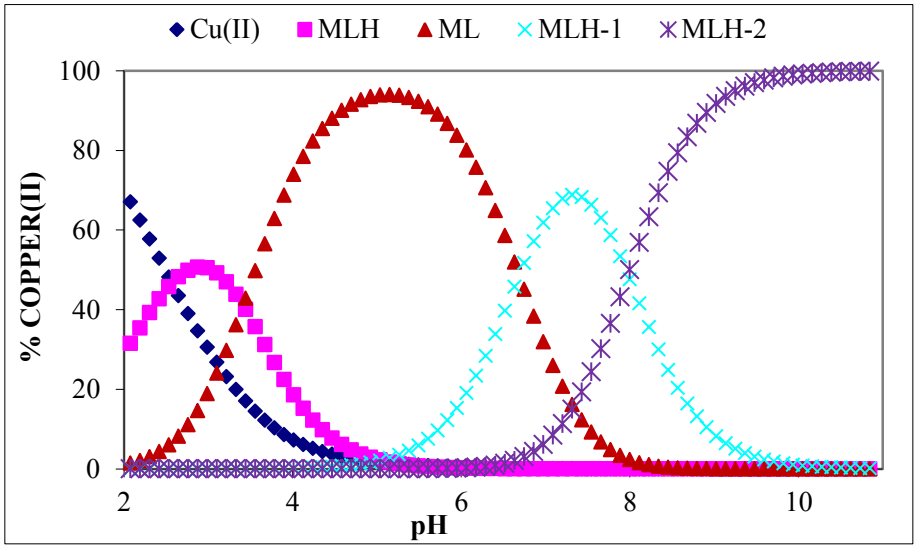

Figure 3.16 : The distribution curve for Cu(II)-$[H_2(555)NH_2]$ Complex. Metal to Ligand ratio 1:1.

3.5.2.1.4 Cu(II)-$[H_2(565)NH_2]$ System

The complexation of $[H_2(565)NH_2]$ with Cu(II) seems to be different from that of the $[H(555)NH_2]$, $[H(555)NMe_2]$ and $[H_2(555)NH_2]$ systems as observed from the formation and deprotonation functions in Figure 3.17(a) and 3.17(b) respectively. The Z_M-bar function does not level off at a value of 1.0, clearly indicating that an ML species in the

Cu(II)-[H_2(565)NH_2] system is not predominant in solution. The graph flags back at low pL's corresponding to lower metal to ligand concentration ratios. This indicates loss of the amide protons in this ligand system upon metal ion coordination due to formation of MLH_{-2} species at Low pH. The deprotonation function rises to maximum value of about 3.0 at pH 5.1 indicating that approximately three protons have been released from the ligand due to complexation. At this pH the ligand has only two protons or rather Q_M-bar(=3.0) > n-bar (=1.5) suggesting the formation of MLH_{-1} species as a result of the release of an amide proton. The falling of Q_M-bar curves parallel to the n-bar curve indicates no further complexation.

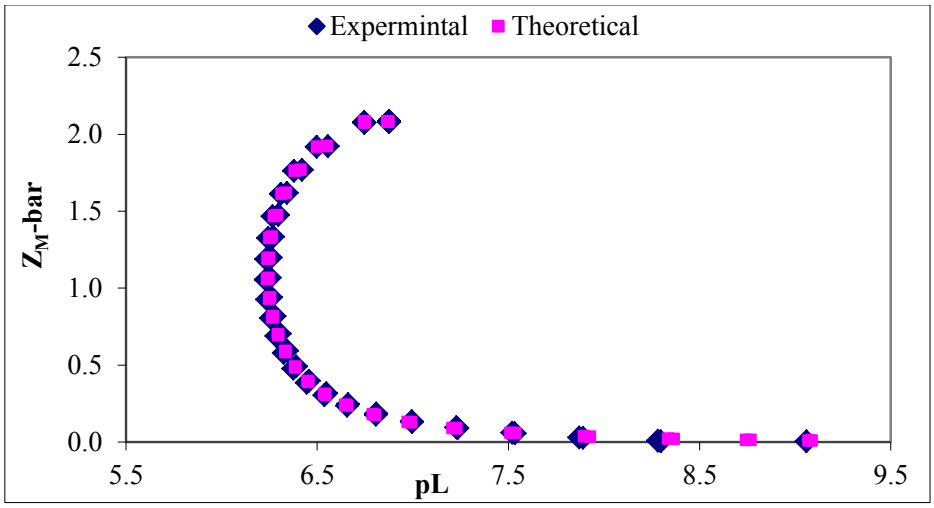

(a)

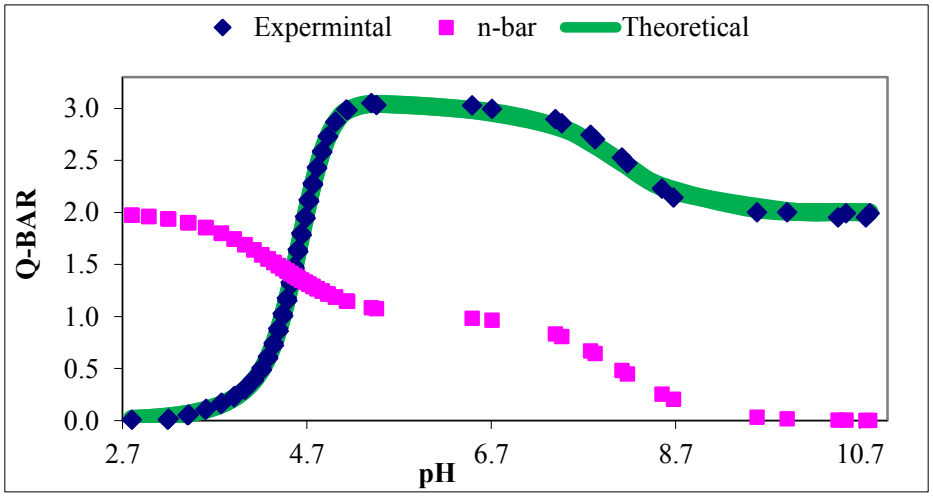

(b)

Figure 3.17 (a): Z_M-bar as a function of pL for Cu(II)-[H_2(565)NH_2] Complex. **(b):** Q_M-bar as a function of pH Cu(II)-[H_2(565)NH_2] Complex.

The stability constants for species formed between Cu(II) and [H_2(565)NH_2] from pH 2.0 to pH 11.0 are given in Table 3.10. The excellent agreement between the theoretical and experimental formation as well as small standard deviations and $R_f^H \approx R_{lim}^H$. These show that the model is accurate. Note in this case there is no MLH_{-1} species. Different models were tried but this species was always rejected.

Table 3.10: Stability constants (log β_{pqr}) for Cu(II) of [H_2(565)NH_2] complexes. $\beta_{pqr} = [M_pL_qH_r]/[M]p[L]q[H]r$, I = 0.15 mol.dm^{-3} (NaCl), T = 25 ºC. S. dev denotes standard deviation in log β_{pqr}; R_f^H is the Hamilton R-factor and R_{lim}^H its limit.

Metal	p	q	r	log β_{pqr}	S.dev	R_f^H	R_{lim}^H	$n_T(n_p)$
Cu(II)	1	1	1	10.04	0.09	0.009	0.009	2(72)
	1	1	0	5.93	0.02			
	1	1	-2	-3.06	0.01			

The speciation graphs are given in Figure 3.18. Mixed species are observed at all pH values except at pH below 2.5 where there is about 100 % Cu(II) in solution, and at pH above 5.3 where almost all Cu(II) ion in solution exist in MLH_{-2} form.

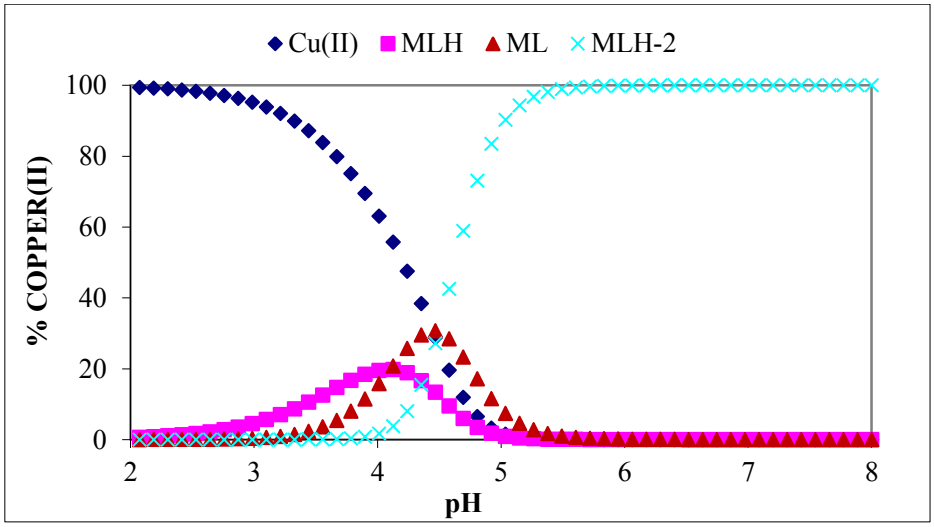

Figure 3.18: The distribution curve for Cu(II)-[H_2(565)NH_2] Complex. Metal to Ligand ratio 1:2.

3.5.2.1.5 Cu(II)-[H(56)NH_2] System

A plot of the complex formation function is given in Figure 3.19(a). From pL 10.44 to pL 9.00, the Z_M-bar is equal to zero. Then the Z_M-bar rises from pL 8.68 to pL 7.36. From pH 7.02 to pH 5.02, Z_M- bar = 2. Figure 3.19(b) shows that at pH 3.2 the deprotonation function Q_M-bar of zero indicates that no protons have been displaced due to complexation. For pH values above 3.41, the deprotonation function Q_M-bar rapidly rises to intersect the protonation curve (n-bar) at a pH of 4.43, reaching a maximum value of about 2.01 at pH 5.03. This indicates that metal-assisted deprotonated MLH_{-1} and MLH_{-2} are being formed although Z_M-bar shows is not fanning back at pL 5.0. Above pH 5.03, the Q_M-bar curve runs parallel to the protonation curve, indicating no complexation being formed.

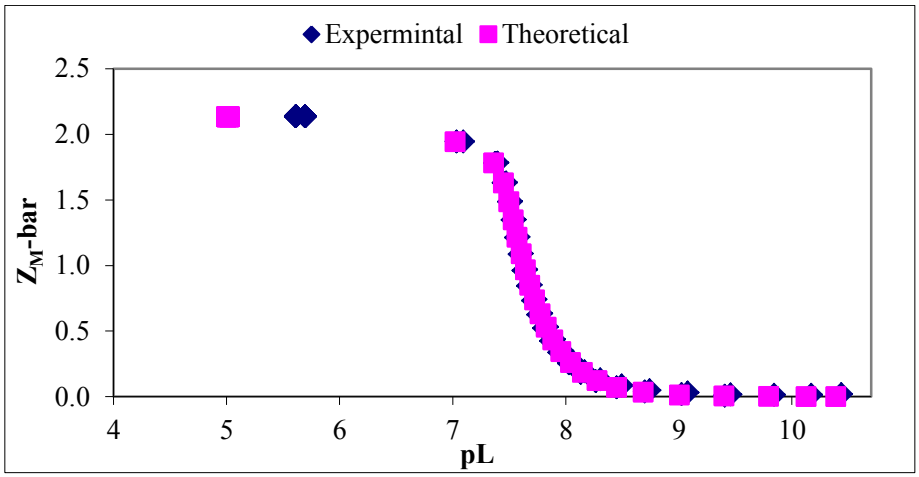

(a)

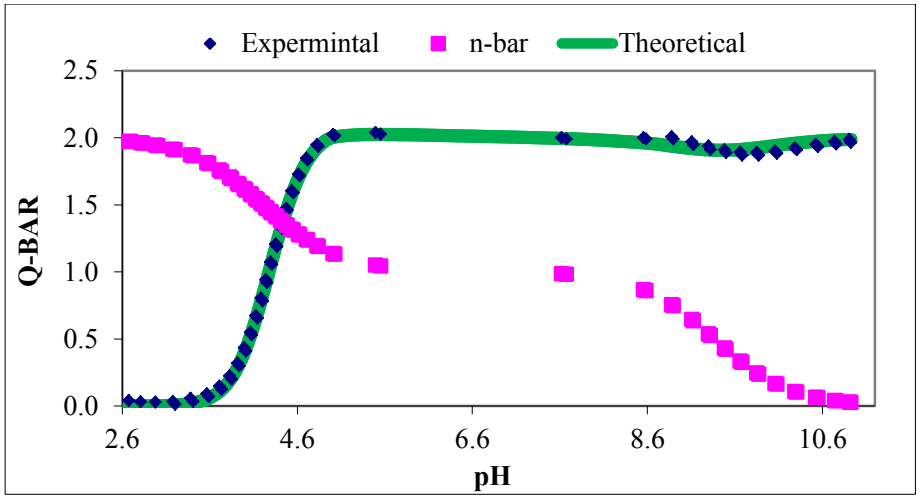

(b)

Figure 3.19 (a): Z_M-bar as a function of pL for Cu(II)-[H(56)NH_2] Complex. **(b):** Q_M-bar as a function of pH Cu(II)-[H(56)NH_2] Complex.

The standard deviations are reasonably low, and the Hamiltonian R-factor is low thus giving confidence for the model chosen in Table 3.11.

Table 3.11: Stability constants (log β_{pqr}) for Cu(II) of [H_2(565)NH_2] complexes. β_{pqr} = $[M_pL_qH_r]/[M]p[L]q[H]r$, I = 0.15 mol.dm^{-3} (NaCl), T = 25 ºC. S. dev denotes standard deviation in log β_{pqr}; R_f^H is the Hamilton R-factor and R_{lim}^H its limit.

Metal	p	q	r	log β_{pqr}	S.dev	R_f^H	R_{lim}^H	$n_T(n_p)$
	1	1	0	6.83	0.07			
Cu(II)	1	1	-1	3.21	0.008	0.009	0.008	2(74)
	1	1	-2	-6.32	0.01			

Figure 3.20 shows the speciation graph for Cu(II)-[H(56)NH_2] system. ML, MLH_{-1} and MLH_{-2} are present in significant levels at different pH values i.e. 11.07% (pH 4.24), 99.60% (pH 7.09) and 95.45% (pH 10.85) respectively.

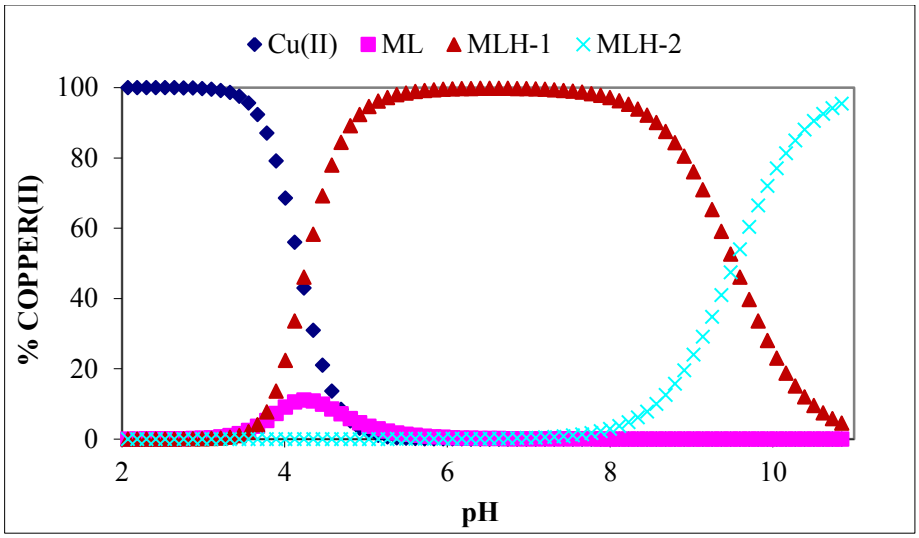

Figure 3.20: The distribution curve for Cu(II)-[H(56)NH_2] Complex. Metal to Ligand ratio 1:2.

3.5.2.2 Ni(II) System

Several of Ni(II)-systems in this study were kinetically slow. This was shown by a drift in pH and measurements could only be taken after a stable pH was reached. These data were analysed with the ESTA suite of programs, the results are given in Table 3.12 in the

same way as for the Cu(II)-systems and will not be discussed. The Z_M-bar, Q_M-bar and speciation curves are presented in appendix Figure A1-A15.

Table 3.12: Stability constants (log β_{pqr}) for Ni(II) of [H(555)NH_2], [H(555)NMe_2], [H_2(555)NH_2], [H_2(565)NH_2] and [H(56)NH_2] complexes. β_{pqr} = $[M_pL_qH_r]/[M]p[L]q[H]r$, I = 0.15 mol.dm^{-3} (NaCl), T = 25 ºC. S. dev denotes standard deviation in log β_{pqr}; R_f^H is the Hamilton R-factor and R_{lim}^H its limit.

Ligands	p	q	r	log β_{pqr}	S.dev	R_f^H	R_{lim}^H	$n_T(n_p)$
[H(555)NH_2]	1	2	0	14.84	0.02			
	1	1	0	8.02	0.01	0.01	0.01	2(82)
	1	1	-1	-0 .95	0.07			
	1	1	-2	-10.76	0.05			
[H(555)NMe_2]	1	2	0	11.47	0.09			
	1	1	0	6.83	0.02	0.02	0.009	2(71)
	1	1	-1	-1.05	0.06			
	1	1	-2	-12.78	0.1			
[H_2(555)NH_2]	1	1	0	5.98	0.03			
	1	1	-1	-1.48	0.02	0.01	0.01	3(67)
	1	1	-2	-8.33	0.04			
[H_2(565)NH_2]	1	1	0	4.04	0.04			
	1	1	-1	-2.44	0.01	0.01	0.01	5(127)
	1	1	-2	-9.38	0.02			
[H(56)NH_2]	1	1	0	4.98	0.04			
	1	1	-1	-2.55	0.03	0.01	0.01	4(98)
	1	1	-2	-11.37	0.04			

3.5.2.3 Zn(II) System

The Z_M-bar and Q_M-bar functions, as well as the speciation graphs, are given in Figures B1 – B15. The data were analysed by using the ESTA suite of programs and the results are given in Table 3.13. The Z_M-bar function for Zn(II) with [H_2(555)NH_2] and

[H_2(565)NH_2] systems levelling off to a value of 1.0, clearly indicates the formation of ML as the predominant species. In the other Zn(II)-ligand systems studied, the ML species is never dominant and hence the Z_M-bar curves do not level off at 1.0.

Table 3.13: Stability constants (log β_{pqr}) for Zn(II) of [H(555)NH_2], [H(555)NMe_2], [H_2(555)NH_2], [H_2(565)NH_2] and [H(56)NH_2] complexes. β_{pqr} = $[M_pL_qH_r]/[M]p[L]q[H]r$, I = 0.15 mol.dm^{-3} (NaCl), T = 25 ºC. S. dev denotes standard deviation in log β_{pqr}; R_f^H is the Hamilton R-factor and R_{lim}^H its limit.

Ligands	p	q	r	log β_{pqr}	S.dev	R_f^H	R_{lim}^H	$n_T(n_p)$
[H(555)NH_2]	1	1	0	6.41	0.01			
	1	1	-1	-0.51	0.02	0.01	0.01	2(92)
	1	1	-2	-10.46	0.02			
[H(555)NMe_2]	1	1	0	5.41	0.12			
	1	1	-1	-1.13	0.05	0.01	0.01	2(37)
	1	1	-2	-9.93	0.08			
[H_2(555)NH_2]	1	1	0	5.11	0.05			
	1	1	-1	-2.77	0.05	0.01	0.007	2(36)
	1	1	-2	-11.31	0.08			
[H_2(565)NH_2]	1	1	0	3.68	0.02			
	1	1	-1	-4.32	0.01	0.01	0.01	4(100)
	1	1	-2	-12.45	0.02			
[H(56)NH_2]	1	1	0	3.98	0.09			
	1	1	-1	-3.37	0.02	0.01	0.01	4(99)
	1	1	-2	-12.62	0.02			

3.5.2.4 Discussion – Stability and Structure of Complexes

The five ligands used in this study were chosen to test the effect of the number of amide groups and the effect of methyl substitution upon the stability of the metal complexes. All five ligands have the same N-((pyridin-2-yl)methyl)acetamide moiety. The calculated equilibrium constants are given in Table 3.14

Table 3.14: Stability constants (log β_{pqr}) for Cu(II) of [H(555)NH_2], [H(555)NMe_2], [H_2(555)NH_2], [H_2(565)NH_2] and [H(56)NH_2] complexes. β_{pqr} = $[M_pL_qH_r]/[M]p[L]q[H]r$, I = 0.15 mol.dm^{-3} (NaCl), T = 25 ºC.

Ligands	p	q	r	log β_{pqr}
[H(555)NH_2]	1	1	1	13.89
	1	1	0	11.81
	1	1	-1	7.45
[H(555)NMe_2]	1	1	0	10.90
	1	1	-1	6.18
	1	1	-2	-3.63
[H_2(555)NH_2]	1	1	1	12.80
	1	1	0	9.39
	1	1	-1	2.71
	1	1	-2	-5.27
[H_2(565)NH_2]	1	1	1	10.04
	1	1	0	5.93
	1	1	-2	-3.06
[H(56)NH_2]	1	1	0	6.83
	1	1	-1	3.21
	1	1	-2	-6.32

The effect of methyl substitution is shown by a comparison of the formation constants for the mononuclear ML species of [H(555)NH_2] and [H(555)NMe_2], which are the same except for the two terminal methyl groups. Addition of the methyl groups decreases the stability of the Cu(II) complex from 11.8 to 10.9. The reason for this could be inductive or steric. The inductive effect is shown by the protonation constants, as H^+ is too small to have a steric effect. The difference in protonation constants (log β_{011}) for these two ligands is ~0.4, which is too small to account for the difference in the Cu(II) complex stability. Hence the predominant effect must be steric.

The effect of the amido group is shown by comparing [555-N][31], [H(555)NH_2] and [H_2(555)-NH_2]. All three ligands have the same structure but [555-N] has no amide group, [H(555)NH_2] has one amide group and [H_2(555)-NH_2] has two amide groups. The three stability constants are 18.62, 11.81 and 9.39 respectively. This shows that the amide group decreases the stability of the complex substantially. This result is not unexpected as it is in complete accordance with the base-weakening effect of the CONH-group.[33] Again this could be an inductive effect or the actual structures of the different complexes could be different. This is shown by comparing [H_2(555)NH_2] and [H_2(565)-NH_2]. When the second amido group is moved so that the two carbonyls are no longer adjacent the stability decreases from 9.39 to 5.93. Since in [H_2(565)-NH_2] the carbonyl is closer to the terminal amine, the basicity of the amine decreases from 8.96 to 8.08, a change of 0.9 log units. This change is not big enough to account for the decreased stability of the Cu(II) complex. Rather there must be a change in coordination geometry. For this reason we need to discuss the possible geometries of the different species, remembering however, that thermodynamics tells us about the stability of the complex and not its structure. This structure has to be inferred from comparison with related complexes of known structure or determined spectroscopically.

Ligands used in this study have four main electron donor atoms; amino nitrogen (amine-N); amide nitrogen (amide-N); pyridine nitrogen (pyridyl-N) ; amide carbonyl (amide-O) and hydroxide oxygen (OH^-); water oxygen (H_2O).

3.5.2.4.1 The structures of [H(555)NH_2] and [H(555)NMe_2]

The MLH formation constants for [H(555)NH_2] is 13.89. Proposed structures of this complex are given in Figure 3.21. They are formed by the coordination of one/two amino-N's with the pyridyl-N protonated or by the pyridyl-N with the amino group protonated. The amide-O is also coordinated. Of the two structures, a(i) seems a more likely coordination geometry than structure a(ii) due to the formation of stable 5,5 membered chelate rings rather than 7,5 chelate rings. In addition the pK_a of this species (MLH $\rightleftharpoons$ ML + H) is ~2, which is close to the pK_a of the pyridine. However, coordination through the pyridyl-N is also feasible and has been demonstrated for Cu(II) *N,N'*-di(aminoethylene)-2,6-pyridine-dicarbonylamine (Figure 3.31)[38], where coordination is *via* one amino-N, the pyridyl-N and the amide-O. The other amine group is protonated.

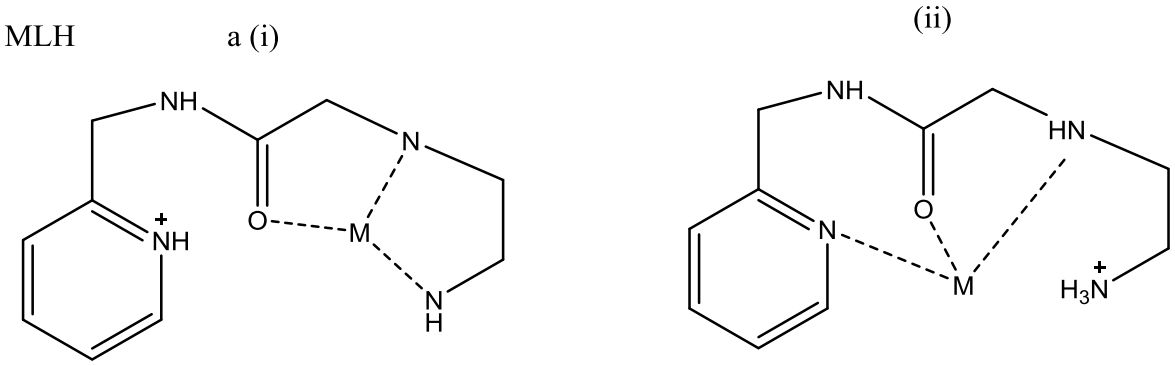

Figure 3.21: Possible structures for MLH of Cu(II)- [H(555)NH_2] system.

The log β_{110} values for ML in Cu(II)-[H(555)-NH_2] and Cu(II)-[H(555)-NMe_2] are 11.81 and 10.90 respectively. This is much higher than the stability of $[Cu(II)(NH_3)]^{2+}$ (4.8), suggesting that the ligands are not monodentate. In fact the log β_{110} values are similar to the log β_{110} value for the $[Cu(II)(en)]^{2+}$ (10.5), suggesting that the ligands have a similar binding mode. However, since the basicity of ethylenediamine is less than our two ligands one would expect its Cu(II) complexes to be more stable. In fact they are ~ 1 log unit more stable, implying that there is an extra weak binding in these complexes. Figure 3.22 b(i) and b(ii) show possible structures for these complexes. The weak binding is due to a pyridyl -N and an amide-O present in these ligand systems giving these complex species extra stability. The formation of three stable membered chelate rings, as shown in structures Figure 3.22 b(i), are responsible for the increase stability. Even though both structures 3.22 b(i) and b(ii) are coordinated *via* 3N they have smaller log β_{110} than $[Cu(II)(dien)]^{2+}$ (15.9). This is consistent with the amino (-NH_2) group being a stronger base than pyridine. Of the two possible structures, we prefer 3.22b(i) because it has two amine-N's coordinated giving rise to 2 five membered and 1 seven membered chelate rings. In addition, in structure 3.22b(ii) the amide, whose pK_a is ~15 is deprotonated rather than the amine, which has a pK_a of ~9.

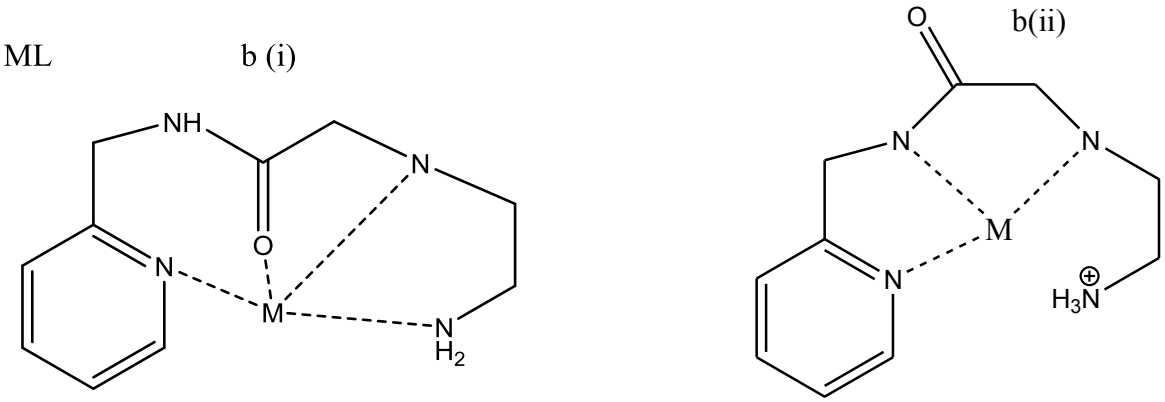

Figure 3.22: Possible structures for ML of Cu(II)-[H(555)NH_2] and [H(555)NMe_2] systems.

Based on the two possible structures for ML, the transformation to MLH_{-1} could form by deprotonation and coordination of the terminal amine or a swap from O to N coordination of the amide. The pK_a for this process (log β_{110} – log β_{11-1}) is 4.36 and 4.72 for Cu(II)-[H(555)-NMe_2] and Cu(II)-[H_2(555)-NH_2] respectively. This can be compared to the same process occurring with 3,5-diaminodiamido-4-oxahexacyclododecane (cageL) (pK_a = 5 for the process log β_{110} – log β_{111}) where it is known that coordination is accompanied by deprotonation of the terminal amine.[39] However, this is also the range expected for metal-assisted deprotonation of the amide proton.[24,40,41] Both of these process give the same structure for MLH_{-1} (Figure 3.23 c(i)). This is the same geometry that was suggested for Cu(II)-[H(555)N]H_{-1}.[31]

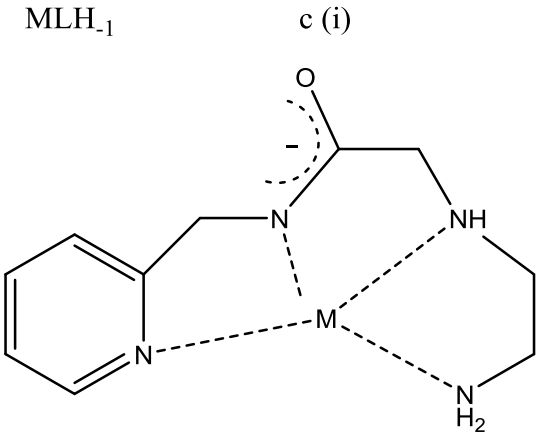

Figure 3.23: Possible structures for MLH_{-1} of Cu(II)-[H(555)NH_2] and [H(555)NMe_2] systems.

The pK_a value determined for MLH_{-1} the Cu(II)-[H(555)NMe_2] system ($CuLH_{-1} \rightleftharpoons CuLH_{-2}+H^+$) is 9.81. This is higher than the pK_a for $[Cu(H_2O)_6]$ (8.00) and is presumed to be associated with deprotonation of an axially coordinated water molecule. Note the structure for MLH_{-1} does not have any equatorial waters.

3.5.2.4.2 The Structures of $[H_2(555)NH_2]$

The postulated structures of the MLH species in $[H_2(555)NH_2]$ are shown in Figure 3.24, where a(i) is more favourable than structure a(ii). The equilibrium constant of the reaction M + LH $\rightleftharpoons$ MLH is ~ 4. Given the basicity of the pyridine, this value is too high for monodentate coordination (2-methylpyridine, pK_a =6.14; 1og β_{110} = 1.69).[23,42] The obtained value suggests predominant pyridine coordination (perhaps together with weak coordination of the amide-O) in this species. The terminal amine is still protonated giving the correct stoichiometry.

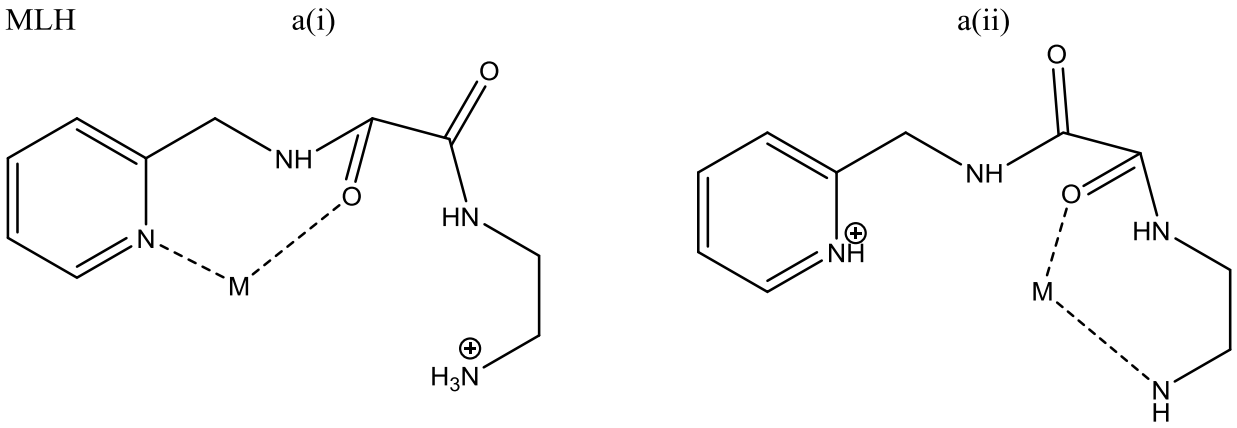

Figure 3.24: Possible structures for MLH_{-2} of Cu(II)-$[H_2(555)NH_2]$ system.

Loss of a proton from MLH gives rise to the ML complex. A possible structure of ML is depicted in Figure 3.25b. The complex is formed at pH 6 which means that the amine must either be coordinated or protonated. While this structure has the amine-N and the pyridyl-N both coordinated it has a very large chelate ring. Copper binding constants are 9.96 for Cu(II) cageL (pK_{a1}= 9.52; pK_{a2}= 8.28) which forms 7 and 8 membered rings; and 8.6 for 1,4-butylenediamine (pK_{a1}= 10.72; pK_{a2}= 9.44) which form 7 membered chelate rings.[39,43] The increase in basicity of the amines should increase the stability of the complex but this is countered by the decrease in chelate effect.

A possible structure for MLH_{-1} is depicted in Figure 3.25c. The pK_a of CuL in solution, $CuL \rightleftharpoons CuLH_{-1}+H^+$, is 6.68. This can be compared to the same process occurring with Cu(II) glycinamide (pK_a 6.8), where it is known that deprotonation causes exchange from the amide-O to the amide-N.[44] Similarly, Odisitse *et al*.[39] have proposed a structure in which deprotonation of an amide occurs at pH 5.5.

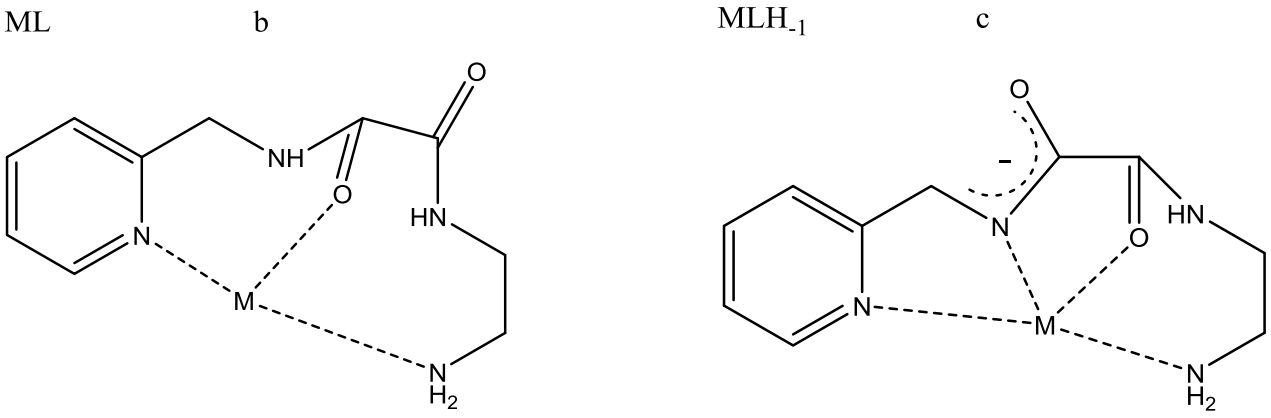

Figure 3.25: Possible structures for **(b)** ML and **(c)** MLH_{-1} of Cu(II)-[H_2(555)NH_2] system.

The pK_a value corresponding to the deprotonation of MLH_{-1} is 7.98. This could be due to metal-assisted deprotonation and coordination of the second amide[25,45] or loss of a proton from a coordinated water molecule. Even though the hydrolysis constant of $Cu(H_2O)_6$ is 8.0 we believe that deprotonation of the amide has occurred. The structure of the resulting complex is given in Figure 3.26.

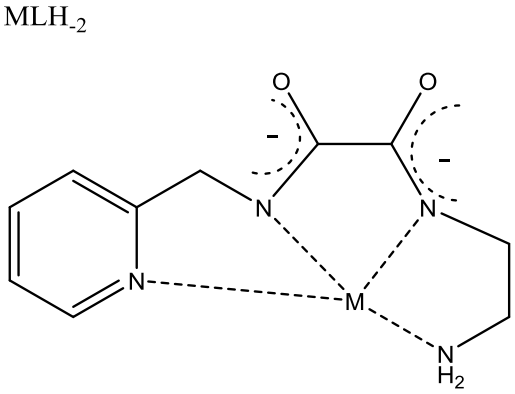

Figure 3.26: Possible structures for MLH_{-2} of Cu(II)-[H_2(555)NH_2] system.

3.5.2.4.3 The Structures of $[H_2(565)NH_2]$

The proposed structures of the MLH species for the Cu(II)-$[H_2(565)\text{-}NH_2]$ system is given in Figure 3.27a (i and ii). The species MLH is not very stable and is present in very low concentration. Log K for the equilibrium M + LH $\rightleftharpoons$ MLH is 1.96. This is quite similar to the stability of 2-methylpyridine, log β_{110} = 1.69.[42] Structures in Figure 3.27 a (i and ii) have the metal bi- or tri-dentate coordinated to one the pyridyl-N and one/two the amide-O. The terminal amine is still protonated. In the postulated structure given in Figure 3.27 a(i), a pyridyl-N and one amide-O donor are coordinated forming a 7 chelate ring system. However, the feasibility of this structure is unlikely based on the low stability of the chelate rings. The structure given in Figure 3.27 a(ii) is favoured because of formation of two chelate rings in contrast with the one chelate ring of structure 3.27 a(i). Further support for this conclusion comes from the demonstration that with [Cu(II)en] (log β_{110} = 10.5) where two donors are present, log β_{110} is 0.46 log units higher than log β_{111} = 10.04.

MLH a(i) a(ii)

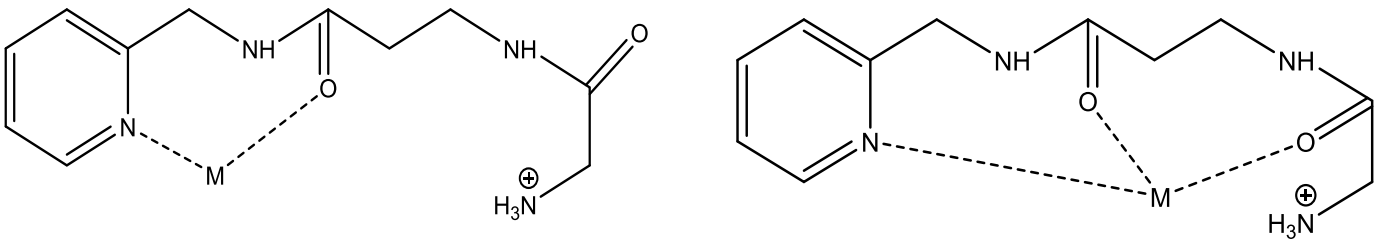

Figure 3.27: Possible structures for MLH of Cu(II)-$[H_2(565)NH_2]$ system.

In the formation of the ML species from MLH, the ML could be formed by deprotonation of the terminal amine to give structure 3.28b(ii). Alternatively, one of the amides could deprotonate to give structure 3.28b(i) where the second amide-O is coordinated. The pK_a for this process CuLH $\rightleftharpoons$ CuL +H is 4.36. Again this can be compared to the same process occurring with glycinamide (pK_a 6.8) where it is known that coordination exchanges from the amide-O to the amide-N.[44] For $[H_2(555)NH_2]$ the pK_a was 6.68 while here it is 2.4 log units lower. This could be due to the position of the second amide group which changes the size of the chelate ring. Comparing 1,2-ethylenediamine (pK_{a1} =9.89; pK_{a2} =7.08), 1,3-propylenediamine (pK_{a1} = 10.56; pK_{a2} = 8.76) and 1,4-butylenediamine

(pK_{a1} =10.72; pK_{a2} =9.44), which form 5, 6 and 7 membered chelate rings respectively, the copper binding constants are 10.5, 9.7 and 8.6, respectively.[43,39] The increasing basicity of the amines should increase the stability of the complex but this is countered by the decreased chelate effect. ML of the Cu(II)-[H_2(565)NH_2] complex starts to form just past pH 3 and rapidly reaches a maximum value over a small pH range of less than 1.5 units. This means once the first coordination bond is formed, the chelate effect will aid in formation of the next coordination bonds to the central Cu(II) ion. However, from the potentiometric data we cannot distinguish between these structures.

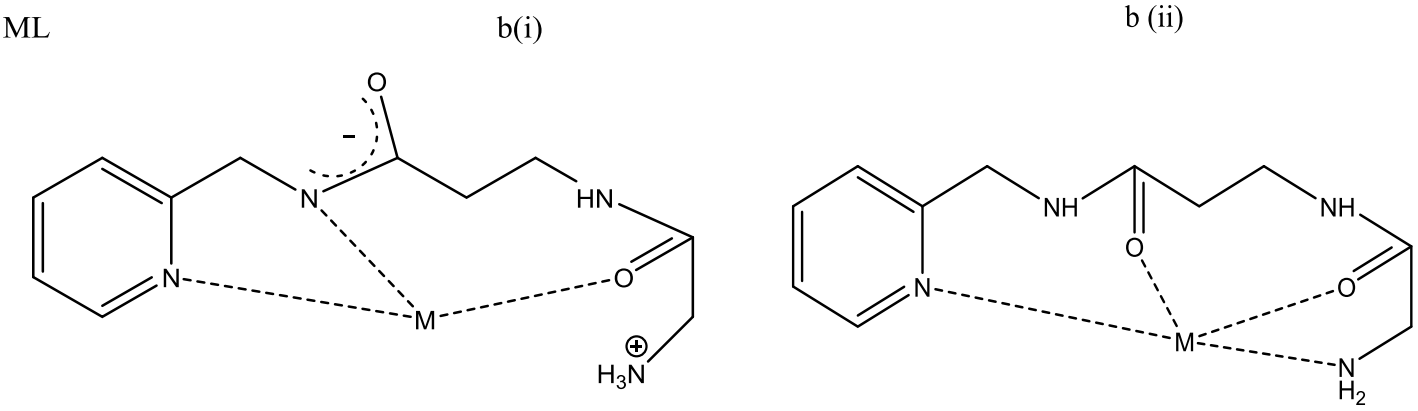

Figure 3.28: Possible structures for ML of Cu(II)-[H_2(565)NH_2] system.

The MLH_{-2} is the predominant species of Cu(II)-[H_2(565)NH_2] with deprotonation and coordination of two amide-N's to give the structure 3.29c. The log*K* for the equilibrium $M + LH_2 \leftrightarrow MLH_{-2}$ is 9.4. The formation of MLH_{-2} complex is observed at high pH. This species is formed when all the four nitrogens in the ligand are coordinated to the metal ion thus making a 5,6,5 membered ring. It is reported that an increase in number of chelate rings around the metal ion results in large girdle strains, thus influencing the stability of complexes formed.[46] However the formation constants determined for Cu(II)-[H_2(565)NH_2] showed a somewhat lower coordination ability of MLH_{-2} species compared to the analogous ligands containing an imidazole ring, a methyl group, or having additional O-donor group(s) (amide and/or carboxylate). For instance glycylglycylhistamine (ggha)[47], alanylglycyl-histamine (Ala-Gly-Ha)[48], and Gly-Gly-His[49,50], formation constants have been reported as: log β_{11-2} ~ -2.48; -2.86; and -1.80 respectively. Also Cu(II)-[H_2(565)NH_2] has higher coordination with log β_{11-2} = -3.06 compared to the analogous ligand containing pyridine ring

$[H_2(556)\text{-}N]$[27] which has shown log $\beta_{11\text{-}2}$ = -4.09. The difference can be attributed to the basicity of an imidazole and weak axial coordination of the O-donor group. The analogous ligands bearing side chain substituents are given in Figure 3.31.

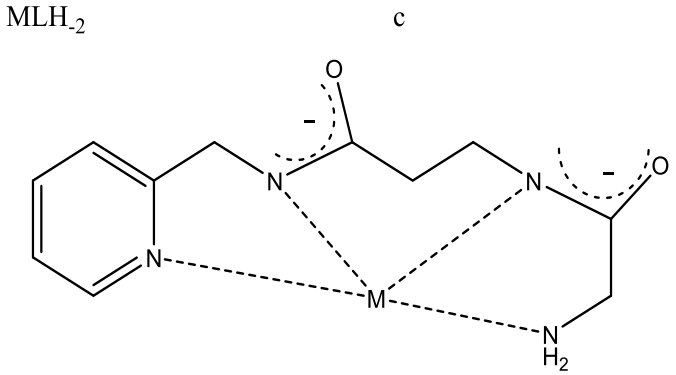

Figure 3.29: Possible structures for MLH_{-2} of Cu(II)-$[H_2(565)NH_2]$ system.

3.5.2.4.4 The Structures of $[H(56)NH_2]$

The log β_{110} value for an ML in the Cu(II)-$[H(56)NH_2]$ (6.83) is observed to be similar to the log β_{110} value for ML of GlyGlyHis (7.60).[51] This supports binding of the amino-N, a pyridyl-N, and an amide-O to the metal ion. Thus structure a(i) in Figure 3.30 is more likely than a(ii). The formation of the MLH_{-1} species could then arise from deprotonation of the amide group. The pK_a for this reaction (log β_{110} – log $\beta_{11\text{-}1}$) is 3.62, in the range expected for metal-assisted deprotonation of the amide proton[24,31,41], rather than a water molecule from the coordination sphere of the complex. The ligand is postulated to coordinate to Cu(II) ion through three nitrogen donor atoms leaving two axial sites occupied by water molecules. The structure is given in Figure 3.30b. The pK_a value determined for MLH_{-2} system (log $\beta_{11\text{-}1}$ – log $\beta_{11\text{-}2}$ = 9.53) is assigned to deprotonation of an axial water molecule. This pK_a is higher than that $[Cu(H_2O)_6]$ (8.00), but this is ascribed to the fact that in $[Cu(H_2O)_6]$ an equatorial water proton is deprotonated rather than an axial water. This would therefore suggest the postulated structure shown in Figure 3.30c as the most likely for the MLH_{-2} complex species.

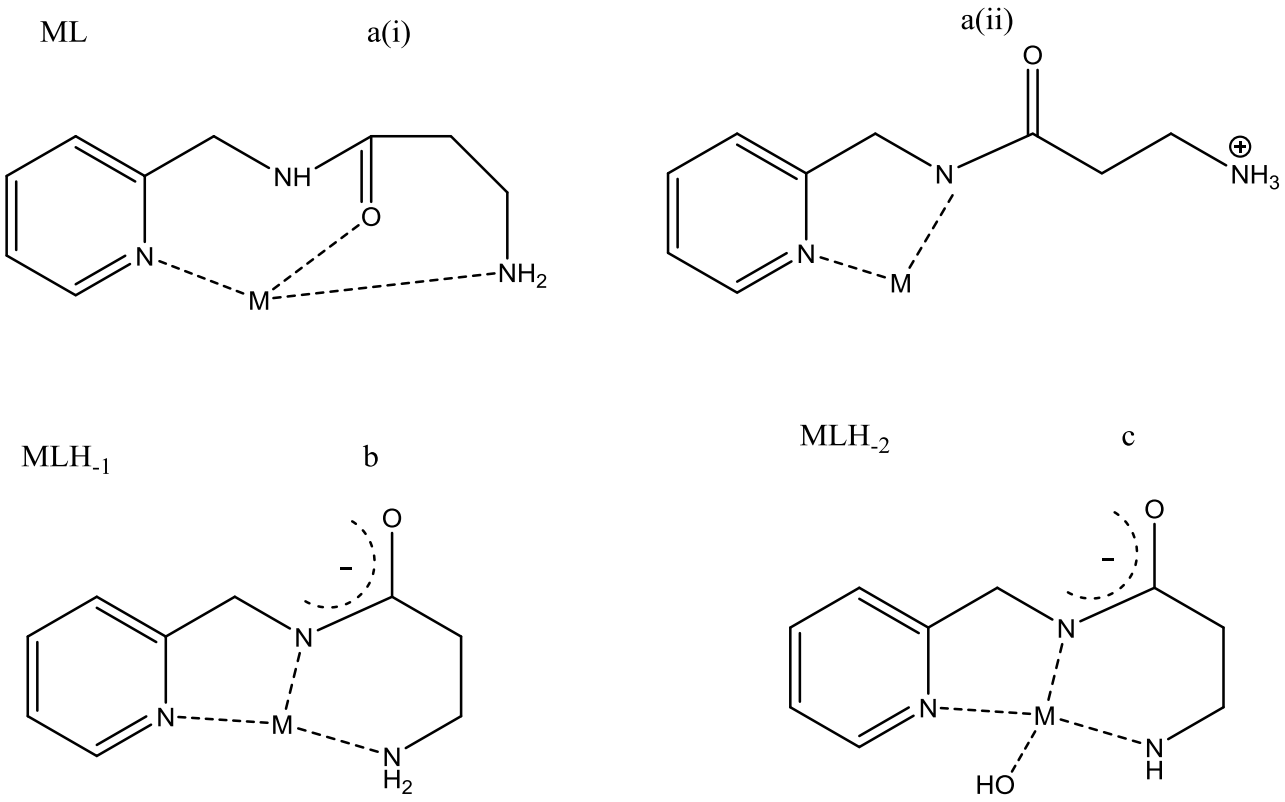

Figure 3.30: Possible structures for (a) ML, (b) MLH_{-1} and (c) MLH_{-2} of Cu(II)-[H_2(565)NH_2] system.

The potentiometric results alone cannot unambiguously predict the correct structure of a complex in solution. To get more evidence of the solution structures formed between Cu(II) and these ligand systems, as well as the coordination geometry of these structures, they have also been determined spectroscopically and these will be discussed in detail in chapter four.

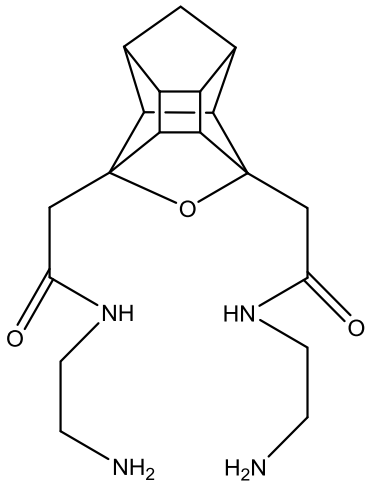

CageL

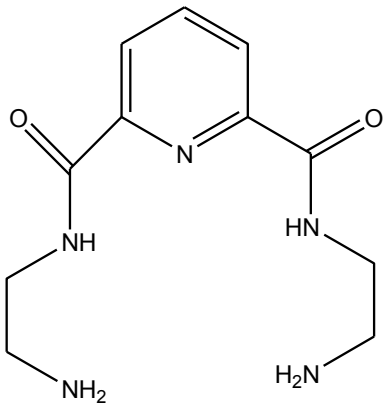

N,N'-di(aminoethylene)-2,6-pyridine-dicarbonylamine

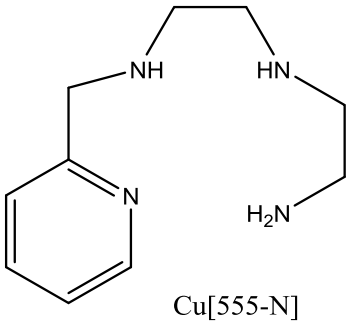

Cu[555-N]

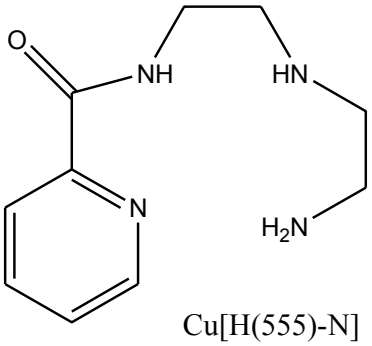

Cu[H(555)-N]

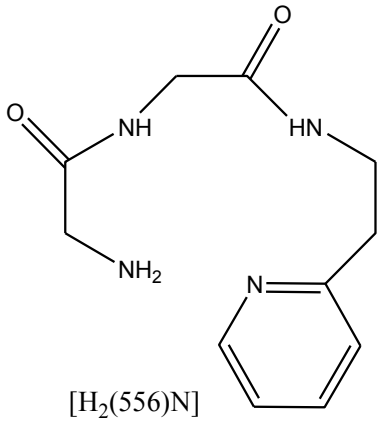

[H_2(556)N]

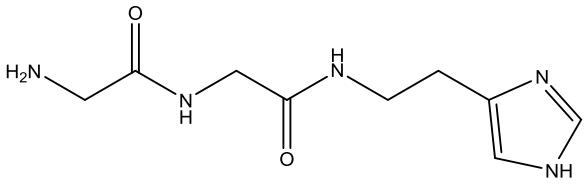

Gly-Gly-Ha

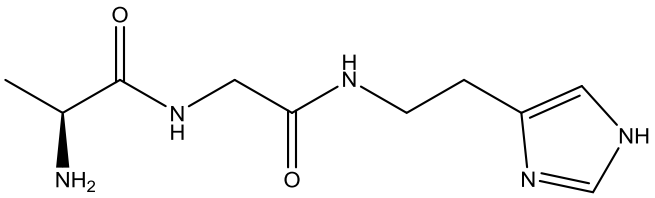

Ala-Gly-Ha

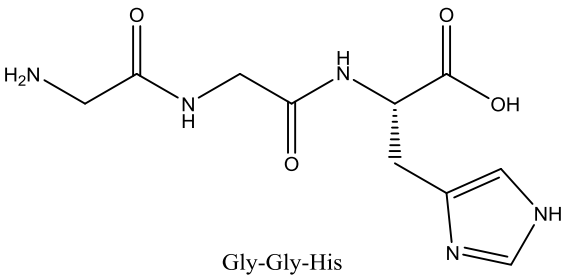

Gly-Gly-His

Figure 3.31: Some analogous ligands mentioned in the discussion.

3.5.2.4.5 Possible Structures of Ni(II) and Zn(II) Complexes

The formation equilibria for Ni(II) and Zn(II) show that these metal ions also form relatively stable complexes with $[H(555)NH_2]$, $[H(555)NMe_2]$, $[H_2(555)\text{-}NH_2]$, $[H_2(565)NH_2]$ and $[H(56)NH_2]$ although their stability is lower than that of Cu(II). The equilibrium constants for Ni(II) and Zn(II) are shown in Tables 3.12 and 3.13. Trends in these equilibrium constants are in accordance with the Irving-Williams stability series.[52] Although Zn(II) is a weaker chelators than Cu(II), the *in vivo* concentration of this essential metal ions is much higher than that of Cu(II) and so could potentially compete for the ligands. For example, the stability constants (log β's) of the ML species of $[H(555)NH_2]$ with Cu(II), Ni(II) and Zn(II) are 11.81, 8.02 and 6.41, respectively. The difference in stability of some 4-5 log units is observed between Cu(II) and the *in vivo* competitors Ni(II) and Zn(II). This indicates the metal ion's reduced affinity for complexation and lower binding strength of the ligand $[H(555)NH_2]$ towards Ni(II) and Zn(II).

A noticeable feature about the complexation of $[H(555)NH_2]$ and $[H(555)NMe_2]$ with these two metal ions is the prevalence of the ML_2, ML, ML_{-1} and MLH_{-2} species. For the ML species, the difference in stability observed between Cu(II), Ni(II) and Zn(II) with $[H(555)NH_2]$ and $[H(555)NMe_2]$ were 3 - 5 log units. The explanation for this observation is that the arrangement of the ligand donor atoms is such that the metal ion is constrained to adopt the square planar coordination geometry. Zn(II) prefers a tetrahedral coordination geometry as observed in the majority of its simple systems[53] and in biological metallo-enzymes.[54] In such enzymes, the Zn(II) ion is coordinated to three nitrogen atoms while a water molecule occupies the fourth coordination site constituting the tetrahedral arrangement of donor atoms. On the other hand, Cu(II) and Ni(II) prefers a tetragonally distorted or square planar arrangement of ligand(s) donor atoms around the metal ion.[55-59]

In the deprotonation of ML to form MLH_{-1} species, the calculated pK_a values for the complexation of $[H(555)NH_2]$ and $[H(555)NMe_2]$ with Ni(II) were 8.97 and 6.92, respectively and 7.88 and 6.54, respectively for Zn. For Ni(II), these pK_a values were 0.9-2.0 log units lower than the first hydrolysis constant of Ni(II) ($pK_{M\text{-}OH} = 9.86$).[60] Furthermore, the pK_a values of the formation of MLH_{-1} species for Zn(II) were 2.3-2.6 log units lower than the first hydrolysis constant of Zn(II) ($pK_{M\text{-}OH} = 9.17$).[60] This implies that it is the amide that is being deprotonated. While the MLH_{-1} species could be attributed to deprotonation of the

amide group, the MLH_{-2} species are a result of the ionisation of coordinated water molecules. We conclude this because the pK_a for this process is very similar to the hydrolysis constant of the respective metal ions. For Ni(II) the pK_a values are 9.81 and 11.73 for $[H(555)NH_2]$ and $[H(555)NMe_2]$, respectively. For Zn(II) the pK_a values are 9.95 and 8.80.

The ligands $[H_2(555)NH_2]$ and $[H_2(565)NH_2]$ form ML, MLH_{-1} and MLH_{-2} species with Ni(II) and Zn(II). Once again the deprotonation constant of ML suggests that it is the amide that is deprotonated to form MLH_{-1}. Similarly, the calculated pK_a ($\log\beta_{11-1} - \log\beta_{11-2}$) values for the second deprotonation to form MLH_{-2} is also lower than the hydrolysis constant of the respective metal ions. This again suggests that it is an amide that is being deprotonated. Note that this is a different conclusion to the one made for $[H(555)NH_2]$ and $[H(555)NMe_2]$. Here we concluded that the second proton was lost from a coordinated water molecule. The reason for this difference is that $[H(555)NH_2]$ and $[H(555)NMe_2]$ only have one amide group while $[H_2(555)NH_2]$ and $[H_2(565)NH_2]$ have two amide groups.

The coordination of $[H(56)NH_2]$ with Cu(II), Ni(II) and Zn(II) indicates that three different mononuclear species are formed in solution. The ML and MLH_{-1} species form at low pH and the speciation graphs show that there is already complexation at the start of the titration. The calculated pK_a ($\log \beta_{110} - \log \beta_{11-1}$) values were 7.53 and 7.35 for Ni(II) and Zn(II) respectively. These processes are close to the first deprotonation constants of the previous four ligands. Meanwhile the calculated pK_a ($\log \beta_{11-1} - \log \beta_{11-2}$) values for the second deprotonation were 8.82 and 9.25 log units for Ni(II) and Zn(II), respectively. These values are closer to the hydrolysis constant of the metal ion suggesting that the deprotonation comes from a coordinated water molecule in the complex.

References:

1. F. R. Hartley, C. Burgess and R. M. Alcock, *Solution Equilibria*, Ellis Horwood, Chichester, 1980.

2. K. B. Murray and P. M. May, *ESTA, Equilibrium Simulation for Titration Analysis*, University of Wales Institute of Science and Technology, Cardiff, 1984.

3. C. (Carl) Zhang, *Fundamentals of Environmental Sampling and Analysis*, John Wiley & Sons, Inc, New Jersey, 2007.

4. V. Tomi, T. Gopurenko, K. Majorinc and V. Simeon, *Croat. Chem. ACTA*, 2006, **79**, 613–618.

5. T. Nishio, *Biophys. Chem.*, 1998, **71**, 173–84.

6. N. N. Golovnev, O. S. Romanova and N. V. Busygina, *J. Anal. Chem.*, 2000, **55**, 457–460.

7. G. Sharma and J. P. Tandon, *J. Inorg. Nucl. Chem.*, 1970, **32**, 1273–1278.

8. A. E. Martell and R. D. Hancock, *Metal Complexes in aqueous Solutions, Modern Inorganic Chemistry Series*, Plenum Press, New York, 1996.

9. A. E. Martell and R. J. Motekaitis, *Determination and Use of Stability Constants*, VCH, New York, 1988.

10. P. W. Linder, R. G. Torrington and D. R. Williams, *Analysis Using Glass Electrodes*, Open University Press, Milton Keynes, 1984.

11. J. Francis, C. Rossotti and H. Rossotti, *The Determination of Stability Constants, and other Equilibrium Constants in Solution*, McGraw-Hili Book Company, Inc., New York, 1961.

12. M.T. Beck and I. Nagypal, *Chemistry of Complex Equilibria*, Ellis Horwood Limited:, New York, 1990.

13. S. Odisitse, *PhD Thesis*. University of Cape Town, 2006.

14. K. Mokalane, *MSc Thesis*. University of Cape Town, 2011.

15. G. E. Jackson and M. J. Kelly, *J. Chem. Soc. Dalt. Trans.*, 1989, 2429.

16. G. E. Jackson and B. S. Nakani, *J. Chem. Soc. Dalt. Trans.*, 1996, 1373–1377.

17. A. O. Santini, H. R. Pezza, J. E. De Oliveira and L. Pezza, *J. Braz. Chem. Soc.*, 2008, **19**, 162–168.

18. P. M. May, K. Murray and D. R. Williams, *Talanta*, 1988, **35**, 825–830.

19. P. M. May and K. Murray, *Talanta*, 1988, **35**, 927–932.

20. A. Vacca, A. Sabatini and M. A. Gristina, *Coord. Chem. Rev.*, 1972, **8**, 45–53.

21. B. S. Furniss, A. J. Hannaford, P. W. G. Smith and A. R. Tatchell, *Vogel's Practical Organic Chemistry.*, Longman Scientific & Technical., Harlow, 5th edn., 1989.

22. G. Gran, *Analyst*, 1952, **77**, 661–671.

23. S. Odisitse and G. E. Jackson, *Polyhedron*, 2008, **27**, 453–464.

24. C. Jubert, A. Mohamadou, C. Gérard, S. Brandes, A. Tabard and J.-P. Barbier, *J. Chem. Soc. Dalt. Trans.*, 2002, 2660.

25. G. E. Jackson, P. W. Linder and A. Voye', *J. Chem. Soc. Dalt. Trans.*, 1996, 4605–4612.

26. E. T. Nomkoko, G. E. Jackson and B. S. Nakani, *Dalton Trans.*, 2004, 1432–40.

27. J. N. Zvimba and G. E. Jackson, *Polyhedron*, 2007, **26**, 2395–2404.

28. K. S. Bai and A. E. Martell, *J. Am. Chem. Soc.*, 1969, **91**, 4412–4420.

29. M. W. A. Steenland, I. Dierck, G. G. Herman, B. Devreese, W. Lippens, J. Van Beeumen and A. M. Goeminne, *J. Chem. Soc. Dalt. Trans.*, 1997, **6**, 3637–3642.

30. L. E. Kapinos and H. Sigel, *Inorganica Chim. Acta*, 2002, **337**, 131–142.

31. J. N. Zvimba and G. E. Jackson, *J. Inorg. Biochem.*, 2007, **101**, 148–58.

32. A. E. Martell and R. M. Smith, *Critical Stability Constants*, Plenum Press, New York and London, vol. 1., 1974.

33. J. Clark and D. D. Perrin, *Q. Rev. Chem. Soc.*, 1964, **18**, 295–320.

34. F. Khalili, A. Henni and A. L. L. East, *J. Chem. Eng. Data*, 2009, **54**, 2914–2917.

35. A. E. Martell and R. M. Smith, *Critical stability constants*, Plenum Press, New York and London, Vol 2., 1975.

36. M. Kodama, T. Yatsunami and E. Kimura, *J. Chem. Soc. Dalt. Trans.*, 1979, 1783.

37. R. J. Motekaitis, Y. Sun, A. E. Martell and M. J. Welch, *Can. J. Chem.*, 1999, **77**, 614–623.

38. S. Odisitse and G. E. Jackson, *Inorganica Chim. Acta*, 2009, **362**, 125–135.

39. S. Odisitse, G. E. Jackson, T. Govender, H. G. Kruger and A. Singh, *Dalton Trans.*, 2007, 1140–9.

40. D. Chen, Y. Sun, A. E. Martell and M. J. Welch, *Inorganica Chim. Acta*, 2002, **335**, 119–124.

41. M. Amélia Santos, M. Gaspar and M. Teresa Amorim, *Inorganica Chim. Acta*, 1999, **284**, 20–29.

42. A. I. Mishustin, *Russ. J. Inorg. Chem.*, 2008, **53**, 1376–1383.

43. A. E. Martel, R. M. Smith and R. J. Motekaitis, *NIST Critical Stability Constants of Metal Complexes Database*, A&M University college Station, TX, Taxas, 1993.

44. H. Sigel and R. B. Martin, *Chem. Rev.*, 1982, **82**, 385–426.

45. T. A. Zuberbühler and Th. KadenKaden, *Helv. Chim. Acta*, 1968, **51**, 1805–1811.

46. S.-H. Liu and C. Chung, *Polyhedron*, 1984, **3**, 559–566.

47. T. Gajda, B. Henry, A. Aubry and J. Delpuech, *Inorg. Chem.*, 1996, **35**, 586–593.

48. P. Gizzi, B. Henry, P. Rubini, S. Giroux and E. Wenger, *J. Inorg. Biochem.*, 2005, **99**, 1182–92.

49. T. P. A. Kruck and B. Sarkar, *Inorg. Chem.*, 1975, **14**, 2383–2388.

50. S. Lau and B. Sarkar, *J. Chem. Soc. Dalt. Trans.*, 1981, **4**, 491.

51. K. Várnagy, J. Szabó, I. Sóvágó, G. Malandrinos, N. Hadjiliadis, D. Sanna and G. Micera, *J. Chem. Soc. Dalt. Trans.*, 2000, 467–472.

52. H. Irving and R. J. P. Williams, *J. Chem. Soc.*, 1953, 3192.

53. T. Koike and E. Kimura, *J. Am. Chem. Soc.*, 1991, **113**, 8935–8941.

54. E. Kimura, T. Shiota, T. Koike, M. Shiro and M. Kodama, *J. Am. Chem. Soc.*, 1990, **112**, 5805–5811.

55. S. Mukhopadhyay, D. Mandal, D. Ghosh, I. Goldberg and M. Chaudhury, *Inorg. Chem.*, 2003, **42**, 8439–45.

56. C. Anitha, C. D. Sheela, P. Tharmaraj and R. Shanmugakala, *Int. J. Inorg. Chem.*, 2013, **2013**, 1–10.

57. A. S. Gaballa, *J. Chem. Pharm. Res.*, 2013, **5**, 206–217.

58. R. A. Schoonheydt, F. Velghe, R. Baerts and J. A. N. B. Uytterhoeven, *Clays Clay Miner.*, 1979, **27**, 269–278.

59. M. Hakimi and T. S. Aliabadi, *World Appl. Program. J.*, 2012, **2**, 431–443.

60. C. F. Baes and Jr., R. E. Mesmer., *The hydrolysis of cations*, Wiley-Interscience publication., New York, 1976.

Chapter Four

Ancillary Studies and Molecular Mechanics

4.1 UV - Visible spectroscopy

4.1.1 Introduction

Spectroscopy is a technique that measures the interaction of molecules with electromagnetic radiation.[1] The UV-visible range of the electromagnetic spectrum covers the range 200–800nm (depending on the detector type).[2] The interaction of electromagnetic radiation of wavelength in the UV-visible region with transition metal chelates gives rise to UV-visible spectra of these complexes. Transition metal complexes give rise to a fascinating variety of colours. These colours come from electronic transitions between energy levels whose spacings correspond to the wavelengths of visible light. Since this spacing of transition depends on factors such as the geometry of the complex, the nature of the ligands present, and the oxidation state of the central metal atom, electronic spectra of complexes can provide valuable information related to bonding and structure.[1,3] The ultraviolet and visible spectra of coordination compounds of transition metals involve transitions between the d orbitals of the metals. These transitions are frequently referred to as d-d transitions because they involve molecular orbitals that are mainly metal d in character.

Absorption spectroscopy is usually performed with molecules dissolved in a transparent solvent. The absorbance of a solute depends linearly on its concentration and, therefore absorption spectroscopy is ideally suited for quantitative measurements. The wavelength of absorption and the strength of absorbance of a molecule depend not only on the chemical nature but also on the molecular environment of its chromophores. Therefore, absorption spectroscopy is an excellent technique for following ligand-binding reactions, enzyme catalysis and conformational transitions in proteins and nucleic acids.[4] As a result, UV-visible spectrophotometry is used as a supplementary technique to glass electrode potentiometry when ionic equilibria are investigated.

4.1.2 Theory

Studies of electronic spectra of metal complexes provide information about structure and bonding. The absorption bands caused by the promotion of an electron from a lower to a higher d orbital of the metal ion are labelled as d → d bands. The relative intensities of absorption bands are governed by a series of selection rules. According to the spin selection rule, transitions between states of different spin multiplicity are forbidden. For example, transitions between $^4A_2$ and $^4T_1$ states are "spin-allowed," but between $^4A_2$ and $^2A_2$ are

"spin-forbidden". The Laporte selection rule states that the only allowed transitions are those with a change of parity, gerade to ungerade (g → u) or ungerade to gerade (u → g) but not g → g or u → u. This would mean that all d-d transitions in octahedral complexes are Laporte forbidden and therefore many complexes will be colourless. However, most ions do not have perfect symmetry, and are distorted so that the centre of symmetry is destroyed, resulting in mixing (hybridization) of d and p orbitals. This d,p mixing leads to a partial break-down of the Laporte selection rule and hence an increase in signal intensity.

Most Cu(II) complexes and compounds show broad absorption band corresponding to the three overlapping transitions $^2A_{2g} \leftarrow {}^2B_{1g}$, $^2B_{2g} \leftarrow {}^2B_{1g}$ and $^2E_g \leftarrow {}^2B_{1g}$ which are spin-allowed transitions characteristic of a d^9 tetragonally distorted Cu(II) complex.[5,6] However, octahedral complexes of Cu(II) (d^9) are appreciably distorted due to the Jahn-Teller effect and so there is more than one peak. These peaks overlap forming a broad and unsymmetrical band. Since this is a d^9 system, the crystal-field splitting is in turn affected by the coordination sphere of copper into lower energy e_g and high energy t_{2g} levels. The nine d electrons are arranged into two levels, i.e. $(e_g)^3$ and $(t_{2g})^6$. Since the e_g level is not symmetrically filled, Jahn-Teller distortion occurs. Thus the complex is distorted.[7]

The Ni(II) ion (d^8) exhibits a variety of coordination geometries giving different electronic-spectra characteristic of these geometries. The most common geometry for this metal ion is an octahedral arrangement of donor atoms around the central metal ion. For octahedral complexes, three spin-allowed transitions[1] are expected which can be assigned in order of energies as:

$$\nu_1 = {}^3T_{2g}(F) \leftarrow {}^3A_{2g}(F),$$
$$\nu_2 = {}^3T_{1g}(F) \leftarrow {}^3A_{2g}(F)$$
$$\nu_3 = {}^3T_{1g}(P) \leftarrow {}^3A_{2g}(F)$$

These absorption bands generally fall within the ranges 7, 000 - 13, 000; 11, 000 - 20, 000 and 19, 000 - 27, 000 cm^{-1} respectively, with intensities less than 30 $dm^3\ mol^{-1}cm^{-1}$ in a regular octahedral system. These three spin-allowed absorption bands, two spin-forbidden bands are often observed, and these correspond to transition to the ^{1}Eg and $^1T_{2g}$. Generally square planar complexes differ from octahedral complexes in the absence of any band below 10, 000 cm^{-1} because the ligand field strength in these complexes is very high.[1]

UV-visible spectroscopy commonly obtains spectra as plots of absorbance versus wavelength. The molar absorptivity is characteristic of the species that is absorbing the light and is highly dependent on wavelength. This wavelength is related to the energy of the absorbed radiation as shown by the equation (4.1):

$$E = h\nu = hc/\lambda \tag{4.1}$$

Where:

E = energy

h = Planck's constant = 6.626 X 10^{-34} J s

c = speed of light = 2.998 X 10^{8} m s^{-1}

ν = frequency (s^{-1})

λ = wavelength (nm)

A measure of the ligand field stabilization energy is given by the equation (4.1). This does not, however, give a direct measure of the strength of bonding, but only the amount by which the degenerate d-orbitals of the metal ion have been split due to the crystal field. Particularly when the study is performed in solution, the spectra do not depend only on structural conditions, but also on environmental elements (nature of the solvent, pH value of the aqueous solutions, *etc*.) which make the acquired spectroscopic data assume a "conditional" character.[8]

The fraction of light absorbed by a species at a certain wavelength is its absorptivity (ε) at that wavelength. UV-visible spectroscopy is used for quantitative analysis, in terms of Beer-Lambert's law, which states that, for a given ideal solution, there is a linear relationship between concentration and absorbance provided that the path length is kept constant. This can be expressed in the following form:

$$\log_{10}\left(\frac{I_0}{I}\right) = \varepsilon cb \tag{4.2}$$

where I_0 and I are the intensities of incident and transmitted radiation respectively, c is the molar concentration in mol dm^{-3} of the absorbing species, b is the optical path length (cm) and ε is the molar absorption coefficient of the absorbing species (dm^3 mol^{-1} cm^{-1}). The term $\log_{10}\left(\frac{I_0}{I}\right)$ is called the absorbance and is represented by the symbol A, with this law

becoming, A = Ɛcb. If the analyte solution is a mixture of different species, the total absorbance at a specific wavelength (A^{λ}) for each individual species can be expressed as:

$$A^{\lambda} = b(\varepsilon_1{}^{\lambda}C_1 + \varepsilon_2{}^{\lambda}C_2 + \varepsilon_3{}^{\lambda}C_3 + \cdots \varepsilon_n{}^{\lambda}C_n)$$

(4.3)

where all the terms are as defined earlier. The molar absorptivities or extinction coefficients are characteristics of the molecular electronic spectra and should be positive and give smooth curve when plotted as a function of wavelength.[9] Equation 4.3 can be simplified to:

$$A^{\lambda} = b\sum \varepsilon_i{}^{\lambda}C_i$$

(4.4)

If A, b and C are known at a particular wavelength, then Ɛ can be calculated at that wavelength. Different species absorb light at different wavelengths and the maximum wavelengths of absorption can be correlated with the structure of the species.

Values of λ_{max} can therefore be used to predict structures of complexes. Billo's method[10] is one of the most popular methods of structure determination using values of λ_{max} for a tetragonally distorted Cu(II) complex with axially coordinated water molecules. The λ_{max} of the d → d band of the Cu(II) complex in spectra of an aqueous solution can be expressed as the sum of individual ligand-field contributions from the four donor atoms which, with Cu(II), define the square planar complex. Calculated λ_{max} is expressed as:

$$\lambda_{max} = \frac{10^3}{n_i \nu_i}$$

(4.5)

where n_i is the number of equatorial donor groups and ν_i is the ligand field of the complex. This equation gives the contribution of each of the four coordinating groups to the calculated absorption frequency.

Several authors[11-15] have used UV-visible to predict the structures of Cu(II) complexes with donor groups located only on the equatorial plane of the distorted octahedron of copper(II) ion.

The electron donor groups and their corresponding ligand fields are given in Table 4.0, according to Billo[10,11,16] and subsequently Sigel and Martin.[17]

Table 4.0: Electron donor groups and corresponding ligand field.

Electron donor groups	Ligand field (vi 10^{-3} cm^{-1})
amino group ν_{NH}	4.60
amide group ν_{N}	4.94
pyridine nitrogen - ν_{py}	4.22
Water ν_{O}	2.96
Carbonyl ν_{O}	2.96
Hydroxide ν_{O}	2.96

4.1.3 Experimental

Aqueous solutions of Cu(II) 1:1, 1:1.5 and 1:2 ratio with $[H_2(555)NH_2]$, $[H(555)NMe_2]$, $[H(555)NH_2]$, $[H_2(565)NH_2]$, and $[H(56)NH_2]$ were prepared over the pH range 2-11. Small amounts of 0.1 mol dm^{-3} NaOH and 0.02 mol dm^{-3} HCl were used to adjust the pH during the titration. A CRISONmicro pH meter equipped with a Metrohm glass electrode was used to measure the pH. The exact amount of NaOH/HCl added was noted. The concentrations of the absorbing species were calculated at every pH. The solutions were kept at a temperature of 25 ^{o}C. The electronic spectra in the aqueous solutions of Cu(II) and Ni(II) complexes were recorded in 1.00-cm quartz cells using a Hewlett Packard 8452A Diode Array Spectrophotometer which was set at 300 -820 nm. A blank (water) was used to correct the absorbance. Since there are different absorbing species in solution at the same time, and their concentration changes with pH, it was necessary to use known concentration of each species (obtained from potentiometry) to deconvolute the spectra. This was done using UV_SPECTRA.EXE, an in-house computer program that uses single value decomposition to solve the set of linear equations. Note that each wavelength is solved independently and so the smoothness of the resultant spectrum of

each species can be used to check the method. In addition, the spectrum of $[Cu(H_2O)_6]^{2+}$ is calculated and compared to the experimental spectrum of this species.

4.1.4 Results and Discussion

4.1.4.1 Cu(II)-L Systems

Colour changes were noticed during the progression of the potentiometric titrations of Cu(II) with all the ligands in this study. This was due to the changing speciation of the solutions with pH, forming different complex species with different absorption spectra. The absorption spectra for these Cu(II)-ligand systems were obtained in the pH range 2-11 and wavelength region 400 - 800 nm.

The wavelengths and molar extinction coefficient values corresponding to maximum absorption of the Cu(II) species formed in solution with ligands of this study together with those calculated as well as those of $[Cu(NH_3)_n(H_2O)_{6-n}]^{2+}$ [18]are given in Table 4.1. The proposed structures for the various species have already been given in Figures 3.21 and 3.30, in Chapter Three. For convenience, structures of some of the literature ligands used in the discussion are given in Figure 4.42.

Table 4.1: UV-visible λ_{max} (nm) and ε_{max} ($dm^3.mol^{-1}.cm^{-1}$) for different Cu-Ligand species. Calculated λ_{max} is from Billo's method using the postulated donor groups.

Ligands	Species	Experimental λ_{max} **(nm)**	ε_{max} **($dm^3.mol^{-1}.cm^{-1}$)**	Calculated λ_{max} **(nm)**	Postulated donor groups
$[H(555)NH_2]$	CuLH	-	-	-	-
	CuL	574	109.15	598	$-NH_2$, N^-, N_{Py},H_2O
	$CuLH_{-1}$	556	149.92	545	$-2NH_2$, N^- , N_{Py}
$[H(555)NMe_2]$	CuL_1	623	101.94	611	$-2NH_2$, N_{Py},CO
	CuL_1H_{-1}	588	118.51	545	$-2NH_2$, N^-, N_{py}
	CuL_1H_{-2}	608	86.6	545	$-2NH_2$, N^-, N_{py},HO^-
$[H_2(555)NH_2]$	CuLH	741	26.87	766	$-N_{py}$, CO , 2 H_2O
	CuL	682	87.98	680	$-NH_2$, N_{Py}, CO,H_2O
	$CuLH_{-1}$	575	58.96	598	$-NH_2$, N^- , N_{Py}, CO^-
	$CuLH_{-2}$	524	121.84	534	$-NH_2$, $2N^-$, N_{Py}
$[H_2(565)NH_2]$	CuLH	746	19.78	766	$-N_{Py}$, 2CO, H_2O
	CuL	747	47.45	766	$-N_{Py}$, 2CO, H_2O
	$CuLH_{-2}$	532	80.03	534	$-NH_2$, N_{Py}, $2N^-$
$[H(56)NH_2]$	CuL	-	-	-	-
	$CuLH_{-1}$	608	70.37	598	$-N_{Py}$, NH_2, N^-, H_2O
	$CuLH_{-2}$	573	67.62	598	$-N_{Py}$, NH_2, N^-, OH^-
NH_3 in $[Cu(NH_3)_n(H_2O)_{6-n}]^+$	CuL	-	-	745(n=1)	-
	$CuLH_{-1}$	-	-	680(n=2) 645(n=3)	-
	$CuLH_{-2}$	-	-	590(n=4)	-

4.1.4.1.1 Cu(II)-[H(555)NH_2]

Figure 4.1 shows the UV-visible electronic spectra of the Cu(II)-[H(555)NH_2] system as a function of pH. At low pH, there is little complex formation and the spectrum is that of $[Cu(OH_2)_6]^{2+}$ with maximum absorption >800 nm. As the pH is increased, the absorption band increases in intensity and shifts to shorter wavelengths. From the potentiometric results, the species formed between pH 2.53 and 3.44 is MLH. Further increase in pH, up to a value of 3.74, causes the absorption band to increase in intensity and shift to shorter wavelengths due to Cu-O to Cu-N bond substitution. From the potentiometric results, the species formed in this region are ML and MLH_{-1}. No further changes were observed in the pH range 7.33 - 8.65.

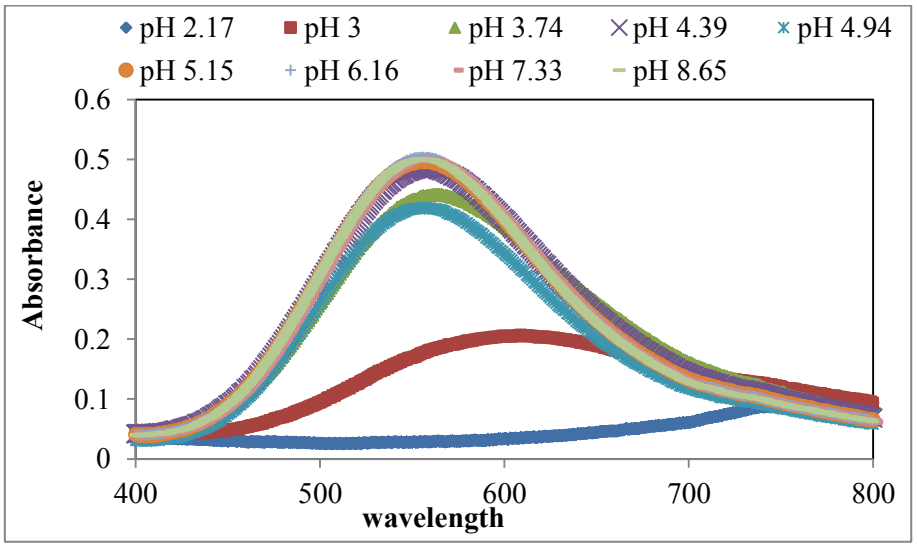

Figure 4.1: UV-visible electronic absorption spectra for Cu(II)-[H(555)NH_2] with [M(0.003 mol dm^{-3})-L(0.006 mol dm^{-3})] at different pH values.

Deconvolution of the spectral data leads to the spectra of the individual species (Figure 4.2). The λ_{max} and molar extinction coefficient (Ɛ) are listed in Table 4.1. Unfortunately, under the conditions of this experiment, the concentration of the MLH species was too low for the spectrum of this species to be calculated. The ML species exhibits λ_{max} = 574 nm and Ɛ = 109.15 dm^3 mol^{-1} cm^{-1}. Using Billo's method, and assuming coordination by a pyridyl-N, an amide-N and an amine-N, the value of λ_{max} is 574 nm. A similar value was found by Odisitse for the ML species (570 nm) of

Cu(II)–*N,N′*-di(aminoethylene)-2,6-pyridine-dicarbonylamine.[11] MLH_{-1} has a λ_{max} of 556 nm and ε = 149.92 dm^3 mol^{-1} cm^{-1}. The shifting in λ_{max} suggests coordination of two amino-N's, a pyridyl-N and an amide-N in a tetragonally distorted arrangement. The similar value was found by Zvimba for the MLH_{-1} species (550 nm) of Cu(II)-[H(555)-N].[12] The calculated λ_{max} for this coordination geometry is 545 nm, which is in good agreement with the experimental value.

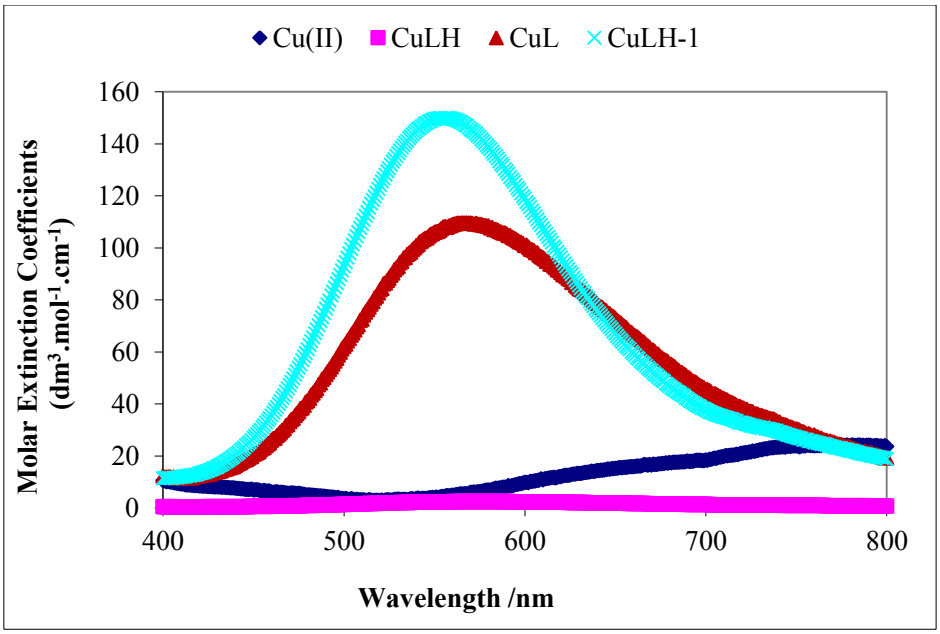

Figure 4.2: Calculated spectra of Cu(II)-[H(555)NH_2] individual species.

4.1.4.1.2 Cu(II)-[H(555)NMe_2]

Figure 4.3 shows the UV-visible electronic spectra of the Cu(II)-[H(555)NMe_2] system as a function of pH. Before the titration by base, complex formation has already taken place at low pH (pH 2.95). The dominant complex species at this pH is CuN_3 with maximum absorption at 623 nm, instead of CuO_6 with H_2O as ligands, which normally forms at such low pH. The band maximum shifts to shorter wavelengths and increases in intensity up to a pH value of 9.01. At pH > 9.01, the intensity decreases with the typical blue shift. The MLH_{-2} is the species in this pH range. From the potentiometric results, we have proposed that this species is derived from the MLH_{-1} species by hydrolysis of a coordinated

water molecule.[13] It is well known that increased axial coordination decreases the energy of the three spin allowed Cu(II) d → d transitions.[19]

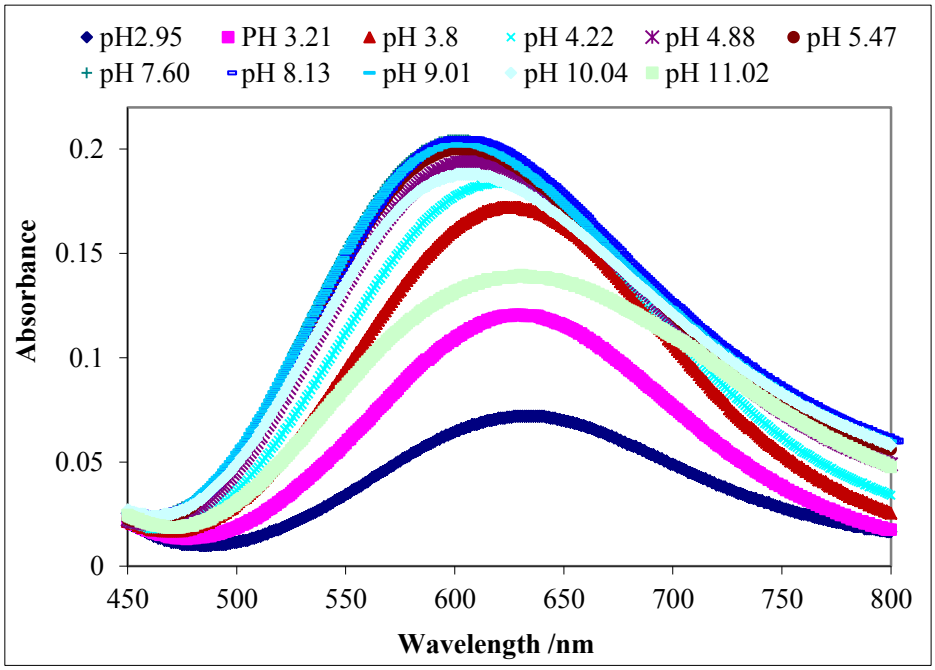

Figure 4.3: UV-visible electronic absorption spectra for Cu(II)-[H(555)NMe$_2$] with [M(0.004 mol dm^{-3})-L(0.006 mol dm^{-3})] at different pH values.

Figure 4.4 and Table 4.2 show the absorption spectra of the experimental species for the Cu(II)-[H(555)NMe$_2$] system. The smooth graphs indicate that the model is appropriate. A single absorption band was observed for each species. The $\lambda_{max}(\varepsilon)$ values for the ML is 623 (101.94) which suggests that Cu(II) coordinates with two amine-N's, a pyridyl-N and an amide-O. This was the same coordination for ML, where L is Bis-(*N,N*-dimethylethyl)-2,6-pyridine-dicarboxamide[11] with λ_{max} (600 nm). λ_{max} 588 (118.51) shifts to a shorter wavelength when MLH$_{-1}$ forms. This is a result of a Cu-O$_{amide}$ to Cu-N$_{amide}$ rearrangement. The λ_{max} value of 580–590 nm is consistent with 4 nitrogens coordination.[12] The alteration of MLH$_{-1}$ to MLH$_{-2}$ is followed by a significant blue shift of the d–d absorption maximum with drop in the molar extinction coefficient. As well as, the observed λ_{max} (MLH$_{-2}$) is 63 nm less than the calculated maximum wavelength. A difference of 63 nm between the calculated and the observed λ_{max} may be due the fact that coordination to hydroxide (-OH$^-$) is axial while coordination to amide-N, two amines-N's and a pyridyl-N are equatorial. Billo's method[10,16] assumes no axial coordination.

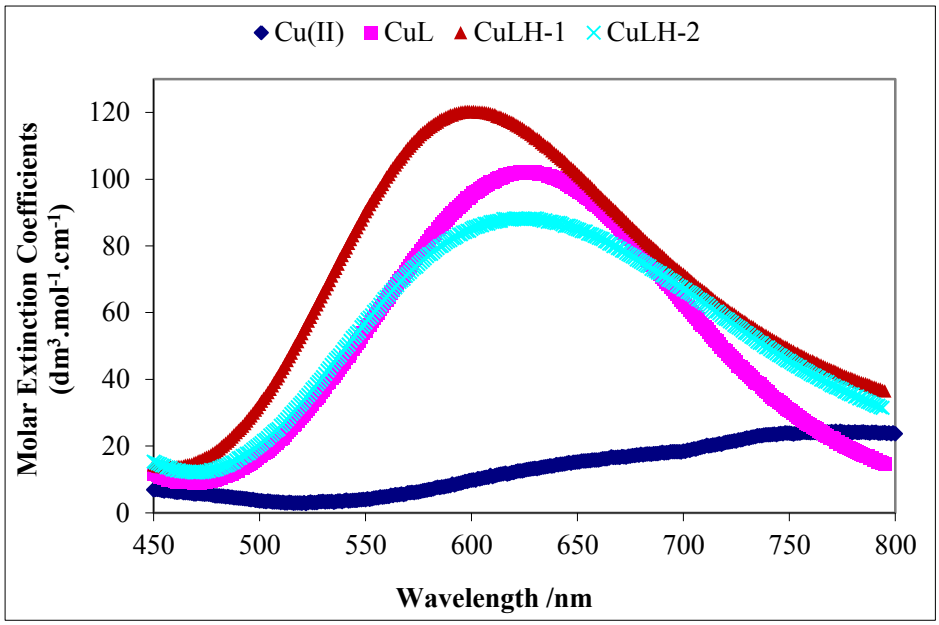

Figure 4.4: Calculated spectra of Cu(II)-[H(555)NMe_2] individual species.

Two possible structures are suggested by the potentiometric results for the ML with [H(555)NH_2] and [H(555)NMe_2]. The stability constants for both ML are similar with a log difference of ~ 1 log units. The ML of [H(555)NMe_2] formed before the titration starts between pH range 2.1 - 6.06 while ML of [H(555)NH_2] between pH range 2.60 - 5.38. Although the two ligands have the same environment, the difference was the two methyl groups on the terminal amine. From the UV-visible spectroscopy it is clear that the complexes of these two ligands have different structures. They have very different λ_{max} values; 569 and 623 nm, for [H(555)NH_2] and [H(555)NMe_2], respectively. These values suggest that ML of [H(555)NH_2] has structure in Figure 3.22 b(ii) and [H(555)NMe_2] structure in Figure 3.22 b(i).

4.1.4.1.3 Cu(II)-[H_2(555)NH_2]

The electronic absorption spectra for the Cu(II)-[H_2(555)NH_2] system are shown in Figure 4.6. At low pH, the spectrum is the same as that of $[Cu(OH_2)_6]^{2+}$. The red shift in λ_{max} when forming MLH from hydrated Cu(II) reflected the increased ligand field splitting in the presence of the ligand as opposed to H_2O. As the pH increases, the band maximum increases in intensity (curves for pH 2.27 and 3.10). Further increase in pH (curves for pH 3.7; 3.65 to 6.24) causes the absorption band to shift to shorter wavelengths due to the Cu-O to Cu-N bond rearrangements. Above pH 8.35, the colour changes to purple and the band

maximum increases in intensity as Cu(II) complexes of the type CuN4 are formed and the deprotonation reaction at the amide site occurs. The gradual colour changes with changing pH are shown in Figure 4.5.

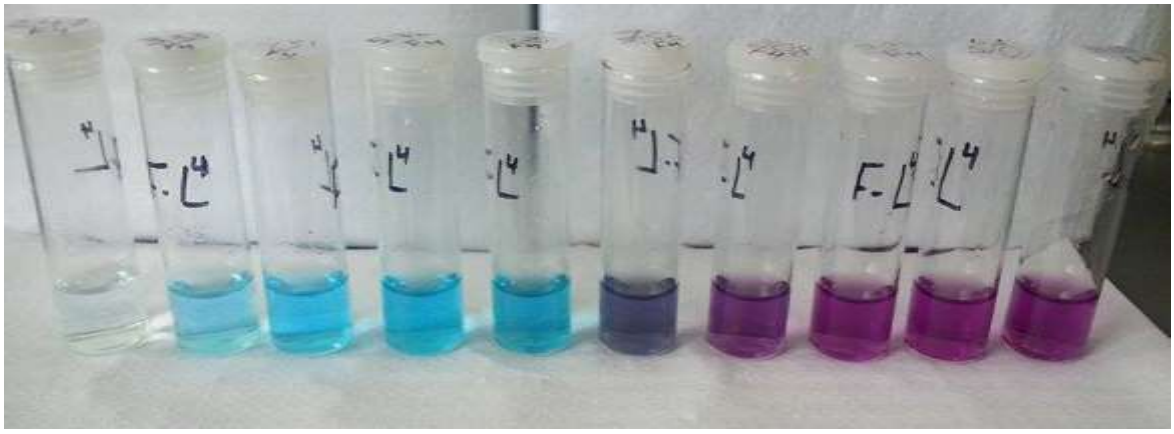

Figure 4.5: Cu(II)-[H_2(555)NH_2] showing gradual colour change from pH 1.83 to 10.08.

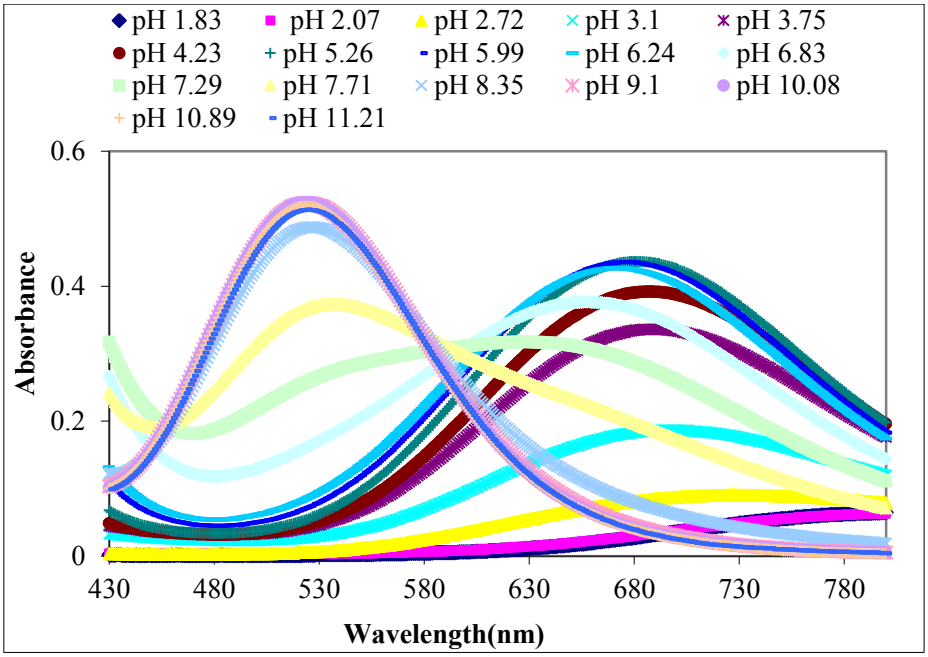

Figure 4.6: UV-visible electronic absorption spectra for Cu(II)-[H_2(555)NH_2] with [M(0.005 mol dm^{-3})-L(0.005 mol dm^{-3})] at different pH values.

The calculated absorption spectra for the individual species are shown in Figure 4.7. The λ_{max} and molar extinction coefficient (Ɛ) are listed in Table 4.1. It is interesting to note

that between pH 6.8 and 7.7 there appears to be an isosbestic point at λ 584 nm (Figure 4.6). In this pH range ML, MLH_{-1} and MLH_{-2} are in equilibrium (see Figure 3.16). Normally an isobestic point is only seen when two species are in equilibrium. Looking at Figure 4.7, we see that these three species have very similar extinction coefficient at λ 599 nm and hence the isobestic point. The λ_{max} of the MLH species is 741 nm which is close to the calculated λ_{max} of 766 nm. The λ_{max} value obtained for MLH is compatible with the coordination of Cu(II) Ala–Gly–Ha (λ_{max} 740 nm).[20] The λ_{max} of the ML species is 682 nm. This is close to 680 nm for $[Cu(NH_3)_2(H_2O)_4]^{2+}$ which is also coordinated by 2N.

The λ_{max} 575nm for the MLH_{-1} species suggests coordination of the pyridyl-N, an amide-O, an amide-N and an amino-N. This value is close to the λ_{max} of 570 nm for the ML species of the Cu(II)-*N,N′*-di(aminoethylene)-2,6-pyridine-dicarbonylamine system.[11] The calculated λ_{max} of MLH_{-2} species is 534 nm which clearly indicates the presence of four nitrogen atoms in the coordination sphere. The Cu(II) ion coordinated with two amide-N, one amine-N and a pyridyl-N in a square-planar arrangement.[11] The predicted λ_{max} is close to the observed value of 524nm. A high extinction coefficient value of 121.84 $dm^3mol^{-1}cm^{-1}$ and a change in colour at this pH range supports such geometry. Thus, the ligand is postulated to coordinate the metal ion as shown in the structure given in Figure 3.26 as suggested by the potentiometric data.

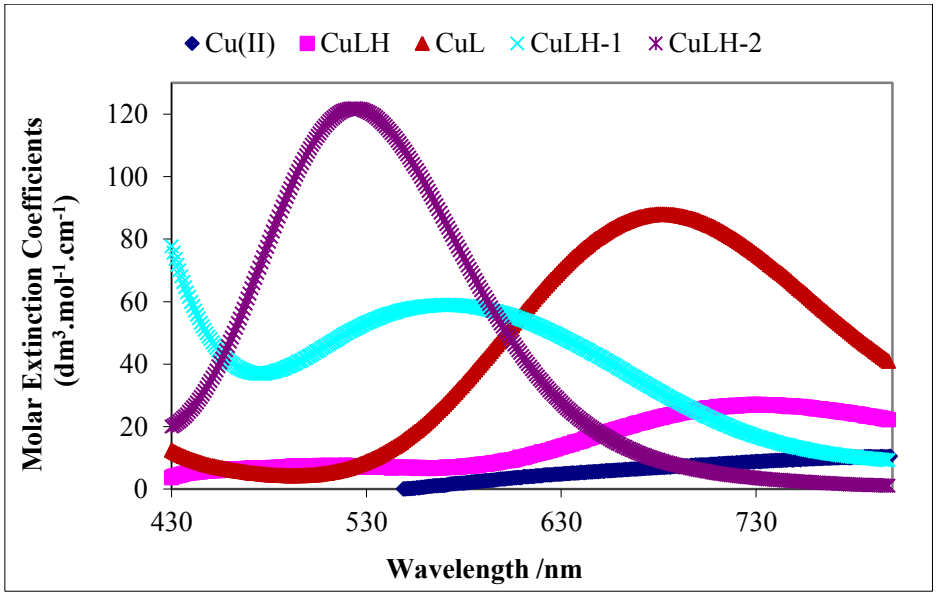

Figure 4.7: Calculated spectra of Cu(II)-$[H_2(555)NH_2]$ individual species.

4.1.4.1.4 Cu(II)-[H_2(565)NH_2]

The UV-visible electronic absorption spectra detected for the Cu(II)-[H_2(565)NH_2] system are shown in Figure 4.8. At low pH 2.22 and 3.07, the spectrum is the same as that of $[Cu(OH_2)_6]^{2+}$. As the base concentration increased, the absorption bands shift towards shorter wavelength with an increase in intensity (curves for pH 4.33, 4.75 and 5.03). A noticeable feature about the absorption bands is that they remain the same in the pH range 5.79 – 8.19 when deprotonation of the second amide occurs to form the MLH_{-2} species. This result suggests that there is no change in the coordination sphere of the Cu(II) above pH 7.65.

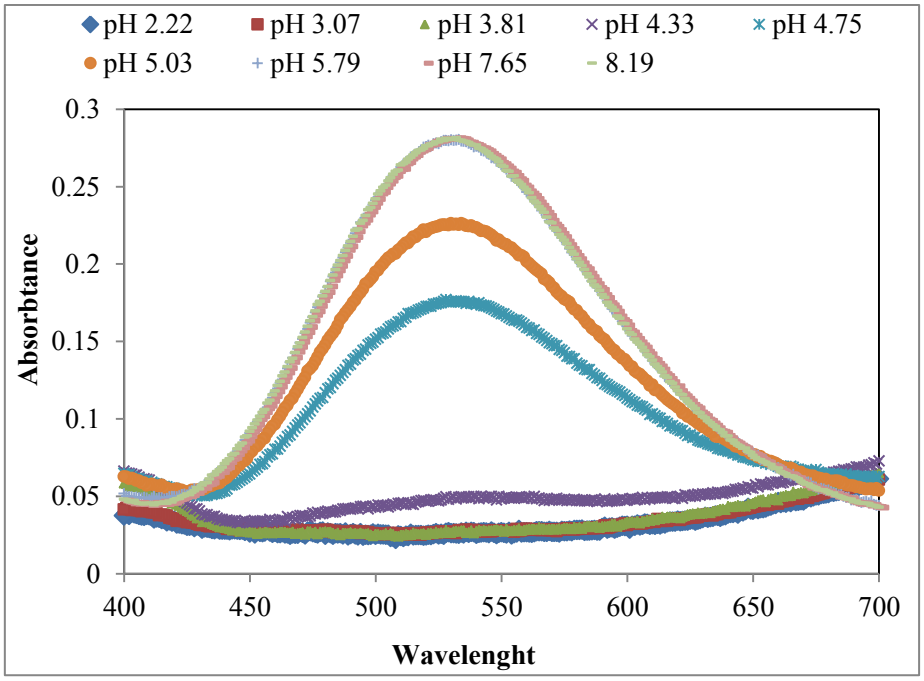

Figure 4.8: UV-visible electronic absorption spectra for Cu(II)-[H_2(565)NH_2] with [M(0.003 mol dm^{-3})-L(0.006 mol dm^{-3})] at different pH values.

The calculated absorption spectra for the individual species are shown in Figure 4.9. The λ_{max} and molar extinction coefficient (ε) for the three [H_2(565)NH_2] species are given in Table 4.1. At pH 3.07, the formation of MLH species has already begun, this is in support of the speciation curves in Figure 3.18. The values of λ_{max} and ε_{max} for CuLH are (746 nm, 19.78 $dm^3mol^{-1}cm^{-1}$) which is in good agreement with one nitrogen donor atom in the coordination sphere of the Cu(II) ion of this species. A similar value was obtained for Cu(II)

coordinated with Ala–Gly–Ha[20] (λ_{max} = 740 nm) and $[Cu(NH_3)(H_2O)_5]^{2+}$ (λ_{max} = 745 nm).[12] The coordinating groups are the pyridyl-N and two amide-O groups. The individually calculated d–d spectrum for the CuL species shows a band with λ_{max} at 747 nm (ε_{max} = 47.45 $dm^3\ mol^{-1}cm^{-1}$). The d-d electronic absorption bands of MLH and ML (Figure 4.9) have the same λ_{max} (~746 nm) but different extinction coefficients. This suggests that there is no change in the coordination of the ligand. However, there is a substantial change in extinction coefficient which indicates some change in the symmetry of the molecule. The bands are also slightly asymmetric at the low-frequency side. In general, the more distorted the molecule, the higher the extinction coefficient. Therefore, a CuN type of coordination is most likely to be formed in this speciation range.[21] However, λ_{max} of 532 nm for the MLH_{-2} species indicates the presence of four nitrogen atoms in the coordination sphere of the Cu(II) ion in a square-planar arrangement. Calculated absorption spectra of 534 nm, as given in Table 4.1, confirm the experimental results which are consistent with the presence of an amine-N, a pyridyl-N and two amide-N's in the coordination sphere of the Cu(II) ion.[11]

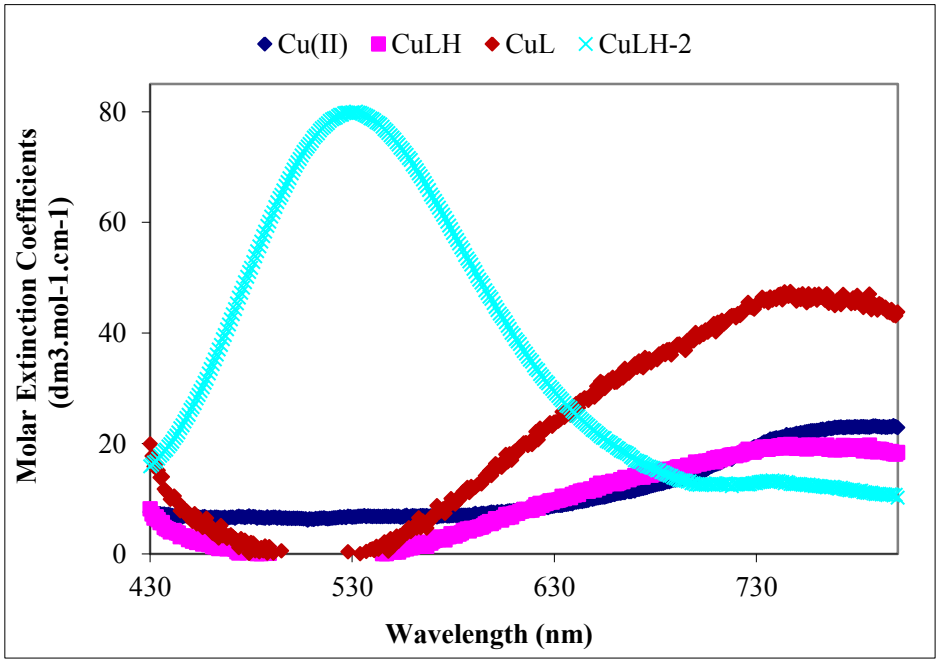

Figure 4.9: Calculated spectra of Cu(II)-$[H_2(565)NH_2]$ individual species.

4.1.4.1.5 Cu(II)-[H(56)NH_2]

The UV-visible electronic absorption spectra for the Cu(II)-[H(56)NH_2] system are shown in Figure 4.10. As the pH is increased, the band maximum increases in intensity and shifts to shorter wavelength. This indicates the presence of different species in solution at different pH values. A noticeable feature about the absorption bands is that they remained the same in the pH range 5.51 – 9.18. Above pH 9.18, a drop in the absorbance value was found after the formation of the MLH_{-2} species. This result suggests that there is no further reaction between this species and the base above pH 9.18. However, this proton could come from a coordinated water molecule.

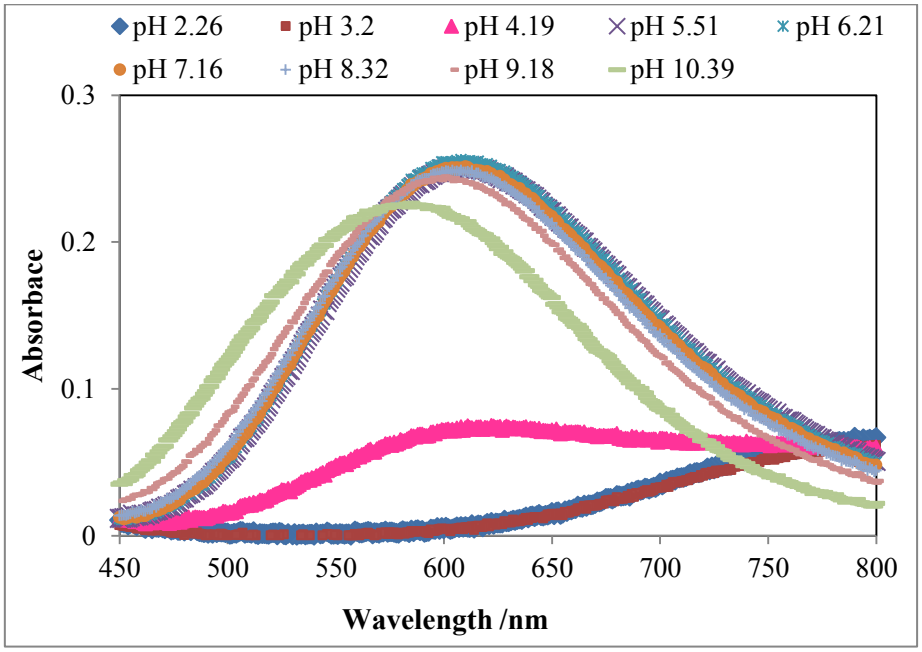

Figure 4.10: UV-visible electronic absorption spectra for Cu(II)-[H(56)NH_2] with [M(0.003 mol dm^{-3})-L(0.006 mol dm^{-3})] at different pH values.

The CuL species were not detected spectroscopically due to very low concentration as shown in Figure 3.20. The values of λ_{max}= 608 nm and ε_{max} = 70.37 dm^3 mol^{-1} cm^{-1} of $CuLH_{-1}$ are in very good agreement with MLH_{-1} of glycyl-L-histidine[22] (λ_{max}= 606 nm) and glycyl-L-histidylglycine[23] (λ_{max}= 605 nm). The calculated λ_{max} 598 nm shows that the coordinating groups are an amino-N, an amide-N and a pyridyl-N in addition to a water molecule and this is in good agreement with the experimental λ_{max} value. There is a drop in

the molar extinction coefficient when an MLH_{-2} species was formed. This observation support a mechanism of water hydrolysis[11] since, for $CuLH_{-2}$, water is the only possible source of protons.[24] However, a drop in the extinction coefficient value suggests that the loss of this proton is from an axially coordinated water molecule, an observation consistent with the potentiometric results.

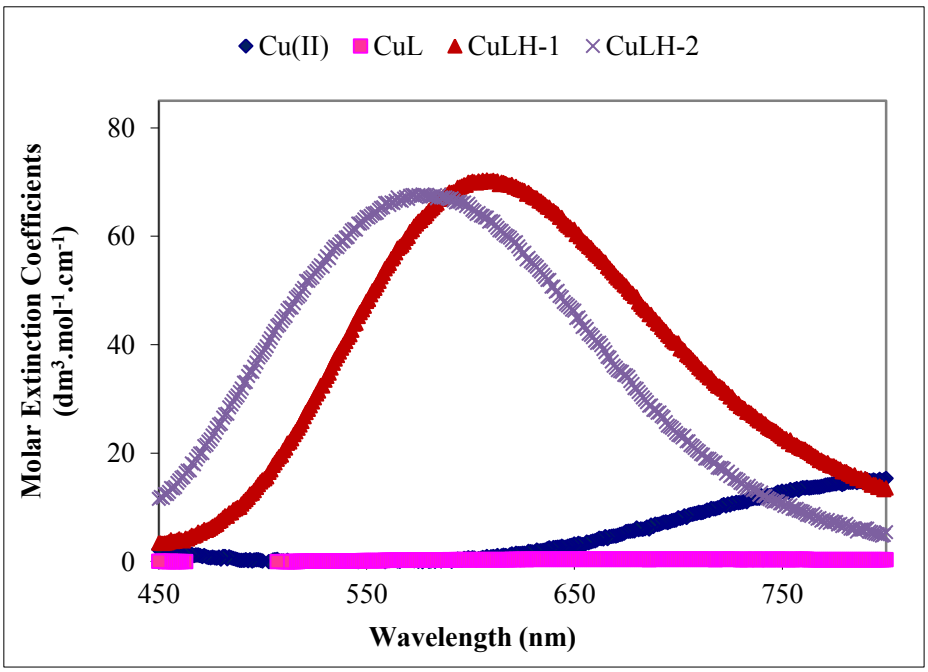

Figure 4.11: Calculated spectra of Cu(II)-[H(56)NH_2] individual species.

Any slight discrepancy between the calculated and the experimental λ_{max} values given above could be due to failure of Billo's method[10] for solution mixtures containing axially coordinating solvent molecules such as water. Previous studies showed that the rearrangement of donor atoms in the coordination sphere results in the splitting or significant shift of the absorption bands.[25,26] The predicted results indicate the same structures as proposed by the potentiometric results and are in good agreement with the observed λ_{max}.

4.1.4.2 Ni(II)-L Systems

The colour changes were only observed for the Ni(II)-[H(555)NH_2] and Ni(II)-[H_2(565)NH_2] systems, while the Ni(II)-[H(555)NMe_2], Ni(II)-[H_2(555)NH_2] and Ni(II)-[H(56)NH_2]] systems remained uncoloured during the potentiometric titrations. The

absorption spectra and electronic spectra, as a function of pH, for individual species of the Ni(II)-[H(555)NH_2] and Ni(II)-[H_2(565)NH_2] are shown in Figure 4.12 and 4.13 respectively. The wavelength and molar extinction coefficient values corresponding to maximum absorption of the Ni(II) species formed in solution with these two ligands are given in Table 4.2. These values were obtained as a result of the changing speciation of the solution with pH, forming different complex species with different absorption spectra. The absorption spectra were obtained in the pH range 2-11. In this study, the Ni(II) spectrophotometric spectra are less informative than the Cu(II) spectra.

Table 4.2: UV-visible spectra λ_{max} (nm) and ε_{max} ($dm^3.mol^{-1}.cm^{-1}$) experimental values with possible donor groups for Ni(II) with [H(555)NH_2] and [H_2(565)NH_2] complexes.

Ligands	Species	Experimental λ_{max} **(nm)**	ε_{max} **($dm^3.mol^{-1}.cm^{-1}$)**	Possible donor atoms
[H(555)NH_2]	NiL2	425	71.59	$2NH_2$, $2N_{py}$,
	NiL	425	38.22	$-NH_2$, N^-, N_{py}, H_2O
	$NiLH_{-1}$	425	78.08	$-NH_2$, N^-, N_{py}, H_2O
	$NiLH_{-2}$	425	26.33	$-NH_2$, N^-, N_{py}, OH^-
[H_2(565)NH_2]	NiL	-	-	-
	$NiLH_{-1}$	445	110.51	NH_2, N^-, N_{py}, H_2O
	$NiLH_{-2}$	445	50.46	NH_2, $2N^-$, N_{py}

4.1.4.2.1 Ni(II)-[H(555)NH_2]

At low pH values, the solution is made up of the hydrated [$Ni(OH_2)_6$] species. As the base concentration is increased, the intensity of the absorption band at 425 nm increases (curves from pH 5.59 to 10.95). The NiL_2, NiL, $NiLH_{-1}$ and $NiLH_{-2}$ species presented similar spectroscopic parameters, supporting the same coordination in all modes of Ni(II) ions. At pH 5.59, the solution colour starts to change from light green to yellow. This change in colour, which can be attributed to a single absorption band (λ_{max} = 425 nm), strongly suggests the formation of square-planar complexes. The analysis of the data suggests that the bonding mode of NiL formed with [H(555)NH_2] is the same as that for $NiLH_{-2}$ of Gly-Gly-Gly, but the amino group is still protonated.[27] Most Ni(II) complexes

coordinated with deprotonated amide nitrogen atoms have been reported to be diamagnetic and square-planar.[28-31] Furthermore, similar behaviour was observed for the Ni(II)-Gly-His complex, which is formed below pH 8, and where the most stable coordination mode occurred *via* the terminal amino-N, amide-N and imidazole-N donors.[32] As a consequence, the latter coordination mode can be suggested for the high stability, planar complex-$NiLH_{-2}$, for which the individually calculated spectrum has a λ_{max} at 425 nm and ε = 26.33 $dm^3.mol^{-1}.cm^{-1}$, suggesting the coordination of a hydroxide ion at the fourth equatorial site.[22]

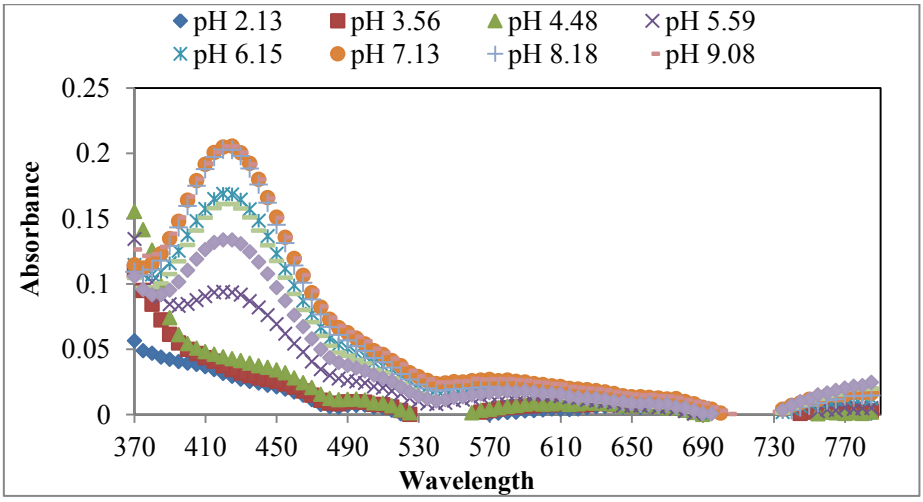

(a)

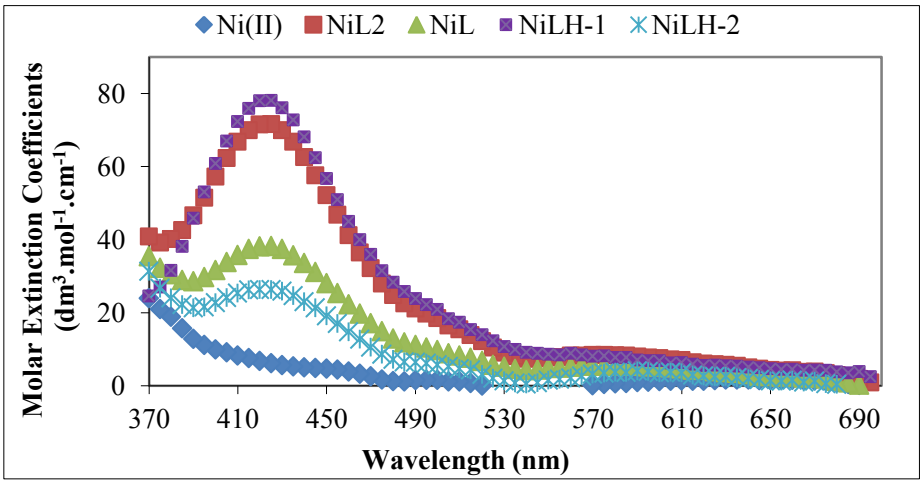

(b)

Figure 4.12: UV-visible electronic absorption spectra for **(a):** Ni(II)-[H(555)NH_2] with [M(0.003 mol dm^{-3})-L(0.006 mol dm^{-3})] and **(b):** calculated species spectra for Ni(II)-[H(555)NH_2] in aqueous solution.

4.1.4.2.2 Ni(II)-[H_2(565)NH_2]

Above pH 6.55, the previously colourless sample turns yellow. At pH value around 6.12, the first complex formed is probably NiL. As can be seen from species distribution diagrams in Figure A12, the NiL complex with [H_2(565)NH_2] was not detected spectroscopically due to the formation of a colourless solution complex at the pH range of its existence.

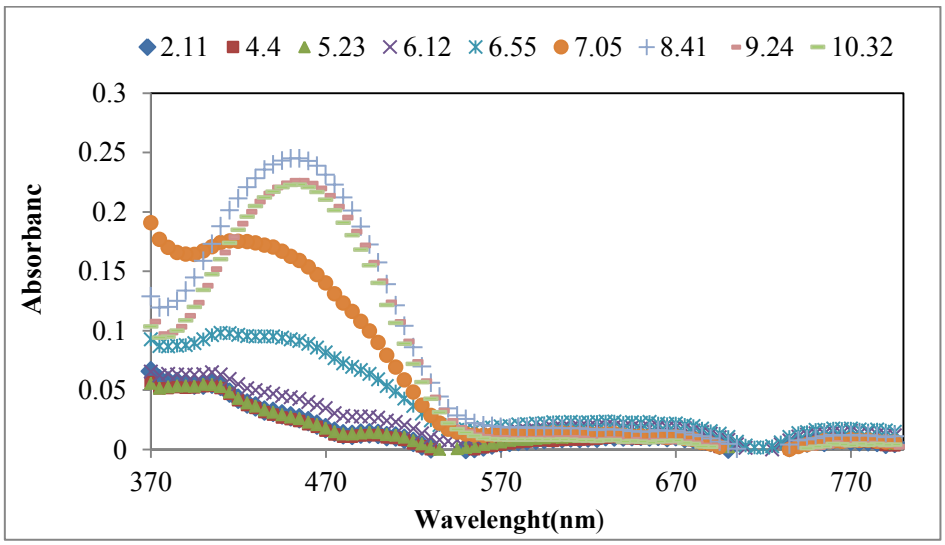

(a)

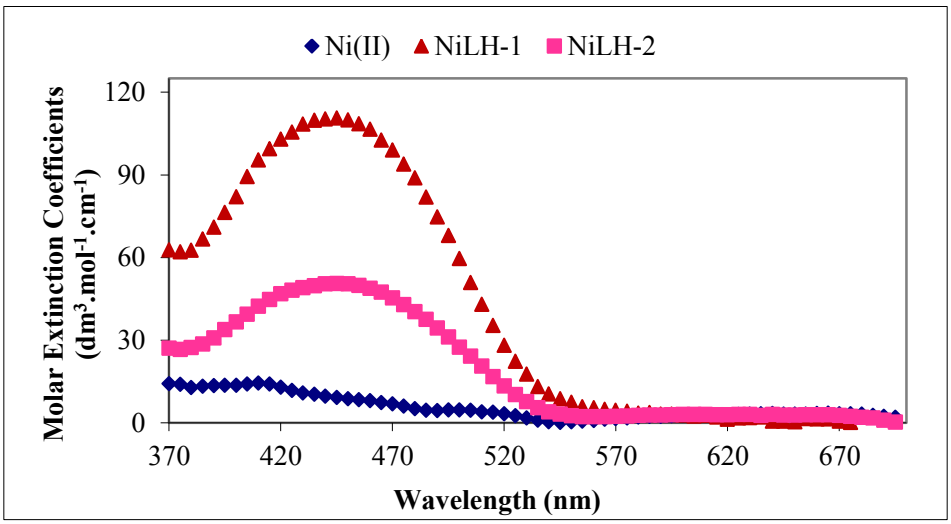

(b)

Figure 4.13: UV-visible electronic absorption spectra for **(a):** Ni(II)-[H_2(565)NH_2] with [M(0.003 mol dm^{-3})-L(0.006 mol dm^{-3})] and **(b):** calculated species spectra for Ni(II)-[H_2(565)NH_2 in aqueous solution.

Table 4.2 shows the wavelength and molar extinction coefficient values corresponding to maximum absorption of the Ni(II) species formed in solution with possible donor groups for this ligand. The deprotonation of two or more amide nitrogens in Ni(II) peptide complexes is often followed by fundamental changes of UV-visible spectra, representing a geometry shift of the complexes from octahedral (light green) to square planar (yellow) structures.[33-35] λ_{max} band of $NiLH_{-1}$ (λ_{max} = 445 nm, ε = 110.51 $dm^3.mol^{-1}.cm^{-1}$) unambiguously supports the amino-N, amide-N, pyridyl-N and water in the coordination sphere.[34] As a consequence, the latter coordination mode found in the high stability planar complex of $NiLH_{-2}$, for which the individually calculated spectrum has a λ_{max} at 445 nm and ε = 50.46 $dm^3.mol^{-1}.cm^{-1}$, suggests the coordination of a deprotonated amide-N^{20} at the fourth equatorial site. The two deprotonated amide groups provide a strong ligand field leading to singlet ground state of Ni(II).

4.2 ^{1}H-NMR Spectroscopy

4.2.1 Introduction

NMR spectroscopy is one of the most important analytical tools available today. It is a flexible technique with many applications.[37-40] ^{1}H-NMR observation yields structures of organic molecules, organometallic complexes, proteins, peptides, and nucleic acid oligomers. It is also widely used in medicine where it is often called magnetic resonance imaging (MRI). Furthermore, it gives detailed information for selected nuclei, information about the chemical bonding, the local electronic structure and the local site dynamics. Small changes to the environment at an NMR-active nucleus can be detected and identified.

In this study ^{1}H-NMR has been used to gain insights in to the site of metal coordination upon complexation by Cu(II). The presence of the metal ion is expected to broaden and shift the signals arising from protons attached to the neighbouring carbons most affected.[41] Cu(II) is paramagnetic which can affect both the chemical shift and relaxation time of the protons.[11,41] This manifests in a broadening and shifting of the ^{1}H-NMR signals. The broadening effect of the metal is attenuated by $1/r^{6}$ where r is the internuclear distance between the Cu(II) and the observed proton. Cu(II) exchange is usually very rapid and so only average spectra are seen. The differential effect of the metal ion on the ligand can then be used to determine the structure of the complex.

4.2.2 Experimental

All solutions between 0.009 and 0.017 mol dm^{-3} of ligands were prepared in D_2O at 25°C. The ^{1}H-NMR spectra were recorded on a Bruker Avance 400MHz spectrometer. The comparison of shifting and broadening of the spectra from the ligand protonation and copper complexes were determined using the Mestre Nova version 9.1 program. The pD of the solutions was adjusted using concentrated NaOD and DCl. A CRISONmicro pH meter equipped with a Metrohm glass electrode was used to measure the pH. The spectra were recorded from pH 2 to pH 11. Tertiary butyl alcohol was used as an internal reference. Small aliquots of dilute Cu(II) solution were added into the ligand solution. Since a pH electrode was used to measure pD, corrections were made as described by Popov[42] and Glasoe[43];

$$pD = pH \text{ meter reading} + 0.44 \quad (4.6)$$

4.2.3 Results and Discussion

4.2.3.1 Protonation Titrations

A spectrum for ^{1}H-NMR is a plot of signal intensity against chemical shift. If D_2O is used as solvent, the amine protons are not observed as they exchange with the deuterium of the water. It is possible to record spectra in H_2O/D_2O and observe the amide protons below a pH of ~6. Above this pH the amide proton are in rapid exchange and so cannot be observed. Since we were interested in the pH range 2- 11 the spectra were all run in D_2O, which is technically much easier and does not require solvent suppression.

In this study NMR has been used to determine the sequence of protonation of the ligands. Thus, a plot of chemical shift *vs.* pH can be used to determine the site of protonation[42,44], while the inflection point in the chemical shift curves can be used to estimate pK_a values. Many authors have used ^{1}H-NMR to determine the sequence of protonation of the ligands, to estimate the protonation constants and to predict the structures of metal to ligand complexes.[45-52]

4.2.3.1.1 Protonation of [H(555)NH_2]

The assignments of the spectra are indicated and follow the numbering in Figure 4.14. Figure 4.15 shows the proton ^{1}H-NMR spectra for [H(555)NH_2] as a function of pH. From pH 1.94 – 6.29, the signals **d, e, f, g** and **h** were the first to shift from low to high field. This is ascribed to protonation of the pyridine nitrogen group.

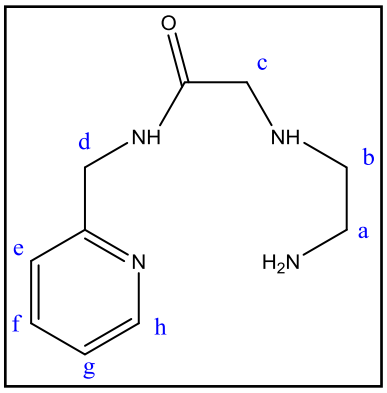

Figure 4.14: The structure of the [H(555)NH_2] showing the proton labels in Figures 4.15 and 4.16.

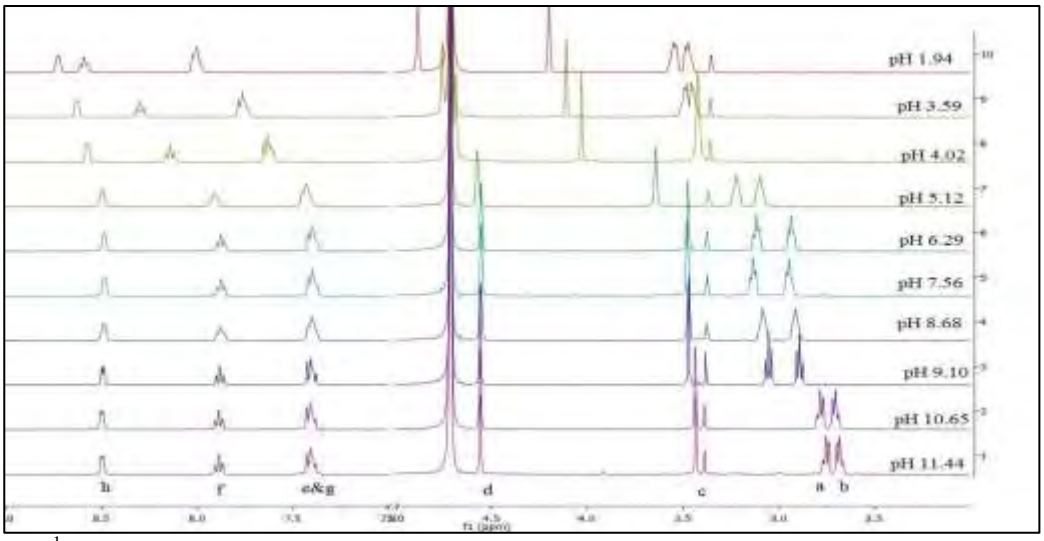

Figure 4.15: ^{1}H-NMR spectra of [H(555)NH_2] as a function of pH. Note the break in the f1 dimension at 5.0 ppm. The assignments are given under the pH11.44 spectrum and follow the numbering scheme given in Figure 4.14.

Also, the signal **c** shifts between pH 1.94 and 6.29. This indicates that the secondary amine is being protonated in this pH range. At pH 5.12, the signal **b** crossover the signal **a,** with shifting to high field for all signals. From pH 6.29 to high pH the most significant shifting to high field were signals **a** and **b**. This indicates protonation of the terminal amine. The change in chemical shifts as a function of pH of protons near to possible coordination sites is shown in Figure 4.16. The plots of change in proton chemical shift show approximate pK_a values of about 3.59, 5.10 and 9.10, corresponded to the protonation of the pyridine nitrogen, the secondary amine and the terminal amine respectively. These are in good agreement with the values obtained from potentiometric results.

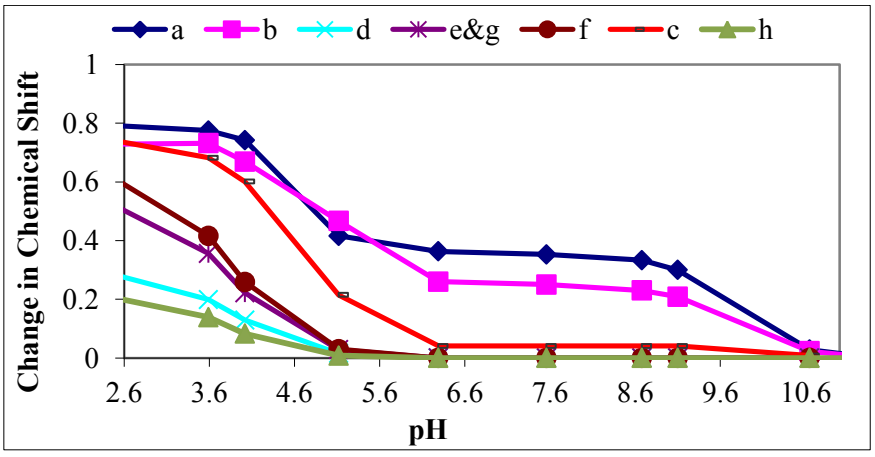

Figure 4.16: Change of chemical shifts of selected protons of [H(555)NH2] as a function of pH. The assignment is given in Figure 4.14.

4.2.3.1.2 Protonation of [H(555)NMe$_2$]

The numbering of the protons is given in Figure 4.17 and their assignment in Figure 4.18 which shows the ^{1}H-NMR spectra obtained at different pH values. Note the crossover of the **b** and **c** signals at pH 9.69. The changes of chemical shifts of selected protons are given in Figure 4.19. Between pH 3.35 and 6.07, the aromatic signals **f, h**, **g** and **i** shift significantly to high field as the pyridine nitrogen is protonated.

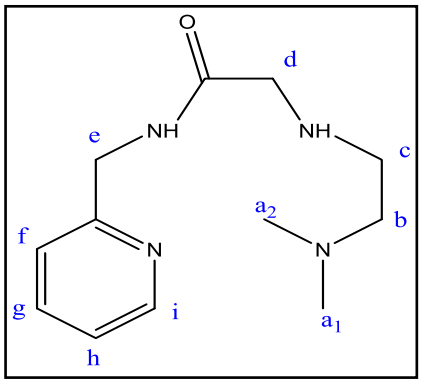

Figure 4.17: The structure of the [H(555)NMe$_2$] showing the proton labels in Figures 4.18 and 4.19.

Signal **b, c** and **d** shifted from pH 3.35 to pH 6.07. This is due to the protonation of the secondary amino group. At high pH, the methyl signals, $\mathbf{a_1}$ and $\mathbf{a_2}$, undergo a big shift to high field. This indicates protonation of the terminal amine.

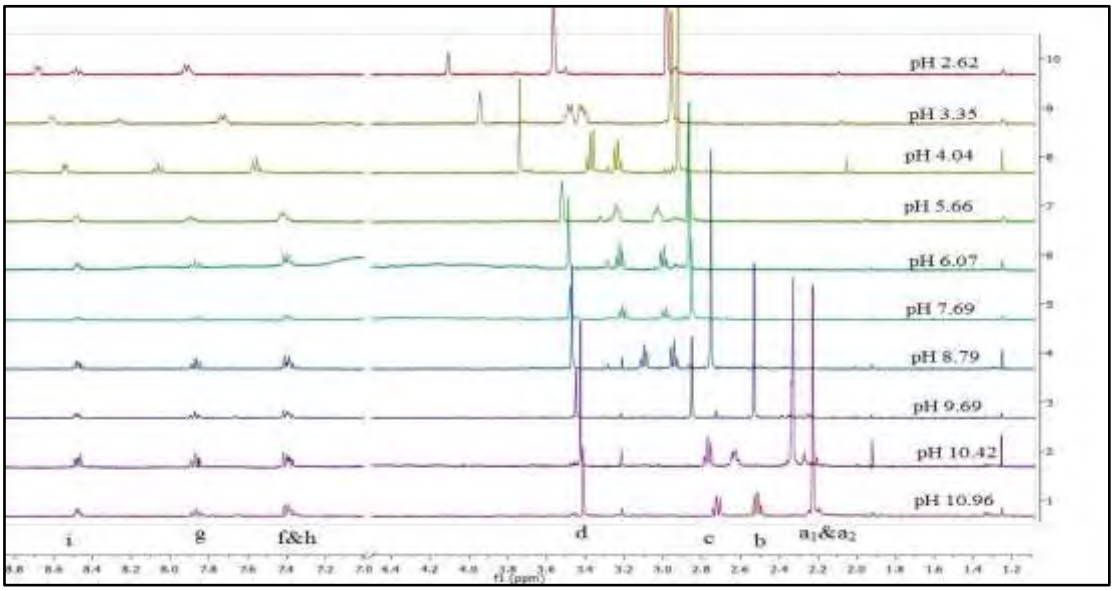

Figure 4.18: ^{1}H-NMR spectra of [H(555)NMe$_2$] as a function of pH. Note the break in the f1 dimension at 4.5 ppm. The assignments are given under the pH10.96 spectrum and follow the numbering scheme given in Figure 4.17.

The inflection is seen in Figure 4.19, with significant change in the chemical shift of protons. The inflection point in the chemical shift curves can be used to estimate the pK_a values of the three protonation sites. The pK_a values of 3.35, 4.04 and 8.79, confirm that it is the pyridyl nitrogen and two amino groups are being protonated. The observed result agree with those from the potentiometric results. Note, in this case the spectra were recorded with water suppression in 90:10 D_2O/H_2O in order to see the amide protons. The signal for proton **e** is close to the water signal and so was also suppressed. However the amide protons were still not observed and so all subsequent spectra were recorded in D_2O.

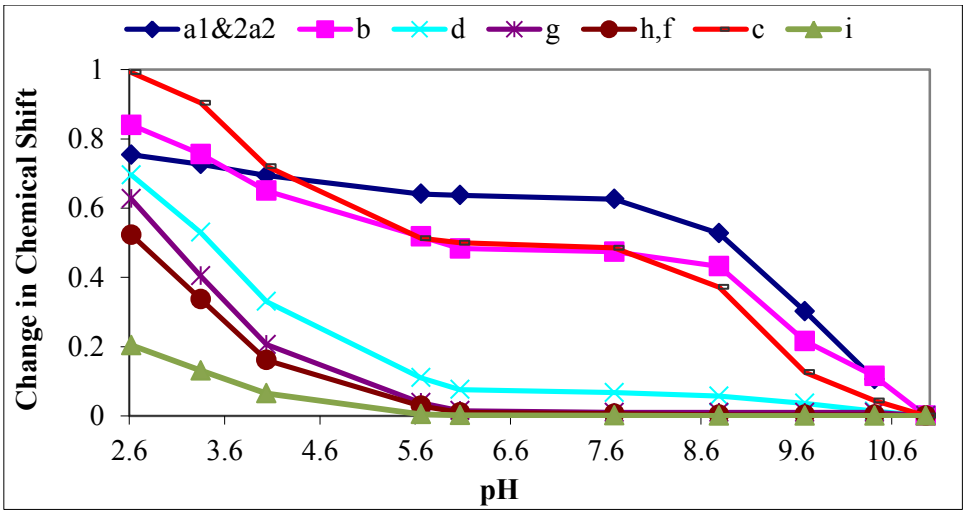

Figure 4.19: Change of chemical shifts of selected protons of [H(555)NMe_2] as a function of pH. The assignment is given in Figure 4.17.

4.2.3.1.3 Protonation of [H_2(555)NH_2]

The proton labels used in the ^{1}H-NMR spectra are given in Figure 4.20.

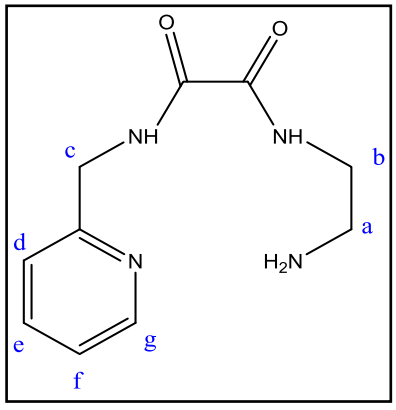

Figure 4.20: The structure of the [H_2(555)NH_2] showing the proton labels in Figures 4.21 and 4.22.

Figure 4.21 shows the ^{1}H-NMR spectra. Change of chemical shifts of protons near the possible coordination sites of the free $[H_2(555)NH_2]$ as a function of pH are shown in Figure 4.22. Going from pH 2.03 to 6.51, the signals **c, d, f, e,** and **g** were the first to shift to high field. This is due to the protonation of the pyridine nitrogen. Signals **a** and **b** shifted from pH 8.08 to pH 11.21. This is due to the protonation of the N-terminal amino group.

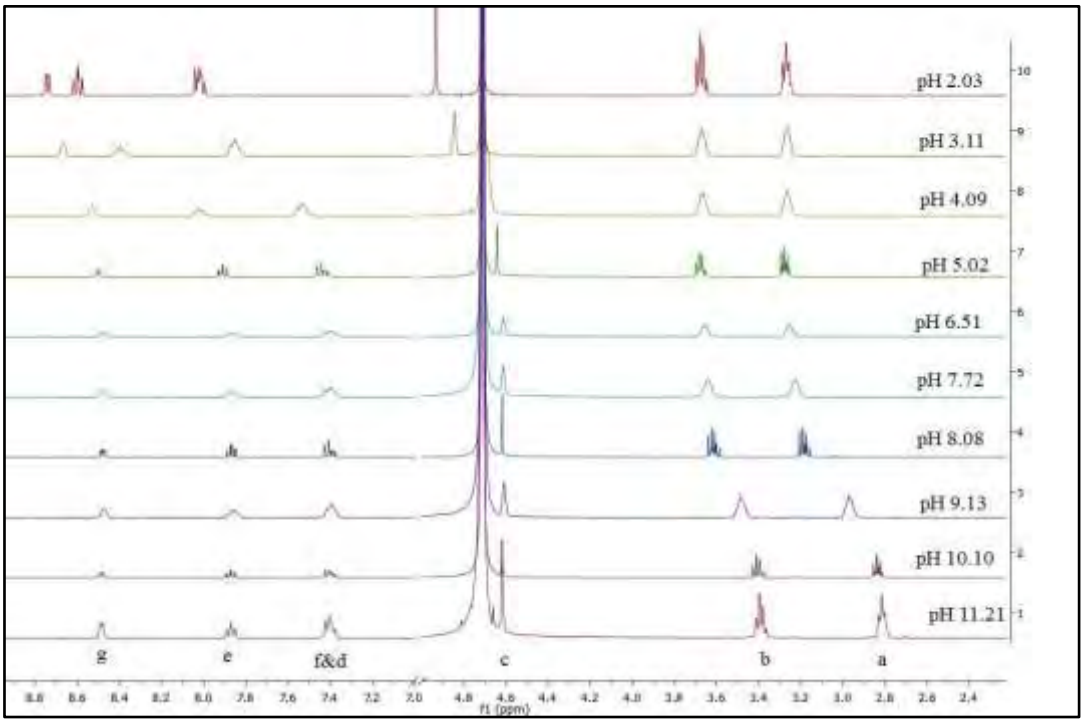

Figure 4.21: ^{1}H-NMR spectra of $[H_2(555)NH_2]$ as a function of pH. Note the break in the f1 dimension at 5.0 ppm. The assignments are given under the pH11.21 spectrum and follow the number in scheme given in Figure 4.20.

Figure 4.22 shows the plots of chemical shifts as a function of pH. The inflection point in the chemical shift curve can be used to estimate the average pK_a of the two protonation sites. From potentiometric data, $[H_2(555)NH_2]$ has a pK_a value of 8.96, and this is in very good agreement with the pK_a value of 9.00 determined from the NMR data given in Figure 4.22. The protonation constant for the pyridyl nitrogen donor as determined from NMR data was 3.11. Odisitse[53] reported the pK_a of the pyridyl nitrogen as 3.51 in *N,N'*-bis[2(2-pyridyl)-methyl]pyridine- 2,6-dicarboxamide which is quite similar to the pK_a of the pyridyl nitrogen in $[H_2(555)NH_2]$.

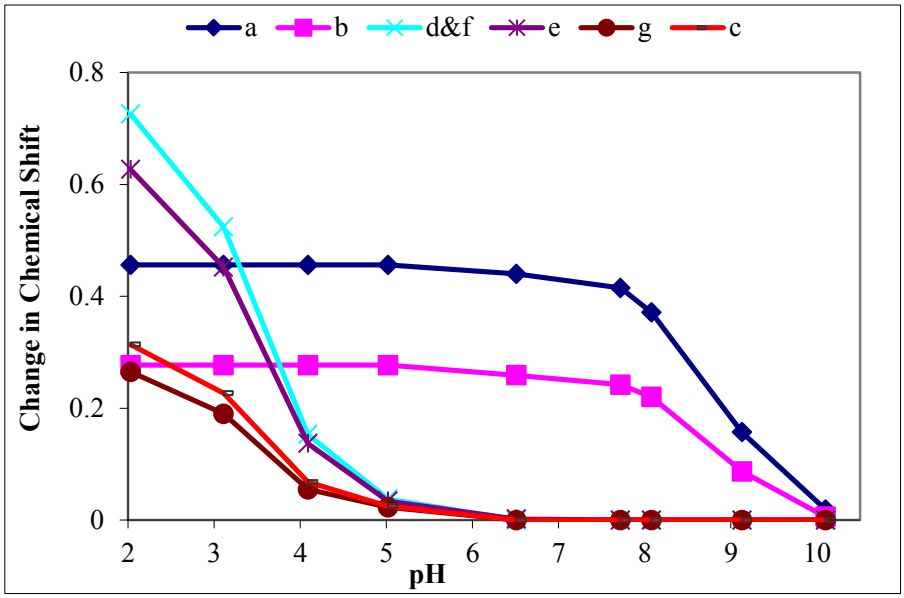

Figure 4.22: Change of chemical shifts of selected protons of [H2(555)NH2] as a function of pH. The assignment is given in Figure 4.20.

4.2.3.1.4 Protonation of $[H_2(565)NH_2]$

Figure 4.24 shows the ^{1}H-NMR spectra obtained at different pH values. The numbering of the protons is given in Figure 4.23.

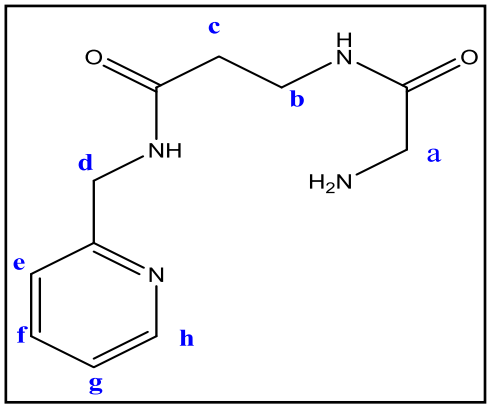

Figure 4.23: The structure of the $[H_2(565)NH_2]$ showing the proton labels in Figures 4.24 and 4.25.

From pH 3.74 to 5.79, the signals **d, e,g, f** and **h** are shifting to high field. That was due to the protonation of the pyridine nitrogen. At pH 7.47 the signal **a** start shifts to high field and then, crossover the signal **b** at pH 8.06 going to high field. This was due to the protonation of the terminal amino group

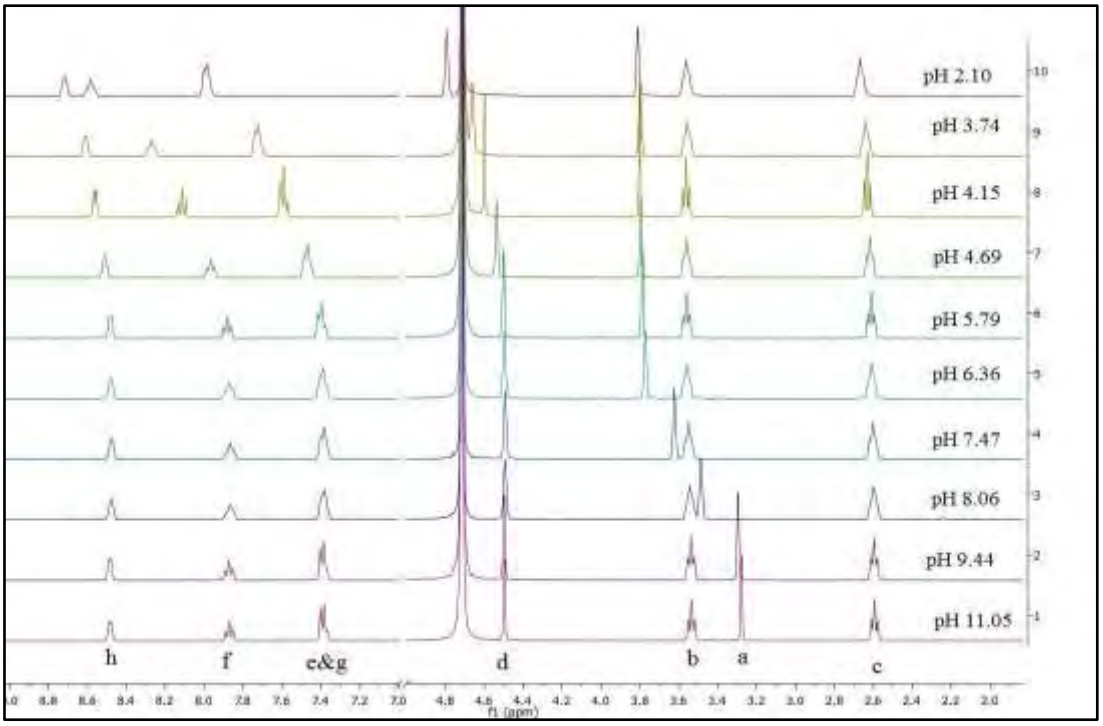

Figure 4.24: ^{1}H-NMR spectra of [H_2(565)NH_2] as a function of pH. Note the break in the f1 dimension at 5.0 ppm. The assignments are given under the pH11.05 spectrum and follow the number in scheme given in Figure 4.23.

Figure 4.25 shows plots of proton chemical shifts as a function of pH. This plots given the approximate pK_a values of the first protonation (4.60) and the second protonation step (8.06). That value is very similar to those for the protonation of the pyridine nitrogen and the amine group from the potentiometric results.

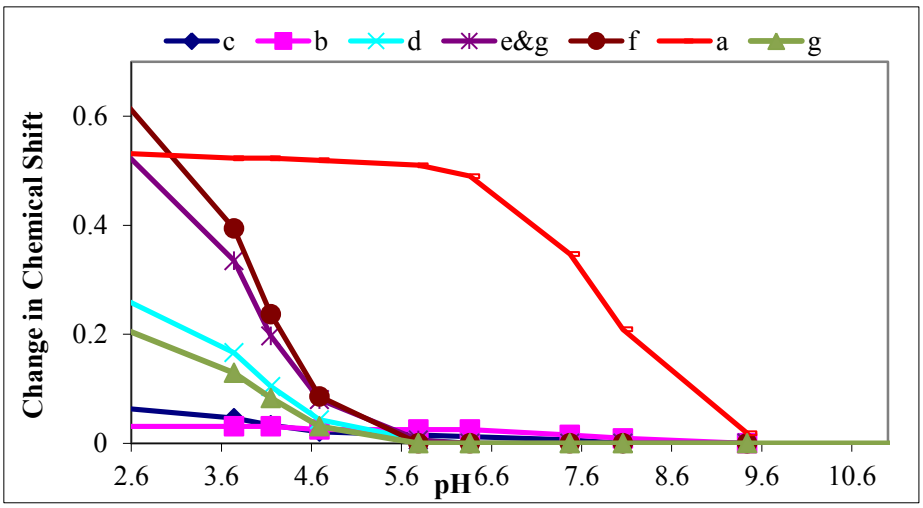

Figure 4.25: Change of chemical shifts of selected protons of [H_2(565)NH_2] as a function of pH. The assignment is given in Figure 4.23.

4.2.3.1.5 Protonation of the [H(56)NH_2]

The assignments of the protons are given in Figure 4.26.

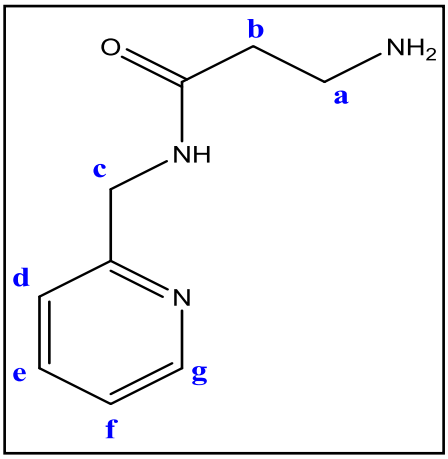

Figure 4.26: The structure of the [H(56)NH_2] showing the proton labels in Figures 4.27 and 4.28

The ^{1}H-NMR spectra obtained at different pH values are shown in Figure 4.27. The changes of chemical shifts of selected protons are given in Figure 4.28. From the potentiometric results, [H(56)NH_2] has two dissociable protons; the pyridine proton and the terminal amine proton. The signals **c**, **d, f, e** and **g** were the first to shift from low to high field from pH 3.12 to 6.35, which indicates the protonation of the the pyridine nitrogen (pK_a = 4.31). Protonation of the terminal amine occurs from pH 8.38 to 11.46 where signals **a** and **b** start shifting substantially. The pK_a value of 8.38 agrees with that from the potentiometric results.

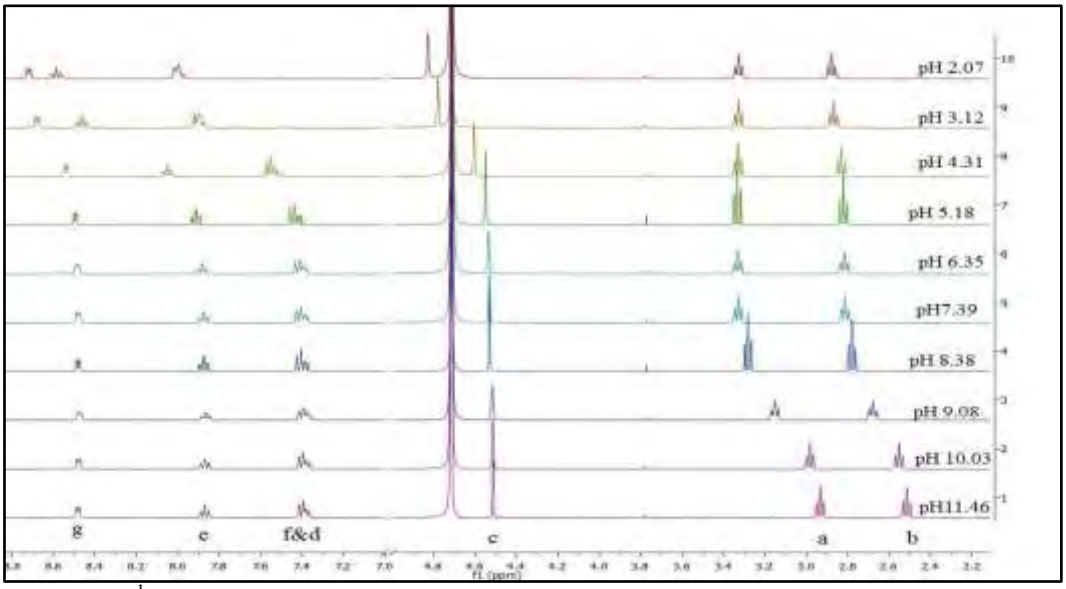

Figure 4.27: ^{1}H-NMR spectra of [H(56)NH_2] as a function of pH. Note the break in the f1 dimension at 5.0 ppm. The assignments are given under the pH11.46 spectrum and follow the number in scheme given in Figure 4.26.

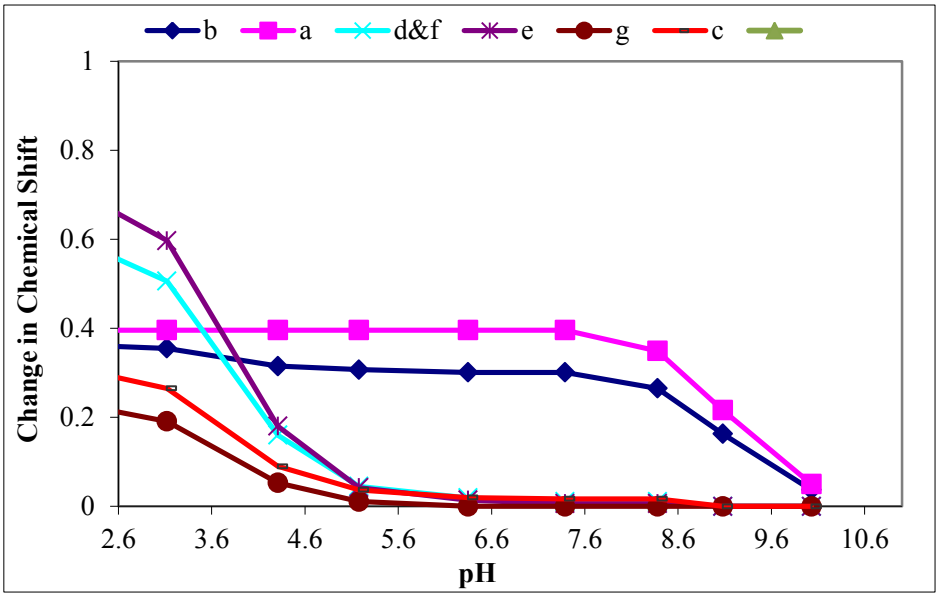

Figure 4.28: Change of chemical shifts of selected protons of [H(56)NH2] as a function of pH. The assignment is given in Figure 4.26.

4.2.3.2 Complex Formation Titrations

^{1}H-NMR was used to study the structure of Cu(II) complexes with [H(555)NH_2], [H(555)NMe_2], [H_2(555)NH_2], [H_2(565)NH_2], and [H(56)NH_2]. The active binding sites for these ligands are the pyridyl-N, the amide-N and the amine-N's. The ^{1}H-NMR spectra in D_2O were investigated at different pH values, where the maximum concentrations of the various species are observed, as deduced from the speciation diagrams in Chapter 3. Gradual addition of Cu(II) ions to solutions of ligand causes important paramagnetic perturbations and produces considerable changes in the ^{1}H-NMR spectrum.

4.2.3.2.1 Cu(II)-[H(555)NH_2] complexes

Figure 4.29 shows the effect of Cu(II) upon the spectra of [H(555)NH_2] as a function of pH. Since Cu(II) is paramagnetic, it tends to broaden the signals arising from protons attached to neighbouring carbons as observed in Figure 4.29. From the speciation graphs in Figure 3.12, complexation starts at pH 2.76 and therefore a change in NMR spectra signals is expected at pH > 2.76. The signals in Figure 4.29 broaden with the addition of Cu(II). The very broad peak for the aromatic protons of the pyridyl group ($\delta = 8$) indicates that at pH 3.59 the pyridyl-N is coordinated to the Cu(II). At the same pH, **c** and **d** are also very broad indicating that the amide-N and secondary amine-N are also coordinated. There is some differential broadening of **a** and **b** indicating that perhaps the terminal amine-N is not

coordinated. The results are not unambiguous; however, as more than one species may be present at the same time. Since Cu(II) exchange is fast on the NMR time scale only average signals would be observed. Similarly, at pH 4.02 and 6.26, all the protons broaden indicating that all four nitrogens are coordinated. Note the broadening cannot be due to a change in the magnetic susceptibility of the solution as the reference peak does not broaden.

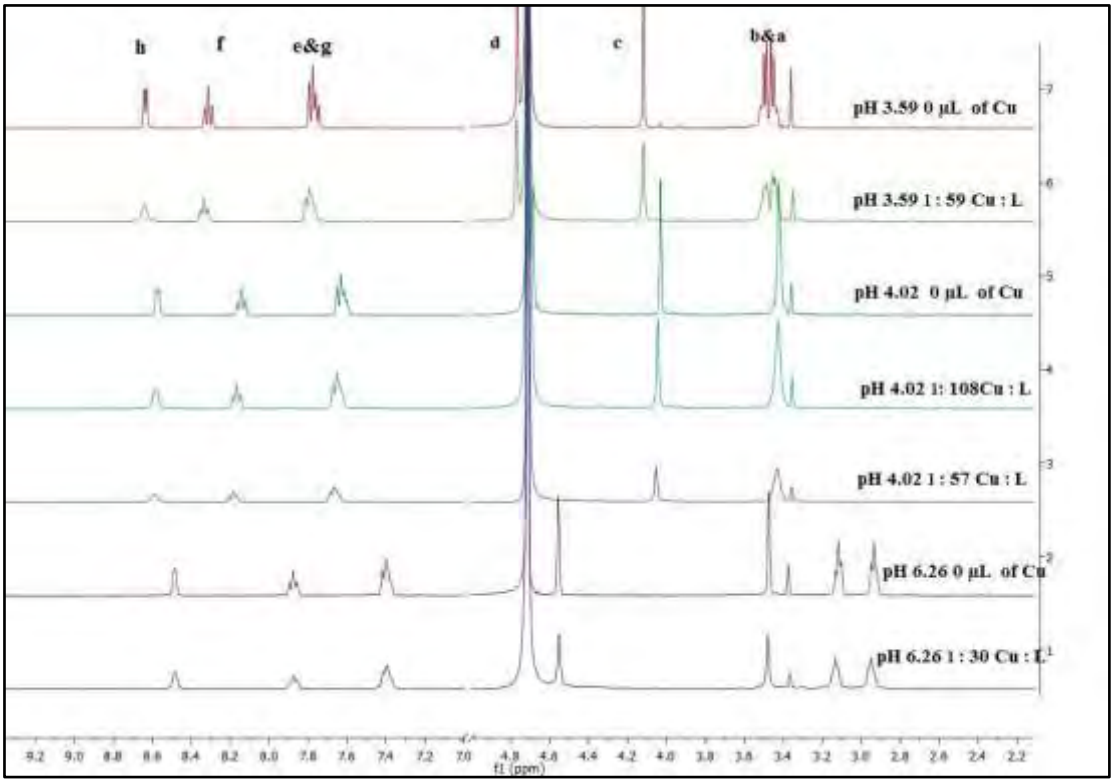

Figure 4.29: ^{1}H-NMR titration for the complexation of [H(555)NH_2] (0.099 M) in D_2O. Note the break in the f1 dimension at 5.0 to 7.0 ppm. The proton assignments are according to Figure 4.14.

4.2.3.2.2 Cu(II)-[H(555)NMe_2] complexes

^{1}H-NMR results for the complexation of [H(555)NMe_2] with Cu(II) are given in Figure 4.30. The small amounts of Cu(II) used in the ^{1}H-NMR study should enable the observation of significant differential broadening of the resonances of protons close to the copper binding. At pH 3.49, ML is the most predominant species in solution. Signals from **b** to **i** were already broadened at the beginning of the Cu(II)/ligand titration. Signal $\mathbf{a_1}$ and $\mathbf{a_2}$ broadened upon further titration with Cu(II). The broadening of signals **h**, **f, g** and **i** indicate coordination to the pyridyl-N. The broadening of signals $\mathbf{a_1}$, $\mathbf{a_2}$, **b** and **c** indicate coordination to the two amino-N's. The broadening of **d** and **e** indicate coordination to the

amide-N or the amide-O. The stoichiometry supports coordination to the two amino-N's, a pyridyl-N and the amide-O for this species. When the pH was increased from 3.49 to higher, signals **d** and **i** disappeared. The stoichiometry supports coordination to the two amino-N's, a pyridyl-N and the amide-N when MLH_{-1} forms. The change in ^{1}H-NMR spectra signals is similar to that of the Cu(II)-[H(555)NH_2] system, indicating that indeed complexation takes place at all the nitrogen donor. Further coordination at pH 10.67 to deprotonation of water when MLH_{-2} forms due to is not a change in coordination mode.

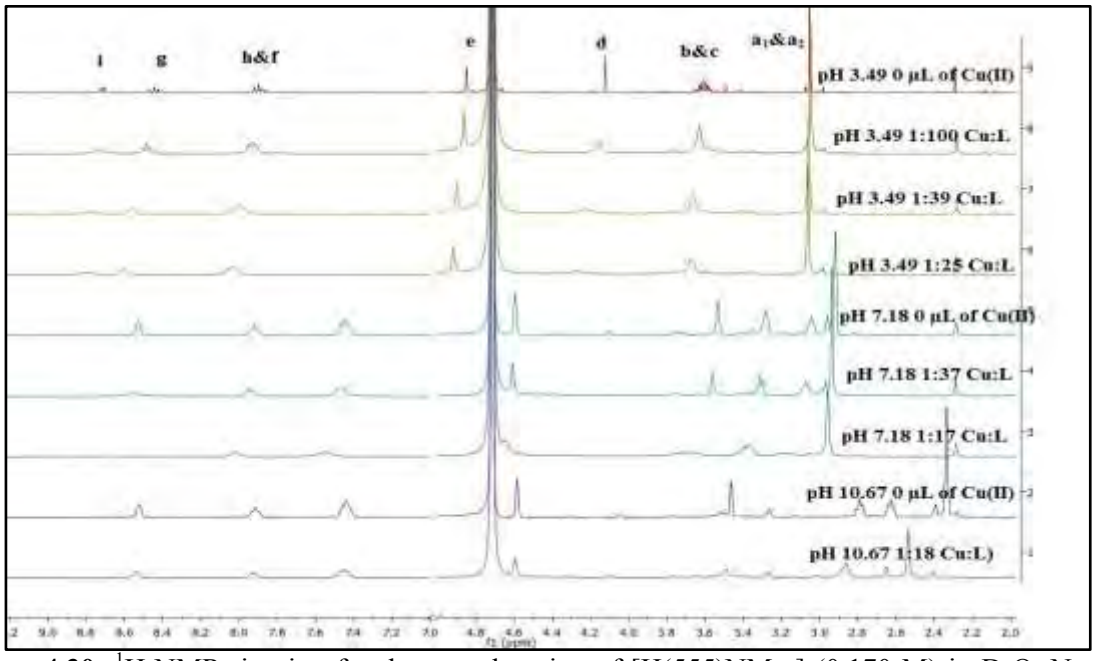

Figure 4.30: ^{1}H-NMR titration for the complexation of [H(555)NMe_2] (0.170 M) in D_2O. Note the break in the f1 dimension at 5.5 ppm. The proton assignments are according to Figure 4.17.

4.2.3.2.3 Cu(II)-[H_2(555)NH_2] complexes

Figure 4.31 shows the effect of Cu(II) on the spectrum of [H_2(555)NH_2]. At pH 3.11, MLH is the most predominant species in solution. At this pH, signals **f, d,** and **e** are substantially broadened. The **g** signal has broadened so much that it has virtually disappeared into the baseline. The broadening of **c** indicates coordination to the amide-N or the amide-O. Since the other proton signals are not substantially broadening, this implies that the terminal amine is not coordinated. This is a clear indication that Cu(II) binds to the pyridyl-N and the amide-O for this species. However, in a more basic solution at pH 5.02, the signals for protons **a** and **b** also broaden, indicating that the terminal amine also

coordinates to the Cu(II). At this pH the ML species predominates. At pH 7 and 10, all the peaks are broadening. This is consistent with the structures postulated for MLH_{-1} and MLH_{-2} from potentiometry, where the two amide-N's are coordinated.

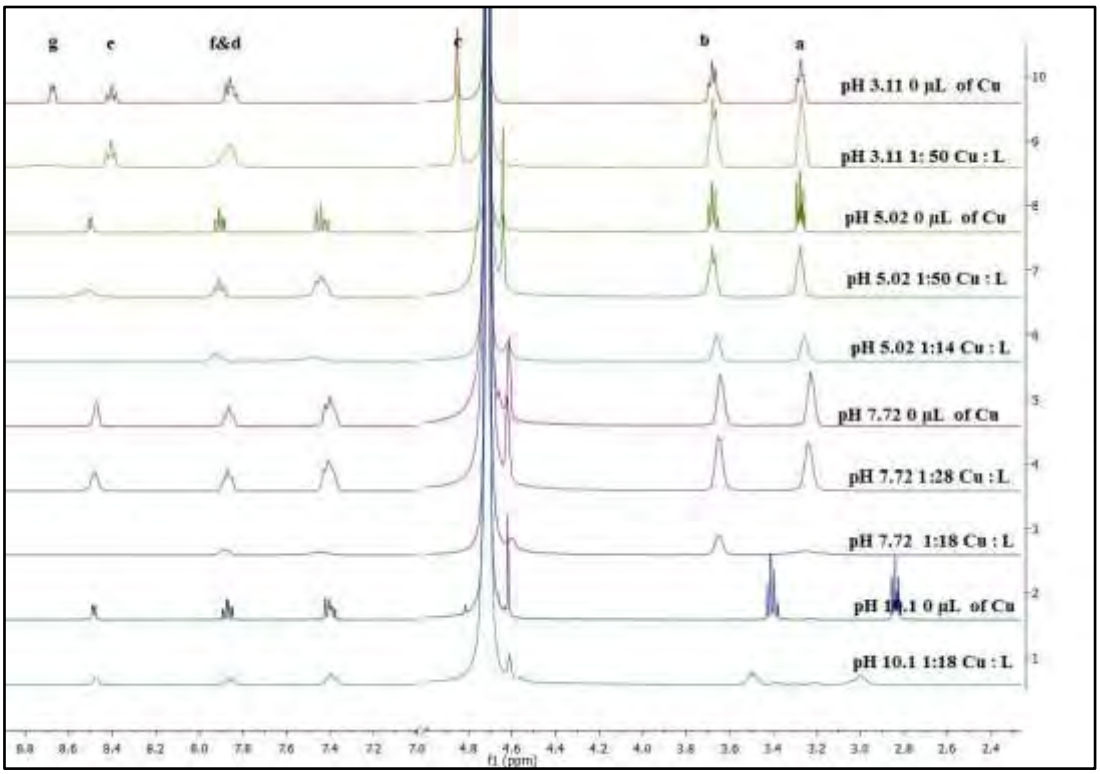

Figure 4.31: ^{1}H-NMR titration for the complexation of $[H_2(555)NH_2]$ (0.100 M) in D_2O. Note the break in the f1 dimension at 5.0 ppm. The proton assignments are according to Figure 4.20.

4.2.3.2.4 Cu(II)-$[H_2(565)NH_2]$ complexes

Figure 4.32 shows the spectra for complexation of Cu(II) with $[H_2(565)NH_2]$ as a function of pH. The interpretation of these spectra is difficult as, from the potentiometric studies, the formation of MLH, ML and MLH_{-2} overlap. Since the different species are likely to be in rapid chemical exchange only average effects will be seen. When the amount of Cu(II) titrated into the $[H_2(565)NH_2]$ solution increased, the signals broadened extensively. At pH 4.15, with the exception of **h**, all the proton signals are broaden the same. For the MLH species we postulate that the Cu(II) is coordinated to the pyrdyl-N, and the two amide-O's. This structure is consistent with the UV-visible results. At pH 4.69, the **a** proton signal preferentially broadens, indicating that the terminal amine is now coordinated. This is also consistent with the structure postulated for ML from potentiometry, but is not

consistent with the UV-visible results where the same λ_{max} was found for ML and MLH. At pH 7.5 the most predominant species is MLH_{-2}. Here the same broadening of signals was seen as that observed at pH 4.69. From potentiometry and UV-visible we postulated that for this species the coordination swapped from amide-O to amid-N. Since this should not have an effect on the Cu(II)-proton distances the same broadening would be expected. Note, in strongly basic conditions, the signals appear again and sharpen when the amount of Cu(II) was increased. Since, in solution the concentration of the ligand is very much greater than that of Cu(II), the effect of Cu(II) coordination is transferred to the bulk free ligand *via* chemical exchange. The sharpening of the signals with increasing pH is explained by the slowing down of the exchange.[54-56] Similar observations have been made on the Cu(II)- glycylglycylhistamine (GlyGlyHa) system.[57]

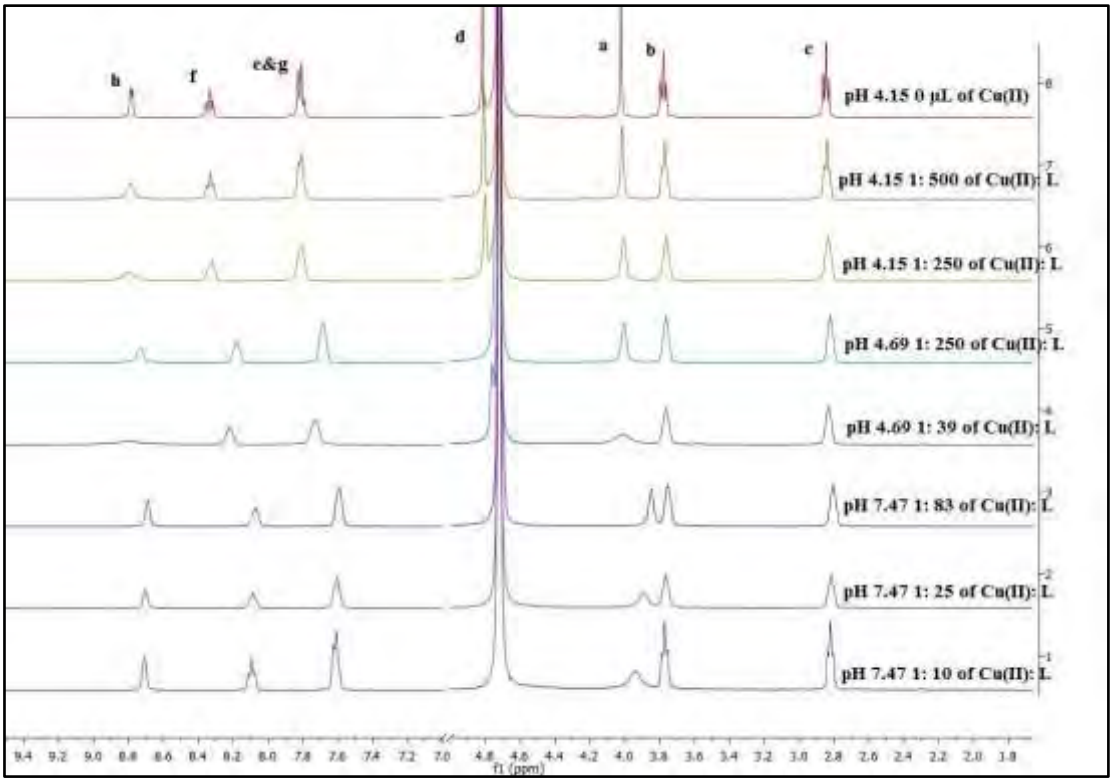

Figure 4.32: ^{1}H-NMR titration for the complexation of $[H_2(565)NH_2]$ (0.099 M) in D_2O. Note the break in the f1 dimension at 5.0 ppm. The proton assignments are according to Figure 4.23.

4.2.3.2.5 Cu(II)-[H(56)NH_2] complexes

The effects of Cu(II) addition on the ^{1}H-NMR spectrum of [H(56)NH_2] are shown in Figure 4.33. The addition of small amounts of Cu(II) to [H(56)NH_2] caused differential broadening of resonances, which provided an indication of the location of Cu(II) binding. At pH 4.31, the most predominant species is ML. Only signals **c, d, f, e** and **g** are broadening at this pH. This implies that Cu(II) binds to the pyridyl-N and the amide-O in this species. This is interesting, particularly as ML was not detected spectroscopically due to its very low concentration. At pH 7.39, the $CuLH_{-1}$ species predominates. The signal of proton **g** broadens so much that it disappears into the baseline while those for the **a** and **b** protons also broaden substantially. The stoichiometry supports coordination to the pyridyl-N, an amino-N and the amide-N when $CuLH_{-1}$ forms. Above pH 7.39, all the resonances were observed to broaden. However, the signals **a** and **g** disappeared completely. These results indicate that coordination of $CuLH_{-2}$ is the same as $CuLH_{-1}$. MLH_{-2} forms from the deprotonation of a coordinated water molecule.

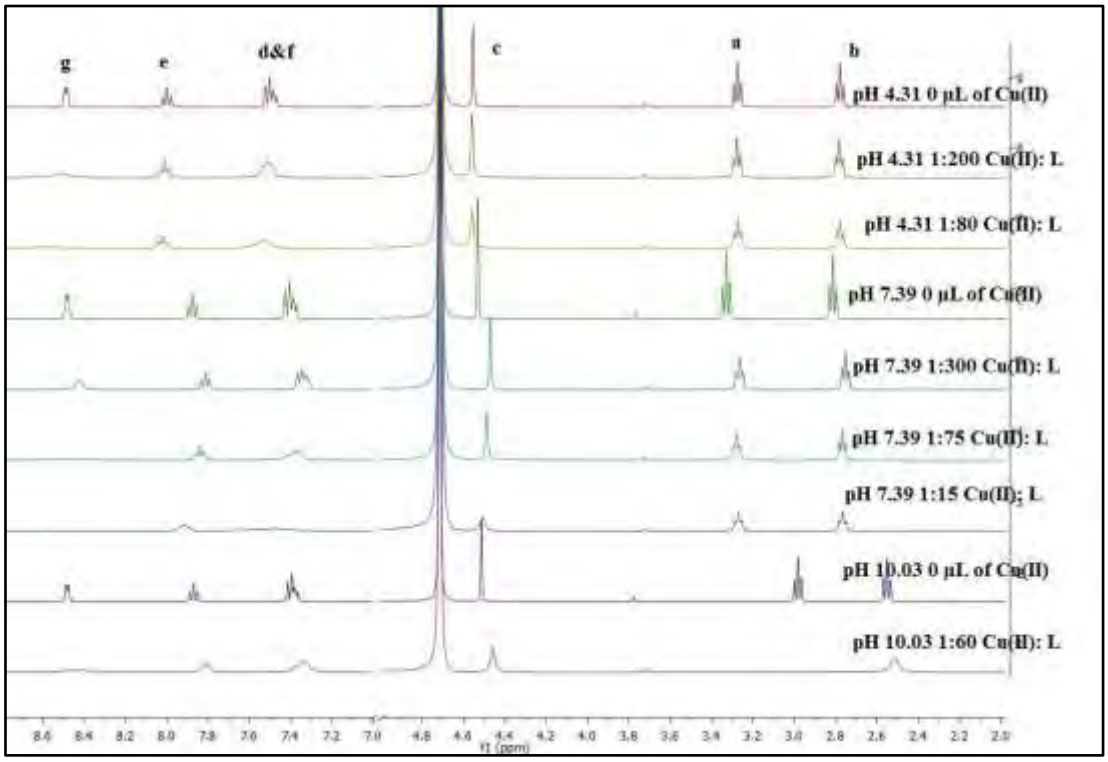

Figure 4.33: ^{1}H-NMR titration for the complexation of [H(56)NH_2] (0.099 M) in D_2O. Note the break in the f1 dimension at 5.0 ppm. The proton assignments are according to Figure 4.26.

4.3 Crystallography

4. 3.1 Introduction

Single-crystal X-ray diffraction, is a study of crystal structure through X-ray diffraction techniques which may lead to an understanding of the molecular and crystal structure of a substance. X-ray crystallography gives information on the structure and properties of the crystalline state by determining the arrangement of atoms within a crystal. It can be applied to a wide range of sizes of structures ranging from very small molecules and simple salts to complex minerals and synthetically prepared inorganic and organometallic complexes. X-ray crystallography is the only technique capable of providing detailed information on interatomic distances, bond angles, molecular architecture, absolute configuration, thermal vibration parameters and crystal packing, as well as possible order-disorder and/or non-stoichiometry from the same experiment.[58] The solid state structure only provides an indication of the solution speciation as one cannot guarantee that the species that crystalizes survive in solution.

4.3.2 Experimental

4.3.2.1 Single-crystal data collection for Cu(II)-[H(56)NH_2Cl]H_{-1}

A single crystal of Cu(II)-[H(56)NH_2Cl]H_{-1}, suitable for X-ray structure determination was grown by slow evaporation of a 1:1 mixture of EtOH:$ClHCl_3$ and an aqueous solution of the title compound at pH 11.03. X-ray single crystal intensity data were collected on a Nonius Kappa-CCD diffractometer using graphite monochromated MoKα radiation (λ = 0.71073 Å). The temperature was controlled by an Oxford Cryostream cooling system (Oxford Cryostat). The strategy for the data collections was evaluated using the Bruker Nonius "Collect" program. Data were scaled and reduced using DENZO-SMN software.[59] Absorption correction was performed using SADABS.[60] The structure was solved by direct methods and refined employing full-matrix least-squares with the program SHELXL-97[61] refining on F^2. The program PovRay in the X-seed interface was used to generate pictures.[62]

4.3.2.2 Single-crystal data collection for Cu(II)-[H_2(565)NH_2]H_{-2}

A single crystal of Cu(II)-[H_2(565)NH_2]H_{-2}, suitable for X-ray structure determination was grown by slow evaporation of a 1:1 mixture of MetOH:$ClHCl_3$ and an aqueous solution of the title compound at pH 11.06. Single-crystal X-ray diffraction data

were collected on a Bruker KAPPA APEX II DUO diffractometer using graphite-monochromated Mo-Kα radiation (χ = 0.71073 Å). Data collection was carried out at 173(2) K. Temperature was controlled by an Oxford Cryostream cooling system (Oxford Cryostat). Cell refinement and data reduction were performed using the program SAINT[1]. The data were scaled and absorption correction performed using SADABS.[63] The structure was solved by direct methods and refined by full-matrix least-squares methods based on F^2 using SHELXL version 2014/7[61] and using the graphics interface program X-Seed.[62,64] Diagram were produced using the program Pov-Ray.[65]

The structure was refined to an R factor of 0.0267 and 0.0309 for $[H(56)NH_2]H_{-1}$ and $[H_2(565)NH_2]H_{-2}$ respectively. The crystallographic data and refinement parameters for both copper complexes are given in Table 4.3.

Table 4.3: Details of data collection and structure refinement for the crystal analysis of the Cu(II)-$[H(56)NH_2Cl]H_{-1}$ and Cu(II)-$[H_2(565)NH_2]H_{-2}$ complexes.

Compound	**Cu(II)-[H(56)NH_2Cl] ($CuLH_{-1}$)**	**Cu(II)-[H_2(565)NH_2] ($CuLH_{-2}$)**
Formula	Cu C_9 H_{12} N_3OCl, 2(H_2O)	C_{11} H_{14} Cu N_4 O_2, 2(H_2O)
Molecular weight (g mol^{-1})	313.25	333.84
Temperature (K)	173(2)	173(2)
Crystal system	Monoclinic	Monoclinic
Space group	$P2_1/c$	$P2_1/c$
a (Å)	7.3116(2)	6.9351(7)
b (Å)	22.4070(9)	16.6491(17)
c (Å)	7.3570(2)	11.5189(12)
α (˚)	90	90
β (˚)	90.080(2)	95.176(2)
γ (˚)	90	90
Volume of unit cell ($Å^3$)	1205.30(7)	1324.6(2)
Z	4	4
No. of reflections collected	5280	18562
No. unique reflections	2860	3046
Calculated density (g cm^{-3})	1.726	1.674
Absorption coefficient (mm^{-1})	2.034	1.669
F(000)	644	692
Crystal Size (mm)	0.05 x 0.07 x 0.10	0.13 x 0.14 x 0.17
Radiation	Mo Kα (λ= 0.71073 A˚)	Mo Kα (χ= 0.71073)
theta range for data collection (∘)	3.3 - 27.9	2.2, 27.5
Reflections measured	2860	3046
R, R_w, goodness-of-fit	0.0267, 0.0668, 1.07	0.0309, 0.0764, 1.05
Min and max residual density (e $A^{\circ -3}$)	-0.65, 0.43	-0.46, 0.30

All non-hydrogen atoms for $[H(56)NH_2Cl]H_{-1}$ and $[H_2(565)NH_2]H_{-2}$ were refined anisotropically. All hydrogen atoms, except those of NH_2 and H_2O, were placed in idealised

positions and refined in riding models with U_{iso} assigned the values 1.2 times those of their parent atoms, and the C-H bond distances were constrained to 0.95 Å for aromatic hydrogen atoms and 0.99 Å for CH_2. The hydrogen atoms of $[H(56)NH_2]H_{-1}$ (H1C, H1D, H2C, H2D, H3A and H3B) and for $[H_2(565)NH_2]H_{-2}$ (H3A, H3B, H4A, H4B, H4C and H4D) were located in the electron difference maps and refined with simple bond lengths restraints.

4.3.3 Results and discussion

4.3.3.1 Crystal structure of Cu(II)-$[H(56)NH_2Cl]H_{-1}$

The Cu(II)-$[H(56)NH_2]H_{-1}$ complex crystallises in monoclinic crystal system space group $P2_1/c$. The structure and the atom-labeling of the complex are shown in Figure 4.34. The structure of the complex consists of a Cu atom surrounded in a pentadentate manner through the pyridyl-N, amino-N, and amide-N of the ligand. One Cl atom in this complex occupies an equatorial plane and another chloride atom is in the axial positions, which makes the Cu(II) coordination 3+2 as shown in Figure 4.35. The principal atomic distances and angles are summarized in Table 4.4.

Table 4.4: Principal atomic distances and angles in Cu(II)-$[H(56)NH_2Cl]H_{-1}$ complex.

Distances (Å)							
Cu1	-Cl1	2.6736(5)		C1	-C2	1.518(3)	
Cu1	-N1	1.9896(17)		C2	-C3	1.514(3)	
Cu1	-N2	1.9756(15)		C4	-C5	1.501(3)	
Cu1	-N3	1.9783(16)		C5	-C6	1.391(3)	
Cu1	Cl1_a	2.3229(5)		C6	-C7	1.383(3)	
O1	-C3	1.277(3)		C7	-C8	1.390(3)	
O2	-H2D	0.97(2)		C8	-C9	1.373(3)	
O2	-H2C	0.968(16)		C1	-H1B	0.9900	
O3	-H3A	0.97(2)		C1	-H1A	0.9900	
O3	-H3B	0.97(2)		C2	-H2A	0.9900	
N1	-C1	1.478(3)		C2	-H2B	0.9900	
N2	-C3	1.317(3)		C4	-H4A	0.9900	
N2	-C4	1.464(3)		C4	-H4B	0.9900	
N3	-C5	1.344(3)		C6	-H6	0.9500	
N3	-C9	1.350(3)		C7	-H7	0.9500	
N1	-H1D	0.879(9)		C8	-H8	0.9500	
N1	-H1C	0.880(11)		C9	-H9	0.9500	
Angles(°)							
Cl1	-Cu1	-N1	88.88(4)	O1	-C3	-C2	117.31(17)
Cl1	-Cu1	-N2	113.46(4)	O1	-C3	-N2	124.24(19)
Cl1	-Cu1	-N3	88.98(4)	N2	-C4	-C5	110.32(17)
Cl1	-Cu1	-Cl1_a	95.55(2)	C4	-C5	-C6	122.63(19)
N1	-Cu1	-N2	94.12(6)	N3	-C5	-C4	116.29(17)
N1	-Cu1	-N3	175.17(6)	N3	-C5	-C6	121.08(17)

Cl1_a	-Cu1	-N1	91.63(5)	C5	-C6	-C7	119.1(2)
N2	-Cu1	-N3	82.77(6)	C6	-C7	-C8	119.53(19)
Cl1_a	-Cu1	-N2	150.49(5)	C7	-C8	-C9	118.46(19)
Cl1_a	-Cu1	-N3	92.88(5)	N3	-C9	-C8	122.30(19)
Cu1	-Cl1	-Cu1_b	107.58(2)	N1	-C1	-H1A	109.00
H2C	-O2	-H2D	98.1(19)	C2	-C1	-H1B	109.00
H3A	-O3	-H3B	104.9(19)	H1A	-C1	-H1B	108.00
Cu1	-N1	-C1	111.07(12)	N1	-C1	-H1B	109.00
Cu1	-N2	-C3	130.45(14)	C2	-C1	-H1A	109.00
C3	-N2	-C4	115.20(16)	C3	-C2	-H2A	108.00
Cu1	-N2	-C4	113.80(12)	C1	-C2	-H2A	108.00
Cu1	-N3	-C9	124.99(13)	C1	-C2	-H2B	108.00
C5	-N3	-C9	119.50(16)	H2A	-C2	-H2B	107.00
Cu1	-N3	-C5	115.51(12)	C3	-C2	-H2B	108.00
H1C	-N1	-H1D	107(2)	N2	-C4	-H4B	110.00
C1	-N1	-H1C	110.5(13)	C5	-C4	-H4A	110.00
C1	-N1	-H1D	107.1(15)	H4A	-C4	-H4B	108.00
Cu1	-N1	-H1C	110.4(13)	C5	-C4	-H4B	110.00
Cu1	-N1	-H1D	110.8(16)	N2	-C4	-H4A	110.00
N1	-C1	-C2	112.21(17)	C5	-C6	-H6	121.00
C1	-C2	-C3	118.80(17)	C7	-C6	-H6	120.00
N2	-C3	-C2	118.45(18)	C8	-C7	-H7	120.00
C6	-C7	-H7	120.00	C8	-C9	-H9	119.00
C7	-C8	-H8	121.00	N3	-C9	-H9	119.00
C9	-C8	-H8	121.00				

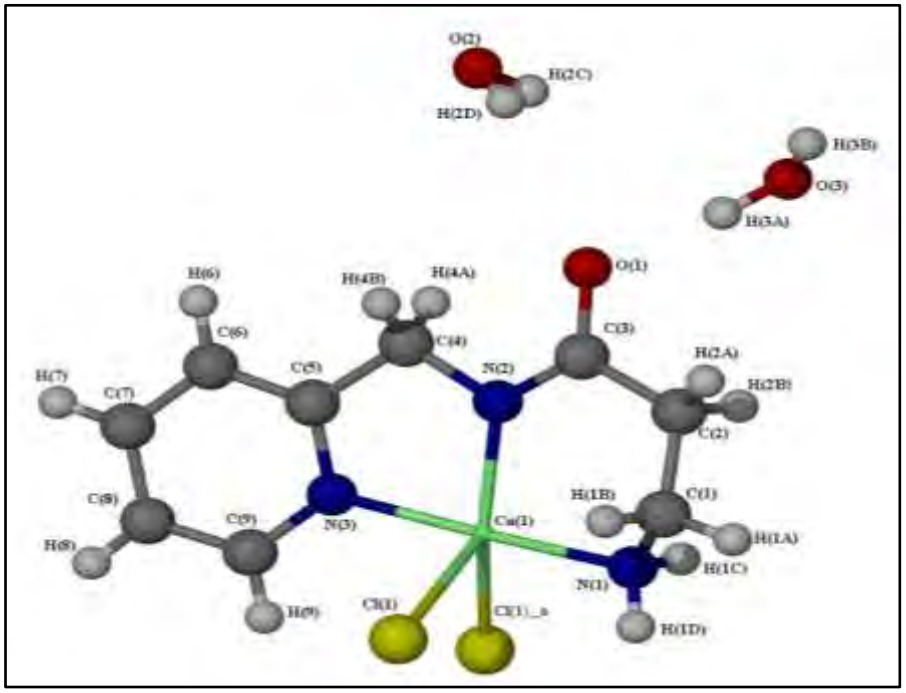

Figure 4.34: Crystal structure of complex Cu(II)-[H(56)NH_2Cl]$H_{.1}$.

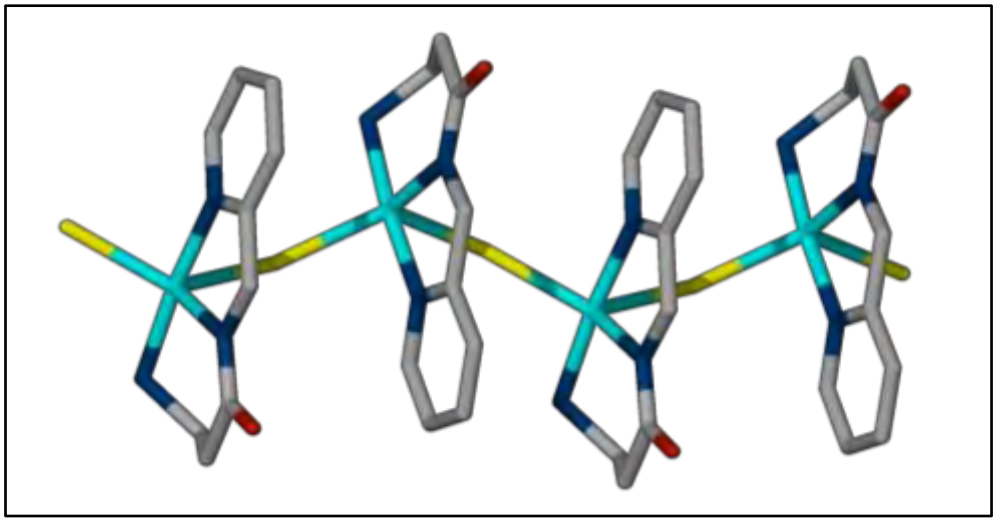

Figure 4.35: View of dimer made of two Cu(II)-[H(56)NH_2Cl]H_{-1} complexes.

Each chloride atom acts as a bridge and links two Cu atoms as shown in Figure 4.35. The coordination has typical Cu–N bond lengths[66] as in the case of $[Cu(Mepy_2)en]^{2+}$.[67,68] A geometry parameter τ, which is defined τ = (β - α)/60, is applicable to five-coordinate structures within the structural continuum between trigonal bipyramidal and tetragonal or rectangular pyramidal. For perfect tetragonal symmetry, τ is zero, and for perfect trigonal-bipyramidal geometry τ becomes 1.0.[69,70] In this complex, β = 175.11(6)° for N1–Cu1–N3, and α = 150.49 (5)° for Cl1_a–Cu1–N2. Thus, τ is (175.11 – 150.49)/60 = 0.410, indicating a 90% rectangular pyramidal geometry. Furthermore, the bridging chlorine atoms are positioned at distances of 2.67(5) Å for Cl(1) and 2.32(5) Å for Cl(1a) and make an angle of 95.55(2)◦ at each metal centre, in agreement with previous reports.[71-73] However, in this complex $CuLH_{-1}$ has a slightly rectangular pyramidal geometry structure which is essentially a D_{2h} symmetric. In addition, the bond lengths are Cu1–N1 1.98 Å, Cu1–N2 1.97 Å, Cu1–N3 1.97 Å and Cu1–Cl1 2.67-2.32Å. The angles around the copper atom are N1–Cu1–N2 94.12(◦), N1–Cu1–N3 175.17(◦) and N2–Cu1–N3 82.77(◦). Thus, values of bond angles and bond distances are in good agreement with those reported for some analogous Cu(II)complexes in a rectangular pyramidal geometry.[68,70]

4.3.3.2 Crystal structure of Cu(II)-[H_2(565)NH_2]H_{-2}

The solid-state structure of Cu(II)-[H_2(565)NH_2]H_{-2} determined by single-crystal X-ray diffraction, together with atom labelling, is shown in Figure 4.36. The bond lengths and bond angles are presented in Table 4.5.

Table 4.5: Principal atomic distances and angles in Cu(II)-[H_2(565)NH_2]H_{-2} complex.

Distances (Å)					
Cu1	-N1	2.0007(18)	C2	-C3	1.386(3)
Cu1	-N2	1.9327(18)	C3	-C4	1.379(3)
Cu1	-N3	1.9205(18)	C4	-C5	1.393(3)
Cu1	-N4	2.0083(19)	C5	-C6	1.497(3)
O1	-C7	1.259(3)	C7	-C8	1.516(3)
O2	-C10	1.265(3)	C8	-C9	1.528(4)
O3	-H3B	0.970(14)	C10	-C11	1.513(3)
O3	-H3A	0.969(17)	C1	-H1	0.9500
O4	-H4C	0.967(15)	C2	-H2	0.9500
O4	-H4D	0.97(2)	C3	-H3	0.9500
N1	-C1	1.355(3)	C4	-H4	0.9500
N1	-C5	1.344(3)	C6	-H6A	0.9900
N2	-C7	1.317(3)	C6	-H6B	0.9900
N2	-C6	1.460(3)	C8	-H8A	0.9900
N3	-C10	1.307(3)	C8	-H8B	0.9900
N3	-C9	1.456(3)	C9	-H9B	0.9900
N4	-C11	1.481(3)	C9	-H9A	0.9900
N4	-H4B	0.879(17)	C11	-H11A	0.9900
N4	-H4A	0.880(11)	C11	-H11B	0.9900
C1	-C2	1.374(3)			
Angles(˚)					
N1	-Cu1	-N2	83.41(8)	C4	-C5	-C6	121.4(2)
N1	-Cu1	-N3	168.17(9)	N1	-C5	-C6	116.94(18)
N1	-Cu1	-N4	100.64(7)	N2	-C6	-C5	110.26(18)
N2	-Cu1	-N3	94.97(8)	O1	-C7	-C8	118.44(19)
N2	-Cu1	-N4	167.72(9)	N2	-C7	-C8	117.8(2)
N3	-Cu1	-N4	83.39(8)	O1	-C7	-N2	123.8(2)
H3A	-O3	-H3B	109(3)	C7	-C8	-C9	115.9(2)
H4C	-O4	-H4D	108(3)	N3	-C9	-C8	111.12(19)
C1	-N1	-C5	118.71(18)	N3	-C10	-C11	114.74(19)
Cu1	-N1	-C5	113.96(14)	O2	-C10	-N3	127.3(2)
Cu1	-N1	-C1	127.32(15)	O2	-C10	-C11	117.94(19)
Cu1	-N2	-C6	115.34(14)	N4	-C11	-C10	111.02(19)
Cu1	-N2	-C7	128.29(15)	C2	-C1	-H1	119.00
C6	-N2	-C7	116.08(18)	N1	-C1	-H1	119.00
Cu1	-N3	-C9	122.32(14)	C1	-C2	-H2	120.00
C9	-N3	-C10	119.83(18)	C3	-C2	-H2	120.00
Cu1	-N3	-C10	117.71(15)	C4	-C3	-H3	120.00
Cu1	-N4	-C11	108.75(14)	C2	-C3	-H3	120.00
C11	-N4	-H4B	106.6(16)	C5	-C4	-H4	120.00
Cu1	-N4	-H4B	120.5(17)	C3	-C4	-H4	120.00
C11	-N4	-H4A	109.5(16)	N2	-C6	-H6B	110.00
Cu1	-N4	-H4A	105.0(17)	N2	-C6	-H6A	110.00
H4A	-N4	-H4B	106(2)	H6A	-C6	-H6B	108.00
N1	-C1	-C2	122.2(2)	C5	-C6	-H6A	110.00
C1	-C2	-C3	119.1(2)	C5	-C6	-H6B	110.00
C2	-C3	-C4	119.1(2)	C9	-C8	-H8A	108.00
C3	-C4	-C5	119.2(2)	C9	-C8	-H8B	108.00

N1	-C5	-C4	121.65(19)	H8A	-C8	-H8B	107.00
C7	-C8	-H8A	108.00	C8	-C9	-H9B	109.00
C7	-C8	-H8B	108.00	N4	-C11	-H11B	109.00
C8	-C9	-H9A	109.00	N4	-C11	-H11A	109.00
N3	-C9	-H9A	109.00	H11A	-C11	-H11B	108.00
N3	-C9	-H9B	109.00	C10	-C11	-H11A	109.00
H9A	-C9	-H9B	108.00	C10	-C11	-H11B	109.00

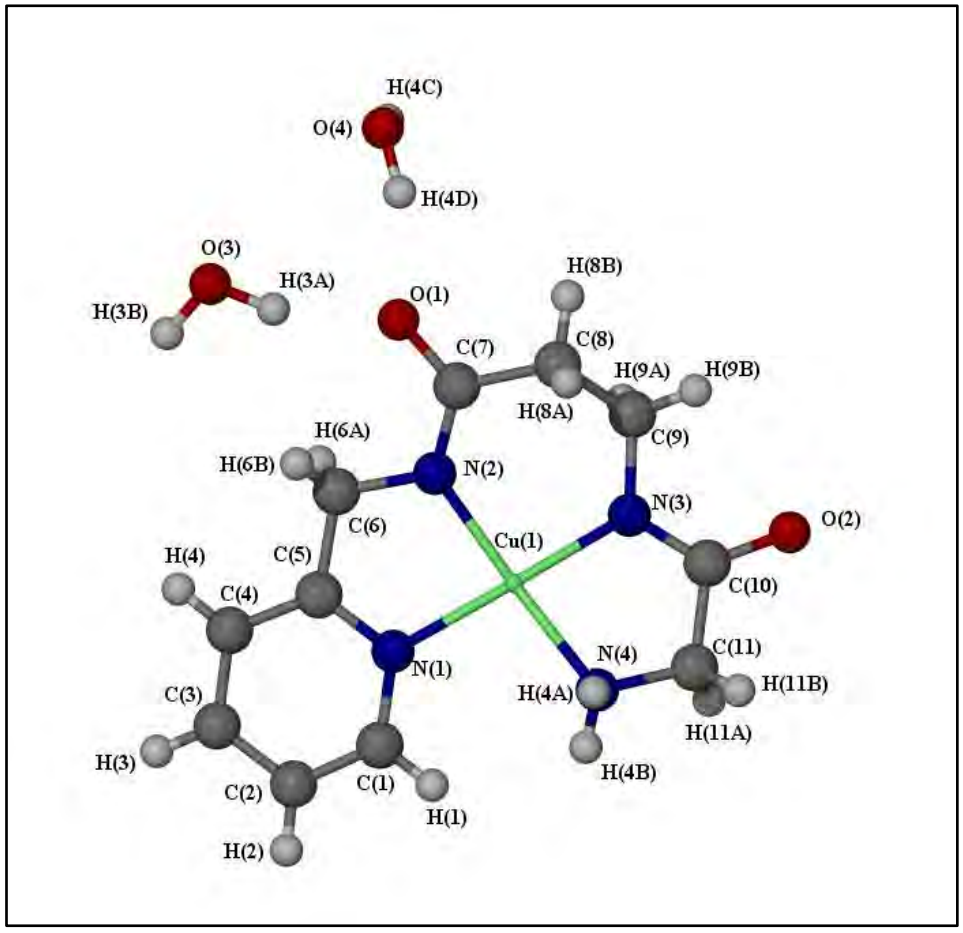

Figure 4.36: Crystal structure of complex Cu(II)-$[H_2(565)NH_2]H_{-2}$.

The crystal structure of the Cu(II)-$[H_2(565)NH_2]H_{-2}$ complex consists of a monomer of Cu(II) coordinated to the ligand *via* the pyridyl-N, the amine-N and the two amide -N. In this complex Cu(II) has a slightly distorted square planar geometry, with the two amides in *cis* positions. The structure is essentially of D_{4h} symmetry. The Cu-N_{amine}, Cu-N_{amide} and Cu-N_{py} distances fall within the expected ranges of, 1.990– 2.004 Å[74], 1.91–1.96 Å[75], and 2.00-2.11 Å[76,77], respectively. The Cu–N_{amine} and Cu–N_{py} distances are almost equal to each other. Furthermore the bond angles N1-Cu-N2 83.41(8)° and N3-Cu-N4 83.39(8)° deviate only slightly from the ideal 90° for regular square planar geometry. The angle (θ) between

the N1-Cu-N2 and N3-Cu-N4 planes is found to be 17.64° rather than 0^o for a regular square plan. The trans angles N1-Cu-N3 and N2-Cu-N4 are 168.17(9)◦ and 167.72(9)◦ respectively which deviates from the ideal bond angle 180◦. These results suggest that Cu(II) in this complex is located in a geometry much closer to square planar. The angular distortions in the complex are caused by the different bite angles in the five and six membered chelate rings.

In summary, the $[H(56)NH_2Cl]H_{-1}$ ligand was reacted with Cu(II) chloride and the resulting complex analysed. The X-ray single crystal structure revealed that the motif consists of a monomeric Cu(II), with the copper bound to the three nitrogens of the ligand, as well as two chloride atoms. The fifth coordination site is occupied by Cu–3N and 2Cl to form a rectangular pyramidal geometry. On the other hand, the $[H_2(565)NH_2]H_{-2}$ ligand was coordinated with copper by four nitrogens to form distorted square planar geometry. The X-ray results support the structures suggesting by potentiometric and Uv-Vis studies. In particularly the X-ray result show the loss of the amide proton from both ligands. Unfortunately, it has not been possible to prepare a single crystal of either CuL or $CuLH_{-1}$ suitable for X-ray structure analysis. Furthermore, we were not able to perform crystal structure analyses of Cu(II) complexes of the other ligands.

4.4 Molecular Mechanics

4.4.1 Introduction

Molecular mechanics (MM) is a very popular tool used to express the structures and relative energies of a molecule as a function of its resistance to bond stretching, bond bending, and atom crowding.[78-81] Advances in computing have greatly increased the interest in computer-based molecular modelling. As such, it is now used as an aid in the interpretation of experimental results and design of new materials with desirable properties. In this study MM was used to determine the lowest energy conformation of possible geometries of the complex species in solution. These calculations of the strain energy of a molecule are done using force fields. The choice of a force field used in a calculation is entirely dependent on the type of complex or molecule (i.e. organic or inorganic) of interest and the software program used to run the simulation.[82] There are a limited number of reliable force fields to use for the MM calculation involving metal ions. Therefore, MM calculations involving transition metal ions are not used to the same extent as those for organic molecules.[83,15]

4.4.2 Theory

The basis of the molecular mechanics method is that a good estimate of the geometry of a molecule can be obtained by taking into account all the forces between atoms calculated using a mechanical approach.[78,79]

Molecular mechanics expresses the strain energy E^{strain} ; meaning that it reflects the "strain" inherent to a "real" molecule relative to some idealized form. However, it arises from four principle energy terms[78,79,84] the general form of which is given as;

$$E^{strain} = \sum_{A}^{bonds} E_A^{stretch} + \sum_{A}^{bond\ angles} E_A^{bend} + \sum_{A}^{torsion\ angles} E_A^{torsion} + \sum_{A}^{non-bonded\ atoms} \sum_{B} E_{AB}^{non-bonded} \quad (4.7)$$

Bond deformation strain is the energy exerted on a bond between atoms, either by stretching the bond or compressing it. Due to a bond's ability to stretch/compress and the ability of the angle between the bonds to bend, the total bond deformation strain can be estimated using Hooke's law.

$$\mathrm{E}^{stretch}(r) = \frac{1}{2}k^{stretch}(\mathrm{r} - \mathrm{r}^{eq})^2$$

(4.8)

$$\mathrm{E}^{bend}(\alpha) = \frac{1}{2}k^{bend}(\alpha - \alpha^{eq})^2$$

(4.9)

where $k^{stretch}$ and k^{bend} are the so-called stretch and bend "force constants" respectively, while r and α are the bond distance and angle respectively, and r^{eq} and α^{eq} are the "ideal" (equilibrium) bond length and bond angle respectively, taken either from performing experiments or from accurate quantum chemical calculations.

Proper description of the torsional potential requires a form that reflects its inherent periodicity. However, torsional strain is experienced when a molecule undergoes a complete rotation around one bond.

$$E^{torsion}(\omega) = k^{torsion3}[1 - \cos 3(\omega - \omega^{eq})]$$

(4.10)

ω is the torsion angle, ω^{eq} is the ideal torsion angle and $k^{torsion3}$ is treated as a parameter. Bond torsion contributions to the overall energy may also need to include terms which are one-fold and two-fold periodic.

$$E^{torsion}(\omega) = k^{torsion1}[1 - \cos(\omega - \omega^{eq})] + k^{torsion2}[1 - \cos 2(\omega - \omega^{eq})] + k^{torsion3}[1 - \cos 3(\omega - \omega^{eq})]$$

(4.11)

$k^{torsion1}$ and $k^{torsion2}$ are additional parameters

Non-bonded interactions typically involve a sum of van der Waals (VDW) interactions and coulombic interactions.

$$\mathrm{E}^{non\text{-}bonded}(\mathrm{r}) = \mathrm{E}^{VDW}(\mathrm{r}) + \mathrm{E}^{Coulombic}(\mathrm{r})$$

(4.12)

Additional non-bonded terms may be included to account explicitly for interactions such as hydrogen bonding.

Most commonly, van der Waals interactions are represented as a sum of repulsive and attractive terms.[85] This occurs when the distance between these substituents is less than van der Waals radii.[86]

$$E^{VDW}(r) = \varepsilon \left[\left(\frac{r^{\circ}}{r}\right)^{12} - 2\left(\frac{r^{\circ}}{r}\right)^{6} \right] \tag{4.13}$$

r is the non-bonded distance, and ε and r^{o} are parameters. This functional form provides a very steep energy barrier inside the sum of van der Waals radii for the two atoms involved.

The coulombic term takes account of the interaction of charges.

$$E^{Coulombic}(r) = \frac{qq'}{r} \tag{4.14}$$

r is the non-bonded distance, and the atomic charges, q, may either be treated as parameters or be taken from quantum chemical calculations.

Many different kinds of force fields have been developed over the years. Some include additional energy terms that describe other kinds of deformations. Some force fields account for coupling between bending and stretching in adjacent bonds in order to improve the accuracy of the mechanical model. In general force field terms are derived empirically with the target of reproducing experimental structures and energy distributions.[78,79] The extension of MM to inorganic chemistry and especially to transition-metal (TM) systems presents greater challenges.[82,87,88] A generic force field, Extensible Systematic Force Field (ESFF)[89] has been developed. This force field[90] attempts to provide the widest possible coverage of the periodic table, including transition metals, with reasonable accuracy and has been successfully used to model several proteins containing metals.[89,91,92] ESFF employs semi-empirical rules to translate atomic-based parameters to parameters typically associated with a covalent valence force field. The atomic parameters depend not only on atom type, but also on internal type, thus resulting in a more accurate force field. The force field has been applied to molecular simulations of a wide variety of systems including nucleic acids,

peptides, hydrocarbons, -porphyrins, transition metal complexes, zeolites, and organometallic compounds.[89] The agreement with the experimental results indicates that ESFF is a valuable tool in molecular simulations for understanding and predicting both crystal and gas phase molecular structures. The valence bond, angle, torsion, and out-of-plane energies in the mathematical expression of the ESFF are used to describe the internal interactions, while van der Waals and electrostatic energies represent the nonbonded interactions.[91] An advantage of using the ESFF force field is the ease in automatic parameterization of all atom types.[93] The ESFF force field has been used extensively to study the geometry of Cu(II) complexes[91,92,94], including complexes with amide coordination.[94-96] However, it should be noted that MM does not calculate the absolute energy of a system as it does not take into account bond enthalpies or entropy of the system. Instead, it calculates the energy brought about by changes in bond angles and lengths from their idealised (parameterized) values. When a complex forms the ligand has to adopt a conformation that is different from its lowest energy structure. This increased conformational energy is compensated for by the formation of new bonds to the metal ion. For this reason it is not really valid to compare two structures that have different bonding. However, the strain introduced into the ligand as a result of metal ion coordination can be used as an indication of stability or likelihood of formation.

4.4.3 Calculations

The MM calculations were performed using the force field ESFF[97] as implemented in the InsightII v. 2004.1 package.[98] The different chemical species in solution were constructed from fragments using the BUILDER module of the Accelrys Biosym/MSI software package and were based on the speciation models obtained from UV-visible spectroscopy and potentiometry (see Chapter 3 and 4.1). The energy minimizations of the copper speciation complexes were carried out using the Discover_3 program which was run as an application in the Insight II package.[98]

4.4.4 Results and Discussion

In this study, MM has been used to provide more evidence in support of the solution structures postulated from potentiometric and spectroscopic data. In this regard, structures of two sets of species were considered for each Cu(II) ligand system.

The energy-minimised structures for the Cu(II)-[H(555)NH_2], [H_2(565)NH_2] and [H(56)NH_2] systems are given in Figures 4.37-4.41. The output data for the deformation energies including internal (strain) energy for these structures are given in Tables 4.6 - 4.10. The energy-minimised structures are compared in terms of internal energy. The internal energy indicates the strain energy introduced into the ligand when it coordinates to the central metal ion. It is a one of the contributing factor in the overall stability of the complex.

Strain energy elevates the internal energy contribution to the overall potential energy of the molecule resulting in low complex stability. On other hand, the strain contribution to the differences in stability is the energy associated with torsion of bonds as the different donor atoms are oriented for coordination to the metal ion. Bond stretching seems to make a less significant contribution to the differences in strain energies of these structures. The main differences in internal energy contribution arise from twisting of bonds and bending of angles as coordinating atoms are accommodated around the central metal ion.

4.4.4.1 ML of [H(555)NH_2] System

For the Cu(II)-[H(555)NH_2] system, it is possible to propose two structures for the ML complex (Figure 4.37). In one structure (Figure 4.37**a**), the Cu(II) is coordinated to the pyridyl-N, two amine-N and an amide-O. In the other structure (Figure 4.37**b**) the Cu(II) is bound to the pyridyl-N, amine-N and amide-N, while the terminal amine is not coordinated. In order to maintain the stoichiometry, the amine will have to be protonated as the amide has lost a proton. The optimised, MM structures for these two structures show that the Cu(II) in Figure 4.37**a** is very distorted from an idealised tetragonal geometry, while Figure 4.37**b** has a square planar arrangement of ligands in the equatorial plane. Figure 4.37**a** has a much higher total internal energy (E_{int}) (84.58 kcal mol^{-1}) than Figure 4.37**b** (40.81 kcal mol^{-1}) (see Table 4.6). This is mainly as a result of angular and torsional distortions, which are 27 and 16 kcal mol^{-1} higher in Figure 4.37**a** than Figure 4.37**b**. Hence from MM calculations, the structure in Figure 4.37**b** is preferred. This conclusion supports both the potentiometric and spectroscopic data.

Table 4.6: Internal energy ($E_{internal}$), bond (E_{bond}), angle (E_{angle}), torsion ($E_{torsion}$) and out-of-plane (E_{Oop}) deformation energies (kcal mol^{-1}) for **(a)** 7,5,5 and **(b)** 5,5 membered chelate rings of ML Cu(II)-[H(555)NH_2] systems.

	[H(555)NH_2] ML	
	7,5,5 (a)	**5,5 (b)**
E_{int}	84.58	40.81
Bond	11.18	11.03
Angle	47.90	20.57
Torsion	24.23	8.35
Oop	1.26	0.84

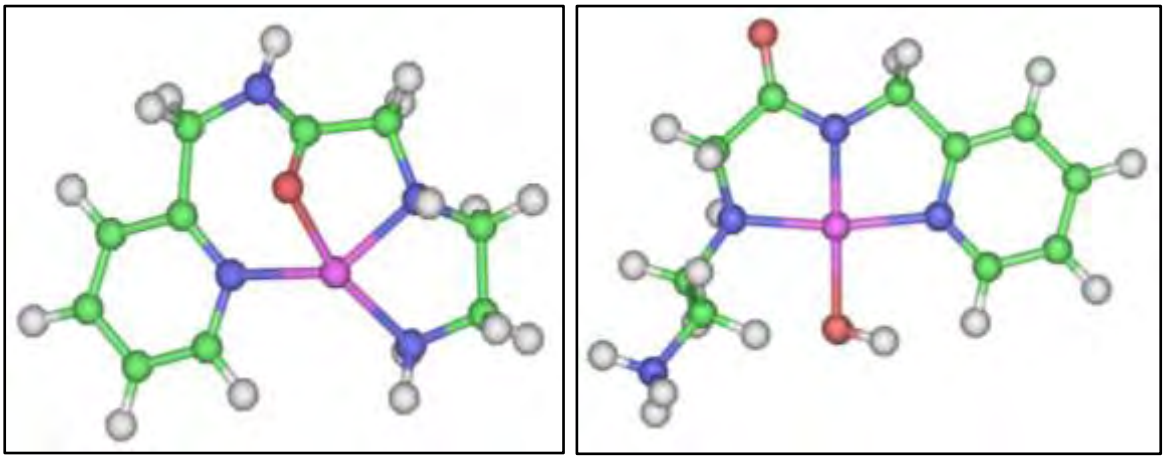

(a) **(b)**

Figure 4.37: Two possible energy-minimised structures of Cu(II)-[H(555)NH_2] (ML). **(a):** 7,5,5 membered chelate rings and **(b):** 5,5 membered chelate rings. For clarity the axial waters are not displayed.

4.4.4.2 MLH_{-1} of [H(555)NH_2] System

Figures 4.38**c** and 4.38**d** show the two proposed structure of MLH_{-1} species for the Cu(II)-[H(555)NH_2] system. In Figure 4.38**c**, the Cu(II) is coordinated to the pyridyl-N, two amine-N and amide-N to form 5,5,5 membered chelate rings. Meanwhile, the Cu(II) in Figure 4.38**d** is coordinated to the pyridyl-N, an amine-N and an amide-N to form 5,5 membered chelate rings; the terminal amine is not coordinated. The 5,5,5 chelate structure given in Figure 4.38**c** has a higher internal energy than the 5,5 chelate structure given in Figure 4.38**d**. The high strain energy associated with the 5,5,5 chelate structure is mainly due to the high angle bending and torsional energies in this structure (Table 4.7). From the MM calculations, the proposed structure with 5,5-membered ring in Figure 4.38**d** is preferred

for MLH_{-1}. This conclusion does not support the structure postulated from potentiometric and spectroscopic data, which favours 4.38c. Such a result clearly demonstrates the limitations of MM calculations as a computational tool for Cu(II) complexes since it does not take into account the bond enthalpy of the extra Cu-N bond, the electronic contributions of the metal or entropy effects, both in terms of the chelate effect of the ligand and the solvent.

Table 4.7: Internal energy ($E_{internal}$), bond (E_{bond}), angle (E_{angle}), torsion ($E_{torsion}$) and out-of-plane (E_{Oop}) deformation energies (kcal mol^{-1}) for **(c):** 5,5,5 and **(d):** 5,5 membered chelate rings of MLH_{-1} Cu(II)-[H(555)NH_2] systems

	[H(555)NH_2] MLH_{-1}	
	5,5,5 (c)	**5,5 (d)**
E_{int}	70.76	26.68
Bond	15.60	8.98
Angle	45.60	13.64
Torsion	8.53	3.87
Oop	0.97	0.18

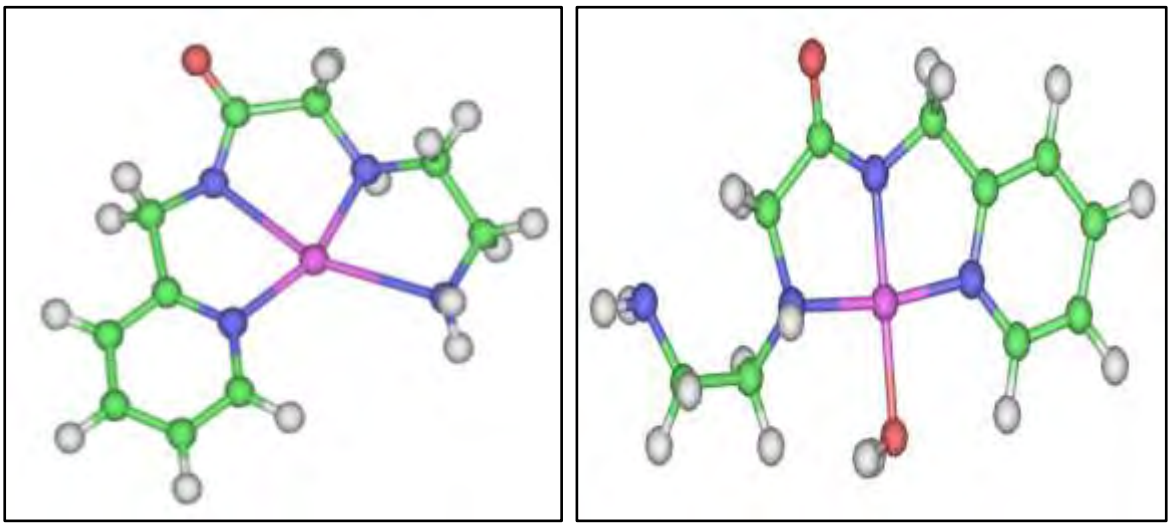

(c) **(d)**

Figure 4.38: Two possible energy-minimised structures of Cu(II)-[H(555)NH_2] (MLH_{-1}). **(c):** 5,5,5 membered chelate rings and **(d):** 5,5 membered chelate rings. For clarity the axial waters are not displayed.

4.4.4.3 ML of $[H_2(565)NH_2]$ System

The three proposed structures of ML species for the Cu(II)-$[H_2(565)NH_2]$ system are shown in Figures 4.39 (**e**, **f** and **g**). In Figure 4.39**e**, Cu(II) is coordinated to the pyridyl-N, an amide-N and an amide-O to form 5,8 membered chelate rings, while the terminal amine is still protonated. In the other two structures, Cu(II) is coordinated to the pyridyl-N and two amide-O to form 7,8 membered chelate rings. However, it could be coordinated as either the meridional isomer (Figure 4.39**f**) or the facial isomer (Figure 4.39**g**) to form an octahedral geometry. The meridional isomer chelate rings have high internal energy (Table 4.8), because it is distorted from an idealised tetragonal geometry. The two structures **e** and **g** have similar internal energies (53.87 kcal mol^{-1}) and (52.39 $kcalmol^{-1}$) respectively. However, the structure in Figure 4.39**e** has a very high angle bending energy. This energy comes from the distortion of the amide geometry. Ideally the amide with a carbonyl group must be planar with sp^2 hybridization. Thus, any distortion of this result leads to loss of electron delocalization with the N-amide partial double bond. From the potentiometric data (see section **3.5.2.4.3**) we postulated a similar structure to that predicted by these MM calculations in Figure 4.39**g**. Moreover, the spectroscopic data giving a λ_{max} value of 747 nm clearly suggests an octahedral geometry by one nitrogen donor atom.

Table 4.8: Internal energy ($E_{internal}$), bond (E_{bond}), angle (E_{angle}), torsion ($E_{torsion}$) and out-of-plane (E_{Oop}) deformation energies (kcal mol^{-1}) for **(e):** 5,8, **(f):** 7,8 Mer and **(g):** 7,8 Fac membered chelate rings of ML Cu(II)-$[H_2(565)NH_2]$ systems.

	$[H_2(565)NH_2]$ ML		
	5,8 (e)	**7,8 (f) mer**	**7,8 (g) fac**
E_{int}	53.87	116.51	52.39
Bond	12.62	18.82	10.39
Angle	33.44	85.61	20.03
Torsion	7.22	11.90	21.22
Oop	0.57	0.16	0.73

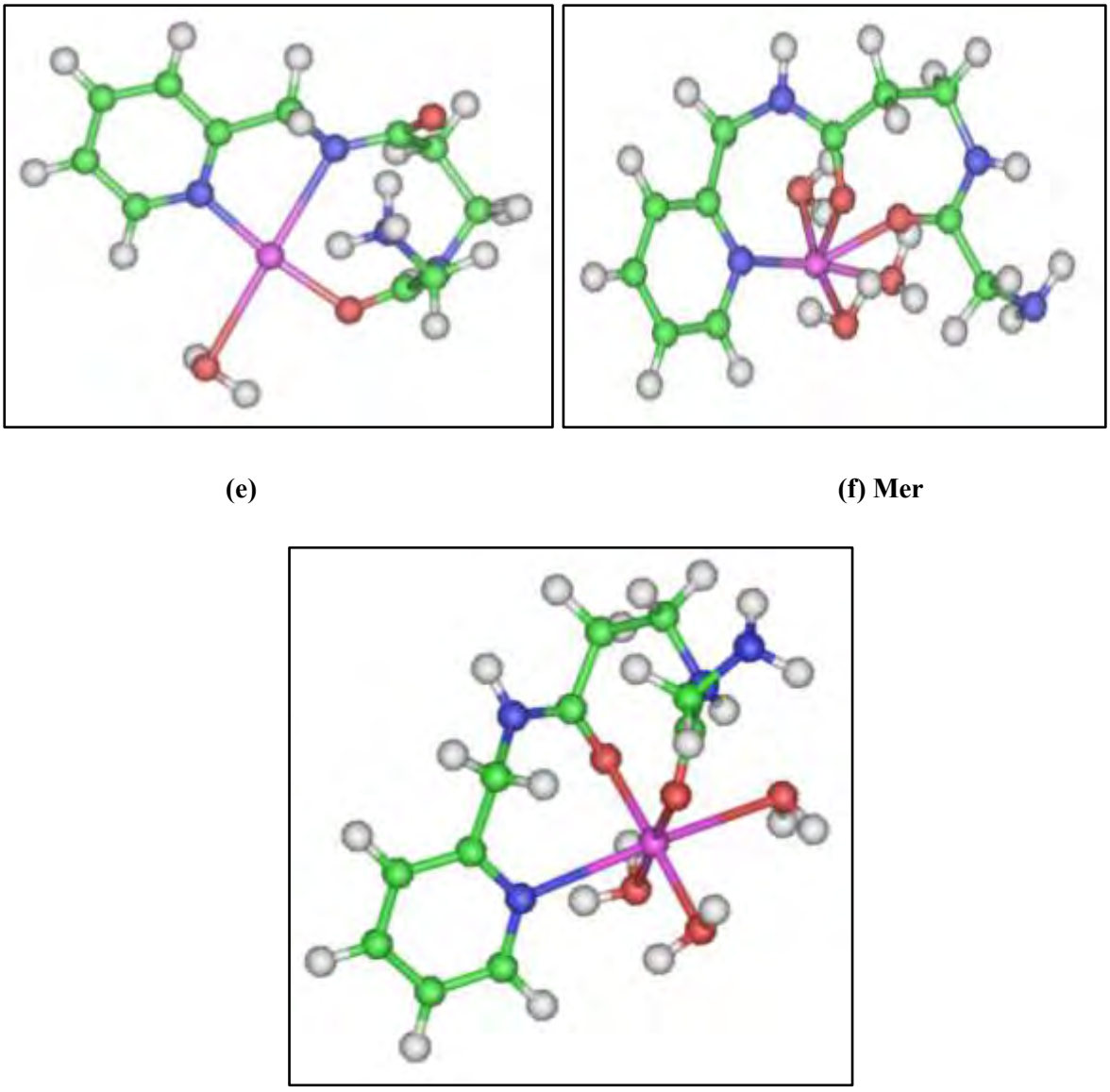

(e) **(f) Mer**

(g) Fac

Figure 4.39: Three possible energy-minimised structures of Cu(II)-[H_2(565)NH_2] (ML). **(e):** 5,8 **(f):** 7,8 Mer and **(g):** 7,8 membered chelate rings Fac. For clarity in the structure (e) the axial waters are not displayed.

4.4.4.4 ML of [H(56)NH_2] System

The two proposed structures of ML species for the Cu(II)-[H(56)NH_2] system are given in Figures 4.40**h** and 4.40**i** with their corresponding energies given in Table 4.9. The Cu(II) in Figure 4.40**h** is bound to the pyridyl-N, an amide-O and an amine-N to form 7,6-membered rings. In Figure 4.40**i**, the Cu(II) is coordinated by the pyridyl-N and an amide-N, while the terminal amine is protonated. The optimised MM structures for these two structures show that the Cu(II) with a 5-membered ring (Figure 4.40**i**) has a lower strain

energy than the 7,6 chelate structure (Figure 4.40**h**). This energy difference arises from a high angle bending energy (22.60 kcal mol^{-1}) and torsion energy (16.68 kcal mol^{-1}) in the 7,6 chelate structure as the amine nitrogen donor is forced into the coordination plane of the metal. From the MM calculations, the structure with a 5-membered ring (Figure 4.40**i)** is preferred. This structure is not consistent with the structure of the ML species determined from potentiometric study (Figure 4.40**h**). The ML result clearly demonstrates the limitations of MM calculations as a computational tool for Cu(II) complexes. This result is in accordance with the established observation that three chelate complexes are more stable than complexes with bidentate ligands.[99]

Table 4.9: Internal energy ($E_{internal}$), bond (E_{bond}), angle (E_{angle}), torsion ($E_{torsion}$) and out-of-plane (E_{Oop}) deformation energies (kcal mol^{-1}) for **(h):** 7,6 and **(i):** 5 membered chelate rings of ML Cu(II)-[H(56)NH_2] systems.

	[H(56)NH_2] ML	
	7,6 (h)	**5 (i)**
E_{int}	59.40	36.68
Bond	19.07	12.06
Angle	22.60	21.62
Torsion	16.68	2.80
Oop	1.03	0.19

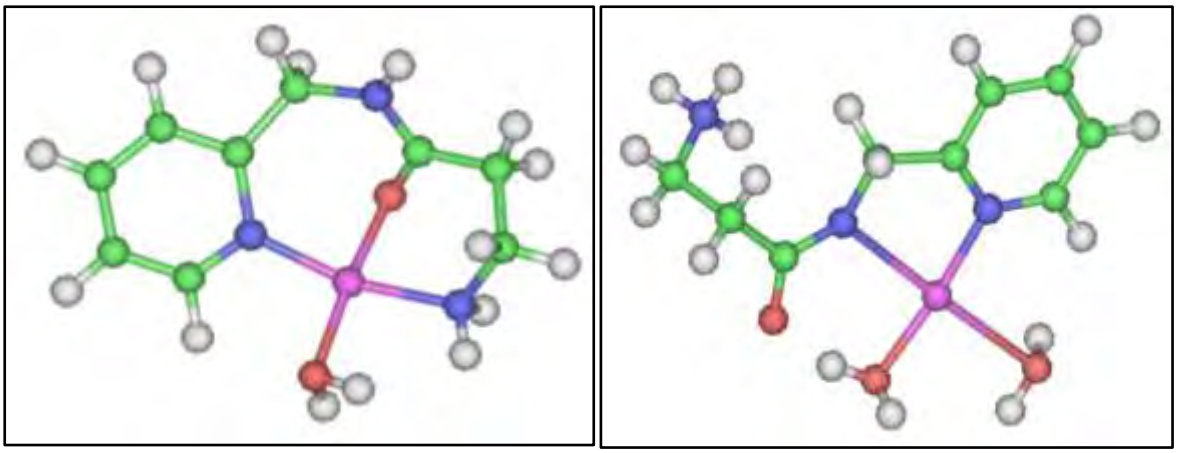

(h) **(i)**

Figure 4.40: Two possible energy-minimised structures of Cu(II)-[H(56)NH_2] (ML). (**h):** 7,6 and **(i):** 5 membered chelate rings. For clarity the axial waters are not displayed.

4.4.4.5 MLH_{-1} of $[H(56)NH_2]$ System

The two possible structures for MLH_{-1} of the Cu(II)-$[H(56)NH_2]$ system, are shown in Figures 4.41**j** and 4.41**k**. In one structure (Figure 4.41**j**), Cu(II) is coordinated to the pyridyl-N and an amide-N. In the other structure (Figure 4.41**k**), Cu(II) is bound to the pyridyl-N, an amine-N, and an amide-N. From the MM optimisation of these two structures, the 5,6 chelate structure (Figure 4.41**k**) had a slightly higher strain energy (Table 4.10) than the 5 chelate structure (Figure 4.41**j**).

Table 4.10: Internal energy ($E_{internal}$), bond (E_{bond}), angle (E_{angle}), torsion ($E_{torsion}$) and out-of-plane (E_{Oop}) deformation energies (kcal mol^{-1}) for **(j):** 5 and **(i):** 5,6 membered chelate rings of MLH_{-1} Cu(II)-$[H(56)NH_2]$ systems.

	$[H(56)NH_2]$ MLH_{-1}	
	5 (j)	**5,6 (k)**
E_{int}	26.57	33.11
Bond	10.49	12.31
Angle	12.47	16.64
Torsion	3.36	4.13
Oop	0.24	0.02

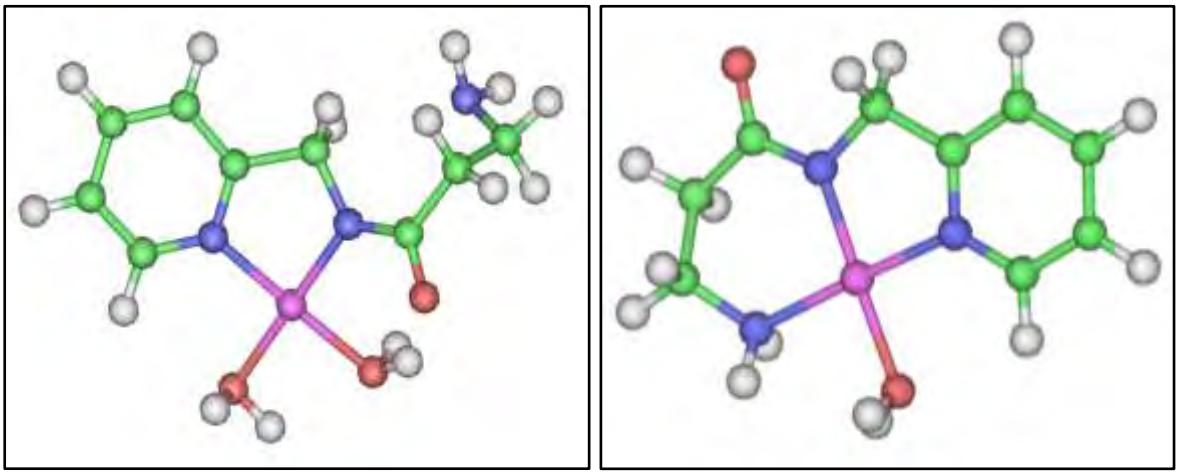

(j) **(k)**

Figure 4.41: Two possible energy-minimised structures of Cu(II)-$[H(56)NH_2]$ (MLH_{-1}). **(j):** 5 and **(k):** 5,6 membered chelate rings For clarity the axial waters are not displayed.

For both structures, the major contributions to the internal strain energy come from the angle bend and bond stretch energies. However, it is not much different in comparison to

the 5 membered ring in Figure 4.41**j**. The 5,6 chelate ring systems in this study seem to be stabilized as compared to the 5 chelate ring system due to the pre-organization of the ligand. The MM calculations were not able to distinguish between the two structures. However, the potentiometric, UV-visible spectroscopy and X–ray studies favour the structure with 5,6 membered rings (Figure 4.41k) for MLH_{-1}.

4.4.5 Conclusion

In this study molecular mechanics has been used as a simple computational tool to provide more information about the possible structures for the different complexes. These results were used to support the potentiometric and spectroscopic (NMR, UV-visible) studies. In all calculations, no account is taken of the electronic contribution, Jahn-Teller distortion of Cu(II), entropy effects, the chelate effect of the ligand and solvent effects. This might explain some of the discrepancies observed between the potentiometric results and the MM calculations.

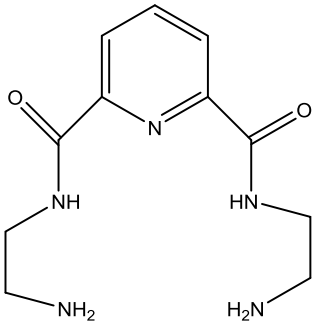

N,N'-di(aminoethylene)-2,6-pyridine-dicarbonylamine

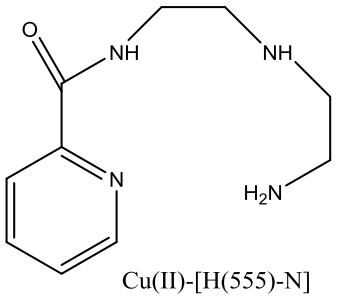

Cu(II)-[H(555)-N]

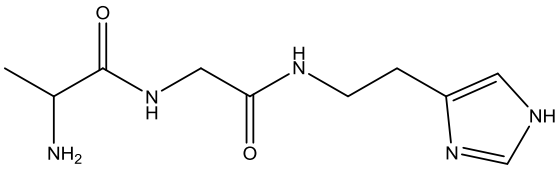

Ala-Gly-Ha

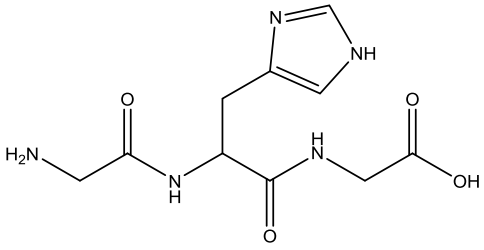

glycyl-L-histidylglycine

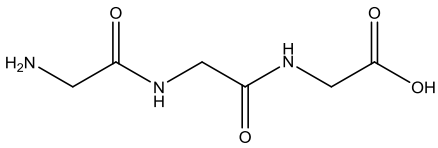

Gly-Gly-Gly

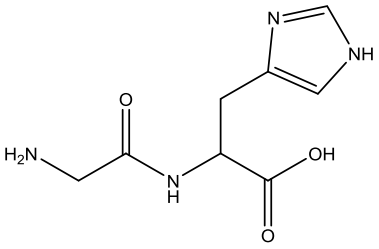

glycyl-L-histidine

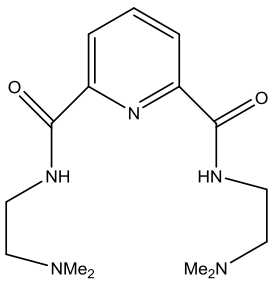

Bis-(N,N-dimethylethyl)-2,6-pyridine-dicarboxamide

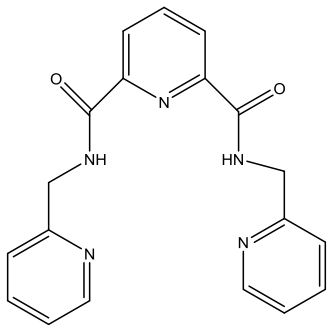

N,N'-bis[2(2-pyridyl)-methyl]pyridine- 2,6-dicarboxamide

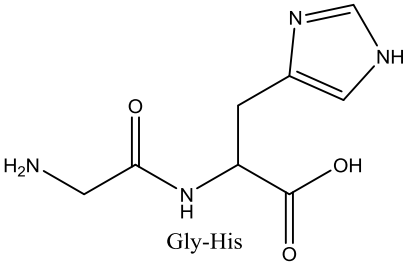

Gly-His

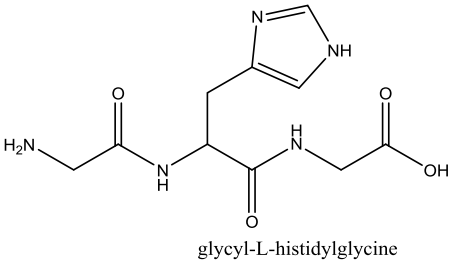

glycyl-L-histidylglycine

Figure 4.42: Some of the literature ligands used in the discussion.

References

1. G. L. Miessler and A. T. Donald, *Inorganic Chemistry*, Prentice Hall, Richmond, TX, U.S.A., 2003.

2. S. L. Upstone, *Ultraviolet/Visible Light Absorption Spectrophotometry in Clinical Chemistry*, John Wiley & Sons Ltd, Chichester, Beaconsfieldr, UK, 2000.

3. J. E. Huheey, E. A. Keiter and A. L. Keiter, *Inorganic Chemistry, Principles of Strucrure and Reactivity*, Harper Collins College Publishers, New York, 4th ed., 1993.

4. F-X Schmid, *Encyclopedia of Life Sciences*, John Wiley & Sons, Ltd, Chichester, UK, 2001.

5. R. S. Drago, *Physical Methods in Inorganic Chemistry*, Reinhold Publishing Corporation, Chapman & Hall Ltd, London, New York, 1965.

6. AB. P. Lever, *Studies in Physical & Theoretical Chemistry Inorganic Spectroscopy*, Pergamon Press., 2nd edn., 1987.

7. J. D. Lee, *Concise Inorganic Chemistry*, Chapman & Hall, London, 4th ed., 1991.

8. E. Prenesti, P. G. Daniele and S. Toso, *Anal. Chim. Acta*, 2002, **459**, 323–336.

9. F. R. Hartley, C. Burgess and R. M. Alcock, *Solution Equilibria*, Ellis Horwood, Chichester, 1980.

10. E. J. Billo, *Inorg. Nucl. Chem. Lett.*, 1974, **10**, 613–617.

11. S. Odisitse and G. E. Jackson, *Inorganica Chim. Acta*, 2009, **362**, 125–135.

12. J. N. Zvimba and G. E. Jackson, *J. Inorg. Biochem.*, 2007, **101**, 148–58.

13. G. E. Jackson and B. S. Nakani, *J. Chem. Soc. Dalt. Trans.*, 1996, 1373–1377.

14. G. E. Jackson, P. W. Linder and A. Voyé, *J. Chem. Soc. Dalt. Trans.*, 1996, 4605.

15. T. E. Nomkoko, G. E. Jackson, B. S. Nakani and R. Hunter, *Dalton Trans.*, 2006, 4029–38.

16. E. Prenesti, P. Daniele, M. Prencipe and G. Ostacoli, *Polyhedron*, 1999, **18**, 3233–3241.

17. H. Sigel and R. B. Martin, *Chem. Rev.*, 1982, **82**, 385–426.

18. H. H. Jaffe and M. Orchin, *Theory & Applications of Ultraviolet Spectroscopy*, John Willey & Sons, New York, London, New York, 1962.

19. D. W. Smith, *Inorganica Chim. Acta*, 1977, **22**, 107–110.

20. P. Gizzi, B. Henry, P. Rubini, S. Giroux and E. Wenger, *J. Inorg. Biochem.*, 2005, **99**, 1182–92.

21. R. R. Khoury, *Ph.D Thesis*, The University of New South Wales, 2013.

22. P. J. Morris and R. Bruce Martin, *J. Inorg. Nucl. Chem.*, 1971, **33**, 2913–2918.

23. P. G. Daniele, O. Zerbinati, V. Zelano and G. Ostacoli, *J. Chem. Soc. Dalt. Trans.*, 1991, **1**, 2711.

24. S. Odisitse, G. E. Jackson, T. Govender, H. G. Kruger and A. Singh, *Dalton Trans.*, 2007, 1140–9.

25. H. Gampp, D. Haspra, M. Maeder and A. D. Zuberbuehler, *Inorg. Chem.*, 1984, **23**, 3724–3730.

26. D. Sanna, G. Micera, C. Kallay, V. Rigo and I. Sovago, *Dalton Trans.*, 2004, 2702–7.

27. W. L. Koltun, R. H. Roth and F. R. Gurd, *J. Biol. Chem.*, 1963, **238**, 124–31.

28. T. Komorita, J. Hidaka and Y. Shimura, *Bull. Chem. Soc. Jpn.*, 1968, **41**, 854–862.

29. T. Komorita, J. Hidaka and Y. Shimura, *Bull. Chem. Soc. Jpn.*, 1971, **44**, 3353–3363.

30. T. Komorita, J. Hidaka and Y. Shimura, *Bull. Chem. Soc. Jpn.*, 1969, **42**, 168–177.

31. M. Nonoyama and K. Yamasaki, *Inorganica Chim. Acta*, 1971, **5**, 124–128.

32. E. Farkas, I. Sóvágó and A. Gergely, *J. Chem. Soc. Dalt. Trans.*, 1983, 1545.

33. M. Mylonas, J. C. Plakatouras, N. Hadjiliadis, A. Krężel, and W. Bal, *Inorganica Chim. Acta*, 2002, **339**, 60–70.

34. W. Bal, H. Kozlowski, R. Robbins and L. D. Pettit, *Inorganica Chim. Acta*, 1995, **231**, 7–12.

35. W. Bal, M. Dyba and H. Kozłowski, *Acta Biochim. Pol.*, 1997, **44**, 467–76.

36. E. Farkas, É. A. Enyedy, G. Micera and E. Garribba, *Polyhedron*, 2000, **19**, 1727–1736.

37. G. Gauglitz and T. Vo-Dinh, *Handbook of Spectroscopy*, WILEY-VCH Verlag GmbH & Co. KGaA, Weinheim, Germany, 2003.

38. E. Purcell, H. Torrey and R. Pound, *Phys. Rev.*, 1946, **69**, 37–38.

39. F. Bloch, W. W. Hansen and M. Packard, *Phys. Rev.*, 1946, **69**, 127.

40. T. N. Mitchell and B. Costisella, *NMR – From Spectra to Structures*, Springer-Verlag Berlin Heidelberg, Berlin Heidelberg, New York, 2nd edn., 2007.

41. P. s. Pregosin, Ed., *Transition metal nuclear magnetic resonance, studies in inorganic chemistry*, Elsevier Science Publisher B.V., Amsterdam, 1991.

42. K. Popov, H. Rönkkömäki and L. H. J. Lajunen, *Pure Appl. Chem.*, 2006, **78**, 663–675.

43. P. K. Glasoe and F. A. Long, *J. Phys. Chem.*, 1960, **64**, 188–190.

44. J. N. Zvimba and G. E. Jackson, *J. Inorg. Biochem.*, 2007, **101**, 1120–8.

45. M. Mohajane, *MSc Thesis,* University of Cape Town, 2010.

46. M. Mohajane, *Ph.D Thesis*, University of Cape Town, 2013.

47. S. Odisitse, *Ph.D Thesis,* University of Cape Town, 2006.

48. M. A. Wells, C. Jelinska, L. L. P. Hosszu, C. J. Craven, A. R. Clarke, J. Collinge, J. P. Waltho and G. S. Jackson, *Biochem. J.*, 2006, **400**, 501–10.

49. J. M. Lázaro Martínez, A. K. Chattah, G. A. Monti, M. F. Leal Denis, G. Y. Buldain, and V. Campo Dall' Orto, *Polymer (Guildf).*, 2008, **49**, 5482–5489.

50. M. Düggeli, C. Bonte and A. Von Zelewsky, *Inorganica Chim. Acta*, 2005, **358**, 41–49.

51. X.-Z. Zhao, T. Jiang, L. Wang, H. Yang, S. Zhang and P. Zhou, *J. Mol. Struct.*, 2010, **984**, 316–325.

52. F. D. Sokolov, M. G. Babashkina, D. a Safin, A. I. Rakhmatullin, F. Fayon, N. G. Zabirov, M. Bolte, V. V Brusko, J. Galezowska and H. Kozlowski, *Dalton Trans.*, 2007, 4693–700.

53. S. Odisitse and G. E. Jackson, *Polyhedron*, 2008, **27**, 453–464.

54. S. J. Lau, J. P. Laussac and B. Sarkar, *Biochem. J.*, 1989, **257**, 745–50.

55. J. P. Laussac, R. Haran and B. Sarkar, *Biochem. J.*, 1983, **209**, 533–9.

56. Z. Szabó, *Coord. Chem. Rev.*, 2008, **252**, 2362–2380.

57. T. Gajda, B. Henry, A. Aubry and J. Delpuech, *Inorg. Chem.*, 1996, **35**, 586–593.

58. M. R. Lee, *Meteoritics*, 1994, **29**, 898–899.

59. Z. Otwinowski and W. Minor, *Methods in Enzymology, Macromolecular Crystallography*, Academic Press, New York, NY, part A, 1997.

60. G. M. Sheldrick, *SADABS*, 1996.

61. G. M. Sheldrick, *Acta Crystallogr. A.*, 2008, **64**, 112–22.

62. L. J. Barbour, *J. Supramol. Chem.*, 2001, **1**, 189–191.

63. G. M. Sheldrick, *SADABS*, 2001.

64. J. L. Atwood and L. J. Barbour, *Cryst. Growth Des.*, 2003, **3**, 3–8.

65. *http://www.povray.org/*.

66. N. Tounsi, L. Dupont, A. Mohamadou, C. Cadiou, M. Aplincourt, R. Plantier-Royon, F. Massicot and C. Portella, *New J. Chem.*, 2004, **28**, 785.

67. M. Melník, M. Kabešová, M. Dunaj-Jurčo and C. E. Holloway, *J. Coord. Chem.*, 1997, **41**, 35–182.

68. E. V Rybak-Akimova, A. Y. Nazarenko, L. Chen, P. W. Krieger, A. M. Herrera, V. V Tarasov and P. D. Robinson, *Inorganica Chim. Acta*, 2001, **324**, 1–15.

69. A. W. Addison, T. N. Rao, J. Reedijk, J. van Rijn and G. C. Verschoor, *J. Chem. Soc. Dalt. Trans.*, 1984, 1349.

70. Q. Wang, C.-F. Bi, D.-Q. Wang and Y.-H. Fan, *Acta Crystallogr. Sect. E. Struct. Rep. Online*, 2009, **65**, m439.

71. P. F. Rapheal, E. Manoj and M. R. Prathapachandra Kurup, *Polyhedron*, 2007, **26**, 818–828.

72. A. Sreekanth and M. R. Prathapachandra Kurup, *Polyhedron*, 2003, **22**, 3321–3332.

73. M. Joseph, M. Kuriakose, M. R. P. Kurup, E. Suresh, A. Kishore and S. G. Bhat, *Polyhedron*, 2006, **25**, 61–70.

74. P. Talukder, A. Datta, S. Mitra and G. Rosair, *Zeitschrift fur Naturforsch. - Sect. B J. Chem. Sci.*, 2004, **59**, 655–660.

75. I. O. Fritsky, H. Kozłowski, P. J. Sadler, O. P. Yefetova, J. Świątek-Kozłowska, V. A. Kalibabchuk and T. Głowiak, *J. Chem. Soc. Dalt. Trans.*, 1998, 3269–3274.

76. R. Balamurugan, M. Palaniandavar and R. S. Gopalan, *Inorg. Chem.*, 2001, **40**, 2246–2255.

77. L. Escriche, M. Sanz, J. Casabó, F. Teixidor, E. Molins and C. Miravitlles, *J. Chem. Soc. Dalt. Trans.*, 1989, 1739.

78. P. Comba, T. W. Hambley, M. Gerloch and E. C. Constable, *Molecular Modeling*, Wiley-VCH Verlag GmbH, Weinheim, Germany, 1995.

79. C. Peter and T. W. Hambley, *Molecular Modeling of Inorganic Compounds.*, Wiley-VCH, Weinheim, 2001.

80. A. M. T. Bygott and A. M. Sargeson, *Inorg. Chem.*, 1998, **37**, 4795–4806.

81. E. Lewars, *Computational Chemistry Introduction to the Theory and Applications of Molecular and Quantum Mechanics*, Kluwer Academic Publishers, Moscow, 2004.

82. P. V Bernhardt and P. Comba, *Inorg. Chem.*, 1992, **31**, 2638–2644.

83. E. T. Nomkoko, G. E. Jackson, B. S. Nakani and S. A. Bourne, *Dalton Trans.*, 2004, 1789–96.

84. A. Hinchliffe, *Molecular Modelling for Beginners*, by John Wiley & Sons Ltd, Chichester, 2003.

85. W. J. Hehre, *A Guide to Molecular Mechanics and Quantum Chemical Calculations*, Wavefunction, Inc, Irvine-California, 2003.

86. A. K. Rappe, C. J. Casewit, K. S. Colwell, W. A. Goddard and W. M. Skiff, *J. Am. Chem. Soc.*, 1992, **114**, 10024–10035.

87. V. S. Allured, C. M. Kelly and C. R. Landis, *J. Am. Chem. Soc.*, 1991, **113**, 1–12.

88. V. J. Burton, R. J. Deeth, J. C. M. Kemp and P. J. Gilbert, *J. Am. Chem. SOC*, 1995, **117**, 8407–8415.

89. S. Shi, L. Yan, Y. Yang, J. Fisher-Shaulsky and T. Thacher, *J. Comput. Chem.*, 2003, **24**, 1059–76.

90. F. Ryvkin and F. T. Greenaway, *Bioinorg. Chem. Appl.*, 2010, **2010**, 724210.

91. N. Jager and U. Schilde, *Struct. Chem.*, 1998, **9**, 77–93.

92. D. V Nicolau and S. Yoshikawa, *J. Mol. Graph. Model.*, 1998, **16**, 83–96.

93. W. Nowak, V. Cody and A. Wojtczak, *Acta Biochim. Pol.*, 2001, **48**, 903–16.

94. C. C. Curtain, F. Ali, I. Volitakis, R. a Cherny, R. S. Norton, K. Beyreuther, C. J. Barrow, C. L. Masters, a I. Bush and K. J. Barnham, *J. Biol. Chem.*, 2001, **276**, 20466–73.

95. I. Daizadeh, E. S. Medvedev and A. A. Stuchebrukhov, *Proc. Natl. Acad. Sci. U. S. A.*, 1997, **94**, 3703–3708.

96. N. Declerck, M. Machius, R. Chambert and G. Wiegand, *Protein Eng. vol.10*, 1997, **10**, 541–549.

97. S. Barlow, A. L. Rohl, S. Shi, C. M. Freeman and D. O'Hare, *J. Am. Chem. Soc.*, 1996, **118**, 7578–7592.

98. Insight II. System Guide. July 2005.

99. F. Ramondo, L. Bencivenni and V. Di Martino, *Chem. Phys.*, 1991, **158**, 41–57.

Chapter Five

Bio-Modelling and Tissue Permeability Studies

5.1 Blood Plasma Model

5.1.1 Introduction

Cu(II) complexes are effective in treating inflammation associated with rheumatoid arthritis. This pharmacological effect was first associated with the free labile copper (II) concentration in the body by Sorenson et al. in 1976.[1] The main objective of the present study was to produce a drug that is able to mobilize Cu(II) in blood plasma. Although the ligands designed in this study form more stable complexes with Cu(II) than with Zn(II) and Ni(II), this is no guarantee that the Cu(II) complex will form *in vivo*. Furthermore, the concentrations of Zn(II) and Ni(II) are much higher than the Cu(II) concentration in the body and there are a myriad of other ligands that bind Cu(II). For example, a small fraction of these metal ions are bound to low molecular weight (l.m.w) compounds, mainly amino acids. The metals bound to l.m.w compounds play a major role in many biological and physiological processes like intestinal absorption, cell absorption and renal excretion.[2] The complexing ability of the ligands *in vivo* was estimated by calculating, their plasma-mobilizing indices (p.m.i).

Most complexes in blood plasma are charged and therefore need a neutral transport molecule that will help them to cross the lipid bilayer found in cell membranes. The May model uses a program called Evaluation of Constituent Concentrations in Large Equilibrium Systems (ECCLES)[3,4] which calculates the p.m.i. Thus, p.m.i defines the ability of a ligand to move Cu(II) from a protein-bound form to a l.m.w form. This means that a strong specific Cu(II) chelator would have high p.m.i. values at low drug concentrations, indicating a potentially useful therapeutic agent.

5.1.2 Blood Plasma Simulations

The present study was carried out to investigate the *in vivo* Cu(II) speciation of the studied ligands using the program ECCLES.[5] This program has a list of species that are found in blood plasma with their cumulative stability constants.[6-9] ECCLES simulates the speciation of species of interest at the physiological pH of 7.4 in blood plasma so as to calculate the plasma-mobilizing indices. This calculation takes into account the competition of species with some 7 metal ions and 40 ligands that generate more than 5000 species present in blood plasma. The total ligand concentration was varied over a range 10^{-1} - 10^{-10} M.

The plasma mobilizing index was defined for Cu(II)[10,11] as;

$$\text{p.m.i} = \frac{\text{total concentration of low molecular weight metal complex species in the presence of a drug}}{\text{total concentration of low molecular weight metal complex species in normal plasma}} \quad (5.1)$$

5.1.3 Results

5.1.3.1 [H(555)NH_2]

Figure 5.1 shows p.m.i curves for Cu(II), Ni(II), and Zn(II) with [H(555)NH_2] plotted against logarithms of the concentration of the ligand. The curves indicate that the mobilizing ability of [H(555)NH_2] *in vivo* was in the order Cu(II) > Ni(II) > Zn(II). The ligand was selective for Cu(II) *in vivo* relative to other metal ions. The remarkably high mobilizing ability of this ligand is related to the stable complexes it forms with Cu(II). In addition, the predominant $CuLH_{-1}$ species of this ligand was present at physiological pH at a total ligand concentration of 10^{-5} and 10^{-4} mol dm^{-3} for [H(555)NH_2] with Ni(II) and Zn(II), respectively. In spite of the higher concentrations of these *in vivo* competitors and the predominance of the MLH_{-2} species for both Ni and Zn metal ions, their weak binding strength with [H(555)NH_2] made them less important competitors of Cu(II) *in vivo*.

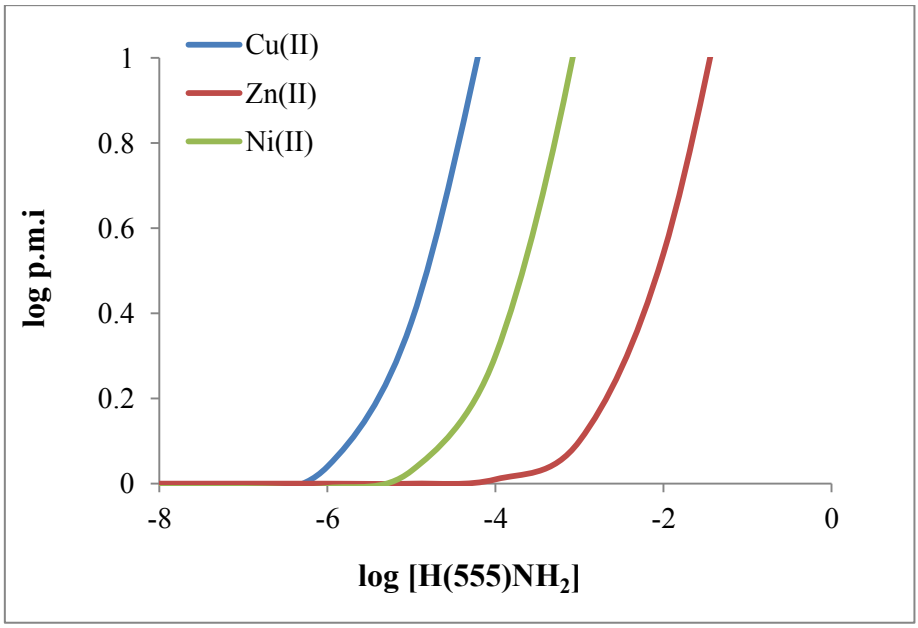

Figure 5.1: Log pmi as a function of log [H(555)NH_2] for Cu(II), Ni(II) and Zn(II) complexes.

5.1.3.2 [H(555)NMe$_2$]

The blood plasma index curves for Cu(II), Ni(II), and Zn(II) as a logarithmic function of concentration of the ligand is given in Figure 5.2. Despite the high *in vivo* concentration of Zn(II), [H(555)NMe$_2$] is able to mobilize Cu(II) to a greater extent. At low ligand concentrations 10^{-5} M, [H(555)NMe$_2$] mobilized Cu(II) but not Ni(II), and the p.m.i of the Cu(II) complexes remains higher than that of the Ni(II) complexes at higher ligand concentration.

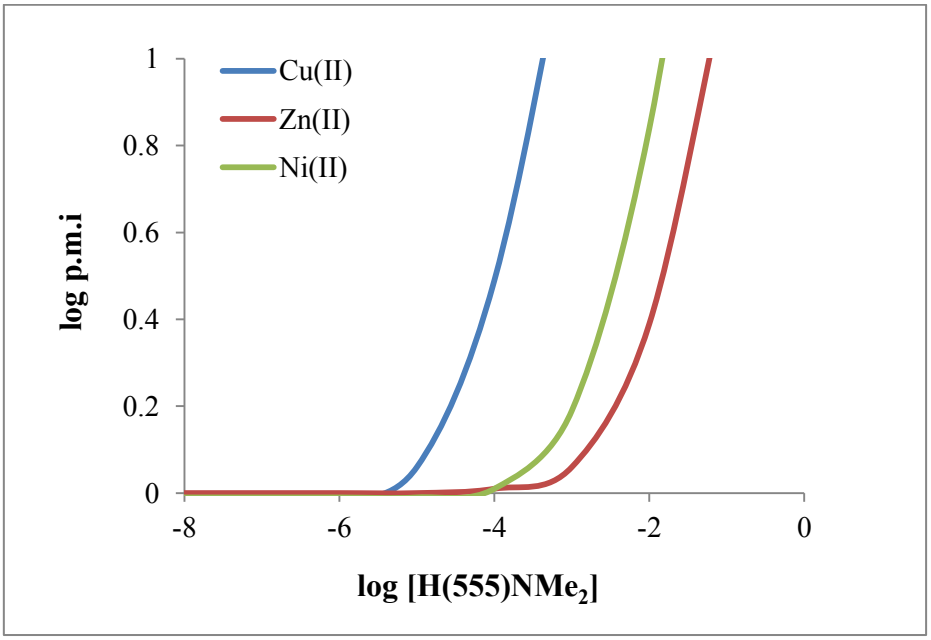

Figure 5.2: Log p.m.i as a function of log [H(555)NMe$_2$] for Cu(II), Ni(II) and Zn(II) complexes.

5.1.3.3 [H$_2$(555)NH$_2$]

Figure 5.3 shows the log p.m.i curves *vs* log of ligand concentration for [H$_2$(555)NH$_2$] with Cu(II), Ni(II) and Zn(II) complexes. The curves indicate that the mobilizing ability of [H$_2$(555)NH$_2$] *in vivo* is in the order Zn(II) > Cu(II) > Ni(II). Therefore, Zn(II) is a good competitor of Cu(II) for [H$_2$(555)NH$_2$] in blood plasma. This ligand mobilized Zn(II) over Cu(II) at the concentration between 10^{-2} M and 10^{-3} M.

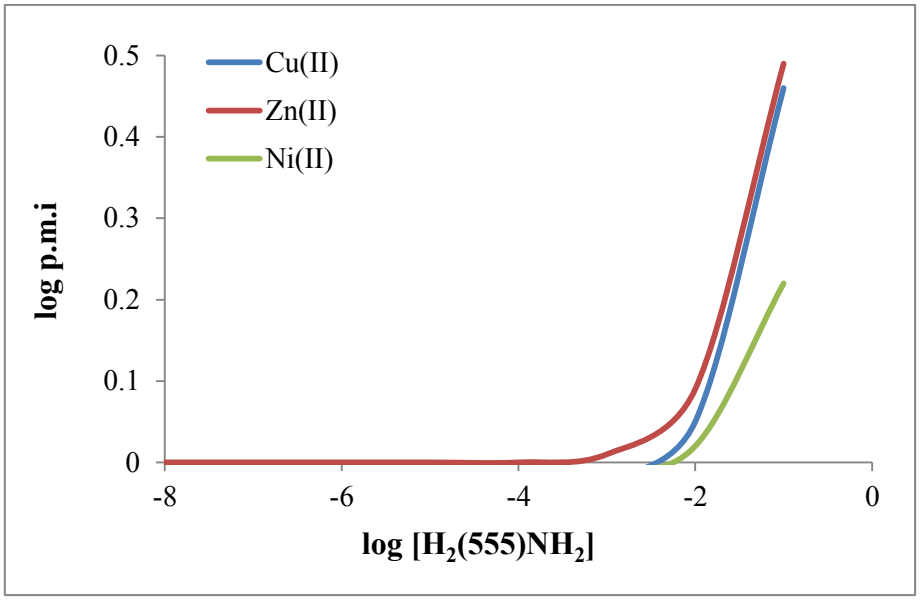

Figure 5.3: Log p.m.i as a function of log [$H_2(555)NH_2$] for Cu(II), Ni(II) and Zn(II) complexes.

5.1.3.4 [$H_2(565)NH_2$]

The p.m.i curve for [$H_2(565)NH_2$] is given in Figure 5.4. [$H_2(565)NH_2$] mobilized Cu(II) at ligand concentrations above 10^{-4} M, while Ni(II) and Zn(II) are mobilized only at ligand concentrations above 10^{-2} M.

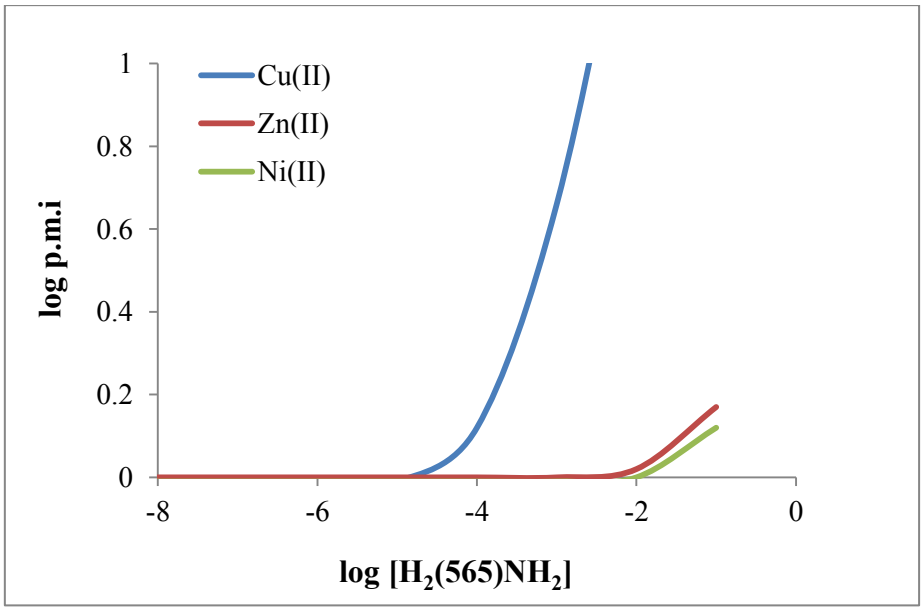

Figure 5.4: Log p.m.i as a function of log [$H_2(565)NH_2$] for Cu(II), Ni(II) and Zn(II) complexes.

5.1.3.5 [H(56)NH_2]

The p.m.i curves for [H(56)NH_2] are given in Figure 5.5. [H(56)NH_2] mobilized Cu(II) almost exclusively over Ni(II) and Zn(II) in blood plasma. Cu(II) is mobilized by [H(56)NH_2] from a ligand concentration of 0.01 M whereas, Zn(II) is mobilized only at ligand concentrations of about 0.1 M. Ni(II) is not mobilized at all.

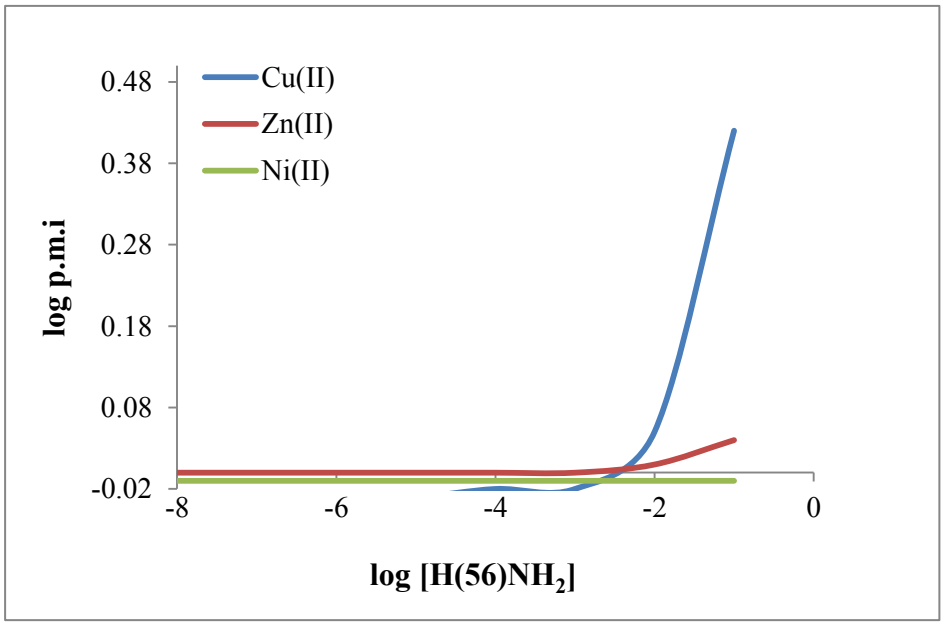

Figure 5.5: Log p.m.i as a function of log [H(56)NH_2] for Cu(II), Ni(II) and Zn(II) complexes.

5.1.4 Discussion

Figure 5.6 shows the Cu(II) p.m.i curves for [555-N], [H(555)NH_2], [H(555)NMe_2], [H_2(555)NH_2], [H_2(565)NH_2] and [H(56)NH_2]. The ligands [H_2(555)NH_2] and [H(56)NH_2] were observed to give a log p.m.i value of ~ 0.46 only at high concentration (0.01 M). This indicates that [H_2(555)NH_2] and [H(56)NH_2] have low mobilizing ability in blood plasma and thus cannot effectively increase the l.m.w Cu(II) fraction. The reason for the low mobilizing ability of these two ligands is the stability of their complexes with Zn(II) and Ni(II). The mobilizing ability of the other ligands for Cu(II) *in vivo* is in the order [H(555)NH_2] > [H(555)NMe_2] > [H_2(565)NH_2] at a total ligand concentration range of 10^{-6}-10^{-2} M. This means that [H(555)NH_2] and [H(555)NMe_2] have the highest ability to mobilize copper *in vivo* in comparison with the other ligands covered in this study. The remarkably high mobilizing ability of [H(555)NH_2] by a factor of one log unit compared to

[H(555)NMe_2] is related to the stable three chelate rings formed with Cu(II) as well as the presence of methyl groups in terminal amine moiety in [H(555)NMe_2].

Zvimba and Jackson[7] reported that a [555-N] ligand containing a pyridine residue and an amine nitrogen is a high mobilizer of Cu(II) *in vivo*. However, better mobilization of [555-N] compared to [H(555)NH_2] and [H(555)NMe_2] could be as a result of stronger coordination of the amino groups as opposed to amidic groups. Such results are not unexpected because the electron withdrawing nature of such a group has been reported[12] to reduce the basicity of the donor atoms for these complex systems. Thus the *in vivo* mobilization of Cu(II) was observed to decrease as amide groups are introduced into the ligand.

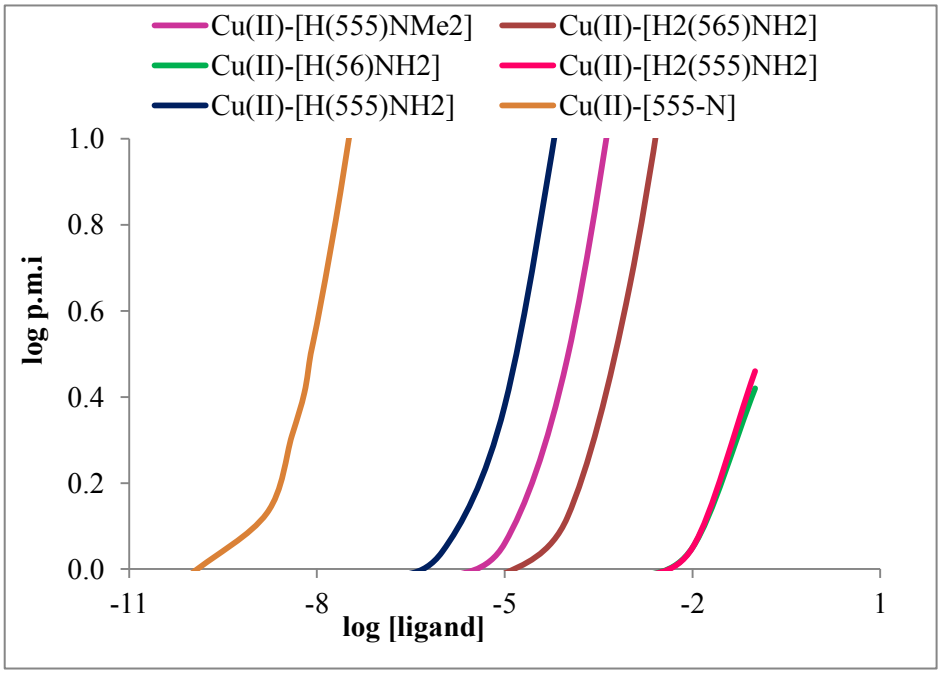

Figure 5.6: Log pmi as a function of log [ligands] for Cu(II) ligands complexes.

5.2 Dermal Absorption Study

Another objective of this work was to establish if the different ligands were able to promote the dermal absorption of Cu(II). This was done by measuring the effect of the ligands on the rate of diffusion of Cu(II) through a Cerasome membrane as a model for skin and determining the partition coefficients in 1-octanol.

5.2.1 Octanol / Water Partition Coefficients

5.2.1.1 Introduction

The partition coefficient between octanol and water (log $P_{oct/aq}$) is an important physicochemical parameter for characterizing the lipophilicity or hydrophobicity of a compound. It is used in many fields, especially in the environmental and pharmaceutical sciences.[13] The octanol/water partition coefficient is a key parameter in the mathematical prediction of percutaneous penetration of chemicals.[14,15] It is widely accepted as the best two-phase system to model the partitioning between biomass and water.[16] Log *P* expresses the partitioning of a chemical between an aqueous (e.g., vehicle) and a lipid phase (e.g., stratum corneum). Octanol is often used as a simplified model of the lipid barrier of the stratum corneum to predict the penetration of chemicals into the skin.[17] One important aspect upon which biological activity depends is the ability of the drug to reach the target area. In general, dermal absorption transport across the skin and bio-membranes is a process of limited diffusion which is governed by the drug's chemical and physical properties such as lipophilicity and protein binding.[18,19] Although Cu(II) complexes, when administered orally and intravenously do increase the availability of copper, it is difficult to move this coordinated metal ion through a series of body compartments without protein binding.[20] In comparison to the classical methods of drug administration such as orally, by injection intravenously, intraperitoneally *etc*., percutaneous absorption offer one obvious advantage of being less painful and hence tolerable to the patient.[20] Accordingly, in this study we have investigated the octanol/water partition coefficients of Cu(II) complexes with a view to establishing whether these species can be administered transdermally. Partition coefficient (log $P_{oct/aq}$) is expressed as;

$$\log P_{\mathrm{oct\backslash aq}} = \log\left(\frac{[\mathrm{Cu(II)}]_{\mathrm{oct}}}{[\mathrm{Cu(II)}]_{\mathrm{aq}}}\right) \qquad (5.2)$$

where $[Cu(II)]_{oct}$ is concentrations of Cu(II) in the organic phase, $[Cu(II)]_{aq}$ is concentrations of Cu(ll) in the aqueous phase.

An investigation of a biphasic system at varying pH values interestingly shows that speciation changes with pH and the different species have different partition coefficients. The skin permeabilities of chemicals are directly proportional to their partition coefficients[22], and therefore this observation is relevant here.

5.2.1.2 Experimental

The classical method for measuring partition coefficients is the shake flask method, which has been adopted as the standard Organisation for Economic Cooperation and Development (OECD) method.[23] However, this technique is not suitable for compounds having higher hydrophobicity because of the formation of octanol emulsions in water.[13]

In this study, partition coefficients were measured using the shake flask method where the organic phase was 1-octanol pre-saturated with water.[23,24] Solutions of Cu(II) (0.005 M) with ligand in ratios of 1:1, 1:2 and 1:1.5 were prepared in distilled/deionised water. 5 ml of Cu(II) complex solutions were dispersed into 10 glass vials in the pH range between pH 2.0 to 11.0 and these solutions were mixed with 6 ml of 1-octanol (99 %). The mixture was shaken for two minutes and left for 5 minutes for the two phases to separate at a constant temperature of 25 °C. The organic layer could not be analysed directly using Microwave Plasma-Atomic Emission Spectrometer (MP-AES) and so the copper had to be back-extracted into an aqueous phase. This was done using 6 ml of 5% HNO_3. 4 ml aliquots were withdrawn from the new aqueous phase (5 % HNO_3). The concentration of copper in each phase does not determine the concentration of the complex species. The total concentration of Cu(II) in each phase was measured using MP-AES. The partition coefficients of Cu(II)-complex as a drug were calculated using Equation 5.2.

5.2.1.3 Results

5.2.1.3.1 Cu(II)-[H(555)NH_2]

Figure 5.7 shows the partition coefficients (log $P_{oct/aq}$) and the speciation graph of Cu(II)-[H(555)NH_2] systems plotted as a function of pH. It is evident that complexes of Cu(II) and Cu(II)-[H(555)NH_2] were more soluble in water than in 1-octanol, since the log $P_{oct/aq}$ values were negative (Figure 5.7). The distribution coefficients did not change

much with pH (from pH 2 to 11). The distribution curves showed that mixed species were observed at some pH values therefore, the log $P_{oct/aq}$ values obtained were not for a single species. All three species (MLH, ML, and MLH_{-1}) had about the same log $P_{oct/aq}$ value. MLH was formed in very small amounts due to the limited amount of Cu(II). The log $P_{oct/aq}$ at pH 7.4 (physiological pH) was -3.3.

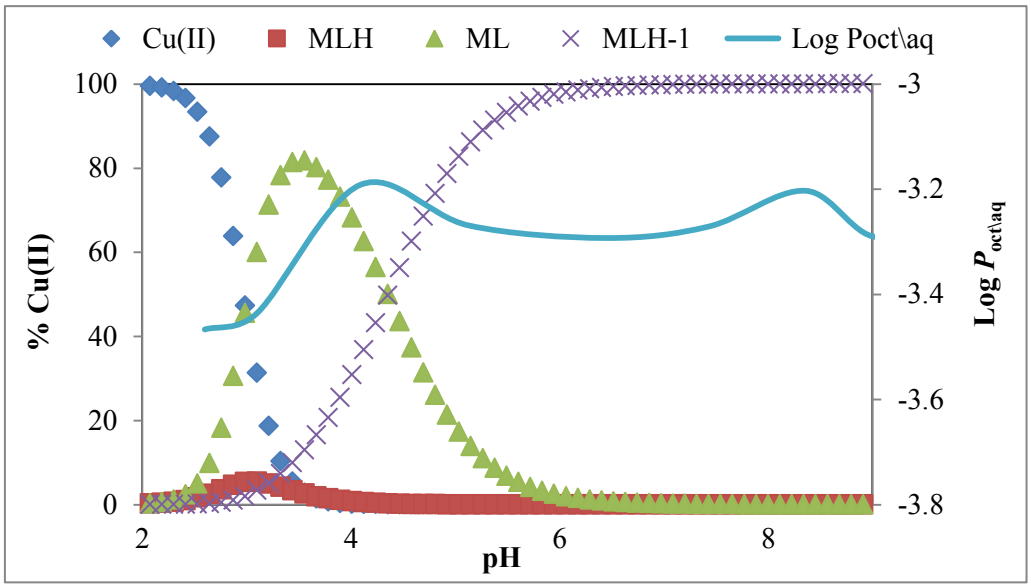

Figure 5.7: Log $P_{oct\aq}$ as a function of pH and speciation graph for 1:2 Cu(II)-[H (555)NH_2].

5.2.1.3.2 Cu(II)-[H(555)NMe_2]

The distribution coefficient curve and the speciation graph for Cu(II)-[H(555)NMe_2] are given in Figure 5.8. The distribution coefficient curve shows that the solubility in 1-octanol increased with an increase in pH (from pH 2 to 11). Figure 5.8 also shows that all log $P_{oct/aq}$ values were negative, indicating that these complexes are largely hydrophilic. The low log $P_{oct/aq}$ values in the acidic pH range for the complex species in this system indicate that the hydrated $[Cu(OH_2)_6]^{2+}$ species predominated in this pH region, although complex formation in the Cu(II)-[H(555)NMe_2] system began at low pH. In the pH range 2.0-3.6, the copper is predominantly present as the ML species. Since log $P_{oct/aq}$ is constant in this pH range we conclude that ML has a distribution coefficient of -2.5. Log $P_{oct/aq}$ = -2.06 at pH 10.10 where 91 % of the Cu(II) is present as MLH_{-2} and so the distribution coefficient was assigned to this species. The log $P_{oct/aq}$ value at physiological pH 7.40 was estimated as -2.19 for the most predominant species MLH_{-1}. There was an increase in log $P_{oct/aq}$ values in the alkaline region (above pH 9.36) for this system.

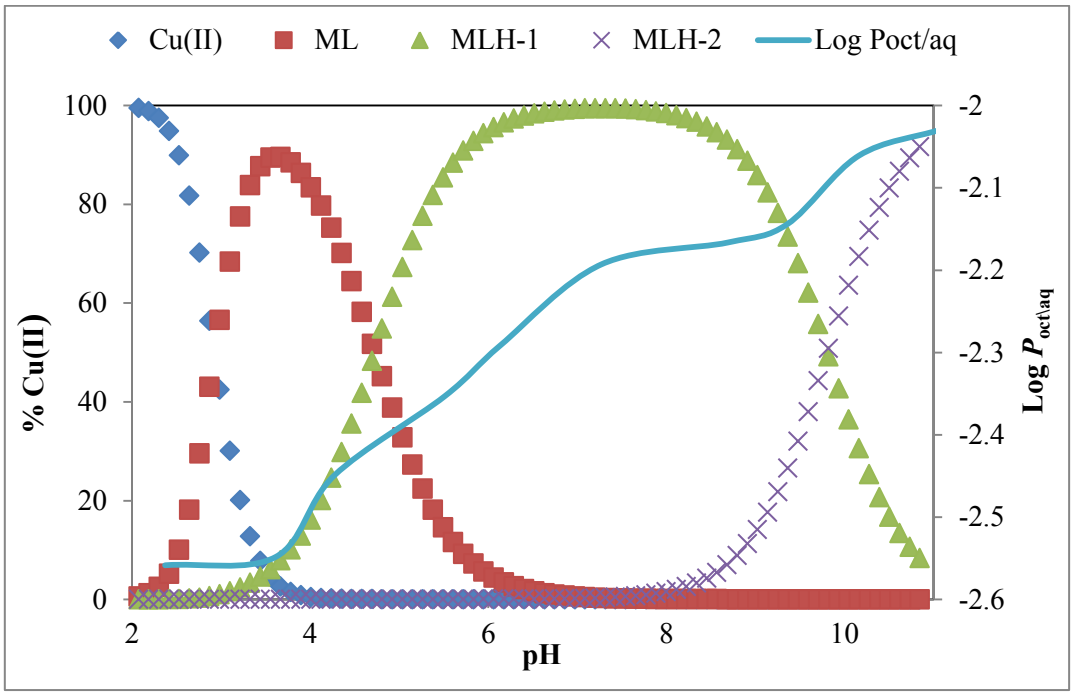

Figure 5.8: Log $P_{oct/aq}$ as a function of pH and speciation graph for 1:1.5 Cu(II)-[H(555)NMe_2].

5.2.1.3.3 Cu(II)-[H_2(555)NH_2]

Figure 5.9 shows the partition coefficients (log $P_{oct/aq}$) and the speciation graph as a function of pH for the Cu(II)-[H_2(555)NH_2] system. From this, it is possible to estimate the log $P_{oct/aq}$ values of the individual species. The MLH species that was formed at the start of the titration (pH 2.07) had a log $P_{oct/aq}$ value of -3.39. The log $P_{oct/aq}$ value is constant in the pH range 3.33 – 6.23 for ML species. At a physiological pH of 7.4, MLH_{-1} was the predominant species and had a log $P_{oct/aq}$ value of -2.8. However, the MLH_{-2} species predominated at pH 9.2 which corresponded to a log $P_{oct/aq}$ value of -2.6. The positively charged species were expected to result in negative log $P_{oct/aq}$ values due to the ability of water to stabilize charges.

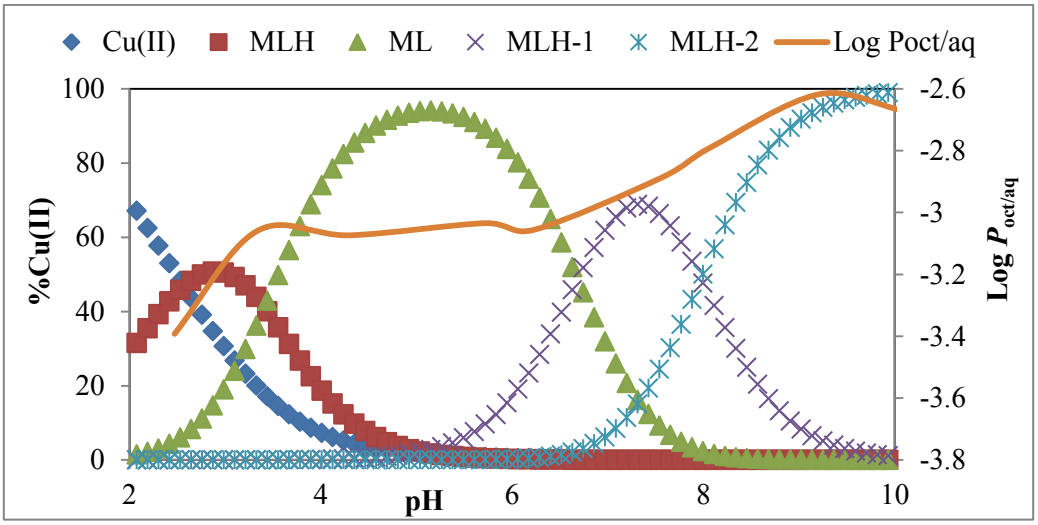

Figure 5.9: Log $P_{oct/aq}$ as a function of pH and speciation graph for 1:1 Cu(II)-[H_2(555)NH_2].

5.2.1.3.4 Cu(II)-[H_2(565)NH_2]

The octanol/water partition coefficients and the speciation graph as a function of pH for the Cu(II)-[H_2(565)NH_2] system are given in Figure 5.10. A noticeable feature about Figure 5.10 is that all log $P_{oct/aq}$ values were negative but increased with pH. Negative values of log $P_{oct/aq}$ suggest that these complexes are largely hydrophilic. From Figure 5.10, the log $P_{oct/aq}$ values for the ligand system at physiological pH (7.40) were estimated as -2.1, indicating a 0.78% extraction of copper into the octanol phase. From the species distribution curves, at this pH, the $CuLH_{-2}$ species predominated and so the partition coefficient was assigned to this species. Above pH 8.00, log $P_{oct/aq}$ was constant.

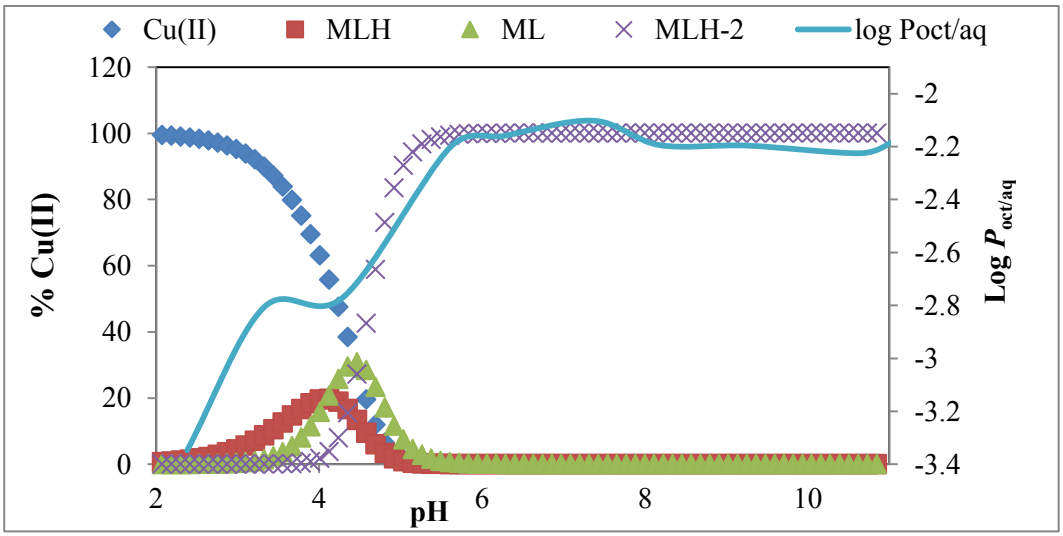

Figure 5.10: Log $P_{oct/aq}$ as a function of pH and speciation graph for 1:2 Cu(II)-[H_2(565)NH_2].

5.2.1.3.5 Cu(II)-[H(56)NH_2]

Results for Cu(II)-[H(56)NH_2] are given in Figure 5.11. The solubility in 1-octanol increased from low pH to high pH. The log $P_{oct/aq}$ value of -2.4 at pH 4.26 was associated with the ML species from the speciation distribution graph in Figure 5.11. At a physiological pH of 7.4, log $P_{oct/aq}$ value of -2.4 is associated with the predominant MLH_{-1} species. At pH 10.1 where 95 % of the Cu(II) was present as MLH_{-2}, the log $P_{oct/aq}$ value was -2.2 and therefore this value was assigned as the distribution coefficient.

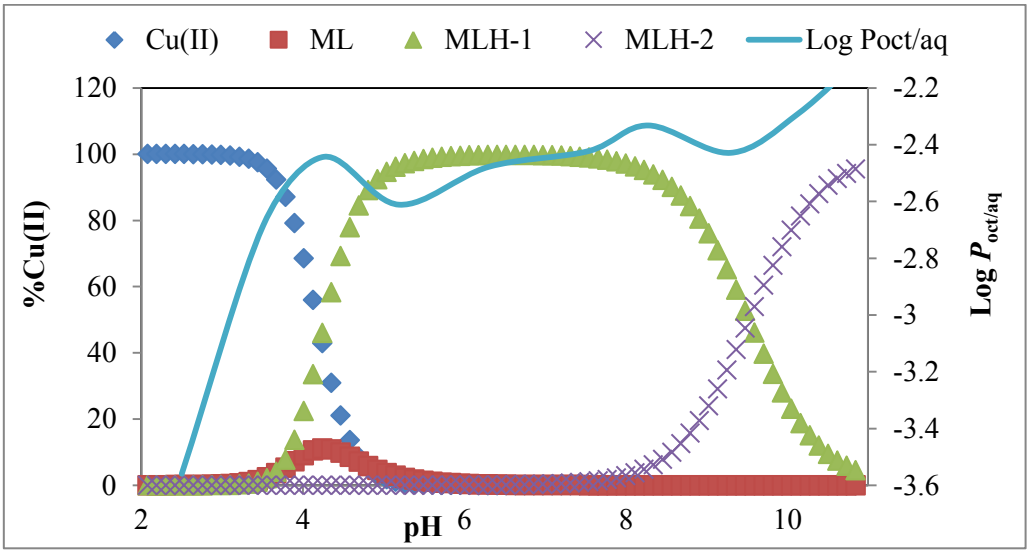

Figure 5.11: Log $P_{oct/aq}$ as a function of pH and speciation graph for 1:2 Cu(II)-[H(56)NH_2].

5.2.1.4 Discussions

Available evidence indicates that compounds having molecular weights less than 600 ($g.mol^{-1}$) are ideally suited for passive diffusion across the skin and other biomembranes.[23-25] This process has been found to depend on the lipophilicity of the drug and the 1-octanol/water partition coefficient of Cu(II). Log $P_{oct/aq}$ is often used by medicinal chemists as a measure of lipophilicity.[23,24] Complex species with a net charge of zero are more lipophilic, than charged complex species.[6-8,16,26-30] The octanol/water partition coefficients of the copper complexes studied have been determined in order to ascertain if they can be applied as topical agents in the alleviation of the anti-inflammatory process in RA.

A summarising table log $P_{oct/aq}$ for complexes of Cu(II) with different ligands at pH 7.4 is given below (Table 5.1).

Table 5.1: Logarithm of partition coefficient -log $P_{oct/aq}$ of Cu(II) at pH 7.4 in the presence of different ligands in octanol/water mixtures.

Ligands	Major Species	- log $P_{oct/aq}$
Cu[H(555)NMe_2]	MLH_{-1}	2.19 ± 0.001
Cu[H_2(565)NH_2]	MLH_{-2}	2.10 ± 0.001
Cu[H(56)NH_2]	MLH_{-1}	2.42 ± 0.001
Cu[H_2(555)NH_2]	MLH_{-1}	2.89 ± 0.004
Cu[H(555)NH_2]	MLH_{-1}	3.27 ± 0.01

The negative values of log $P_{oct/aq}$ indicate that these complexes were largely hydrophilic. The relatively hydrophilic nature of these ligands in addition to the charge distributions explains the preference of the complexes for the aqueous layer, resulting in negative values of log $P_{oct/aq}$.

For a drug to be considered lipophilic, the log $P_{oct/aq}$ value should be at least 0.60. Octanol/water partition coefficient values for highly hydrophobic (log $P_{oct/aq} > 6$) and highly hydrophilic (log $P_{oct/aq} < -2$) substances have been reported recently.[16,31] Although our compounds have log $P_{oct/aq}$ values of less than 0.60, their log $P_{oct/aq}$ values at physiological pH indicate that they do have some lipophilic character and that the presence of bulky groups plays a role to enhance their lipophilicity.

In general, only neutral molecules take part in the partition equilibrium between the aqueous and organic phases, while the charged complexes remain in the aqueous phase. The contributing factors to the hydrophilicity of the present complexes are; the presence of coordinated water molecules, hydrogen bonding between charged groups in these species and the solvent molecules, the overall charge of the MLH, ML, MLH_{-1} , MLH_{-2} complexes and hydrogen bonding between carbonyl oxygen atoms and the bulk of the water molecules.

Cu(II) complexes with a benzyl moiety have been found to have improved lipophilicity.[32] Thus the presence of pyridyl moieties in the ligand systems in this study is expected to

enhance the lipophilicity of their Cu(II) complexes and promote their extraction into the organic phase. Also the N-methyl substituent on the terminal amine increases the lipophilicity of the Cu(II) complexes at pH 7.4 as anticipated.

Positive log $P_{oct/aq}$ values (0.618 - 4.128) of some anti- inflammatory drugs have been reported.[33] Rothwell and coworkers[34] have recently reported the octanol/water partition coefficients of quercetin and related flavonoids to be in the range -1.11 to 3.22. Several workers[35-37] have studied ^{64}Cu-labeled complexes having log $P_{oct/aq}$ values in the range -1.60 to -3.02 for potential use as attaching copper radionuclides to biological molecules for diagnostic imaging and targeted radiotherapy. Jackson and coworkers[38] reported log $P_{oct/aq}$ values for related Cu(II) complexes of dioxo N5-donor ligands to be in the range -3.70 to -6.63 for the MLH, ML, MLH_{-1} and MLH_{-2} species. Nomkoko and coworkers[39] also reported log $P_{oct/aq}$ value of -1.25 at physiological pH (7.4) for the related dioxo N5-donor ligand. Therefore, the results obtained in this study are encouraging considering that they fall in the indicated range. The Cu[H_2(565)NH_2] and Cu[H(555)NMe_2] complexes were reasonably lipophilic at physiological pH (7.4).

Although partition coefficients are traditionally used as a proxy for dermal absorption, these studies have used organic drugs not metal complexes. In order to evaluate that partition coefficients can be used in this way, skin permeability was measured using an artificial membrane.

5.2.2 Franz Diffusion Cells

5.2.2.1 Introduction

Low levels of the bio-available copper in the blood have been associated with the development of chronic inflammation and remission of symptoms has been seen with the administration of exogenous copper supplements.[40,41] The ability of Cu(II) complexes with amino acids to penetrate through the stratum corneum and participate in copper ion transport processes is the key to their cosmetic and pharmaceutical activities Walker *et al.,* have measured the dermal absorption from copper bracelets and found it to be significant.[40] Despite previous successful designs of various useful copper chelating agents capable of enhancing bio-availability of copper in the blood, the challenge remains to develop a system that can enhance exogenous dermal absorption. The topical application of Cu(II)-based drugs is desirable because the current therapy for inflammation disorders relies on intra-articular or intravenous drug injection and causes the patient discomfort.[7] A drug can cross a membrane either by passive or active diffusion.[42] Passive diffusion occurs from a high concentration to a low concentration and does not require an external energy source. In percutaneous absorption studies, the potency of penetration of chemical substances is often described by the permeability coefficient K_p.[44]

For passive molecular diffusion, Fick's first diffusion law[44] is used to calculate the permeability coefficient K_p (cm/h) of Cu(II) ions in the lipid membrane. K_p depends on physiochemical parameters such as solvent temperature, solvent viscosity, nature of substrate and mass of substrate. The relation between the permeability coefficient (K_p) and the steady-state flux is calculated using the equation[45,46];

$$K_P = \frac{J}{C_i} \tag{5.3}$$

where C_i is the initial permeate concentration in the donor solution and J is the mass of permeate that passes through a unit area of the membrane in unit time. This equation implies that in percutaneous absorption studies K_p is theoretically a more reliable parameter than flux, when taking the concentration into consideration. Fick's first law of diffusion is able to describe the distribution of chemicals in fluids and is used in various technical fields.

However, it is not able to characterise the effect of vehicle and consequently the effect of concentration.[44]

When the amounts measured at successive sampling intervals are not significantly different, this is considered steady state flux and C_i is the equilibrium concentration of Cu(II) in the donor phase. Then;

$$J = \frac{Q}{A.t} \tag{5.4}$$

where Q (mg) is the quantity of Cu(II) transported through the membrane in time t (hrs), and A is the area of exposed membrane in cm^2. The steady state flux J units are $mg/(cm^2. h)$. As stated above the permeability coefficient is more reliable than the flux to describe the extent of a dermal absorption potential of chemical substances.

In the Franz diffusion cell, a biological membrane is normally used to determine the diffusion of the metal ion. However, a biological membrane is dependent on the time they were obtained, the conditions of conservation and treatment. In addition, the age, sex and weight have to be specified for a biological membrane. These considerations are not necessary for artificial membranes. The penetration process can be studied *in vitro* in a model system using a Franz diffusion cell with a liposome membrane as an artificial membrane.[44] The artificial membrane gives results that are similar to the actual diffusion through human skin. The Franz diffusion is based on vertical diffusion between donor and acceptor phases, where a liquid crystalline system with physicochemical properties similar to those of the intercellular of stratum corneum is used to model the skin barrier.

5.2.2.2 Experimental

A modified Franz cell was designed based on a normal Franz cell.[47] The cell consisted of two compartments of the same height, diameter and controlled temperature. Figure 5.12 illustrates the apparatus used to study diffusion of Cu(II) complexes.

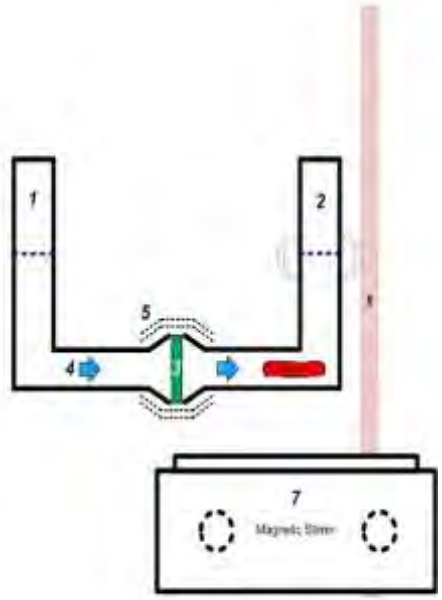

1. Donor phase filled either with 20ml of Cu(II) tripeptide complexes.
2. Receiver phase filled with 20ml blank solution (distilled/deionised water).
3. The artificial membrane (0.094 g).
4. Passive diffusion direction.
5. Clamp.
6. Stirrer bar.
7. Magnetic stirrer.
8. Burette stand with clamp

Figure 5.12: Modified Franz cells apparatus.

The experiments were performed using a Franz diffusion cell. The receiver cell was filled with 20 ml of distilled/deionised water, while the donor phase was filled with solutions having copper to ligand ratio of 1:2 and 1:1.5. The solutions of Cu(II) (0.005 M) were prepared in 20 ml distilled/deionised water. A Physiological pH of 7.4 was maintained in the acceptor cell in all the experiments, as the lower layer of the stratum corneum. The acceptor liquid was in close contact with the membrane during the experiment and was continuously and homogeneously stirred by a rotating magnet placed inside the cell. Duration of experiments (72 h), both cells were covered to prevent water from evaporating. The experiments were maintained at a constant temperature 25°C. The artificial membrane was made using filter paper that was submerged in Cerasome 9005, dried for a few minutes at room temperature and then weighed. The membrane is a lipid solution, which mimics human stratum corneum. The amount of lipid absorbed, determined by mass difference, was 0.094±0.002 g. The membrane sizes (i.e. mass and thickness) were kept constant for every new diffusion experiment undertaken. The available diffusion area between cells was 0.7085 cm^2. Copper concentration (ppm) was determined using a Microwave Plasma-Atomic Emission Spectrometer (MP-AES Agilent 4100). The instrumental detection limit of Cu(II) at wavelength 327.39 nm was 0.2 ppb. The samples were prepared by diluting 1:10

(volume/volume) using 5% HNO_3 immediately prior to analysis. The standard solutions of Cu(II) were prepared as reported.[48-50]

5.2.2.3 Results and Discussion

5.2.2.3.1 Effect of Time on Diffusion

Table 5.2 and Figure 5.13 show the effect of time on the concentration of copper diffusing through the membrane in the presence of $[H(555)NMe_2]$, $[H_2(565)NH_2]$, $[H(56)NH_2]$, $[H_2(555)NH_2]$, $[H(555)NH_2]$ and Cl^-. The pure $CuCl_2.2H_2O$ was determined at pH 4.0 because, at pH 7.00 and the concentration used, $Cu(OH)_2$ would precipitate. From Figure 5.13, it is clear that the ligands used can keep Cu(II) in solution at pH 7.0 and promote the passage of Cu(II) through the membrane, and each complex shows the same general trend. The effect of these ligands on the diffusion of Cu(II) was studied for 72h. From Figure 5.13 it can be seen that there was a slow induction period of ~ 4hrs during which time equilibrium was set up between the donor phase and the membrane and thereafter a rapid increase in diffusion through the Cerasome 9005 membrane is observed. A steady state flux of copper into the receiver phase is shown by the straight line from 6h to 72h. The observed induction period was attributed to the development of equilibrium between the donor phase and the membrane as a result of the complex diffusing through it.[51,48] After ~50 hrs it can be seen that the flux starts to level off as saturation is reached.

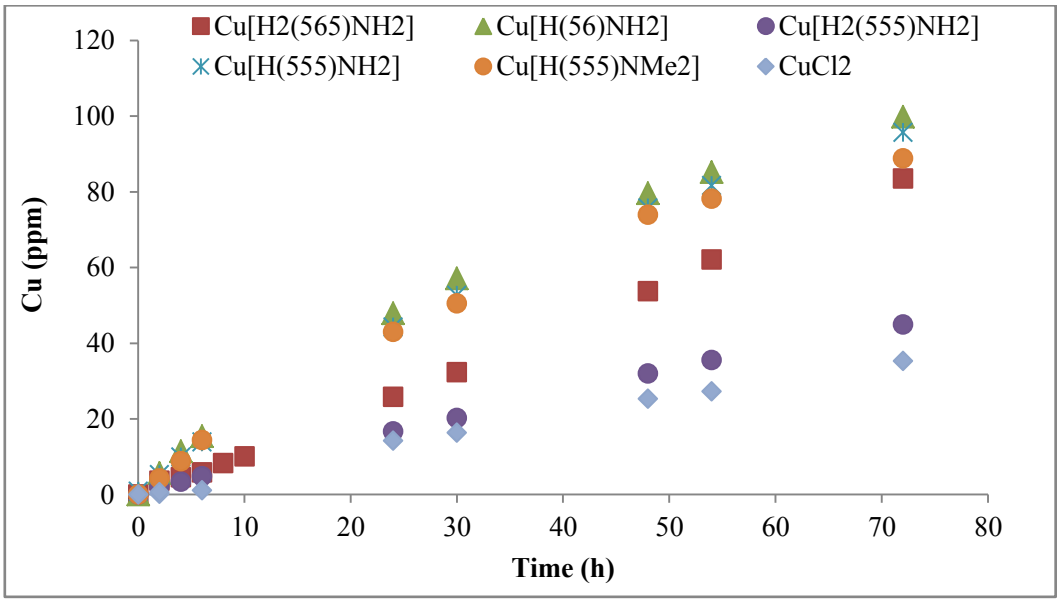

Figure 5.13: Variation of copper conc. of complexes as function of a time through Cerasome 9005 membrane at pH 7.00.

Table 5.2: Concentration (ppm) of Cu(II) in receiver phase in the presence of different ligands at pH 7.00 as function of a time.

Time (h)	[H(555)NMe_2]	[H_2(565)NH_2]	[H(56)NH_2]	[H_2(555)NH_2]	[H (555)NH_2]	Cl^-
0	0	0	0	0	0	0
2	4.2 ± 0.1	3.6 ± 0.1	5.7 ± 0.1	2.2 ± 0.1	5.2 ± 0.1	0.2 ± 0.1
4	8.8 ± 0.1	4.6 ± 0.1	11.4 ± 0.1	3.4 ± 0.1	9.9 ± 0.1	0.6 ± 0.1
6	14.4 ± 0.1	5.8 ± 0.1	15.4 ± 0.1	4.8 ± 0.1	13.9 ± 0.1	1.1 ± 0.1
24	43 ± 0.1	25.8 ± 0.1	47.9 ± 0.1	16.7 ± 0.1	44.2 ± 0.1	14.2 ± 0.1
30	50.5 ± 0.1	32.3 ± 0.1	57.1 ± 0.1	20.2 ± 0.1	52.6 ± 0.1	16.3 ± 0.1
48	73.9 ± 0.1	53.7 ± 0.1	79.6 ± 0.1	32 ± 0.1	75.7 ± 0.1	25.3 ± 0.1
54	78.2 ± 0.1	62.1 ± 0.1	85.2 ± 0.1	35.5 ± 0.1	81.6 ± 0.1	27.2 ± 0.1
72	88.8 ± 0.1	83.5 ± 0.1	99.8 ± 0.2	44.9 ± 0.1	95.7 ± 0.1	35.3 ± 0.2

5.2.2.3.2 The steady state flux *J* and permeability coefficient K_p calculations

The flux values *J*, permeability coefficient K_p and their corresponding standard error (SE) for the copper complexes are shown in Table 5.3. The steady state flux and permeability coefficients were calculated from the gradient of the curves[46] in Figure 5.13. The measurements were done in triplicate. The flux was calculated from the slope of the linear portion of the plot of the cumulative amount of Cu(II) penetrated per square centimetre through the membrane as function of a time.[44]

Figure 5.14 shows the influence of the different ligand systems on the flux of Cu(II) ions through the Cerasome 9005 membrane. These results suggest that the complexation of Cu(II) ions by the different ligands greatly influences the diffusion of Cu(II) ions across the membrane because different flux values were obtained for different Cu(II) complexes.

Table 5.3: Flux of diffusion J (mg/cm^{2}h) and permeability coefficient K_p (cm\h) of copper complexes through Cerasome 9005 membrane.

Complexes	J mg/cm^{2}h	K_p cm/h
Cu[H(555)NMe_2]	0.018 ± 0.01	0.082 ± 0.01
Cu[H_2(565)NH_2]	0.022 ± 0.01	0.078 ± 0.01
Cu[H(56)NH_2]	0.019 ± 0.01	0.069 ± 0.01
Cu[H_2(555)NH_2]	0.011 ± 0.02	0.060 ± 0.02
Cu[H(555)NH_2]	0.02 ± 0.01	0.069 ± 0.01
$CuCl_2.2H_2O$ *pH 4.0	0.003 ± 0.05	0.025 ± 0.07

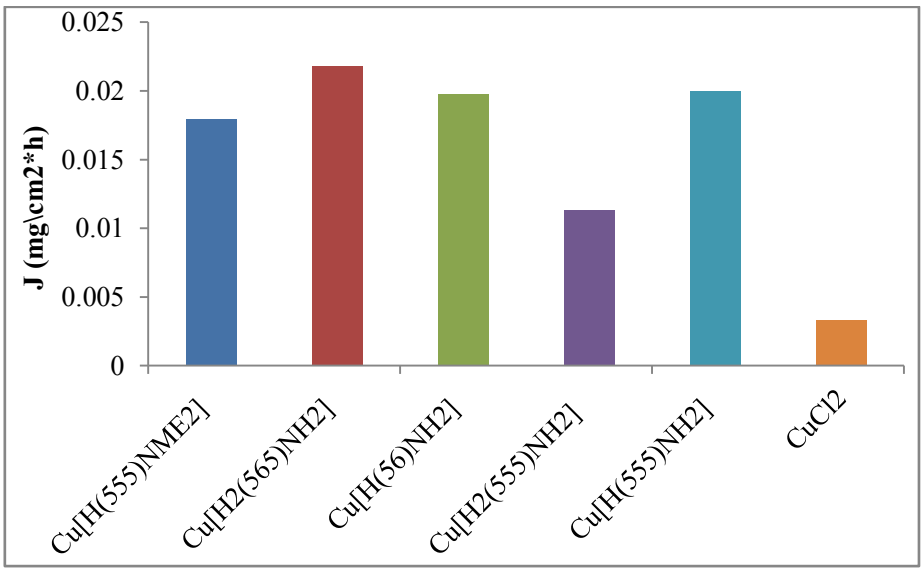

Figure 5.14: Effect of different ligands on the flux of copper through Cerasome 9005 membrane in modified Franz cell from 24 – 72 hrs at pH 7.00.

Lena and Kinga (2007) found that complexation of Cu(II) ions greatly increases the permeation rate of Cu(II) ions as K_p values for complex species are significantly higher (by as much as ten times) than the value for simple Cu(II) ions. The order for the permeability coefficients K_p of Cu(II) ligand complexes as shown in Figure 5.15, is as follows: [H(555)NMe_2] > [H_2(565)NH_2] > [H(555)NH_2] ~ [H(56)NH_2] > [H_2(555)NH_2] > Cl^-. The

obtained results show that different ligands were able to enhance the passage of Cu(II) through an artificial membrane.

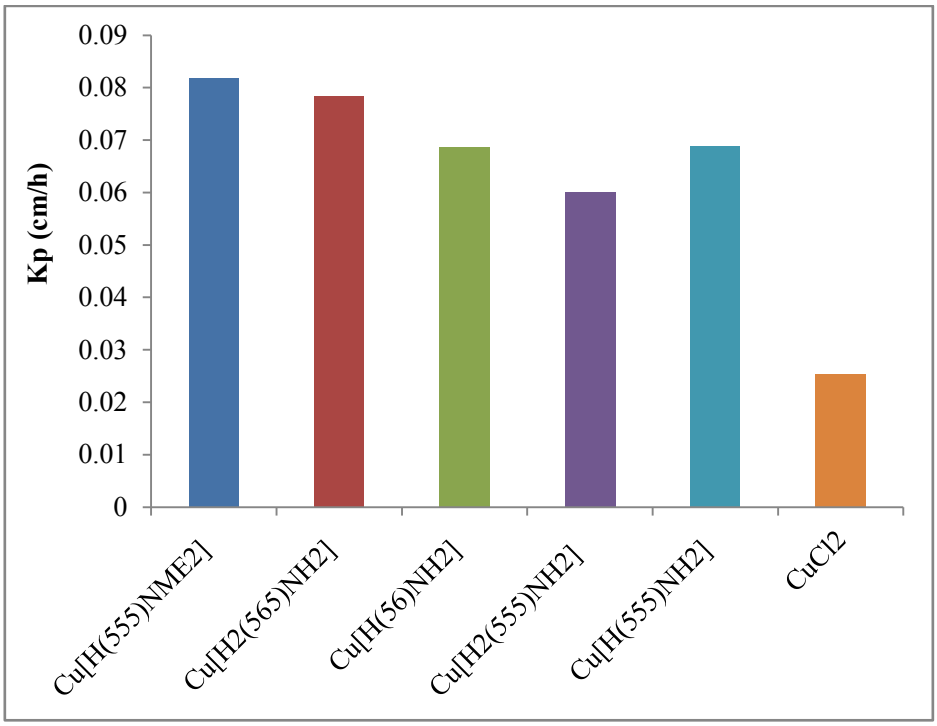

Figure 5.15: Influence of ligands on the permeability of copper complexes through Cerasome 9005 membrane at pH 7.00.

One of the aims of this study was to design ligands that would increase the level of endogenous copper through dermal absorption. This was evaluated using partition coefficient and Franz cell. Partition coefficients are easier to measure than membrane permeability using a Franz cell. For this reason partition coefficients are often used as an indication of tissue permeability. However, for copper complexes it is not known if partition coefficients are a good proxy for tissue permeability. Since in this study we have measured both log $P_{oct/aq}$ and log K_p it is important to see if there is a correlation between the two.

5.2.2.3.3 Relationship between logarithm of permeability coefficient Log K_p and octanol/water partition coefficient Log $P_{oct\backslash aq}$ of copper complexes.

Table 5.4 shows log K_p, log $P_{oct/aq}$ and the major copper species of different ligands at pH 7 present in solution. So it is reasonable to assume that the measured parameters refer to this species.

Table 5.4: The permeability and partition coefficients values of Cu(II) speciation in the presence of different ligands at pH 7.4.

Ligands	Major Species	- log $P_{oct/aq}$	-log K_p
Cu[H(555)NMe_2]	MLH_{-1}	2.19 ± 0.001	1.09± 0.01
Cu[H_2(565)NH_2]	MLH_{-2}	2.10 ± 0.001	1.11± 0.01
Cu[H(56)NH_2]	MLH_{-1}	2.42 ± 0.001	1.16± 0.01
Cu[H_2(555)NH_2]	MLH_{-1}	2.89 ± 0.004	1.22± 0.04
Cu[H(555)NH_2]	MLH_{-1}	3.27 ± 0.01	1.16± 0.02

Figure 5.16 shows the possible correlation between the logarithm of permeability coefficient log K_p and octanol/water partition coefficient log $P_{oct\backslash aq}$ of the Cu(II) complexes. The coefficient of correlation obtained from Figure 5.16 is $R^2 = 0.487 \pm 0.05$. However, it is far from 1 demonstrating that, there is no correlation between the logarithm of permeability coefficient and the logarithm of octanol/water partition coefficient of all Cu(II) complexes. The 48% variability can be explained by octanol/water partition coefficient of the Cu(II) complexes; i.e. that permeability coefficient does not linearly depend on octanol/water partition coefficient for all copper complexes.

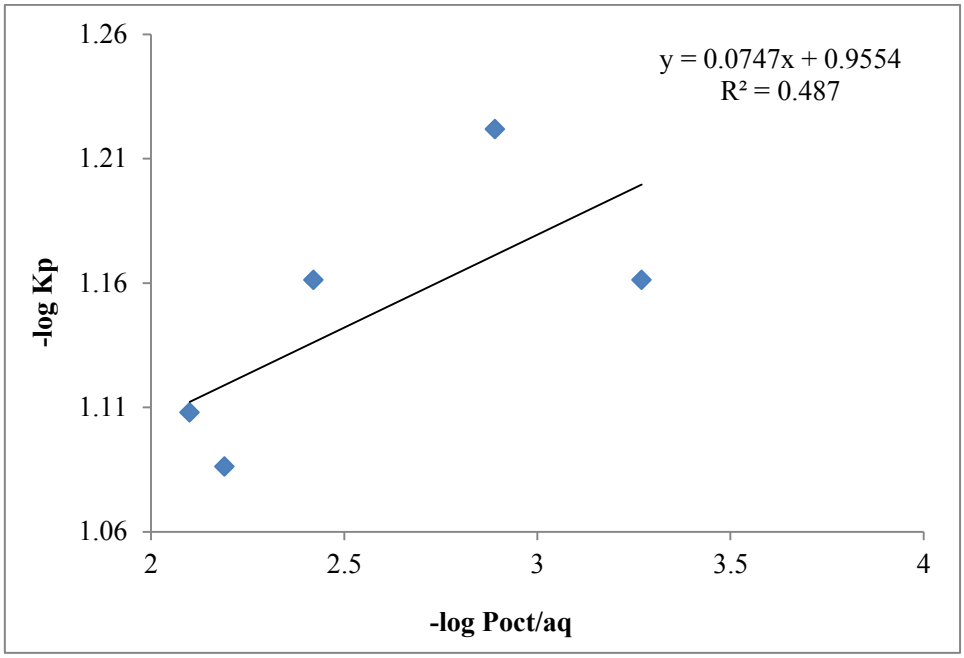

Figure 5.16: Logarithm of permeability coefficient log K_p plotted against logarithm partition coefficient Log $P_{oct\backslash aq}$ of 7 copper complexes.

5.2.2.4 Conclusion

The amount of Cu(II) transferred from aqueous solution to organic layer changes with pH because speciation changes with pH and the different species have different partition coefficients. The results showed that all the Cu(II) complex species studied had log $P_{oct\backslash aq}$ valves below zero indicating that complexes were relatively hydrophilic. However, The Cu[H_2(565)NH_2] and Cu[H(555)NMe_2] complexes were reasonably lipophilic at physiological pH (7.4). In addition, the transport of copper through an artificial membrane with ligands greatly increased the permeation rate of Cu(II) ions since K_p values for complex species were significantly higher than those for simple Cu(II) ions. The obtained results show that the permeability rate of Cu(II) complexes through Cerasome 9005 membrane depends on the ligand. From the partition coefficients results, Cu[H_2(565)NH_2] is predicted to have the highest dermal absorption but K_p says Cu[H(555)NMe_2] should have the highest dermal absorption. A statistical analysis of the results showed that they were no correlation was found between logarithm of partition coefficient and permeability coefficient. This means that log $P_{oct\backslash aq}$ is not as good a measure of dermal absorption of Cu(II) as log K_p.

References

1. J. R. Sorenson, *J. Med. Chem.*, 1976, **19**, 135–48.

2. H. Faure, and A. Favier, *Handbook of Metal-Ligand Interactions in Biological Fluids, Bioinorganic Chemistry*, Marcel Decker, Inc., New York, 2nd edn., 1995.

3. P. M. May, P. W. Linder and D. R. Williams, *J. Chem. Soc. Dalt. Trans.*, 1977, **2**, 588.

4. G. E. Jackson, P. M. May and D. R. Williams, *J. Inorg. Nucl. Chem.*, 1978, **40**, 1227–1234.

5. P. M. May, P. W. Linder and D. R. Williams, *J. Chem. Soc. Dalt. Trans.*, 1977, **2**, 588.

6. J. R. Zeevaart, N. V Jarvis, W. K. . Louw, G. E. Jackson, I. Cukrowski and C. J. Mouton, *J. Inorg. Biochem.*, 1999, **73**, 265–272.

7. J. N. Zvimba and G. E. Jackson, *J. Inorg. Biochem.*, 2007, **101**, 148–58.

8. J. R. Zeevaart, D. R. Jansen, M. F. Botelho, A. Abrunhosa, C. Gomes, L. Metello, Z. I. Kolar, G. C. Krijger, W. K. a Louw and I. C. Dormehl, *J. Inorg. Biochem.*, 2004, **98**, 1521–30.

9. M. Mohajane, *MSc Thesis*, University of Cape Town, 2010.

10. G. E. Jackson, P. M. May and D. R. Williams, *J. Inorg. Nucl. Chem.*, 1978, **40**, 1189–1194.

11. P. M. May and D. R. Williams, *FEBS Lett.*, 1977, **78**, 134–138.

12. J. Clark and D. D. Perrin, *Q. Rev. Chem. Soc.*, 1964, **18**, 295–320.

13. S. Pinsuwan, A. Li and S. H. Yalkowsky, *J. Chem. Eng. Data*, 1995, **40**, 623–626.

14. G. L. Flynn, *Physicochemical determinants of skin absorption. In: Principles of Route-to-Route Extrapolation for Risk Assessment.*, Elsevier, New York, 1990.

15. R. O. Potts and R. H. Guy, *Pharm. Res.*, 1992, **9**, 663–9.

16. J. N. Zvimba and G. E. Jackson, *J. Inorg. Biochem.*, 2007, **101**, 1120–8.

17. G. Korinth, T. Wellner, K. H. Schaller and H. Drexler, *Toxicol. Lett.*, 2012, **215**, 49–53.

18. S. K. Poole and C. F. Poole, *J. Chromatogr. B*, 2003, **797**, 3–19.

19. G. Klopman and H. Zhu, *Mini Rev. Med. Chem.*, 2005, **5**, 127–33.

20. E. T. Nomkoko, G. E. Jackson and B. S. Nakani, *Dalton Trans.*, 2004, 1432–40.

21. B. Idson, *J. Pharm. Sci.*, 1975, **64**, 901–24.

22. X. Q. Kong, D. Shea, W. a Gebreyes and X.-R. Xia, *Anal. Chem.*, 2005, **77**, 1275–81.

23. A. Leo, C. Hansch and D. Elkins, *Chem. Rev.*, 1971, **71**, 525–616.

24. T. X. Xiang and B. D. Anderson, *J. Membr. Biol.*, 1994, **140**, 111–22.

25. T. E. Nomkoko, G. E. Jackson, B. S. Nakani and R. Hunter, *Dalton Trans.*, 2006, 4029–38.

26. B.-Z. Zhu, *Chem. Res. Toxicol.*, 2001, **14**, 222–227.

27. J. Zeevaart, *J. Inorg. Biochem.*, 2001, **83**, 57–65.

28. G. E. Jackson, P. W. Linder and A. Voyé, *J. Chem. Soc. Dalt. Trans.*, 1996, 4605.

29. G. E. Jackson and M. J. Kelly, *J. Chem. Soc. Dalt. Trans.*, 1990, 1889–1893.

30. J. N. Zvimba and G. E. Jackson, *Polyhedron*, 2007, **26**, 2395–2404.

31. J. T. Andersson and W. Schräder, *Anal. Chem.*, 1999, **71**, 3610–3614.

32. J. N. Zvimba, *Ph.D Thesis*, University of Cape Town, 2005.

33. F. Péhourcq, M. Matoga, C. Jarry and B. Bannwarth, *J. Liq. Chromatogr. Relat. Technol.*, 2001, **24**, 2177–2186.

34. J. A. Rothwell, A. J. Day and M. R. A. Morgan, *J. Agric. Food Chem.*, 2005, **53**, 4355–60.

35. X. Sun, M. Wuest, Z. Kovacs, A. D. Sherry, R. Motekaitis, Z. Wang, A. E. Martell, M. J. Welch and C. J. Anderson, *J. Biol. Inorg. Chem.*, 2003, **8**, 217–25.

36. X. Sun, M. Wuest, G. R. Weisman, E. H. Wong, D. P. Reed, C. A. Boswell, R. Motekaitis, A. E. Martell, M. J. Welch and C. J. Anderson, *J. Med. Chem.*, 2002, **45**, 469–77.

37. A. B. Packard, J. F. Kronauge, P. J. Day and S. . Treves, *Nucl. Med. Biol.*, 1998, **25**, 531–537.

38. G. E. Jackson, L. Mkhonta-Gama, A. Voyé and M. Kelly, *J. Inorg. Biochem.*, 2000, **79**, 147–152.

39. E. T. Nomkoko, G. E. Jackson and B. S. Nakani, *Inorg. Chem. Commun.*, 2003, **6**, 335–338.

40. J. J. E. Weder , C. T. Dillon , T. W. Hambley , B. J. Kennedy, P. A. Lay and N. M. D. R. Biffin , H. L. Regtop, *Copper complexes of non-steroidal drugs. a Centre for Heavy Metals Research*, School of Chemistry, University of Sydney, Sydney NSW, 2006.

41. J. R. J. Sorenson, *In Metal Ions in Biological Systems*, Marcel Dekker, New York, Vol.14 edn., 1982.

42. T. Peck , S. Hill and M. Williams, *Pharmacology for Anaesthesia and Intensive Care*, the United States of America by Cambridge University Press, New York, 3rd., 2009, vol. 56.

43. G. Korinth, K. H. Schaller and H. Drexler, *Arch. Toxicol.*, 2005, **79**, 155–9.

44. H. Schaefer and T. E. Redelmeier, *Skin barrier. Principles of percutaneous Absorption.*, Karger, Basel, 1996.

45. L. Mazurowska, K. Nowak-Buciak and M. Mojski, *Anal. Bioanal. Chem.*, 2007, **388**, 1157–63.

46. E. U. Tsumbu, *MSc Thesis*. University of Cape Town, 2010.

47. S. Odisitse, G. E. Jackson, T. Govender, H. G. Kruger and A. Singh, *Dalton Trans.*, 2007, 1140–9.

48. M. Mohajane, *Ph.D Thesis*, University of Cape Town, 2013.

49. P. T. Zvimba N. John, *Ph.D Thesis*, University of Cape Town, 2005.

50. S.-F. Ng, J. Rouse, D. Sanderson and G. Eccleston, *Pharmaceutics*, 2010, **2**, 209–223.

Chapter Six

Concluding Remarks

6.1 Conclusion

The fundamental role of copper and the recognition of its complexes as important bioactive compounds *in vitro* and *in vivo* have aroused an ever-increasing interest in these agents as potential drugs for therapeutic intervention in various diseases.[1] Copper complexes have been reported to have anti-inflammatory activities for the alleviation of inflammation associated with rheumatoid arthritis (RA). Several reviews have been published on the anti-inflammatory activity of copper complexes.[2-6] This study was undertaken in order to develop better Cu(II)-based anti-inflammatory drugs which can be administered orally, intravenously or transdermally. However, the preferred route of administration is through the skin, because percutaneous absorption offers one obvious advantage of being less painful and hence tolerable to the patient.[7] Therefore, the rate of dermal absorption and bioavailability of the copper is important. In the present study five ligands, were designed with the aim of increasing the low molecular weight (l.m.w) copper concentration *in vivo*.

In blood plasma, copper is transported by proteins; human serum albumin (HSA) being the most effective protein.[8-10] The Cu(II) binding site of HSA is Asp-Ala-His residues (shown in Figure 2.1).[11,12] The designs of the ligands in this study were based on the structure of HSA. All the ligands are peptide mimetics, containing one or more amide groups. When the copper coordinates to the amide-N it displaces the amide proton which decreases the charge of the complex. Amines are good, selective coordinators of Cu(II)[13,14] and the pyridyl group has a high Cu(II) mobilizing ability and is found in most NSAID drugs.[3,11,15] For this reason these two groups were incorporated into the ligand design. The pyridyl aromatic ring increases the rigidity of the ligand system and hence the stability and lipophilicity of the metal complex.[15] In addition, N-methyl substitution was used to increase the lipophilicity of the complex. Using these criteria the ligands in this study have been designed.

The effect of the number and position of amide groups as well as, the effect of methyl substitution upon the stability of the metal complexes was studied using a glass electrode potentiometry. The solution equilibria of H^+, Cu^{2+}, Ni^{2+} and Zn^{2+} at 25°C and an ionic strength of 0.15 mol dm^{-3} were measured. The Cu(II) complex species showed significantly different coordination behaviour at physiological pH. The formation equilibria for Ni(II) and Zn(II) showed that these metal ions also form relatively stable complexes with these ligands, although their stability is lower than that of Cu(II).

The CuL species was formed for all the ligands in this study. The stability of the CuL complexes is in the order $[H(555)NH_2]$ > $[H(555)NMe_2]$ > $[H_2(555)NH_2]$ > $[H(56)NH_2]$ > $[H_2(565)NH_2]$. The effect of methyl substitution is shown by comparing $[H(555)NH_2]$ and $[H(555)NMe_2]$ which is a decrease in stability constants by only one log unit. However, the N-methyl substituent on the terminal amine was increased the lipophilicity of the copper complexes.

The effect of the number of amide groups is shown by comparing the CuL species of $[555\text{-}N]^2$, which has no amide group (Figure 3.31), with $[H(555)NH_2]$ and $[H(56)NH_2]$, which have one amide group and $[H_2(555)NH_2]$ and $[H_2(565)NH_2]$, which have two amide groups. In this comparison, the obvious conclusion is reached that the stability decreases with the introduction of amide groups. This comparison, however, is not really valid because the structure of the different complexes is different. In [555-N] (log β 18.62) the copper is coordinated through all 4 nitrogen donor groups, while in $[H(555)NH_2]$ (log β 11.81) only 3 nitrogens are coordinated, the terminal amine being protonated. In $[H_2(555)NH_2]$ (log β 9.39) the copper is coordinated through the pyridyl-N, the terminal amine-N and the amide-O. Thus, the difference in stability reflects the different coordination mode as well as the number of amide groups.

The position of the amide group is shown by comparing $[H_2(555)NH_2]$ and $[H_2(565)NH_2]$. Here, since the stoichiometry is the same, a comparison of the stability constants is valid. The Cu(II) log $\beta_{11\text{-}2}$ for these two are -5.27 and -3.06 respectively. The reason for this is most likely steric strain. $[H_2(555)NH_2]$ forms three, five membered, chelate rings while $[H_2(565)NH_2]$ forms 5,6,5 chelate rings. Previous studies[4,16-18] have shown that three contiguous five membered rings are less stable than when the strain is released by a larger 6 membered ring in the middle.

The reason for designing different ligands with different structural features was to see which is the best at complexing copper at physiological pH. Hence, the best way to evaluate the different ligands is to compare their speciation, in competition, at different pH. This would take into account the different basicities (pK_a's) of the ligand and also their different stoichiometries. Such a speciation diagram is shown in Figure 6.1, where the concentration of Cu(II) and each of the ligands are 1 mM. These results show that $[H(555)NH_2]$ is the best ligand between pH 6 to 7. This ligand has the highest stability with Cu(II) compared to the other ligands as it is coordinated with Cu(II) *via* two amine-N's, an amide-N and a pyridyl-N.

The second ligand binding with Cu(II) in the same pH range is $[H(555)NMe_2]$. At high pH 21% of Cu(II) is bond to this ligand as the MLH_{-1} and MLH_{-2} species. The $[H_2(565)NH_2]$ binds 48% of the Cu(II) at high pH. This is due to forming MLH_{-2} by losing two amide protons. Meanwhile, $[H_2(555)NH_2]$ and $[H(56)NH_2]$ are not able to compete with the other ligands and so their complexes are not formed.

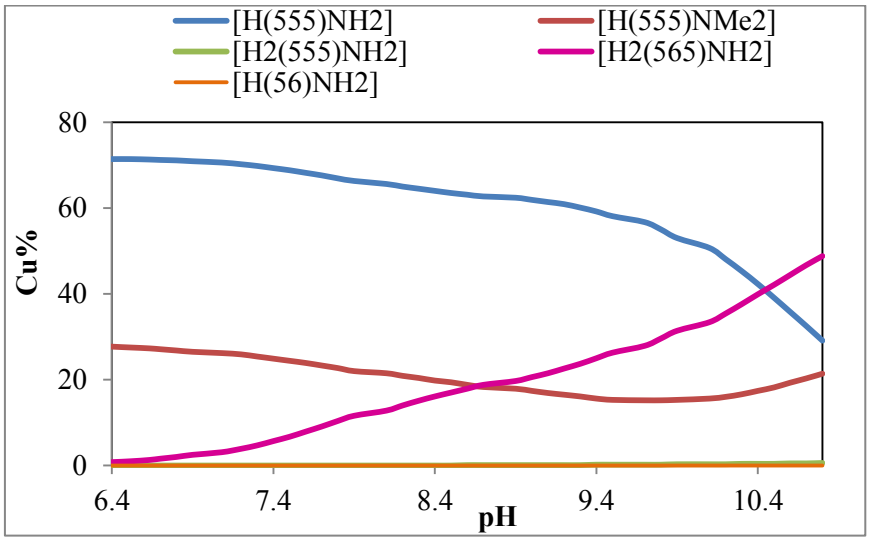

Figure 6.1: Effect of different ligands on the percentage of Cu(II) as a function of pH.

The above discussion centered on the ability of the different ligands to complex copper *in vitro*. What is also important is the ability of the ligands to complex copper *in vivo*. This was evaluated using a computer model of blood plasma, which takes into account competition with endogenous metal ions and ligands. It is particularly important is that the ligands were evaluated using the ECCLES program, an *in vivo* speciation model of blood plasma. The ligands must be selective for Cu(II) over Ca(II) and Zn(II), as these ions are present in plasma at much higher concentrations than Cu(II) and hence are potential competitor *in vivo*.[19-21] The mobilizing ability of the ligands was in the order $[H(555)NH_2]$ > $[H(555)NMe_2]$ > $[H_2(565)NH_2]$ > $[H_2(555)NH_2]$ > $[H(56)NH_2]$. At a concentration of 10^{-6} to 10^{-2} mol dm^{-3} the ligands were able to cause a 10 fold increase in the concentration of low molecular weight Cu(II) complexes. The results showed that the $[H_2(555)NH_2]$ and $[H(56)NH_2]$ have low mobilizing ability in blood plasma and thus cannot effectively increase the l.m.w Cu(II) fraction. The reason for the low mobilizing ability of these two ligands is the stability of their

complexes with Zn(II) and Ni(II), i.e. they are not very selective for Cu(II). [H(555)NH_2] and [H(555)NMe_2] have the highest copper mobilizing capacity as they form the most stable complexes and are selective for Cu(II) over Zn(II).

Figure 6.2 shows the [H(555)NH_2] and [H(555)NMe_2] p.m.i curves. For comparison results with the terminal amino acid sequence of serum albumin, glycylglycylhistamine (GGHA) and L-aspartyl-L-alanyl- L-histidine N-methyl amide (Asp-Ala-His-NHMe) are also shown. From this we see that [H(555)NH_2] is better at mobilizing Cu(II) *in vivo* than GGHA and Asp-Ala-His-NHMe. On the other hand, [H(555)NMe_2] has the same Cu(II) mobilizing ability as GGHA. The remarkably high mobilizing ability of [H(555)NH_2] by one log unit compared to GGHA and three log unit compared to Asp-Ala-His-NHMe is related to the presence of one electron withdrawing CONH-group. At these ligand concentrations, the Zn(II) p.m.i is insignificant. Hence, the speciation of this essential metal ion is not disturbed. In spite of the higher concentration of Zn(II) than Cu(II) *in vivo*, it is unable to compete with Cu(II) for [H(555)NH_2] and [H(555)NMe_2].

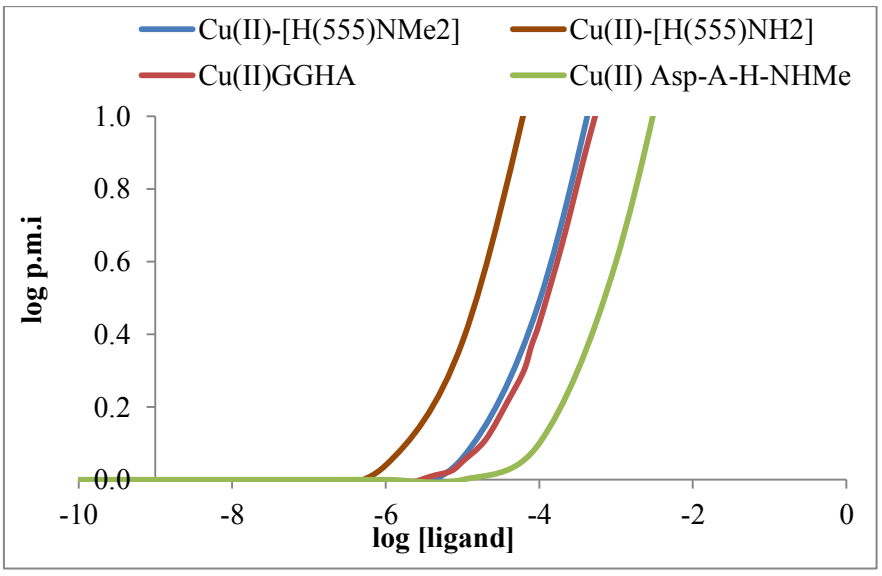

Figure 6.2: Cu(II) plasma mobilizing index for [H(555)NH_2], [H(555)NMe_2], GGHA and Asp-Ala-His-NHMe.

These ligands are able to coordinate Cu(II) *in vivo* and in order to understand the difference in stability of the different Cu(II) complexes their chemical structures were investigated. The geometries of the different species in solution were successfully determined

by potentiometry, ^{1}H-NMR, UV-visible spectroscopy, X-ray crystallography and Molecular Mechanics (MM) calculation studies. At different pH's the colours of the Cu(II) complexes varied from light blue to purple. It was expected that as the pH increased, Cu(II) would induce ionization of the amide protons[22,23], implying a transition from Cu-O to Cu-N in the coordination arrangement.[24] Since several species existed in solution, deconvolution of the spectral data as a function of pH generated extinction coefficient-based data which was used successfully to determine the actual spectra of the complexes in solution. At physiological pH, the predominate species is MLH_{-1} for all the ligands except $[H_2(565)NH_2]$, which has MLH_{-2} as the predominant species. The preference of Cu(II) ion for an environment with four nitrogen donor atoms with a coordination number of four in a tetragonally distorted environment or a square planar geometry were noted. The UV-visible spectroscopy results showed that $[H_2(555)NH_2]$ and $[H_2(565)NH_2]$ formed 4N coordination (NH_2, $2N^-$, N_{py}) with λ_{max} 524 and 532, respectively. Both complexes have the same colour at high pH and are suggested to form a square planar geometry. The MLH_{-1} of $[H(56)NH_2]$ and $[H_2(555)NH_2]$ were coordinated by 3N (NH_2, N^-, N_{py}), where the fourth equatorial position could be a water molecule or carbonyl respectively. The MLH_{-1} species of $[H(555)NH_2]$ and $[H(555)NMe_2]$ are suggested to form tetragonally distorted octahedral geometries *via* 4N coordination ($2NH_2$, N^-, N_{py}) with Cu(II).

From the ^{1}H-NMR results, it is clear that for some of the complexes, more than one species is in solution at the same time. The ^{1}H-NMR study showed that the pyridyl -N is coordinated at the beginning of complexation followed by the amide and terminal amine groups. This is indicated by the broadening of the proton resonances of the ^{1}H-NMR signal arising from protons attached to neighbouring carbons upon complexation by Cu(II). However, coordination by the carbonyl oxygens rather than the amide nitrogen cannot be ruled out. Unfortunately, the amide proton is in rapid exchange and so cannot be observed. The ^{1}H-NMR results confirm the results obtained by potentiometric and UV-visible spectroscopy.

While structures are suggested for different species from potentiometry and spectroscopy, it is not clear that these structures are physically reasonable. For this reason, molecular mechanics (MM) was used to calculate the strain energies (internal) of the different possible geometries for the complexes. By consideration of the differences in strain energy on complexation in various species, the stability of the postulated solution complexes, were successfully explained. Thus, it was shown that molecular mechanics calculations, though not

a comprehensive tool, can still be used to rationalize the stability of related complex species in solution.

Direct evidence for the amide proton dissociation on complexation has been widely reported[25-27] for Cu(II) complexes in solution. The two structures, we were able to isolate and study by X-ray crystallography were the Cu(II) complexes of $[H(56)NH_2]$ and $[H_2(565)NH_2]$. The Cu(II)$[H(56)NH_2]$ complex had an essentially rectangular pyramidal geometry, while Cu(II)$[H_2(565)NH_2]$ formed a distorted square planar geometry. The results of X-ray crystallographic study have shown unequivocally that the amide proton displacement takes place in the solid with the coordination of the resulting negative amide groups occurring to the metal ion

One of the objectives of the study was to develop Cu(II) complexes that could be administered "trans-dermally". This was evaluated by measuring the effect of the ligands on the rate of diffusion of Cu(II) through Cerasome, as an artificial membrane mimetic of skin. These results were then compared with traditional octanol/water partition coefficient measurements.

Traditionally, octanol/water partition coefficients are used as an indication of transdermal absorption. The results showed that all the Cu(II) complex species studied had log $P_{oct\backslash aq}$ values below zero indicating that complexes were relatively hydrophilic. The presence of the pyridyl moieties in the ligand systems, enhanced the lipophilicity of their Cu(II) complexes. The N-methyl substituent on the terminal amine increased the lipophilicity of the Cu(II) complexes. The transport of copper through an artificial membrane with ligands greatly increased the permeation rate of Cu(II) ions since K_p values for complex species were significantly higher than those for simple Cu(II) ions. The order for the permeability coefficient K_p of Cu(II) ligand complexes was as follows: $[H(555)NMe_2] > [H_2(565)NH_2] > [H(555)NH_2] \sim [H(56)NH_2] > [H_2(555)NH_2] > Cl^-$.

Partition coefficients are often used as an indication of tissue permeability as they are easier to measure than membrane permeability using a Franz cell. However, the obtained results showed that, there was no correlation between partition coefficient and permeability coefficient. This means that log $P_{oct\backslash aq}$ is not as good a measure of dermal absorption of Cu(II) as log K_p; this indicates that care must be exercised when using partition coefficients as a proxy for tissue permeability.

In the present study, [H(555)NH_2] and [H(555)NMe_2] have a higher mobilizing capacity than all the other ligands. On the other hand, [H(555)NMe_2] and [H_2(565)NH_2] have the higher Cu(II) permeability. The best mobilizing ligand is not the best transport ligand and so a compromise ligand has to be chosen. This is [H(555)NMe_2], which has a similar mobilizing ability as [H(555)NH_2] and also is the best at promoting dermal absorption. It would be interesting to investigate the copper bio-distribution for this ligand in an animal model of arthritis using ^{64}Cu(II) as a radiotracer.

The overall results in this study are encouraging and merit further evaluation for the use of Cu(II) complexes in chemotherapy. It is therefore hoped that this study has contributed to the understanding of some aspects and factors involved in the development of copper-chelating agents for alleviation of inflammation associated with RA. The study has clearly outlined the approach that could be followed in future studies for the development of new drugs with the aim of introducing Cu(II) into the body.

This study has shown that the [H_2(555)NH_2] system, which has two amide groups next to each other forms weak Cu(II) complexes and hence is not able to mobilize the metal ion *in vivo*. Previous studies have shown that the stability of these complexes can be improved by the addition of a carbon spacer between the two amides. This is certainly something that can be investigated in future. In addition, methyl groups could be added to the terminal amine to improve the lipophilicity. Studies in the future could also focus on a similar system with imidazole replacing the pyridine. Imidazole is a stronger base and is part of the binding terminus of HSA.[28] Based on these considerations the following ligands can be proposed for future studies (Figure 6.3).

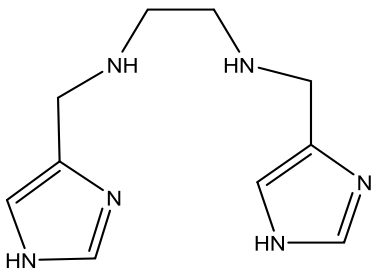

N^1,N^2-bis((1*H*-imidazol-4-yl)methyl)ethane-1,2-diamine

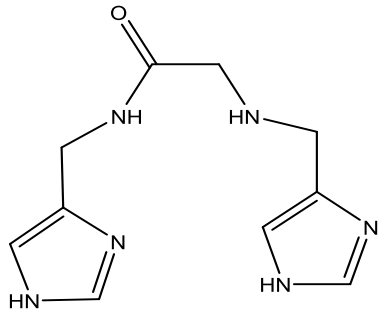

N-((1*H*-imidazol-4-yl)methyl)-2-(((1*H*-imidazol-4-yl)methyl)amino)acetamide

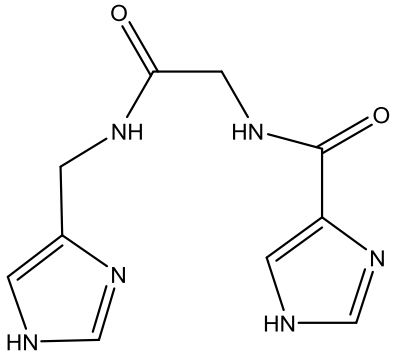

N-(2-(((1*H*-imidazol-4-yl)methyl)amino)-2-oxoethyl)-1*H*-imidazole-4-carboxamide

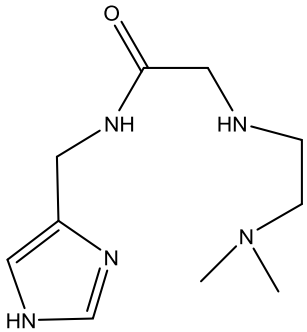

N-((1*H*-imidazol-4-yl)methyl)-2-((2-(dimethylamino)ethyl)amino)acetamide

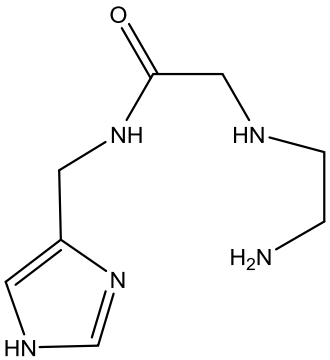

N-((1*H*-imidazol-4-yl)methyl)-2-((2-aminoethyl)amino)acetamide

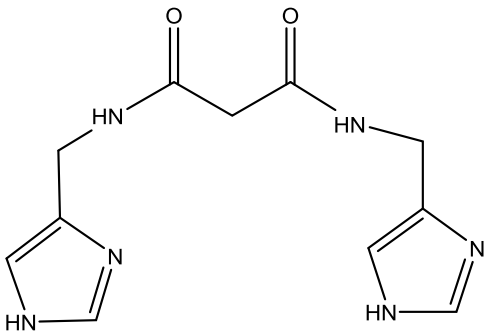

N^1,N^3-bis((1*H*-imidazol-4-yl)methyl)malonamide

Figure 6.3: Schematic representation of structures of ligands for future studies.

References:

1. I. Iakovidis, I. Delimaris and S. M. Piperakis, *Mol. Biol. Int.*, 2011, **2011**, 594529.
2. J. N. Zvimba and G. E. Jackson, *J. Inorg. Biochem.*, 2007, **101**, 148–58.
3. S. Odisitse and G. E. Jackson, *Inorganica Chim. Acta*, 2009, **362**, 125–135.
4. G. E. Jackson, P. W. Linder and A. Voy'e, *J. Chem. Soc. Dalt. Trans.*, 1996, 4605.
5. G. E. Jackson and M. J. Kelly, *J. Chem. Soc. Dalt. Trans.*, 1989, 2429.
6. T. E. Nomkoko, G. E. Jackson, B. S. Nakani and R. Hunter, *Dalton Trans.*, 2006, 4029–38.
7. E. T. Nomkoko, G. E. Jackson and B. S. Nakani, *Dalton Trans.*, 2004, 1432–40.
8. M. Sokołowska, K. Pawlas and W. Bal, *Bioinorg. Chem. Appl.*, 2010, **42**, 1–7.
9. L. Perrone, E. Mothes, M. Vignes, A. Mockel, C. Figueroa, M.-C. Miquel, M.-L. Maddelein and P. Faller, *Chembiochem*, 2010, **11**, 110–8.
10. P. Z. Neumann and A. Sass-Kortsak, *J. Clin. Invest.*, 1967, **46**, 646–58.
11. J. N. Zvimba and G. E. Jackson, *Polyhedron*, 2007, **26**, 2395–2404.
12. M. Dockal, D. C. Carter, and F. Ruker, *J. Biol. Chem.*, 1999, **274**, 29303–29310.
13. R. P. Bonomo, A. De Flora, E. Rizzarelli, A. M. Santoro, G. Tabbí and M. Tonetti, *J. Inorg. Biochem.*, 1995, **59**, 773–784.
14. M. Valko, H. Morris, M. Mazúr, J. Telser, E. J. L. McInnes and F. E. Mabbs, *J. Phys. Chem. B*, 1999, **103**, 5591–5597.
15. S. Odisitse and G. E. Jackson, *Polyhedron*, 2008, **27**, 453–464.
16. G. E. Jackson, P. W. Linder and A. Voy'e, *Polyhedron*, 1991, **10**, 883–884.
17. R. D. Hancock, *J. Chem. Educ.*, 1992, **69**, 615.
18. Y. Arano, M. Yabuki, T. Yahata, K. Horiuchi and A. Yokoyama, *Chem. Pharm. Bull. (Tokyo).*, 1990, **38**, 3099–101.
19. P. M. May, P. W. Linder and D. R. Williams, *J. Chem. Soc. Dalt. Trans.*, 1977, **2**, 588.
20. G. E. Jackson, P. M. May and D. R. Williams, *J. Inorg. Nucl. Chem.*, 1978, **40**, 1227–1234.

21. T. E. Nomkoko, G. E. Jackson, B. S. Nakani, W. K. A. Louw and J. R. Zeevaart, *Dalton Trans.*, 2004, 741–9.

22. K. S. Bai and A. E. Martell, *J. Am. Chem. Soc.*, 1969, **91**, 4412–4420.

23. C. Jubert, A. Mohamadou, C. Gérard, S. Brandes, A. Tabard and J.-P. Barbier, *J. Chem. Soc. Dalt. Trans.*, 2002, 2660.

24. S.-H. Liu and C. Chung, *Polyhedron*, 1984, **3**, 559–566.

25. M. K. Kim and A. E. Martell, *Biochemistry*, 1964, **3**, 1169–1174.

26. M. K. Kim and A. E. Martell, *J. Am. Chem. Soc.*, 1966, **88**, 914–918.

27. M. K. Kim and A. E. Martell, *J. Am. Chem. Soc.*, 1967, **89**, 5138–5144.

28. B. Lenarcik and E. Radzyminska-Lenarcik, *Chemik.*, *2011,*, 2011, **65**, 237–242.

Appendix

3.6.2.2 Ni(II) system

3.6.2.2.1. Ni(II)-[H(555)NH_2] system

Figure A1 shows the Z_M-bar plot for Ni(II)-[H(555)NH_2]. The Q_M-bar and the distribution graph for Ni(II)-[H(555)NH_2]titrations are given in Figure A2 and A3 respectively.

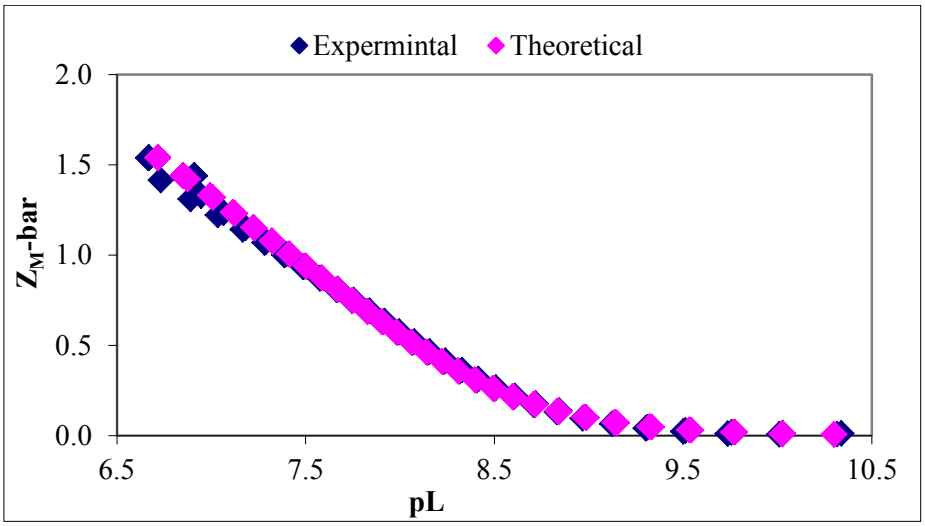

Figure A1: Z_M-bar as a function of pL for Ni(II)-[H(555)NH_2] Complex.

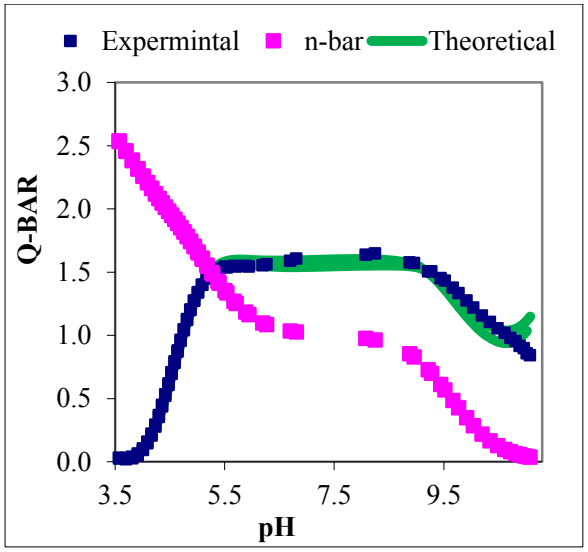

A2

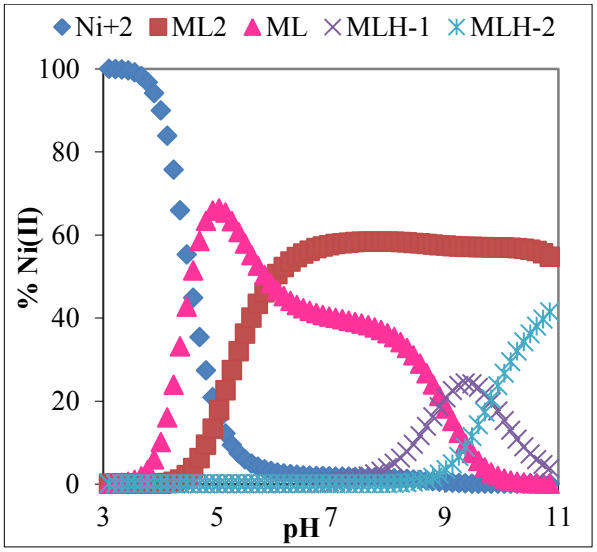

A3

Figure A2: Q_M-bar as a function of pH Ni(II)-[H(555)NH_2] Complex. **Figure A3:** The distribution curve for Ni(II)-[H(555)NH_2] Complex. Metal to Ligand ratio 1:2.

3.6.2.2.2. Ni(II)-[H(555)NMe$_2$] system

Z_M-bar for Ni(II)-[H(555)NMe$_2$] is given in Figure A4. The Q_M-bar curves shown in Figure A4 and the speciation graphs is given in Figure A6. The Ni(II) complex species were not similar to those species obtained from the Cu(II) system.

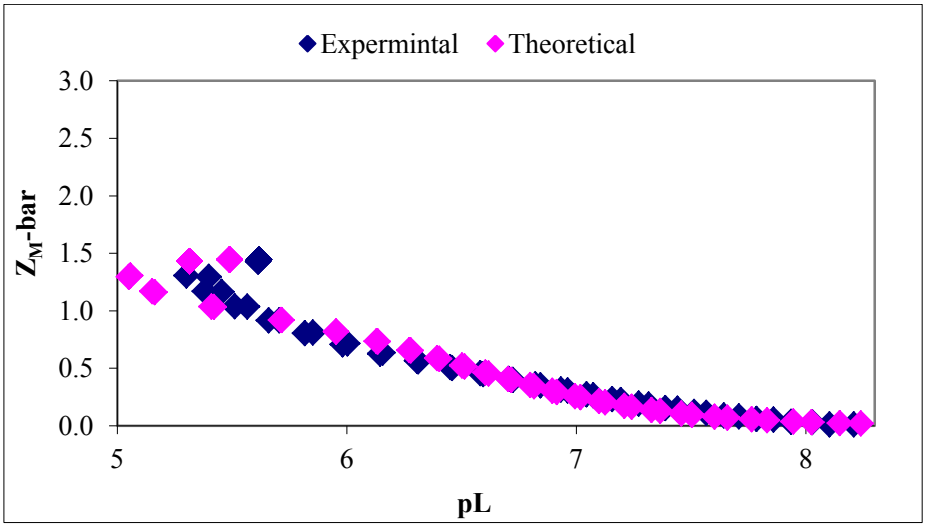

Figure A4: Z_M-bar as a function of pL for Ni(II)-[H(555)NMe$_2$] Complex.

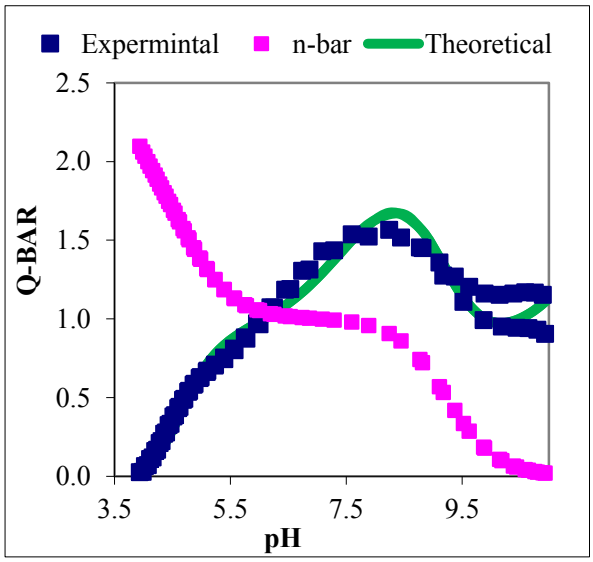

A5

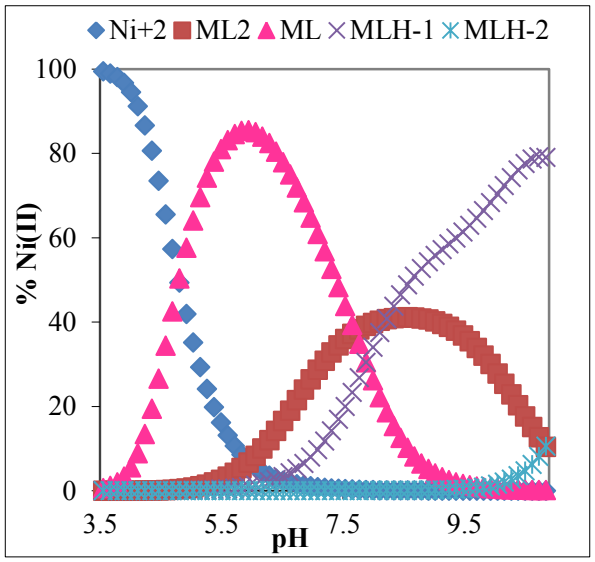

A6

Figure A5: Q_M-bar as a function of pH Ni(II)-[H(555)NMe$_2$] Complex. **Figure A6:** The distribution curve for Ni(II)-[H(555)NMe$_2$] Complex. Metal to Ligand ratio 1:1.5.

3.6.2.2.3. Ni(II)-[H_2(555)NH_2] system

The Z_M-bar is given in Figure A7. Q-bar and the distribution graph for the Ni(II)-[H_2(555)NH_2] system are shown in Figure A8 and Figure A9 respectively.

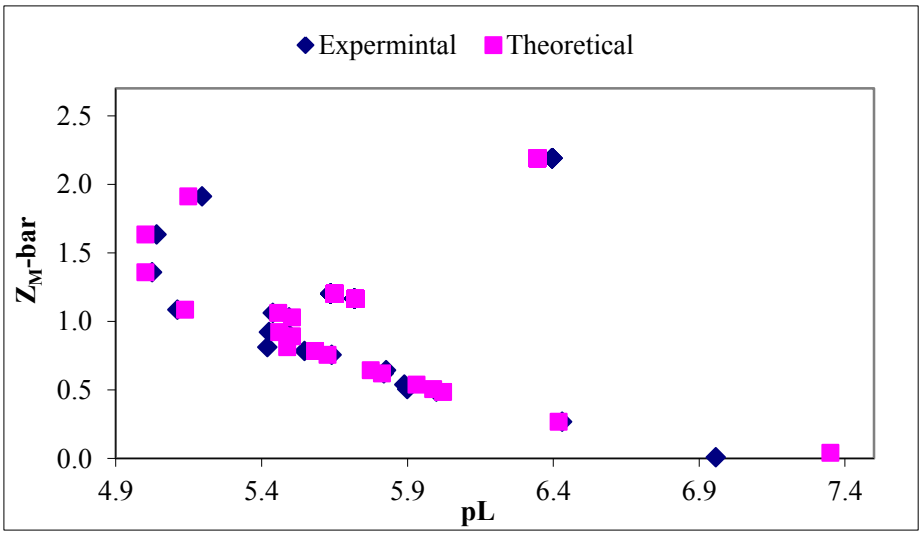

Figure A7: Z_M-bar as a function of pL for Ni(II)-[H_2(555)NH_2] Complex.

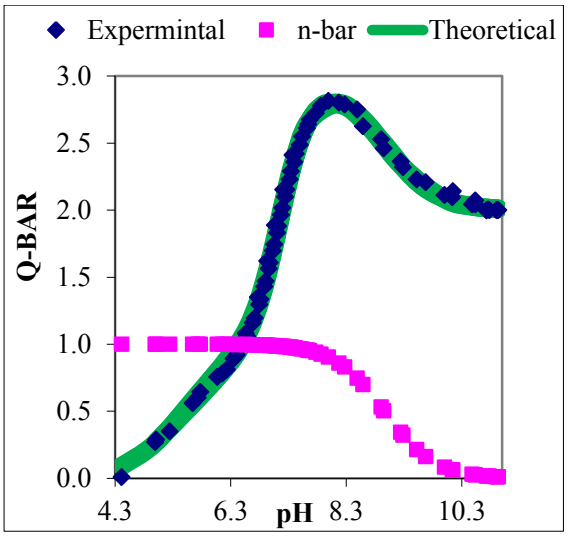

A8

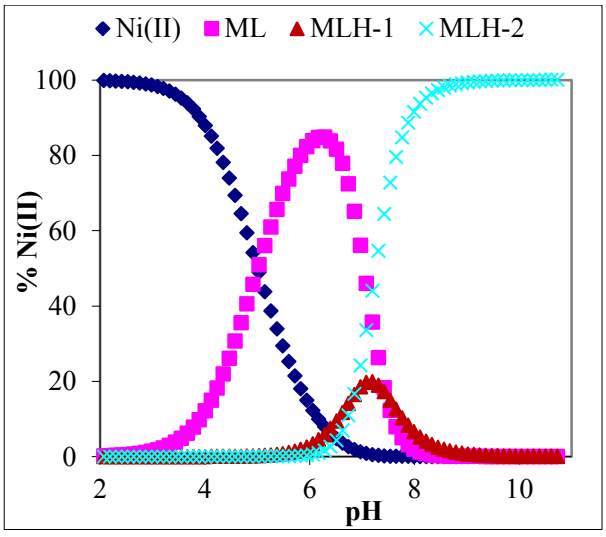

A9

Figure A8: Q_M-bar as a function of pH Ni(II)-[H_2(555)NH_2] Complex. **Figure A9:** The distribution curve for Ni(II)-[H_2(555)NH_2] Complex. Metal to Ligand ratio 1:2.

3.6.2.2.4. Ni(II)-[H_2(565)NH_2] system

The formation function for the Ni(II)-[H_2(565)NH_2] titrations is shown in Figure A10. The plot of Q_M-bar is given in Figure A11. The distribution curve for Ni(II)-[H_2(565)NH_2] titrations is given in Figure A12.

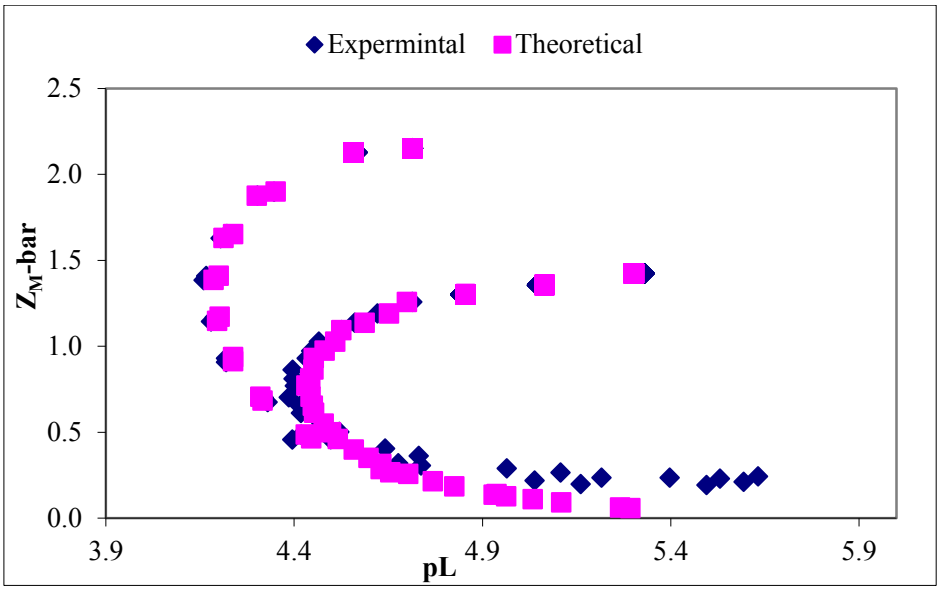

Figure A10: Z_M-bar as a function of pL for Ni(II)-[H_2(565)NH_2] Complex.

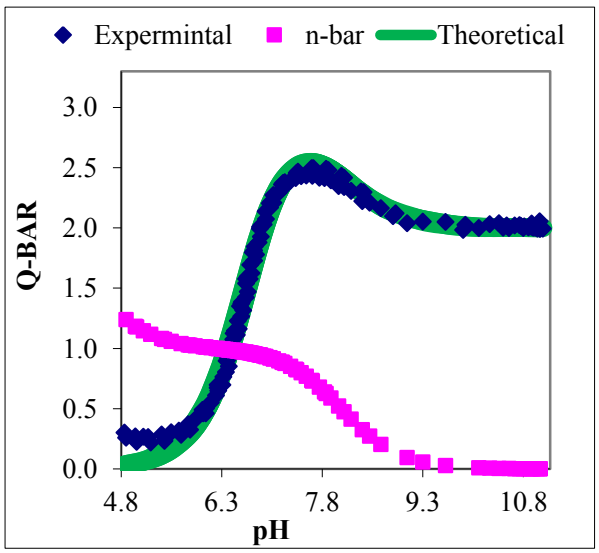

A11

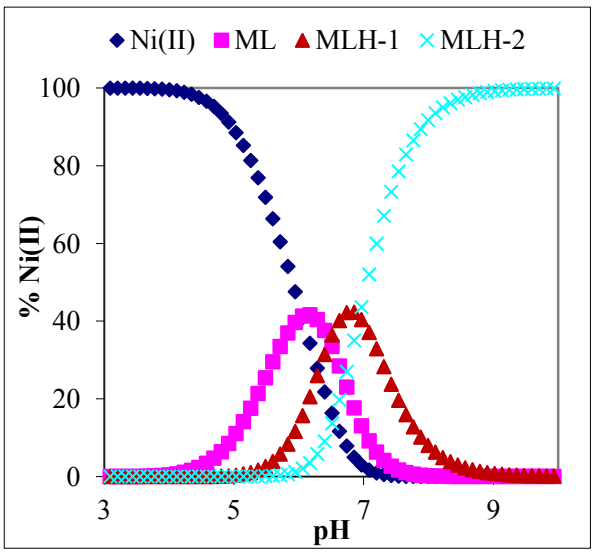

A12

Figure A11: Q_M-bar as a function of pH Ni(II)-[H_2(565)NH_2] Complex. **Figure A12:** The distribution curve for Ni(II)-[H_2(565)NH_2] Complex. Metal to Ligand ratio 1:2.

3.5.2.2.5. Ni(II)-[H(56)NH_2] system

Figure A13 given the Z_M-bar for the Ni(II)-[H(56)NH_2] titrations. Figure A14 and Figure A15 are shown the Q_M-bar curves and the speciation graphs for Ni(II)-[H(56)NH_2] respectively.

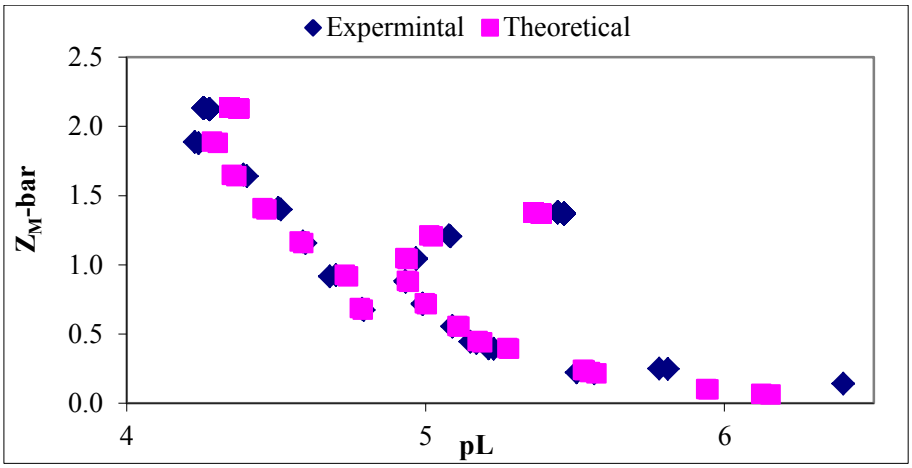

Figure A13: Z_M-bar as a function of pL for Ni(II)-[H(56)NH_2] Complex.

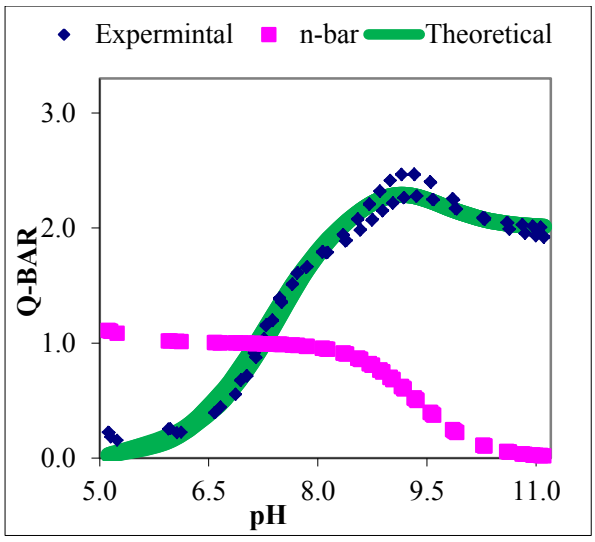

A14

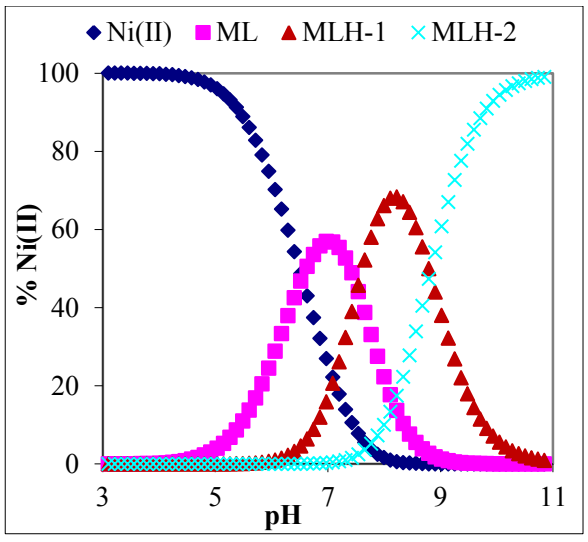

A15

Figure A14: Q_M-bar as a function of pH Ni(II)-[H(56)NH_2] Complex. **Figure A15:** The distribution curve for Ni(II)-[H(56)NH_2] Complex. Metal to Ligand ratio 1:2.

3.5.2.3.1 Zn(II)-[H(555)NH_2] system

The Z_M-bar function for the Zn(II)-[H(555)NH_2] system shown in Figure B1. The deprotonation function (Q_M-bar) curves given in Figure B2. The calculated species distribution curves shown in Figure B3.

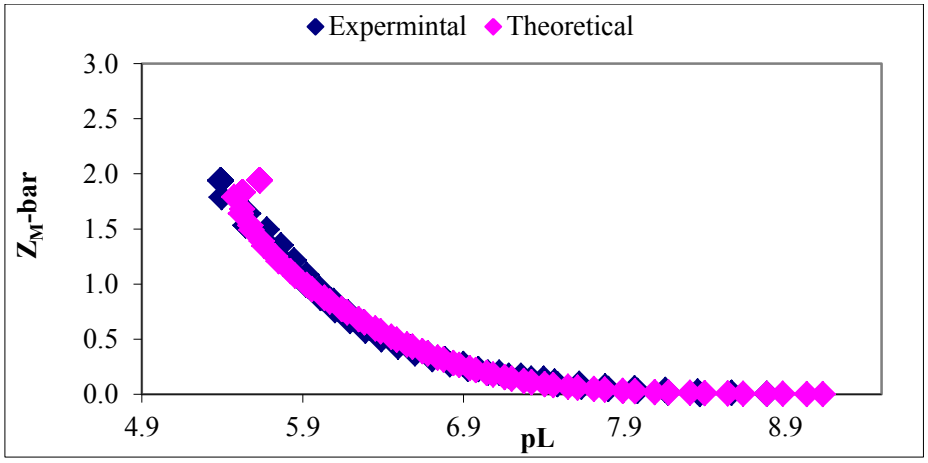

Figure B1: Z_M-bar as a function of pL for Zn(II)-[H(555)NH_2] Complex.

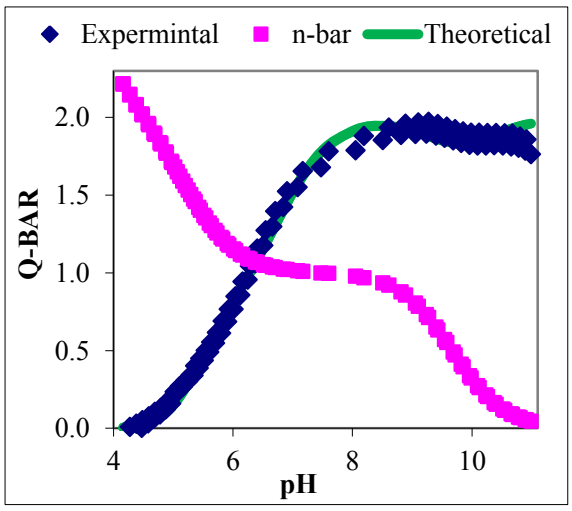

B2

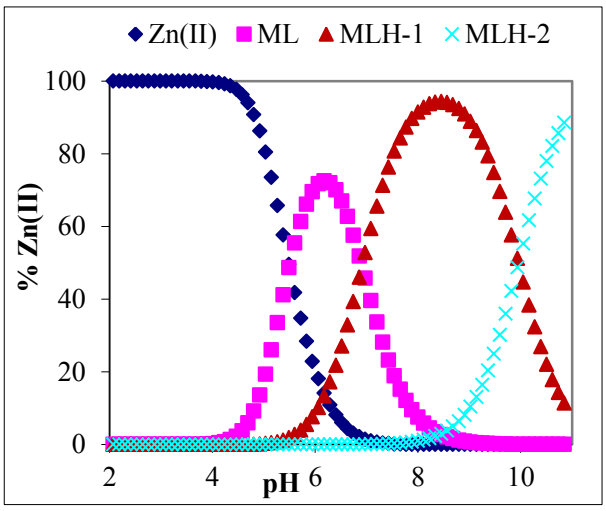

B3

Figure B2: Q_M-bar as a function of pH Zn(II)-[H(555)NH_2] Complex. **Figure B3:** The distribution curve for Zn(II)-[H(555)NH_2] Complex. Metal to ligand ratio 1:2.

3.5.2.3.2 Zn(II)-[H(555)NMe$_2$] system

Z_M-bar for complex formation titrations between Zn(II) and [H(555)NMe$_2$] is given in Figure B4. Q_M-bar and the speciation graph for Zn(II)-[H(555)NMe$_2$] titrations are given in Figure B5 and Figure B6 respectively.

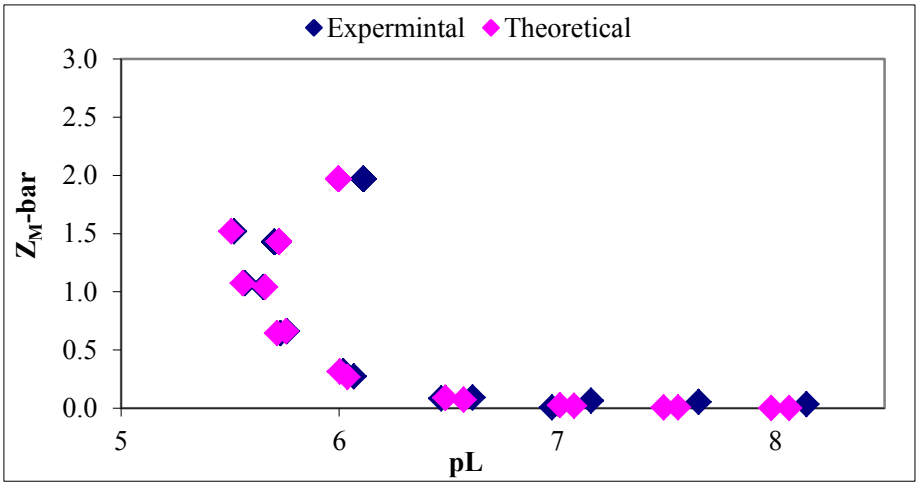

Figure B4: Z_M-bar as a function of pL for Zn(II)-[H(555)NMe$_2$] Complex.

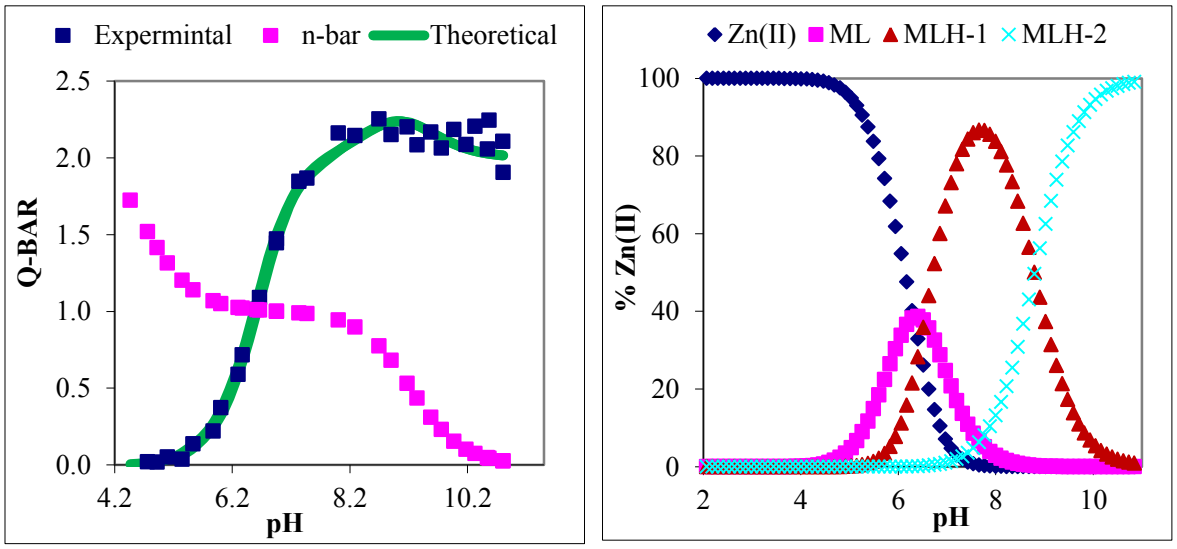

B5 **B6**

Figure B5: Q_M-bar as a function of pH Zn(II)-[H(555)NMe$_2$] Complex. **Figure B5:** The distribution curve for Zn(II)-[H(555)NMe$_2$] Complex. Metal to Ligand ratio 1:2.

3.5.2.3.3 Zn(II)-[H_2(555)NH_2] system

Figure B7 shown the Z_M-bar function for the Zn^{2+}/ [H_2(555)NH_2] system. Figure B8 and Figure B9 show the deprotonation function curves and the distribution graph for the Zn^{2+}/ [H_2(555)NH_2] system respectively.

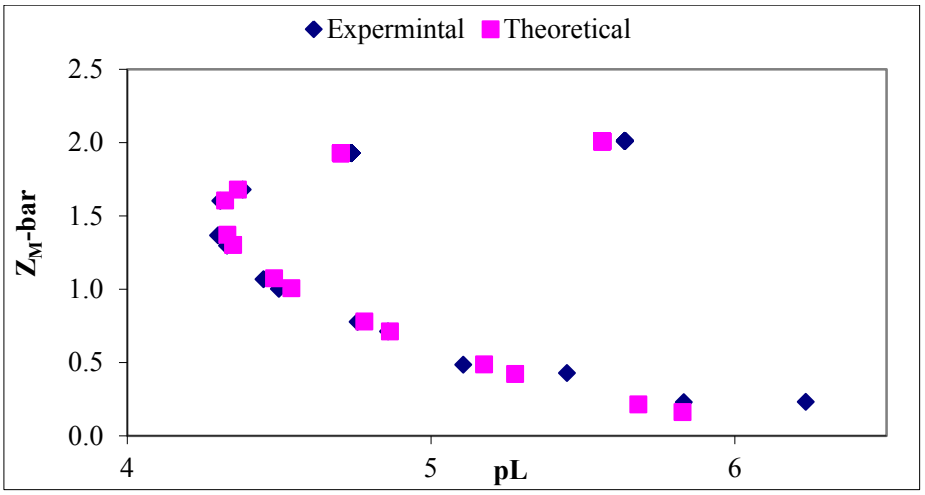

Figure B7: Z_M-bar as a function of pL for Zn(II)-[H_2(555)NH_2] Complex.

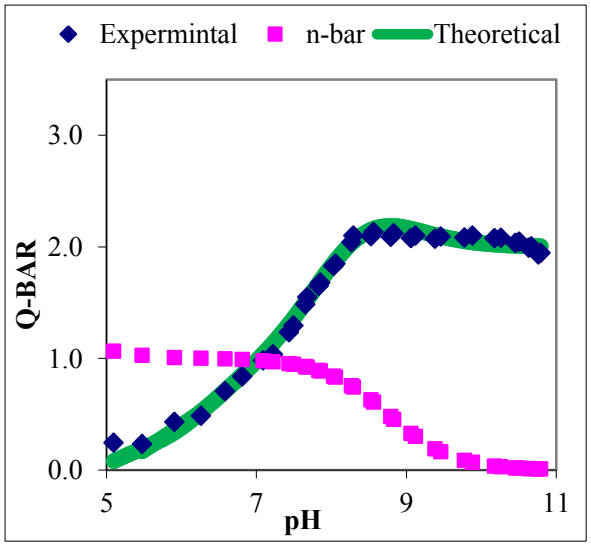

B8

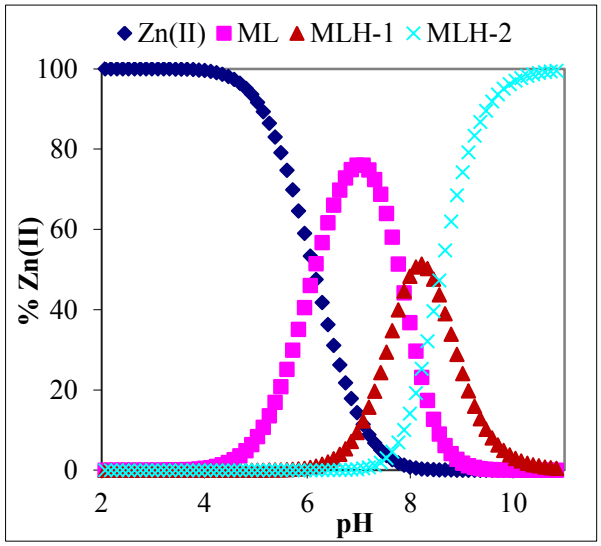

B9

Figure B8: Q_M-bar as a function of pH Zn(II)-[H_2(555)NH_2] Complex. **Figure B9:** The distribution curve for Zn(II)-[H_2(555)NH_2]Complex. Metal to Ligand ratio 1:2.

3.5.2.3.4 Zn(II)-[H_2(565)NH_2] system

Z_M-bar was observed for the Zn(II)-[H_2(565)NH_2] titrations as shown in Figure B10. Q_M-bar for Zn(II)-[H_2(565)NH_2] titrations is given in Figure B11. The distribution curve for Zn(II)-[H_2(565)NH_2] is given in Figure B12.

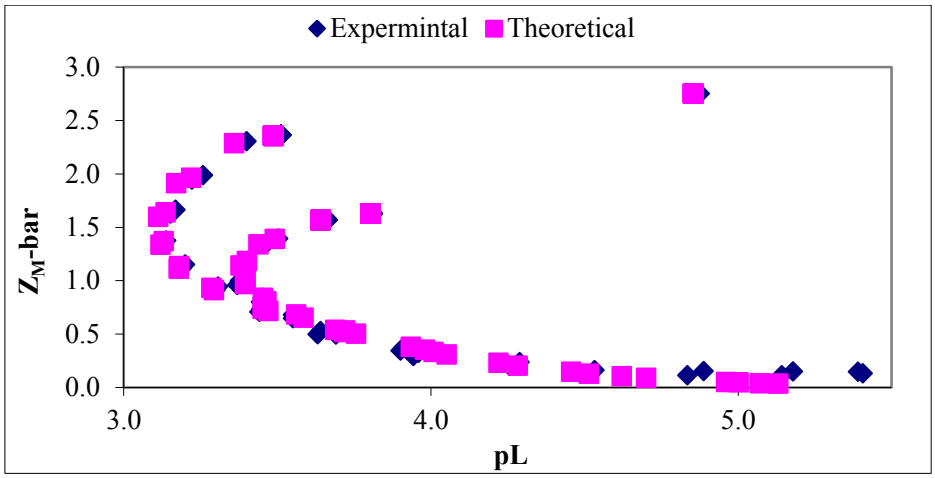

Figure B10: Z_M-bar as a function of pL for Zn(II)-[H_2(565)NH_2] Complex.

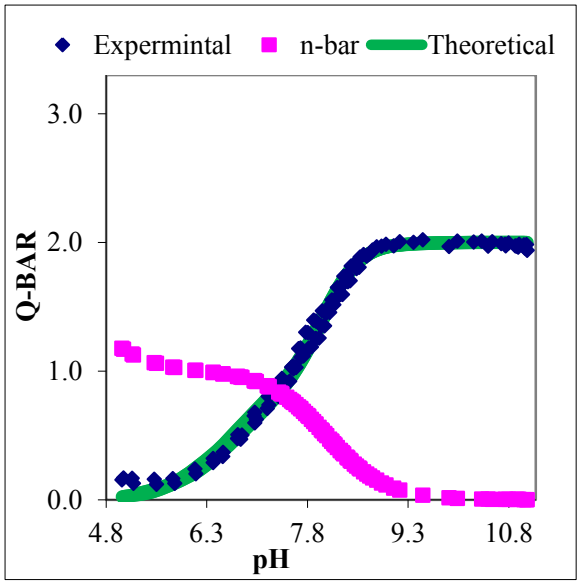

B11

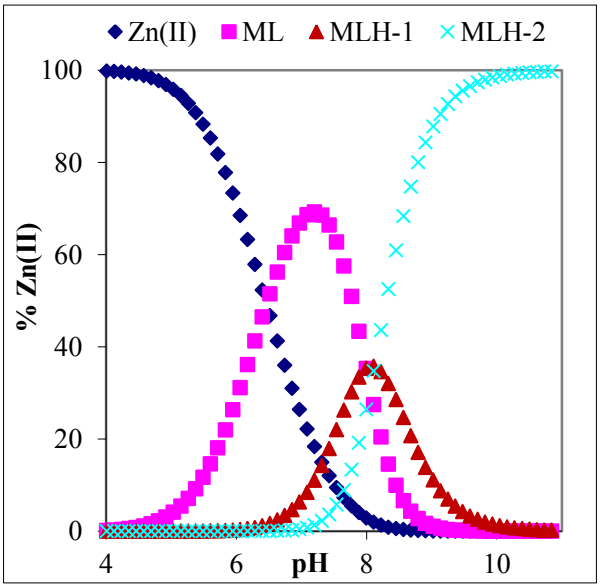

B12

Figure B11: Q_M-bar as a function of pH Zn(II)-[H_2(565)NH_2] Complex. **Figure B12:** The distribution curve for Zn(II)-[H_2(565)NH_2] Complex. Metal to Ligand ratio 1:2.

3.5.2.3.5 Zn(II)-[H(56)NH_2] system

The Z_M-bar for the titration of Zn with [H(56)NH_2] is given in Figure B13. Q_M-bar is given in Figure B14. The speciation graphs in Figure B15 show species formed by the complexation of [H(56)NH_2] with Zn(II).

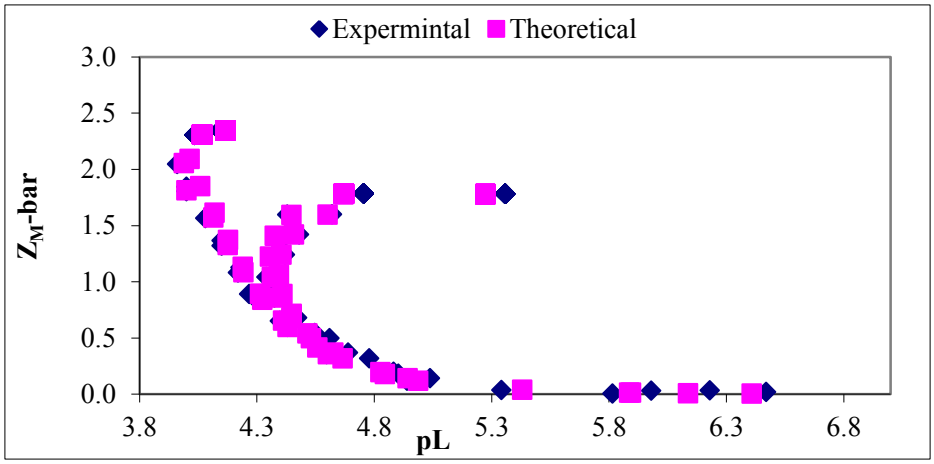

Figure B13: Z_M-bar as a function of pL for Zn(II)-[H(56)NH_2] Complex.

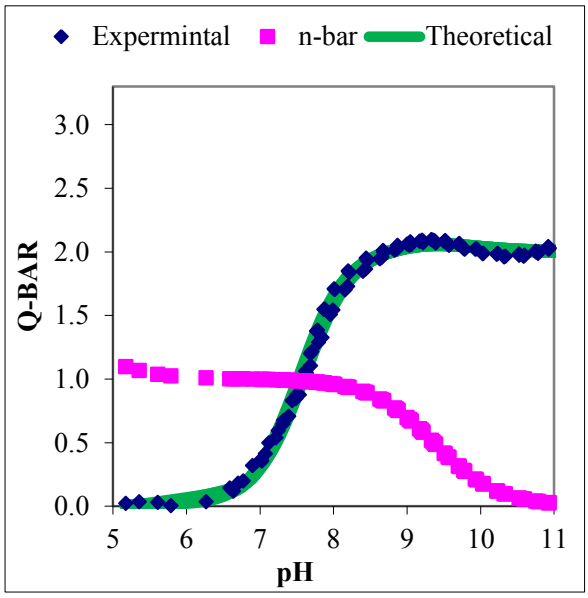

B14

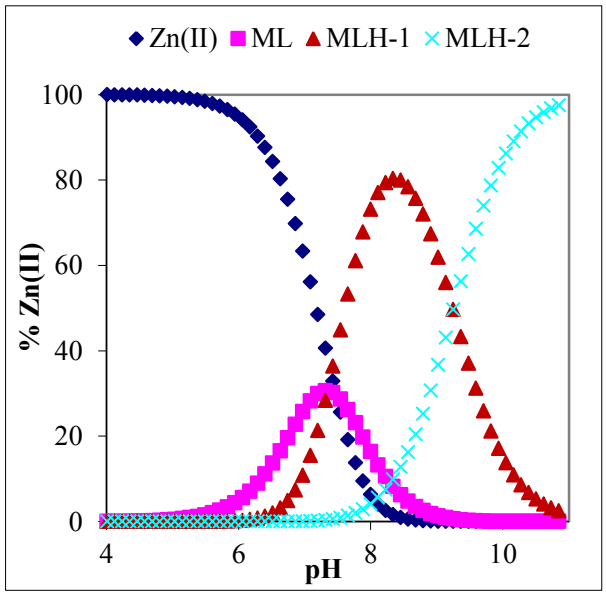

B15

Figure B14: Q_M-bar as a function of pH Zn(II)-[H(56)NH_2] Complex. **Figure B15:** The distribution curve for Zn(II)-[H(56)NH_2] Complex. Metal to Ligand ratio 1:2.